EFFECTS OF MIXTURE DESIGN PARAMETERS AND COMPACTION
METHODS ON THE PROPERTIES OF ROLLER COMPACTED CONCRETE
PAVEMENTS

A THESIS SUBMITTED TO
THE GRADUATE SCHOOL OF NATURAL AND APPLIED SCIENCES
OF
MIDDLE EAST TECHNICAL UNIVERSITY

BY

EMİN ŞENGÜN

IN PARTIAL FULFILLMENT OF THE REQUIREMENTS
FOR
THE DEGREE OF DOCTOR OF PHILOSOPHY
IN
CIVIL ENGINEERING

NOVEMBER 2019

Approval of the thesis:

EFFECTS OF MIXTURE DESIGN PARAMETERS AND COMPACTION METHODS ON THE PROPERTIES OF ROLLER COMPACTED CONCRETE PAVEMENTS

submitted by **EMİN ŞENGÜN** in partial fulfillment of the requirements for the degree of **Doctor of Philosophy in Civil Engineering Department, Middle East Technical University** by,

Prof. Dr. Halil Kalıpçılar
Dean, Graduate School of **Natural and Applied Sciences**   _____

Prof. Dr. Ahmet Türer
Head of Department, **Civil Engineering**   _____

Prof. Dr. İsmail Özgür Yaman
Supervisor, **Civil Engineering, METU**   _____

Prof. Dr. Halil Ceylan
Co-Supervisor, **Civil Engineering, Iowa State University**   _____

Examining Committee Members:

Prof. Dr. Murat Güler
Civil Engineering, METU   _____

Prof. Dr. İsmail Özgür Yaman
Civil Engineering, METU   _____

Assist. Prof. Dr. Hande Işık Öztürk
Civil Engineering, METU   _____

Prof. Dr. Mustafa Şahmaran
Civil Engineering, Hacettepe University   _____

Prof. Dr. İlhami Demir
Civil Engineering, Kırıkkale University   _____

Date: 21.11.2019

I hereby declare that all information in this document has been obtained and presented in accordance with academic rules and ethical conduct. I also declare that, as required by these rules and conduct, I have fully cited and referenced all material and results that are not original to this work.

Name, Surname: Emin Şengün

Signature:

ABSTRACT

EFFECTS OF MIXTURE DESIGN PARAMETERS AND COMPACTION METHODS ON THE PROPERTIES OF ROLLER COMPACTED CONCRETE PAVEMENTS

Şengün, Emin
Doctor of Philosophy, Civil Engineering
Supervisor: Prof. Dr. İsmail Özgür Yaman
Co-Supervisor: Prof. Dr. Halil Ceylan

November 2019, 191 pages

The aim of the thesis is to develop laboratory compaction methodology suitable for simulating field compaction procedures used for creating roller compacted concrete (RCC) mixtures. Based on this methodology, mechanical performance and fracture properties of RCC mixtures of different strength classes were determined and long-term fatigue performance of RCC mixtures with different strength levels was investigated.

In this context, a three-phase experimental study was designed. First, mixtures with different binder content and water amounts were prepared, and samples were made using different compaction procedures. A compaction methodology using a double drum vibratory hand roller was also implemented to represent field compaction procedures in the laboratory and was used to prepare RCC specimens in the later stages of the study. Second, the effects of RCC mixture parameters on RCC properties, especially fracture parameters, were determined for different binder contents and maximum aggregate sizes. Finally, for three RCC mixes of different performance categories, the flexural fatigue performance was determined and expressed as S-N curves. The experimental results show that ideal RCC mixtures can be achieved with

water amounts of 5-6%, Vebe times in the range of 30 ±10 sec, and a compaction ratio higher than 96%. It was also observed that fracture toughness was enhanced with increasing binder dosage and maximum aggregate size, although the increase in binder dosage or maximum aggregate size did not significantly change the fracture energy. Moreover, the average fatigue strength of the RCC mixture, corresponding to 2 million load cycles, was found to be about 62.5% of the ultimate static strength. Above all, compaction ratio, which is influenced by not only compaction methodologies but also mixture designs, is found to be the most important parameters affecting RCC properties.

ÖZ

BETON KARIŞIM TASARIMI PARAMETRELERİNİN VE SIKIŞTIRMA YÖNTEMLERİNİN SİLİNDİRLE SIKIŞTIRILMIŞ BETON KAPLAMA ÖZELLİKLERİNE ETKİSİ

Şengün, Emin
Doktora, İnşaat Mühendisliği
Tez Danışmanı: Prof. Dr. İsmail Özgür Yaman
Ortak Tez Danışmanı: Prof. Dr. Halil Ceylan

Kasım 2019, 191 sayfa

Tezin amacı silindirle sıkıştırılmış beton (SSB) karışımlarının laboratuvar koşullarında doğru ekipman ve tasarımla, saha ortamındaki gerçek performansını yakalayabilmesi için uygun bir sıkıştırma metodolojinin geliştirilmesi ve daha sonra bu sıkıştırma metodolojisi kullanılarak farklı dayanım sınıflarındaki SSB'lerin mekanik ve kırılma özelliklerinin belirlenmesidir. Son olarak ise farklı dayanımlara sahip SSB'lerin uzun süreli yorulma performanslarının araştırılmasıdır.

Bu amaçla üç aşamalı bir deneysel çalışma planlanmıştır. Birinci aşamada, farklı dozaj ve su oranına sahip SSB karışımları hazırlanmış ve bu karışımlardan, farklı sıkıştırma prosedürleri dolayısıyla farklı sıkıştırma dereceleri kullanılarak numuneler hazırlanmıştır. Ayrıca, saha koşullarını laboratuvar koşullarına aktaran çift tamburlu titreşimli el silindiri kullanılarak uygulanan bir sıkıştırma metodolojisi de bu bağlamda geliştirilmiş ve sonraki numune hazırlamada kullanılmıştır. İkinci aşamada, geliştirilen bu sıkıştırma metodolojisiyle SSB tasarımları yapılarak, SSB karışım parametrelerinin (bağlayıcı miktarı, agrega gradasyonu) SSB özelliklerine, özellikle de kırılma parametrelerine etkisi gözlemlenmiştir. Son olarak bir önceki aşamada elde edilen farklı performans kategorisine ait üç tane SSB karışımı için eğilmede yorulma

Gerilme-Çevrim (S-N) ilişkisi belirlenmiştir. Sonuç olarak, ideal SSB karışımlarına %5-6 su oranları, 30±10 sn Vebe süreleri ile %96'dan daha yüksek sıkışma oranlarındaki karışımlar ile elde edildiği görülmüştür. Kırılma parametrelerinden kırılma tokluğu ise bağlayıcı miktarı ve maksimum agrega boyutu ile artış gösterdiği görülürken, karışımların kırılma enerjilerinde bağlayıcı miktarının ve maksimum agrega boyutunun önemli bir etkisi görülememiştir. Son olarak, SSB karışımların yorulma davranışlarına bakıldığında, karışımların ortalama yorulma dayanımları nihai statik dayanımlarının yaklaşık %62,5'i olduğu görülmüştür. Her şeyden öte, sadece sıkıştırma yöntemlerinden değil aynı zamanda karışım tasarımlarından da etkilenen sıkışma oranının, SSB özelliklerini etkileyen en önemli parametrelerden biri olduğu tespit edilmiştir.

Anahtar Kelimeler: Silindirle Sıkıştırılmış Beton (SSB) Kaplama, Sıkıştırma Metodolojisi, Mekanik Performans, Kırılma Parametreleri, Yorulma Davranışı

To my family,

ACKNOWLEDGEMENTS

TABLE OF CONTENTS

LIST OF TABLES

LIST OF FIGURES

FIGURES

xvii

LIST OF ABBREVIATIONS

ABBREVIATIONS

ACI	American Concrete Institute
ACPA	American Concrete Pavement Association
ANOVA	Analysis of Variance
ASTM	American Society for Testing and Materials
CCM	Cohesive Crack Model
CEB	European Committee for Concrete
CMOD	Crack Mouth Opening Displacement
CoV	Coefficient of Variation
CR	Compaction Ratio
CTL	Concrete Technology Laboratory
CTOD	Crack Tip Opening Displacement
DCT	Disc-shaped Compact Tension
DDVHR	Double Drum Vibrating Hand Roller
FCM	Fictitious Crack Model
GBFS	Granulated Blast Furnace Slag
GDH	Turkish General Directorate of Highways
HCF	High Cycle Fatigue
HMA	Hot Mix Asphalt
JCI	Japan Concrete Institute
LCF	Low Cycle Fatigue
LEFM	Liner Elastic Fracture Mechanics
LVDT	Linear Variable Differential Transformer
MPa	Megapascal
MR	Modulus of Rupture

PCA	Portland Cement Association
PCC	Portland Cement Concrete
RCC	Roller Compacted Concrete
RILEM	International Union of Laboratories and Experts in Construction Materials, Systems and Structures
SEM	Size Effect Model
SGC	Superpave Gyratory Compactor
S-N	Stress-Life Fatigue Approach
TPFM	Two-Parameter Fracture Model
VPC	Vibratory Plate Compactor

LIST OF SYMBOLS

SYMBOLS

a_c	Critical effective crack length
C_i	Initial loading compliance value
$CTOD_c$	Critical crack tip opening displacement
C_u	Unloading compliance value
E_c	Elastic modulus
ε	Strain
$\emptyset$	Diameter
f_c	Compressive strength
f_{spt}	Splitting tensile strength
G_F	Fracture energy
G_f	Energy Release Rate/Initial Fracture Energy
K_I	Stress intensity factor
K_{Ic}	Critical stress intensity factor or fracture toughness
K^s_{Ic}	Critical value of stress intensity factor from TPFM
l_{ch}	Characteristic length
N	Number of load cycles to failure
p	Significance level
P_{max}	Maximum load
P_{min}	Minimum load
R^2	Coefficient of determination
S	Stress ratio
S_{max}	Maximum load level
S_{min}	Minimum load level
W_0	Toughness, area below load-CMOD curve

$\Delta\sigma$	Stress range
σ_a	Stress amplitude
σ_m	Mean stress
σ_{max}	Maximum stress
σ_{min}	Minimum stress

CHAPTER 1

INTRODUCTION

Roller compacted concrete (RCC), as the name suggests, is a concrete technology produced from the same components as the traditional concrete that accomplishes compaction using the heavy vibrating-steel-drum rollers and rubber-tired rollers during the fresh state. Aggregates that account for 75-85% of RCC volume have significant effects on RCC properties such as workability, compaction ratio, mechanical performance, and durability. Even though RCC has the same ingredients as conventional concrete, since it must have a stiff consistency to hold the roller when fresh at the same time be wet enough to allow the aggregate to disperse inside the paste. RCC has a higher fine/aggregate content, different gradation, less binding material, and lower water content than conventional concrete pavement (Harrington et al., 2010).

With the development of vibratory compaction equipment in the 1970s, this technology began to be used in Canada and the United States and this use was later continued in other countries, with improved speed, economic, sustainability and advantages provided by RCC accounting for its increased use in dams, airports, industrial warehouse, military fields, pavement structures, and many other applications (Ağar & Taşdemir, 2007; Özcan, 2008; Yaman & Ceylan, 2013). Since 1980s, especially in road construction, RCC pavements have been widely used in France, Germany, Norway, Sweden, Finland, Denmark, Germany, Austria, Argentina and Japan, while in the USA alone RCC pavement usage has exceeded 12 million square meters since 2011 (Yaman & Ceylan, 2013). Preference for using RCC pavements even in countries with little concrete road experience mainly results from the fact that this type of pavement can be constructed using the same equipment used in constructing traditional hot-mix asphalt (HMA) pavements. In addition to its rapid

applicability, the experience gained from many applications abroad has demonstrated its economic benefits, since RCC unit costs are lower than those of conventional concrete and asphalt pavements (Pittman, 2012). Lower cement content, shorter construction times, and lack of need for forms or reinforcing bars during the construction process has significantly proven the economic benefits of RCC pavements.

In Turkey, the proven advantages of RCCs have led to their use in dam construction as well as for urban and rural road construction under both municipal and provincial administrations. The first RCC application in Turkey was the downstream cofferdam of the Karayaka Dam in 1982 and 1983. The first RCC dam in Turkey, Suçatı, was put into service in 2000 (Özcan, 2008), and the first Turkish RCC road applications were tailored as a test strip in Antalya in 2007 under the "Economical and Sustainable Pavement Infrastructure for Surface Transport" (known as Ecolanes) project within the scope of the European Union under the 6th Framework Project (Neocleous, Pilakoutas, & Guadagni, 2009), and more extensive use was carried out by the Denizli Metropolitan Municipality in 2009. Thanks to the principal advantage of RCCs, that they can be produced by the same equipment used for the traditional flexible asphalt pavements, they have been widely used in both rural and urban road construction, mainly by the Samsun Metropolitan Municipality as well as by some other municipalities (Yaman & Ceylan, 2013).

Although there are some RCC pavement specifications, especially in the USA, much work remains to improve these specifications and form new guidelines for use in other countries. Few studies have systematically investigated optimum mixture design, fracture properties, and fatigue performance, all very important, particularly in pavement design. To address the inadequacy of relevant data in this field, a three-phase experimental program was developed in this study.

1) The first phase was aimed at developing appropriate compaction methodology and ensure balanced optimization of strength, density and compactability by simulating

the RCC field compaction process under laboratory conditions. For this purpose, a series of experimental studies were carried out to regulate the proper compaction methodology and secure a satisfactory degree of compaction in the field under laboratory conditions. A compaction methodology using a double drum vibratory hand roller (DDVHR) was also implemented to represent field compaction procedures in the laboratory.

2) During the second phase, flexural and fracture properties of RCCs in different strength classes were determined using beam specimens cut from the plates produced using the DDVHR compaction methodology previously developed for simulating field-compaction procedures. In addition, cores taken from these plates were studied to obtain compressive strength of RCC mixtures 2, 7, and 28 days after fabrication, and the percentage of strength gain with age was determined.

 3) Results of the final phase of the study, which determine the long-term fatigue performance of RCCs with different strength classes, were expressed in terms of S-N curves.

Chapter 2 presents a three-section comprehensive literature review related to the scope of the thesis. The first section covers RCC material selection, mixture design, and their effects on RCC physical and mechanical performance. The second and third sections describe fabrication of RCC specimens under laboratory conditions and physical and mechanical performance of RCC under field conditions. Chapter 3 presents details of the three-phase experimental program. Chapter 4 presents experimental results of each of the three phases separately, with a detailed evaluation of results presented for each phase. Finally, Chapter 5 describes and summarizes the main findings of the study and provides some insights into possible areas of future study.

CHAPTER 2

LITERATURE REVIEW

The literature review is presented in three subsections. Since the first step of the study was development of an appropriate compaction methodology and mixture design to achieve RCC field performance under laboratory conditions, citations on RCC pavement construction are summarized in the first part of the chapter. In the second and third parts of the chapter, the focus is on RCC fracture properties and fatigue behavior to provide a background for determining fracture properties and fatigue behavior of different RCC mixtures produced with the proposed compaction methodology.

2.1. RCC Pavement Construction

Studies based on RCC pavements are found mostly to focus on three main topics: 1- material selection and mixture design, 2- fabrication of RCC specimens under laboratory conditions, and 3- physical and mechanical performance testing of RCC pavements.

2.1.1. RCC Material Selection and Mixture Design

In the first phase of a study conducted by Hazaree, Ceylan, & Wang, (2011), the effects of different cement amounts on the physical and mechanical properties of RCC were investigated. In their study, the amount of cement varied between 100 and 450 kg/m^3 (increasing by 50 kg/m^3) and a single aggregate grading was used (Dmax 19 mm). All mixtures were prepared with a constant Vebe time of 40 ± 10 sec. As a result, the authors indicated that RCCs tend to behave slightly different from conventional concrete, and the optimum amount of cement, considering density, compressive strength, permeable void percentage, and water absorption capacities, was found to lie between 225 ± 25 kg /m^3.

A study conducted by Chhorn & Lee, (2016a) explored, consistency alteration under different amounts of aggregate gradation, water content, and chemical additives. They chose Vebe time as a representative measure of consistency and used three different aggregate gradations and water-contents varying between 3.5-7.4%, while keeping cement dosage constant (280 kg/m^3). However, half of their measurements were excluded because their vebe times were greater than 120 seconds. They had two observations after their experiments were completed. First, Vebe consistency times were greater for mixes with higher finer aggregate content. Second, Vebe consistency times were lower for mixes with higher water content. At the end of the study, the researchers suggested a Vebe consistency time for RCC mixtures between 30 and 75 seconds.

The same authors, Chhorn & Lee, (2016b), investigated, in another publication, the effect of aggregate gradation, cement dosage, water content, curing conditions, and chemical additives on RCC characteristics. In RCC mixes, three different aggregate gradations (with the term Fine Agg./Total Agg. ratio shortened to F/A), F/A=30% (under PCA lower limit), F/A=70% (over PCA upper limit) and F/A=50%, for three cement dosages (220-250-280 kg/m^3). The study concluded that while the highest compressive strength value was associated with the mix with F/A=50%, when cement dosage was considered there were no significant differences among test results. The study, however, did recommend using 280 kg/m^3 to minimize the negative effect of minor changes in water content on compressive strength. It also indicated that 98% compaction degree with respect to modified proctor compaction, could be reached to attain higher compressive strength values.

A study by Aghaeipour & Madhkhan, (2017) investigated the effect of various amounts of granulated blast furnace slag (GBFS), used as binder material in RCC mixtures, on RCC durability (water absorption, percentage of voids, ultimate strength under freeze & thaw, etc.). The study considered two different binder contents (12-15%), three different granulated blast-furnace slag contents (20-40-60% of total cement weight), and five different water contents (4.0-4.75-5.5-6.25-7.0%). The

constant aggregate ratios in the 40 RCC mixes were 7:2:1 for 0-5 mm fine aggregate, 5-12 mm coarse aggregate and 12-19 mm aggregate, respectively. The researchers observed that the optimum water content corresponding to maximum dry density was proportional to the amount of granulated blast furnace slag in the mix, with the optimal portion found to be 40% of binder material weight.

2.1.2. Compaction Methods of RCC Specimens in the Laboratory

The compaction process, in which the amount of air voids in the mixtures decrease and thus the density increases, represents an important stage in RCC applications. Compaction reduces voids by forcing the aggregate particles to rearrange, allowing smaller particles to fill spaces between larger particles, with water in excess of that capable of being absorbed into aggregate particles filling the smallest void spaces. The water in the mixture also has a lubricating effect, helping small particles to fill the voids. On the other hand, if there is insufficient fine material or water in the mixture, or if the compression energy is inadequate, it can be quite difficult to achieve the desired density, as the compaction energy in RCC applications is essential to have sufficient compaction energy (i.e. compaction method) as well as an adequate amount of fine materials and optimum water content in the mixture. The strength and density (i.e. compaction ratio) relationship for RCC mixtures is shown in Figure 2.1, where it can be seen that, especially until the density rises to 96% of the theoretical air free density, mixture strength is quite sensitive to the amount of compaction.
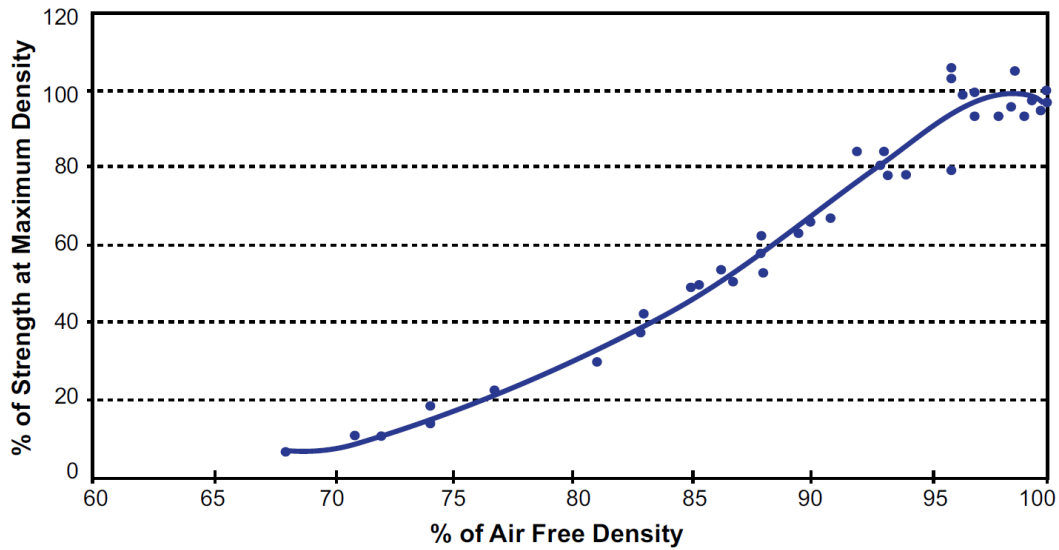
*Figure 2.1. Compressive s*trength vs density relationship for various RCC mixtures (Schrader, 1992)

Although the amount of compaction (i.e., the desired density) can be quite significant for achieving sufficient strength in RCC applications, academic studies on RCC sample production and compaction methods are very limited as compared to those on RCC material selection and mix design. Since it is well-known that it is almost impossible to produce RCC samples using steel drum rollers under laboratory conditions, various methods have been explored for compacting samples for use in academic studies to obtain realistic strength values and compaction degrees similar to those in the field. However, these methods have been highly variable among particular researchers, so they have not been standardized and their test results might not reflect field conditions. The study conducted by Schrader, (2003) should be emphasized, because it describes the effects of different compaction techniques in terms of optimum water content, compressive strength, and unit weights of RCC mixes. This study, a quality control staff member of a RCC dam construction project, was able to apply several compaction techniques the samples taken from the dam construction, and he then described a relationship between compaction technique and characteristic features of RCC such as strength and optimum water content values, as presented in Figure 2.2.

8

Figure 2.2, reveals that the compaction method has a significant effect on maximum achievable strength and moisture content values. Furthermore, when the compaction energy is reduced, optimum moisture content increases while the corresponding strength decreases. A 10-ton vibratory roller, provided the highest available compaction energy, produced higher strength values with lower moisture content. Moreover, the author showed a relationship between the compaction technique and the consistency of RCC for evaluating which technique is more suitable for consistency ranges independent of binder content (Figure 2.2b). Variation in mechanical properties of RCC specimens compacted with different methods under laboratory conditions was also examined. Literature on studies of RCC compaction procedures is rather limited and, and a standard compaction method has not been accepted by researchers. It should also be kept in mind that the concrete mixtures discussed in this study were used for dam construction, hence the binding amount was quite low compared to those for road applications.

Vibrating table (ASTM C1176, 2013) and vibrating hammer (ASTM C1435, 2014) methods are existing compaction methods standardized by the American Society for Testing and Materials (ASTM), and two new compaction methods, the modified proctor (ASTM WK59339, 2017) and the Superpave gyratory compactor (SGC) (ASTM WK33682), have been added to the literature and are about to be standardized. Impact hammer and pneumatic hammer usage has also been described in some studies (ACI Committee 207, 1995; Choi & Groom, 2001). Some researchers have also tried compaction tools specifically designed to simulate field-compaction conditions (Filho, Paulon, Monteiro, Andrade, & Dal Molin, 2008; Neocleous, Angelakopoulos, Pilakoutas, & Guadagnini, 2011).

Compaction Method and Moisture Content
vs
Maximum Achievable Strength (II)

(a)

Lab Compaction Method and Moisture Content
vs
Maximum Achievable Strength (I)
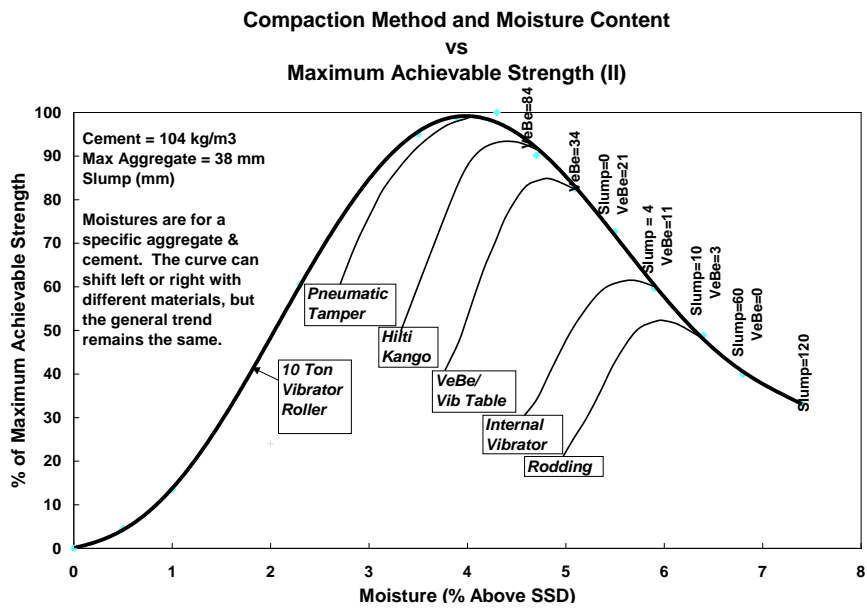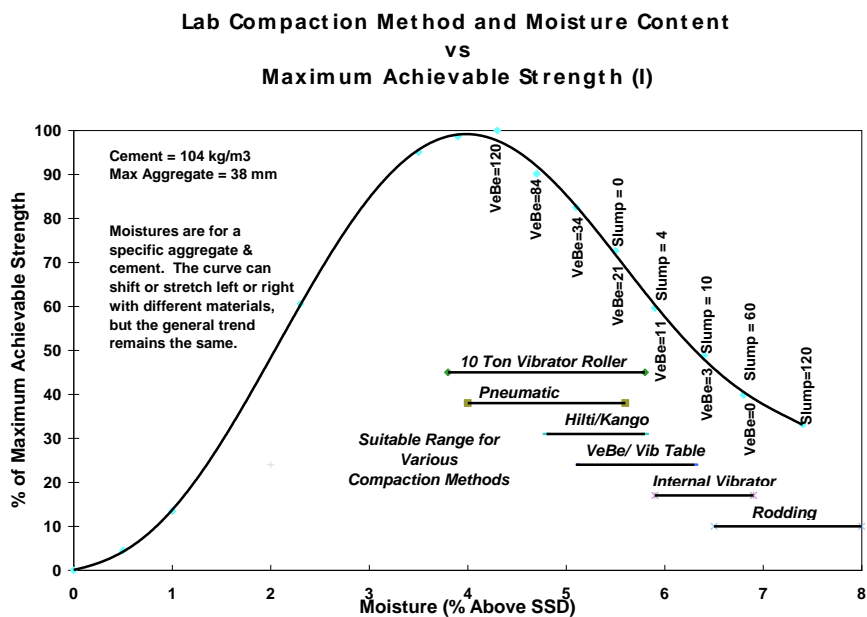
(b)

Figure 2.2. The maximum allowable strength vs. moisture content curve with respect to compaction techniques (Schrader, 2003)

When compared to other compaction equipment, the SGC method is a rather new development mainly used to prepare hot-mix asphalt (HMA) specimens; SGC uses a combination of vertical consolidation pressure and gyratory kneading effort, making it capable of simulating field compaction procedures in the laboratory (Collins, Watson, Johnson, & Wu, 1997; Masad, Muhunthan, Shashidhar, & Harman, 1999; Peterson, Mahboub, Anderson, Masad, & Tashman, 2003; Wang, et al., 2018). SGCs also have various advantages such as: (i) the amount of energy to be applied can be controlled by setting the number of gyrations, (ii) the samples could be compacted to the desired density using a height-based setting, and (iii) the compaction process could be monitored through height versus gyration curves or shear versus gyration curves, etc. (Pasetto & Baldo, 2014).

SGCs were used for the first time for compaction of base and subbase materials in the early 2000s, and the results reflected better simulation of field conditions than the traditional proctor method (Browne, 2006; Cerni & Camilli, 2011; Mokwa, Cuelho, & Browne, 2008). Although the SGC method has most commonly been used to compact HMA mixtures, the study conducted by Amer, Delatte, & Storey, (2003) and Amer, Storey, & Delatte, (2004) stated that this method is also applicable to manufacturing RCC specimens, although the compaction degree and the consistency and density of RCC specimens were strictly dependent on the number of gyrations (Figure 2.3).

Williams, (2013) compared the effects of the proctor method and the Superpave gyratory compactor method for determining optimum water content, with the effect of aggregate gradation on RCC mixes studied during the second stage of the study. The 17 different aggregate gradations and types of aggregates used in this study were sandstone, syenite, limestone and dolomite, with each mix compacted with two of the methods mentioned above, after which the optimum water content and maximum density values were determined. As expected, for the data associated with the mixes compacted with proctor method, a parabolic curve reflected the density/water content relationship, with the peak of the curve corresponding to the optimum water content.

Conversely, the data for the latter method did not reflect such a parabolic curve, and the relationship was linearly proportional to water content. Water leakage was observed during compaction of some mixes with higher water content, and the point at which the first leakage occurred was accepted as the optimum water content (Amer, et al., 2003).
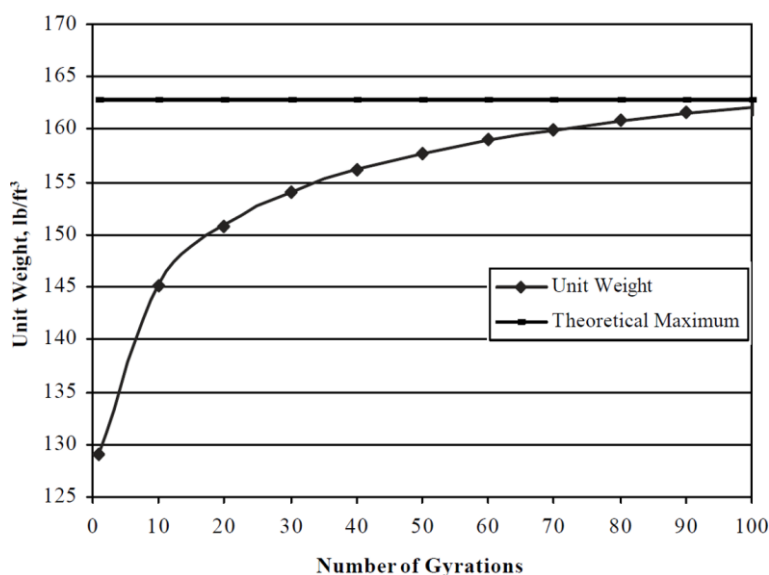
Figure 2.3. Unit weight vs. the number of gyrations curve for Superpave gyratory compactor (Amer et al., 2003)

2.1.3. Performance of RCC Pavements

Research studies performed under field conditions can be considered as the most critical step of this literature review for reasons such as cost and possible difficult field conditions that have resulted in a significant lack of studies performed in the field.

Lee, Cho, & Park, (2014) studied mechanical performance of RCC pavements both in the laboratory and in the field. That study consisted of three stages, with the first stage determining the performance of RCC specimens prepared from six laboratory mixtures with three different binder contents (160-200-250 kg/m^3), 4-6% water content, and constant aggregate gradation, with 20% of the binder replaced with fly

ash. The RCC mixtures were compacted in the laboratory using a vibrating table (ASTM C1176, 2013), and 15x30 cm cylindrical specimens were manufactured, after which strengths after 3,7 and 28 days of RCC fabrication were measured. The second phase involved representing field compaction conditions in a laboratory with a small-scale vibratory roller. A 50x70x20 cm section was poured with RCC and cores then taken. This procedure was followed for eight mixtures reflecting 180-300 kg/m^3 binder content and 4.5-5% water content. In the final phase, four mixtures were selected in accordance with the test results of previous phases. Laboratory test results at the end of the study suggested that the required binder content should be greater than 250 kg/m^3 to provide sufficient strength (a minimum of 28 day strength of 21 MPa was required for bicycle roads) and water content should be greater than 5% to provide sufficient workability. In addition, a 93% compaction degree (core dry unit weight divided by maximum theoretical dry unit weight) was determined when the required strength was reached. With respect to field test evaluations, sufficient results could be obtained for RCC pavements with thickness of 10 cm or less if binder content was lower (250 kg/m^3 or less). When the compaction applications were compared, the vibrating table and the steel drum vibratory roller yielded similar compressive strength values while the small-scale vibratory roller (vibratory hand roller) used in the laboratory yielded 10% higher strength than either of those methods. With respect to surface roughness, they were not able to produce expected results and there were defects on pavement surfaces due to the compaction methodologies used.

Another research study performed by Chhorn, Hong, & Lee, (2017) under field conditions was related to increasing performance of RCC pavements. Similar to the previous study, they used five pavement trial sections of 5 m width, 0.2 m thickness, and 580 m length. The RCC mixtures used 280 kg/m^3 binder content, 4.5% water content, 0.1% air entraining admixture, two maximum aggregate sizes (13 & 19 mm), and 0-0.05% super-plasticizing admixture, so all mixtures had Vebe times varying between 30-75 seconds. Fine and coarse aggregate percentages also remained constant (50-50%). For all mixtures, Vebe consistency times were determined and fresh

concrete were taken to be compacted using a vibrating hammer (ASTM C1435, 2014), and after the field compaction process was completed, core samples were taken to obtain physical and mechanical properties. In addition to standard tests, RCC surface properties were examined in terms of the International Roughness Index (IRI) and skid resistance number (SN). Since the researchers sought to establish relationships between Vebe time and mechanical/physical properties, Vebe time was treated as a control parameter. They also sought to find an optimum range for Vebe time to be used in RCC pavement construction. The final result reflected an optimum Vebe time range of between 47 and 65 seconds for criteria of compressive strength, compaction degree, IRI, and SN.

A study conducted by LaHucik & Roesler, (2017) compared the results obtained from field and laboratory conditions using same material contents and mixture designs in terms of density and mechanical properties of RCC samples. Core samples in that study were taken from four different RCC road projects in Illinois (USA). For laboratory experiments, a vibrating hammer, commonly preferred for RCC compaction, and the SGC method were used, possibly better replicating field compaction conditions. The results coming the vibrating hammer method reflected an optimum moisture content between 5.8% and 6.5%, leading to a fresh density between 2452 and 2508 kg/m^3. Vebe times under a 22.7 kg surcharge load changed by 10 to 20 seconds. To observe mechanical properties of the samples, compressive strength tests (ASTM C39 / C39M-18, 2018), splitting tensile strength test (ASTM C496 / C496M-17, 2017) and disc-shaped compact tension tests (ASTM D7313-13, 2013) were applied. At the end of the study, a t-test with 95% confidence revealed that the compressive strength pairs of laboratory and field core specimens (of the same size) differed statistically, possibly because of lower density and higher density variation in the field. Specifically, the cores taken from sites had approximately 4% lower density values than laboratory samples, resulting in a 45% reduction in compressive strength. It was also stated that since field results were highly different from the laboratory

results, the vibrating hammer method might apply an excessive compaction energy that could not be accomplished in field compaction.

2.1.4. Literature Review Discussion - Part I

Literature studies related to RCC pavement applications generally consist of three components: i) material selection and mixture design, ii) sample production and compaction methodologies under laboratory conditions, and iii) physical and mechanical properties of RCC pavements. The material contents used in the primary studies on RCC, their amounts, and effects of physical and mechanical performance, are summarized in Table 2.1. The mixture design and compaction methods used in the primary studies on RCC are also summarized in Table 2.2. The principal literature based findings in this section are as follows:

- For RCC mix designs, a soil compaction technique that takes maximum density as a reference, was preferred in a number of studies. Some researchers also gave priority while designing the mixtures to RCC workability, correlated with consistency of Vebe times.

- The amount of binder in the mixtures was most often chosen to lie between 250-350 kg/m^3 and the optimum water ratio was generally in the range of 5-6%. The fresh unit weight of RCC also varied between 2450-2550 kg/m^3.

- Aggregates, accounting for 80-85% of RCC mixtures, have been frequently discussed in the literature studies because they significantly affect RCC workability, compactability, strength, thermal properties, and durability. The maximum aggregate size described in the literature was generally selected to lie between 12-19 mm and the percentage of fine aggregate content to total aggregate content changed between 50-70%. While the consistency of the RCC mixtures was not reported in many studies, the studies that did report it observed that Vebe consistency time was generally changed by between 30-50 seconds to achieve a workable RCC mix. Furthermore, RCC mixtures prepared in the field had higher Vebe times than those prepared in the laboratory,

indicating that a mixture specially prepared in the laboratory with a Vebe time of less than 20 seconds might not be stiff enough to carry the heavy compaction equipment used in the field.

- Since RCCs are compacted with 10-12 ton vibratory rollers in the field while they are fresh, the most critical problem for RCC studies is the lack of accepted knowledge about compaction methodology that fully reflects field compaction procedures in the laboratory. It could be observed that RCC samples were prepared by researchers using different compaction methods and procedures under laboratory conditions. It could be observed that RCC specimens were mostly prepared in the laboratory using either a vibrating hammer (ASTM C1435, 2014) or vibrating table (ASTM C1176, 2013), and also seemed that required procedures were not strictly followed in many of the studies. For example, to obtain higher unit weight, the vibrating table method was sometimes applied for a longer time than specified in the standard or the vibrating hammer was held on the specimen for a longer time than written in the standard. Modified proctor, impact hammer, and pneumatic hammer methods were also preferred in some studies. Moreover, use of the SGC method commonly used to compact HMA specimens has increased for RCC compaction in litreature studies, because this method reflects field compaction conditions well in the laboratory and provides higher degrees of compaction. Finally, some researchers used special compaction equipment to prepare RCC specimens.

- The literature indicates that cylindrical specimens were mainly used for RCC strength tests, the most important reason for this choice being that the production and compaction processes of beam and cubic samples is quite difficult compared to those used for cylinder samples, and there is as yet no specification on the production of RCC beam samples under laboratory conditions. In the studies, compressive strengths after 28 days for low cement dosages (300 kg/m^3 and below) were generally between 30-50 MPa.

- A limited number of literature studies comparing field conditions and laboratory conditions revealed that laboratory results generally gave higher density and strength values than those from the field. Compaction methodology is considered to be an essential factor in obtaining different densities in field and laboratory conditions, especially when it is thought that a 1-2% change in RCC sample densities can lead to a 10-15% change in strength (Amer, et al., 2004). The vibrating hammer method commonly used to compact RCC specimens in laboratory conditions may be imparting too much compaction energy to properly simulate field compaction. Also, because the RCC mixtures produced under laboratory conditions have considerably low vebe time, the fact that the RCC specimens may begin to act as conventional concrete can also be a crucial factor. One of the critical problems in RCC field applications is that the density variation depends on the core zone, and it also decreases with depth regardless of the core area. These changes in density reflect the significance of the compaction procedure in field applications, in particular the use of higher density rather than conventional pavers , the use of thicker and stiffer foundation layers beneath the RCC, and the reduction of RCC lift thicknesses, all considered to significantly reduce such variations.

In brief, while there is still a lack of detailed specification(s) to enable researchers reach field compaction conditions in the laboratory, there is an increasing number of studies about RCC pavement. The important points generating discussions can be summarized as: manipulation of existing standards for the sake of higher degree of compaction, possible contradictions between field and laboratory test results, and the uncertainty with respect to how academic studies reflect actual field applications. In light of the limited number of studies, it can be asserted that the compaction procedure used in an RCC applications is the dominant factor explaining why RCC laboratory and field results.

Table 2.1. *Some mixture design and performance values in RCC pavement studies (Sengun, Aykutlu, & Yaman, 2017)*

	References		LR 2015	CL 2016a	CL 2016b	HCW 2011	AM 2017	YUAT 2015	LDRA 2017	GMR 2017	MAT 2012	ADS 2003	ASD 2004	NAPG 2011	CHL 2017	LCP 2013
Binding Materials	Cement	kg/m³	282	220-280	280	225±25	240-280	300	282	330	275	255	260-325	300	280	180-250
	Type and amount of pozzolan	%	-	-	-	-	Slag 0-60%	-	-	Truss 0-20%	N.P 0-30%	Fly Ash 0-20%	-	-	-	Fly Ash 0-25%
	Binder amount by weight	%	12	9-12	13	10-11	12-15	13-15	12	14-15	13	9-14	11-14	13-14	12	8-12
Aggregates	D_{max}	mm	19	19	19	19	19	19	19	19	19	25	13	14	13, 19	25
	Fine/Total Agg. ratio	%	-	30-70	60	-	70	57	-	60	60	-	-	-	50	44
Water	Amount	kg/m³	150-160	-	147	120-125	124-146	120-136	154-172	106	112-143	129	131	-	107	108-120
	Water ratio	%	6-7	5-6	6	5-6	5.5-6.7	5-6	6.5-7.1	4.5	4.7-6.0	5-5.5	5.5	6.25-7.50	4.5	4.5-5.5
Chemical Admixtures	Superplasticizers	% binding weight	-	0.1-0.3	0.1-1.0	1	-	-	-	0-0.8	0-3.0	-	-	-	0-0.05	0-1.0
	Air entraining		-	0.05-0.1	-	0.8	-	-	-	0-0.06	-	-	-	-	0-0.1	-
	Retarders		-	-	1.5	-	-	-	-	-	-	-	-	-	-	-
	Vebe Time	s	-	-	30-75	40±10	-	-	-	36-40	-	-	-	-	47-65	-
	Min. Compaction Degree	%	98	98	-	-	-	99	98	-	-	96	97	-	98	93
	Unit Weights	kg/m³	2330-2437	2211-2311	-	2450-2550	2350-2400	2390-2420	2375-2440	-	2423-2500	2535-2575	2560-2590	2223-2286	2450-2500	2293-2463
Performance parameters	28-day compressive strength	MPa	§ 38-49	26-43	-	45-50	35-40	32-37	47-57	30-45	30-47	46-50	-	31-38	26-37	$$$ 12-29 15-34 18-24
	28-day splitting tensile strength	MPa	§ 3.5-4.4	-	-	-	-	3.5-4.0	4.0-6.8	$$ 3.7-4.6	-	5.5-5.9	3.5-4.3	-	-	-
	Flexural Strength	MPa	-	-	-	-	-	5.3-6.1	4.0-5.0	-	-	-	-	-	-	-

Note: Reference abbreviations; the first letters of the surnames of authors and the year of publication.

§ 14 days results

§§ 90 days results

$$$ Compacted in the laboratory, vibratory hand roller and vibratory roller in the field, respectively.

Table 2.2. *Some mixture design methods and compaction methodologies used in RCC pavement studies (Sengun et al., 2017)*

References	RCC mixture design method	Optimum water amount determination	Specimen Compaction methods
LR2015	Soil Compaction Method	Modified Proctor	Vibrating Hammer
CL2016a	Soil Compaction Method	Vibrating Hammer	Vibrating Hammer
CL2016b	Concrete Consistency Method	Vebe Apparatus	Vibrating Hammer
HCW2011	Concrete Consistency Method	Vebe Apparatus	Vibrating Hammer
AM2017	Soil Compaction Method	Vibrating Hammer	Modified Proctor
YUAT2015	Soil Compaction Method	Vibrating Hammer	Vibrating Hammer
LDRA2017	Soil Compaction Method	Vibrating Hammer	Vibrating Hammer
GMR2017	Concrete Consistency Method	Vebe Apparatus	Vibrating Table
MAT2012	Soil Compaction Method	Vibrating Hammer	Vibrating Hammer
ADS2003	Theoretical Maximum Density Method	Superpave Gyratory Compactor	Superpave Gyratory Compactor (60-75-80-90-100)
ASD2004	Theoretical Maximum Density Method	Superpave Gyratory Compactor	Superpave Gyratory Compactor (50-65-90)
NAPG2011	Soil Compaction Method	Special Equipment	Special Equipment
CHL2017	Soil Compaction Method	Vebe Apparatus	Vibratory Hand Roller and Vibrating Hammer
LCP2013	Concrete Consistency Method	Vibrating Table	Vibratory Steel Drum Roller Vibratory Rubber Tire Roller Vibratory Hand Roller

Note: Reference abbreviations; the first letters of the surnames of authors and the year of publication.

2.2. Fracture Properties of RCC Pavements

The number of studies described in the literature focusing on fracture properties of RCC is limited. While it is clear that studies on determination of fracture parameters are mostly related to metal materials, for conventional concrete, with studies on the use of fibers affecting toughness and fracture parameters most prominent, this field is relatively new with respect to RCCs. Moreover, even the field of conventional concrete has become very difficult for researchers because, unlike steel, concrete is

heterogeneous, making the application of standard procedures for homogeneous materials not useful in concrete, and making result interpretation difficult.

2.2.1. The Application of Fracture Mechanics to Conventional Concrete

Fracture mechanics is the field of mechanics concerned with analyzing the failure of cracked and flawed materials and examining the conditions under which cracks propagate (Anderson, 2017). Cracking is an essential feature of the behavior of concrete applications, with concrete structures normally full of cracks under service loads (Bazant, 2014). Although the first developments of fracture mechanics began with Inglis, (1913) at the beginning of the 20th century, Griffith, (1921) presented a first explanation of the mechanism of brittle fracture using a new energy-based failure criterion. The Liner Elastic Fracture Mechanics (LEFM) concept was later developed by Irwin, (1957) using Westergaard, (1939) equations. Researchers stated that fracture toughness (K_{Ic}), a material parameter used only to describe brittle materials, could be sufficient for defining crack propagation and fracture failure.

In the 1960s, there were some developments related to fracture mechanics of concrete. Kaplan, (1961) adapted application of the LEFM concept to concrete, and while many researchers continued to work on applying LEFM on concrete (Carpinteri, 1982; Cook & Crookham, 1978; Glucklich, 1963; Clyde E Kesler, Naus, & Lott, 1972; Mindess & Nadeau, 1976; Shah & McGarry, 1971; Strange & Bryant, 1979), it seems that classic LEFM should not be applied to normal concrete members because concrete is a heterogeneous material with a fracture process zone (FPZ) in advance of the crack tip, as shown Figure 2.4a.

As shown in Figure 2.4b, many micro failure mechanisms, such as preventing crack propagation of the aggregates at the crack tip, changing the direction of the crack or branching of crack by coinciding with the aggregates, or reducing crack tip sharpness of the cavities, occur inside the FPZ (Akkaya, Bayramov, & Taşdemir, 2003). Therefore, not only do all these effects contribute to energy dissipation in advance of

20

the crack tip, but they also interact with one another, increasing problem complexity (Jimenez Pique, 2002)

(a)

(b)
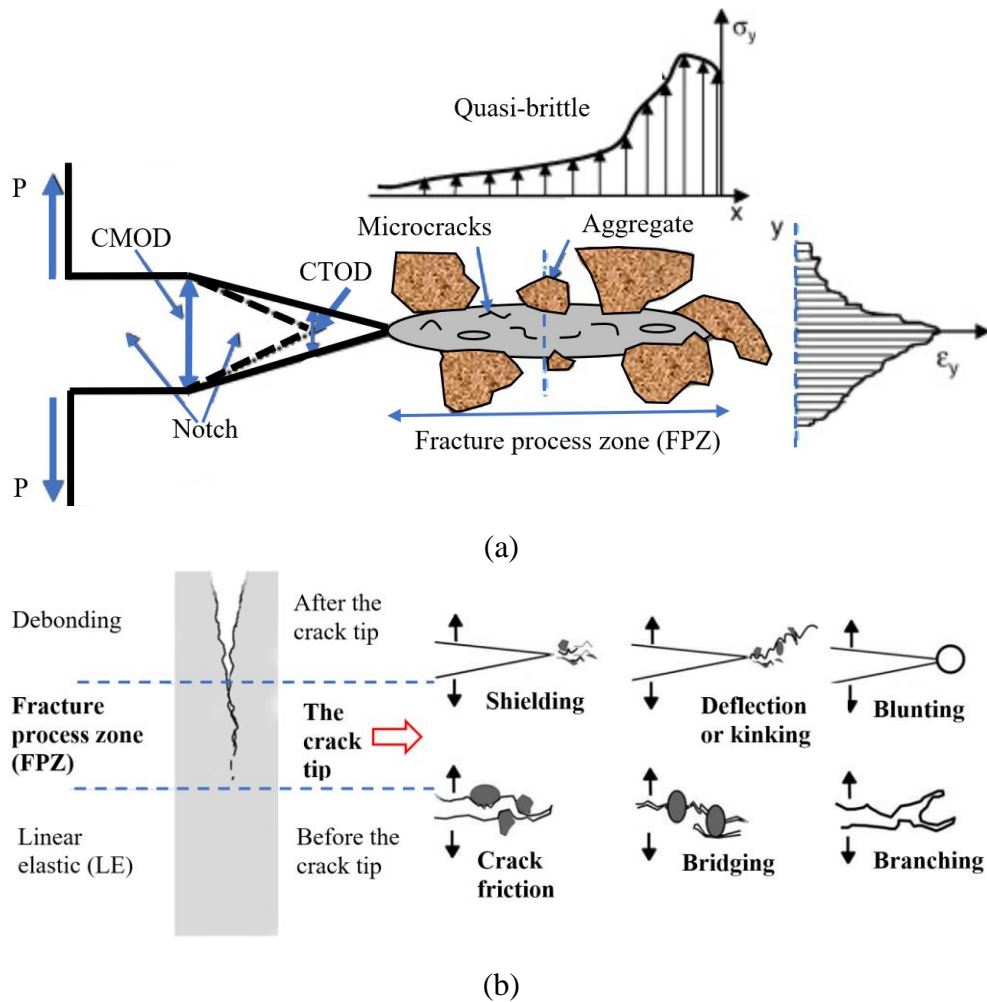
Figure 2.4. a) Concept of FPZ (Kim & Buttlar, 2009), b) Mechanisms of crack propagation for concrete (Akkaya et al., 2003; Jimenez Pique, 2002)

Because of these such mechanisms, since fracture toughness (K_{Ic}) is insufficient for determining fracture properties of semi-brittle materials such as concrete, many different nonlinear fracture models have been developed (Kumar & Barai, 2011). They include:

- Fictitious Crack Model (FCM) (Arne Hillerborg, Modéer, & Petersson, 1976),
- Cohesive Crack Model (CCM) (Barenblatt, 1962; Dugdale, 1960),
- Crack Band Model (CBM) (Bažant & Oh, 1983),
- Two-Parameter Fracture Model (TPFM) (Jenq & Shah, 1985),
- Size Effect Model (SEM) (Bažant, 1984; Bazant & Sun, 1987),
- Effective Crack Model (Nallathambi & Karihaloo, 1986),
- Double-K Fracture Model (Xu & Reinhardt, 1999)
- Double-G Fracture Model (Xu & Zhang, 2008).

The complexity of experimentally determining the fracture parameters of these models has restricted the number of studies found in the literature on fracture mechanics of concrete. A three-point bending test has been applied to a notched beam to determine fracture parameters for three commonly used models (FCM, SEM, TPFM) standardized by RILEM (TC 50-FMC, 1985; TC 89-FMT, 1990). Among these three models, TPFM is particularly advantageous since it does not require the use of different-sized specimens. While two values of K_{Ic} (stress intensity factor or fracture toughness) and $CTOD_c$ (critical crack-tip opening displacement) obtained from this model has been shown to be mostly independent of specimen geometries (Jenq & Shah, 1985), some studies have asserted that the effect of geometry with respect to these parameters is not negligible (Planas & Elices, 1989; Shi, Mirsayar, Mukhopadhyay, & Zollinger, 2018).

 Recent studies on fracture properties of concrete, mostly concentrate on the effect of mixture composition on fracture parameters and fracture energy. Akkaya et al., (2003) investigated how compressive strength, water-to-cement ratio and aggregate concentration can change fracture energy of conventional concrete. The final results of this study revealed that the compressive strength, water-to-binding ratio, maximum aggregate size, concrete age and notch length were the parameters affecting concrete fracture energy. That study observed that the fracture energy of concrete increased with enhance aggregate concentration and maximum aggregate size, while an increase in water-to-cement ratio resulted in decrease in fracture energy.

Because water-to binding ratio and concrete age are directly related to compressive strength the guidelines of the International Federation for Structural Concrete (CEB Bulletin No.189, 1988), compressive strength and maximum aggregate size are taken into consideration in fracture energy prediction. However, Yan, Wu, Zhang, & Yao, (2001) stated that fracture energy would not permanently increase with compressive strength, arguing that the bond strength between matrix and aggregate in high-strength concrete could lead to a smooth fracture surface that absorbs less energy.

A study conducted by C. Tasdemir, M.A. Tasdemir, Grimm, & König, (1995) found that the fracture energy in high strength reinforced concrete was affected by the FPZ. In addition, although there was a significant increase in compressive and splitting tensile strengths in concrete containing silica fume compared to concrete without silica fume, it was observed that fracture energy decreased with increasing compressive strength in high-strength concrete.

Finally, in a current literature review by Khalilpour, BaniAsad, & Dehestani, (2019) related to the fracture energy of concrete and affected parameters, it was stated that all parameters that change the mechanical properties of concrete, such as aggregate size, type, amount, binder ratio, water-to-binder ratio, type of fiber added, type, length, quantity, ambient temperature, etc., can also affect the fracture energy of concrete. A separate examination of these effects indicated that an increase in water-to-binding ratio resulted in a decrease in fracture energy and this was largely related to an increase in porosity at the interface between the cement matrix and the aggregate. It was also seen that an increase in the amount of cement paste might cause a decrease in the fracture energy. In that study, it was also stated that an increase in the maximum aggregate size in concrete both increased the energy required to break the aggregate and enhanced the fracture energy of the concrete because a crack results in a longer path due to crack propagation around the aggregate. The effect of the sample size tested was considered in two ways. The first was the growth in fracture energy due to the longer crack path from increasing the sample size. However, the second was to

decrease fracture energy by increasing notch length resulting from a smaller fracture process zone.

2.2.2. Fracture Properties of RCCs

As it is mentioned at the beginning of the literature review, studies about fracture properties on RCC are quite limited in the literature; the few relevant studies are briefly summarized below.

In a part of a comprehensive study by LaHucik, Dahal, Roesler, & Amirkhanian, (2017) on the determination of mechanical properties of fiber RCCs, fracture properties of RCCs were investigated. The aggregate gradation with 19 mm maximum aggregate size and 280 kg/m^3 cement dosage, was kept constant during the study. A total of twelve different RCC mixtures, one a control mix, were formed using four synthetic fiber types and two steel fiber types with different geometries and volumes. A two-parameter fracture model (TPFM) developed by Jenq & Shah, (1985) was used to determine the RCC fracture properties, but a procedure other than the three-point bending test on notched beam samples proposed by RILEM TC 89-FMT, (1990) was applied. Researchers prepared 15x30 cm cylindrical specimens to apply disk-shaped compact tension (DCT) tests to determine the fracture properties of RCC. In that study, fracture energy (G_F) was determined according to the RILEM TC 50-FMC, (1985) standard procedure, the basis for the fictitious crack model developed by Hillerborg et al., (1976). At the end of the study, fracture parameters of RCC mixtures and conventional concrete (PCC) mixtures were compared, after which, the mixtures were examined with respect to fracture properties such as critical intensity factor (K_{Ic}) and fracture energy (G_F), with RCCs found to produce better results than PCCs. In general, fracture properties of RCC were found to be similar or better than those of PCC. It was also stated by the researchers that RCC fracture performance, especially fracture energy (G_F), improved with increasing fiber content.

In a study conducted by LaHucik & Roesler, (2017), discussed in detail in the previous section, the RCC mixtures with the same binder content and mixture design were

produced both in the field and in the laboratory and their mechanical performances compared. In the last part of the study, the fracture properties of RCC mixtures were discussed, and, as in the previous study, the two-parameter fracture model (TPFM) was used to determine fracture parameters, although they performed a disc-shaped compact tension (DCT) test rather than of a three-point bending test. As a result, similar to density and strength measurements, field results with respect to fracture properties were lower than laboratory results. Since fracture properties are considered to be good indicators of flexural capacity, it was asserted that the lower fracture properties obtained under field conditions could lead to lower structural capacity of RCC pavement than the predicted capacity based on laboratory experiments.

In another study by Ferrebee et al., (2014) related to fracture properties of RCC, the effects of both normal and recycled aggregates on fracture parameters, were examined. In that study, a constant cement amount (267 kg/m^3) was used and optimum water ratios were obtained, between 5.8% and 6.4% for normal and recycled aggregate gradations, respectively, and the RILEM TC 89-FMT, (1990) procedure based on a two-parameter fracture model (TPFM) was used to determine fracture properties. Fracture energy was also determined according to RILEM TC 50-FMC, (1985). At the end of the study, normal and recycled aggregate RCC mixtures exhibited statistically similar results, and when the conventional concrete (PCC) fracture properties obtained from in previous studies were compared for the same aggregate ratios, it was found that RCCs gave better results than PCC in terms of fracture energy (G_F) and critical stress intensity factor (K_{Ic}).

2.2.3. Literature Review Discussion- Part II

Understanding how and under what conditions failure occurs in a cracked material forms the basis of fracture mechanics. The first studies on fracture mechanics were developed on brittle materials such as glass followed by consideration of ductile materials. This concept, used primarily in defense industry designs after the Second World War, came under consideration for in concrete designs after the 1960s. While

many researchers have studied the applicability of a LEFM to concrete, it has been found that LEFM is not applicable since concrete is a semi-brittle and heterogeneous material. Somewhat later, several non-linear fracture mechanics developed for cement binding materials have been applied to determination of the fracture properties of concrete. However, despite the development of many experimental test methods and numerical solutions, some inconsistencies regarding the parameters affecting the fracture parameters of concrete remain in previous research findings. It is unclear to what extent the effect of currently-used laboratory sample size on finding fracture properties changes the results. There are also questions about the extent to which concrete mix designs may affect concrete fracture properties. In any event, examination of the limited number of literature studies investigating RCC fracture behavior produced the following summarized findings:

- It is seen that the non-linear TPFM developed by Jenq & Shah, (1985) and advanced by RILEM TC 89-FMT, (1990) as a standard procedure is preferred for determination of fracture parameters.

- The RILEM TC 50-FMC, (1985) standard procedure that forms the basis of the fictitious fracture model developed by Hillerborg et al. (1976) is preferred for determining the fracture energy (G_F) of RCC samples.

- It has been reported that RCC mixtures exhibit similar or better fracture behavior than conventional concrete mixtures, but since there are very few studies on this subject, it is not possible to make firm generalizations.

- In those studies, since the RCCs were produced by using vibratory hammers under laboratory conditions, it is not known to what extent the RCC samples reflect field conditions.

- The effect of compaction ratio on fracture properties was not considered in the studies found.

Above all, many researchers have indicated that the fracture energy found by RILEM TC 50-FMT, (1985) procedure is strongly affected by sample size. In addition, according to this procedure the deflection at the midpoint of the beam should be referenced in determining fracture energy, although some studies have begun referring to the crack mouth opening displacement (CMOD) to obtain more accurate results. However, in 2003, a standard for determining fracture energy of concrete was developed by the Japan Concrete Institute (JCI-S-001-2003, 2003). According to this standard, fracture energy can be determined using a CMOD-controlled test on notched-beam samples of standard dimensions, even though it has been observed in prior studies that this standard has not been used to determine fracture energy of RCCs. One aim of the present study is to determine fracture energies of RCC mixtures using the more advanced JCI-S-001-2003, (2003) procedure rather than the traditional RILEM TC 50-FMC, (1985) procedure.

2.3. Fatigue Behavior of RCC Pavements

Until recently there have been only a few research studies directly investigating the fatigue behavior of RCC, possibly because fatigue tests are quite time-consuming, complex, and expensive. Another possible explanation is that some researchers have used traditional concrete fatigue behavior in pavement design believing that RCCs have mechanical properties similar to those of traditional concrete. The majority of fatigue studies on RCC have been carried out by highway administrations and concrete pavement associations in the USA, and many have attempted to explain the fatigue behavior of conventional concrete. Before proceeding to examine fatigue studies on RCC, it will be useful to discuss conventional concrete fatigue behavior.

2.3.1. Background to Fatigue Failure

As known, structures or materials exposed to repetitive loads may be subject to permanent damage or sudden failure, revealed by the development of cracks, and such a brittle failure type is called fatigue failure, accounting for at least half of all mechanical fractures, many unexpected. The effects of fatigue have been widely

studied for aircraft, ships, bridges, road pavements, automotive structures, frames, cranes, machine parts, turbines, reactors, channel and dam shutters, and components forming offshore platforms. Another dangerous aspect of fatigue failure is brittle fracture that can occur regardless of a material's ductility.

Studies on fatigue behavior of the materials began with the industrial revolution, with fatigue failure first introduced into the literature during the early years of the 19th century because of a catastrophic failure in railway axles caused by repeated loads. The first systematic study of fatigue effect was reported by the German scientist Wöhler, (1860). Bauschinger, (1886) showed that the stress-strain behavior obtained under a static tensile or compression test might be quite different from the stress-strain behavior obtained under repeated loads. In the period up to the 1950s, at which time significant advancements were made in fracture mechanics, the studies were mostly focused on using fracture mechanics to explain fatigue-related failures (Coffin, 1954; Paris, Gomez, & Anderson, 1961). On the other hand, developments on understanding fatigue behavior were advanced to a significantly different stage with the introduction of closed-loop servo-hydraulic loading systems.

Figure 2.5 shows a typical sinusoidal cyclic fatigue load like those frequently used in fatigue testing. In this typical graph, the mean stress is half the sum of the maximum (σ_{max}) and minimum stresses (σ_{min}), the amplitude stress (σ_a) is the difference between the maximum stress (σ_{max}) and the mean stress (σ_m), and the stress range ($\Delta\sigma$) is the difference between maximum and minimum stress differences. In this graph, strain (ε), moment (M), torque (T), or stress intensity factor (K_{Ic}) can be considered rather than stress, depending on fatigue design and test specimens.
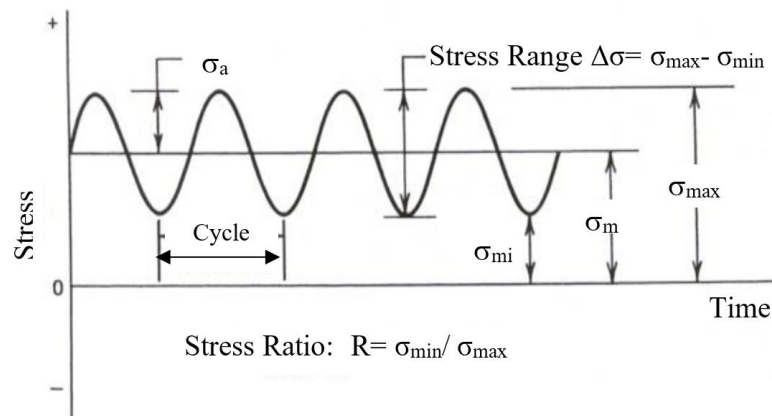
Figure 2.5. Typical sinusoidal constant amplitude fatigue load

Fatigue tests are performed by applying cyclic loads to materials subjected to axial compression or tension, bending, torsion, or simultaneous multiple effects that are representative of real-life loading conditions. On the other hand, for materials such as concrete, where a direct tensile test may be difficult to apply, flexural fatigue tests are often preferred, and fatigue behavior under three-point or four-point bending tests is examined for notched or normal beam specimens. In some special cases where fatigue behavior requires a direct tension fatigue test, fatigue tests can be carried out on compact square or disc-shaped tension samples.

The most commonly-used tool for fatigue analysis and fatigue life estimation for concrete is the stress life (S-N) curve, also known as a Wöhler curve, obtained by plotting the number of load repetitions/cycles to failure (N) corresponding to stress ratios (S) on a logarithmic scale (Figure 2.6). In this approach, the stress ratio (S) is expressed in terms of the ratio of the maximum stress applied to the ultimate strength of the material obtained from static tests and fatigue tests that performed with stress or load control. Basquin (1910) first described the empirical formulation between cyclic loads or stresses applied to materials and the number of load repetitions to failure.

Stress range (S)

Static Failure

Low cycle fatigue (LCF)
low fatigue life, high loading
high plastic deformation

$1 - 10^3$

High cycle fatigue (HCF)
high fatigue life, low loading

$10^3 - 10^7$

Fatigue limit or endurance limit

Fatigue limit does not exit

Log-Log plot

Number of cycles to failure (N)
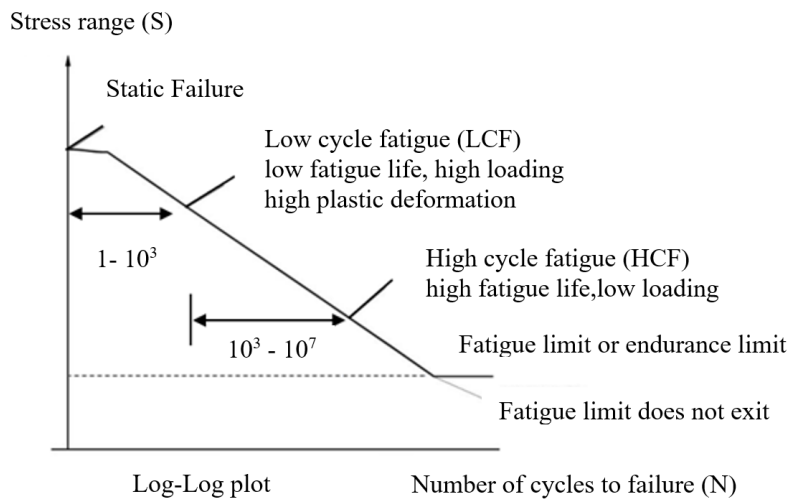
Figure 2.6. Typical S-N curve (R.I., Stephens, Fatemi, R.R., Stephens, & Fuchs, 2000)

Another method uses a Strain-life (Ɛ-N) approach to life estimation for analysis of strain-controlled fatigue tests, with plastic deformations contributing a significant part of the fatigue process. In this method, since fatigue cracks generally arise from areas of plastic strains in certain regions, fatigue life estimates are made taking into consideration regions where such plastic strains are concentrated, so this method is also called the local strain approach method. It is mostly used in fatigue analysis of notched elements where local plastic strains are concentrated. Strain-controlled tests better characterize the fatigue behavior of materials, particularly under low cycle fatigue (LCF) and/or notched samples. Material fatigue may take a very long time, especially in fatigue tests with more than 10^6 load repetition, due to the small size of plastic strains, so high-frequency load/stress-controlled fatigue tests are usually preferred. For this reason, fatigue tests using the strain life Ɛ-N approach are generally known as low-cycle fatigue (LCF) tests. A Ɛ-N approach based on strain-controlled tests are usually preferred over a conventional S-N approach in determining fatigue properties of materials, compositions, or structures, especially in aircraft, automotive, electronics, information, and manufacturing industries where high-precision production in which plastic deformation vital to the design is needed.

30

2.3.2. Fatigue Behavior of Conventional Concrete

Since it is known that the majority of mechanical fractures occur due to fatigue effects, many studies can be found in the literature on the fatigue behavior of metallic materials. Studies on fatigue of concrete, however, began earlier, with concrete fatigue studies first performed by Ornum, (1903). In those studies, cement mortars and concrete cubes were subjected to compression fatigue loads and fatigue strength due to cyclic compression loads was investigated. The result was that cement mortar and concrete displayed similar compressive fatigue strength, approximately 55% of their ultimate static final strength. The fatigue strength of concrete was investigated for the first time in these studies and it was determined that concrete could fail due to cycle loads.

The first research on the flexural fatigue strength of concrete was made by Clemmer, (1922) in the Illinois Department of Transportation to investigate pavement corner breaking, with the result that flexural fatigue strength was found to be 53% of static ultimate flexural strength. Extensive studies on fatigue behavior of traditional plain concrete were carried out in the period up to 1975. These studies, that made significant contributions to the literature, were conducted by researchers such as Crepps, (1923), Hatt, (1925), Williams, (1943), Kesler, (1953), Murdock & Kesler, (1958), McCall, (1958), Neal & Kesler, (1964), Glucklich, (1965) and Antrim, (1967). These studies created scientific knowledge on the fatigue behavior of concrete and shed significant light on the work to be carried out during the following years.

The stress-life (S-N) approach, most commonly used in concrete fatigue tests, is particularly suitable for rigid materials such as concrete that do not exhibit large deformations under stress. The S-N curve of concrete has also been used as a design criterion in the design of concrete pavements. In 1974 a design S-N fatigue curve was used by the Portland Cement Association (PCA) in the USA for the first time, using a S-N fatigue curve created by combining fatigue curves obtained for conventional concrete samples from previous studies (Ballinger, 1971; Kesler, 1970). Such use of

the S-N fatigue curve (1974) in the PCA method yielded some unrealistic results, leading to a minor modification of the high-cycle fatigue section in 1984, and this modified S-N curve (Packard, 1984) is currently used by PCA for testing concrete pavements.

Transverse fatigue cracks are also considered as a performance criterion in mechanistic empirical pavement design (MEPDG), that has recently found use in developed countries, but most especially in the USA and Canada (Öztürk, Tan, Şengün, & Yaman, 2018). To determine the appropriate design concrete thickness, the design guide uses the number of allowable load repetitions based on a given stress level in conjunction with a fatigue-cracking performance curve to predict the level of slab cracking in the field. This is followed by a trial-and-error approach using various input combinations with a trial thickness until the desired fatigue damage (<1.0) or failure criterion (e.g., 20% slab cracking) is met (Bordelon, Roesler, & Hiller, 2009).

2.3.3. Factors Influencing Concrete Fatigue Behavior

There are many parameters that can affect the concrete fatigue behavior, and these parameters generally depend on mixture properties, loading conditions, and environmental factors.

All parameters influencing both fresh and hardened properties of concrete can also affect the concrete fatigue behavior. These include the binder amount and properties, aggregate properties, water-binder ratio, chemical and mineral additives, moisture content, sample age, and curing conditions. Studies related to the effect of concrete mixture parameters on concrete fatigue behavior are briefly summarized in the following discussion.

In a study about the effect of concrete age on fatigue behavior, the researchers investigated the fatigue strength of 28-day, 4-month, and 6-month concrete samples, all with the same content. At the end of the study, the fatigue strengths of 28-day, 4-month, and 6-month concrete specimens were found to be 40-60, 50-55 and 54-55%, respectively. The researchers also stated that it was not clear that the fatigue life of the

concrete increased with age, although they found a significant decrease in variation with age. Also, since fatigue tests generally are continued for a considerable period of time, researchers have recommended that the test should be performed on concrete samples at long-term ages to minimize a concrete gain in strength during the test (Yimprasert & McCullough, 1973).

In another study investigating the effects of different concrete strengths on concrete fatigue behavior, S-N curves were formed by applying compressive fatigue tests on concrete specimens with four different strengths, 26, 52, 84, and 103 MPa. At the end of the study, it was found that fatigue life decreased with an increase in compressive strength, and the unit deformation of high-strength concrete was smaller than that of low-strength concrete, although the unit deformation rate was higher (J.-K. Kim & Kim, 1996).

When studies in the literature have described the effects on fatigue behavior of mixture parameters such as cement dosage, water content, aggregate type, and gradation, all of which significantly affect the static flexural strength of concrete, two different approaches can generally be observed. Some studies state that these parameters do not affect the fatigue behavior of the concrete as much as the static flexural strength, while others claim that they have as much an effect on fatigue behavior as static flexural strength. The European Committee for Concrete (CEB) stated that the effect of these parameters on fatigue strength was small and had less effect on fatigue strength than its effect on static flexural strength (CEB Bultenin No.189, 1988). Conversely, the American Concrete Institute (ACI) stated that many variables affecting the static strength, such as cement ratio, water-cement content, curing methods, test age, air quantity and aggregate type, would have influenced fatigue strength to the same degree (ACI 215R-92, 2002).

There have been a limited number of studies investigating the effects of mineral additives on fatigue behavior of concrete. In one study in which the effect of fly ash and ground granulated blast furnace slag on the fatigue behavior of concrete was

investigated, it was found that use of fly ash and ground granulated blast furnace slag had a positive effect on the fatigue behavior of the concrete (Guo, Carpinteri, Spagnoli, & Sun, 2010), while in some studies it is argued that mineral additives may shorten of fatigue life due to an increase in concrete compressive strength. There are therefore many doubts and disagreements found in the literature about the effects of mineral admixtures on the fatigue behavior of concrete.

Fatigue tests include different loading conditions. In view of the fact that load-controlled fatigue tests on concrete are preferred, investigations of the effects of maximum and minimum stresses, stress range, mean stress, the waveform types, loading frequency and failure probability are mostly found in the literature. As predicted, fatigue behavior is affected by stress range and the mean stress applied to the specimen as well as the maximum and minimum stress during a fatigue test. The fatigue life of a specimen is reduced under high maximum stress and high stress ratio, and the most dangerous fatigue-life situation is the fully reversed condition in which $\sigma_{min}=-\sigma_{max}$.

2.3.4. Fatigue Behavior of RCC

The number of studies in the literature on the determination of fatigue behavior of RCC is very limited, and the main reasons for this is that fatigue tests are quite time-consuming, complex and costly. Another reason for the few studies of RCC fatigue behavior found in the literature is that some researchers have used traditional concrete fatigue behavior in pavement designs because RCC is thought to have mechanical properties similar to those of traditional concrete. Although the majority of RCC fatigue studies have been carried out by highway administrations and concrete pavement associations in the USA, and relatively few academic studies on RCC fatigue behavior have been published, some of the significant studies on RCC fatigue behavior are summarized below.

2.3.4.1. Concrete Technology Laboratory (CTL)

One of the most significant studies on RCC fatigue behavior was performed by CTL (Tayabji & Okamoto, 1987), and the RCC fatigue curve obtained from this study is still used as a reference in fatigue design of RCC pavements. In this study, whose aim was to determine the engineering properties of RCC, four different RCC mixes with binder amounts ranging from 170 to 190 kg/m^3 were cast into test sections 4.0 m wide, 3.6 m long, and 20 cm thick, then compacted with a 10-ton vibratory roller under actual field conditions. The mechanical properties of the RCCs were determined by compressive, flexural, splitting tensile, elasticity and fatigue tests using the cores taken from the field and the beams sawed from the field. In addition, cylindrical and beam specimens were produced from the same mixtures in the laboratory for comparison with field results. When the fatigue-test parts of this study were taken into consideration, 15x15x75 cm^3 beam specimens sawed from the field were maintained under curing conditions for about seven months, after which three-point flexural fatigue testing was performed. The cycling load was applied at stress ratios (applied maximum stress/ultimate static flexural strength) ranging from 0.50 to 0.95. The loading frequency was selected as 10 Hz and the minimum load was chosen to be 10% of the maximum load to eliminate an impact effect on the sample during the fatigue test. Fatigue values and a S-N curve for RCC mixtures obtained from 23 beam samples are shown in Figure 2.7. At the end of this study, researchers stated that RCC and conventional concrete had similar mechanical properties and RCCs could be considered the same as traditional concrete in pavement design. They also indicated that fatigue design procedures used for concrete pavements could be used in RCC pavement design by taking into account the RCC fatigue curve.
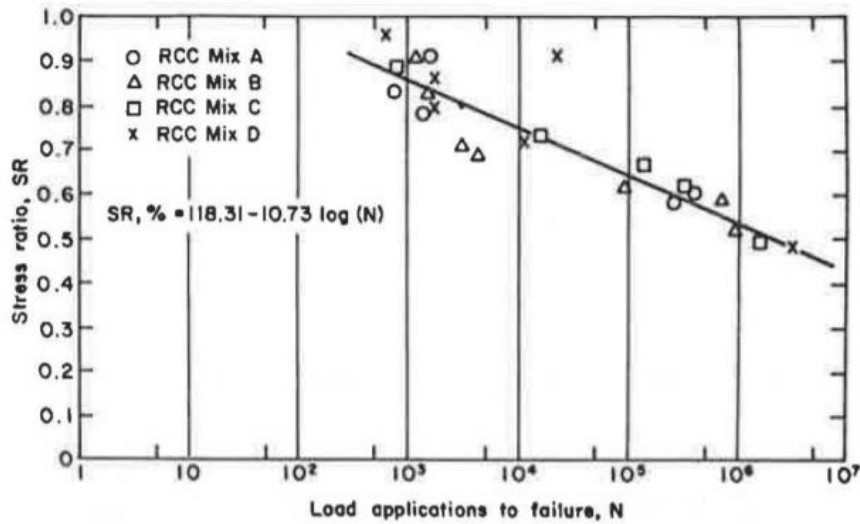
Figure 2.7. S-N fatigue curve for RCC mixtures (Tayabji & Okamoto, 1987).

2.3.4.2. Canada Cement Association (SEM-2002013, 2003)

Another significant studies aimed at determining the mechanical properties of RCCs was performed by the Canadian Cement Association in 2003 (SEM-2002013, 2003). In this study, four different RCC mixtures were formed with different aggregate type (granite and limestone), binder ratio (250 and 300 kg/m^3) and maximum aggregate size (20 mm and 14 mm), with a conventional concrete pavement mixture also prepared for comparison. The water content of the mixtures varied between 4-4.5%. In the fatigue test section of the study, four-point flexural fatigue tests were performed on a total of 37 beams of 10x10x40cm^3 dimensions fabricated from five different mixtures produced in the laboratory. The loading frequency was chosen as 15 Hz and the stress ratio varied between 0.5 and 0.8. The fatigue test was terminated either when a specimen failed or the number of repetitions had reached 1,000,000. A static bending test was then performed and the residual strength determined on samples that had not failed under 1 million repetitive loads. The specimen resilience after fatigue was also determined as the proportion of residual strength and the final static flexural strength.

36

At the end of the study, the fatigue strength of RCC mixtures was found to be 60% of the ultimate static flexural strength after 1 million repetitive loads. For conventional concrete, on the other hand pavement, this value is specified as about 50%. The results of this study showed that RCCs had better fatigue resistance than conventional concrete, making it understood that the use of a conventional concrete fatigue curve in RCC pavement designs can be quite conservative. The design or software guidelines obtained from the conventional concrete fatigue design curves or the Tayabji and Okamoto (1987) RCC design fatigue recommendations for use in the design of RCC pavement made prior to this time were to consider RCC fatigue strengths to lie between 40-50% of the ultimate flexural strength, although in this study that value was about 60% for RCC.

A simple example was also given to show the effect of the difference in fatigue behavior between RCC and conventional concrete in pavement design. In this example, thickness design was chosen roughly for three different fatigue strengths of 40%, 50%, and 60% of the ultimate flexural strength, with resulting slab thicknesses of 185 mm, 160 mm and 145 mm, respectively. As expected for these values, variations in fatigue strength resulted in a significant change in pavement thickness. It should be kept in mind that while this example is quite simple and rough and no other parameters such as load transfer coefficient, resilient modulus of subgrade/subbase/base, curling, environmental conditions, etc. were taken into account, it is clear that fatigue behavior is an effective parameter in RCC pavement design.

It was also observed in that study that maximum aggregate size had an effect on fatigue strength, with RCC mixtures with a maximum aggregate size of 20 mm achieving better fatigue strength than mixtures with a maximum aggregate size of 14 mm. Nevertheless, this effect was not observed to result from static tensile strength.

2.3.4.3. Concrete Technology Laboratory (CTL)-(Okamoto, 2008)

In another study by CTL in 2008, fatigue tests were performed on 37 specimens of size $10x10x40cm^3$ and 44 specimens of size $15x15x75cm^3$ from three different RCC mixtures. In this study, the effect of different aggregate types (limestone, dolomite, etc.) and different beam sample sizes on fatigue behavior were investigated. It was stated that both different aggregate types and different beam sizes gave results-close to a fatigue S-N curve.

2.3.4.4. American Concrete Pavement Association (ACPA) (Roden, 2013)

In 2013, an ACPA study by Roden (2013) was conducted to develop a fatigue model for the design of RCC pavements. For the development of this new fatigue model, reliability levels were considered by using existing RCC fatigue data from the literature (Okamoto, 2008; SEM-202013, 2003; Tayabji & Okamoto, 1987). First, all fatigue data in published studies belonging to different RCC mixtures and different beam sizes (Tayabji & Okamoto, 1987; (SEM-202013, 2003; Okamoto, 2008) were collected and multiplied by a size factor to allow conversion a 15cmx15cm beam size. After the conversion, 141 RCC fatigue data were collected from the three studies and the related figure is shown in Figure 2.8.

In the second phase of the study, the new ACPA-RCC fatigue model and the existing fatigue models were compared and the effect of the pavement thickness was interpreted. The two developed models were first compared to the previously-used fatigue design curve of CTL (Tayabji & Okamoto, 1987). The fatigue models developed for fatigue loads higher than the 40% stress ratio were less conservative, but were still more conservative than the ratio below.

The figure shows a scatter plot with x-axis "Load Applications to Failure, N" (logarithmic scale from 1.E+00 to 1.E+08) and y-axis "Stress Ratio, SR (%)" (from 0% to 100%). The equation shown is:

$$SR = 1.063 - 0.038\ln(N)$$
$$R^2 = 0.6659$$
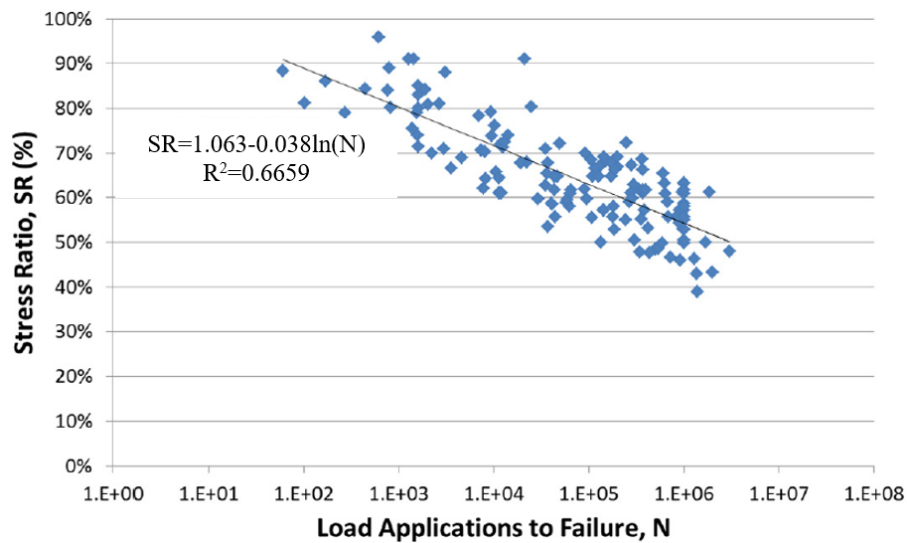
Figure 2.8. A total of 141 RCC fatigue data obtained from the literature for the new fatigue model to be developed by ACPA (Roden, 2013)

Since conventional concrete (PCC) and RCC have generally similar mechanical properties, in some design software or design guides, conventional PCC fatigue models rather than the RCC fatigue model are still used to calculate pavement thickness. Therefore, in the study the fatigue model developed by ACPA for RCC pavement was compared with the PCC fatigue model used for RCC pavement design in some software programs. Since the result of the comparison was a report that these two models exhibited quite different behaviors using conventional PCC fatigue strength in RCC pavement design was not recommended. However, there are some limitations and assumptions in RCC fatigue models developed by ACPA. Above all, RCC fatigue data developed for these models were obtained from previous studies using different mixture contents, different compression methodologies, and different sample sizes. Also, in studies where fatigue data were obtained, there was no standard for RCC specimen production under laboratory conditions.

2.3.4.5. Other studies on RCC fatigue behavior

Sun, et al., (1998) investigated the effects of fly ash on fatigue behavior of RCCs. For this purpose, five different mixes were prepared and a constant aggregate gradation

39

with maximum aggregate size of 20 mm was used. The binding amount of the four mixtures formed from 0%, 15%, 30%, and 45% of fly ash varied between 300-345 kg/cm^3 and the final mixture was prepared as conventional portland cement concrete (PCC). In that study, the beam specimen sizes were selected as $10x10x40$ cm^3. The four-point flexural fatigue test was applied with a stress ratio ranging between 0.55 and 0.85 and the loading frequency was selected as 5-8 Hz. The fatigue test was continued until failure occurred. The S-N curve was drawn for each mixture and regression analysis was performed, and a fatigue equation that included the stress ratio (S), the number of load repetitions to faliure (N) and the fly-ash ratio, was proposed. An increase in the slopes of the S-N curves was observed with increased amount of fly ash in the mixtures. In other words, under constant fatigue load there was a slight increase in the degree of fatigue damage with an increase in fly ash content. On the other hand, fatigue strength was enhanced slightly with an increase in the amount of fly ash. It was also stated that all RCC mixtures yielded better fatigue strength than normal PCC concrete.

The main purpose of the study by Graeff, Pilakoutas, Neocleous, & Peres, (2012) was to investigate how steel fibers obtained from used tires could contribute to the fatigue strength of concrete pavements. Two different mixtures were prepared to represent the concrete road, the first a conventional concrete pavement mixture, and the second was the RCC mixture. Recycled steel fibers were added to the concrete at 0%, 2%, and 6% of the concrete weight. An RCC mixture was also prepared with industrial steel fiber for comparison. The same aggregate gradation was used in both mixtures, although while river gravel was selected for the PCC mixture, basalt gravel was preferred for the RCC mixture. RCC and PCC mixtures had binders amount of 380 and 300 kg/m^3 respectively, while 20% of the binders were formed of fly ash in both mixtures. In the four-point flexural fatigue test, three beam ($15x15x55$ cm^3) specimens were placed on top of one another and fatigue tests performed by applying with three different stress ratios: 0.5, 0.7, and 0.9, at a 15 Hz loading frequency. The minimum fatigue load was selected as 10% of the maximum fatigue load applied. At least three specimens were

used for each stress ratio, and the fatigue test was continued either until failure occurred or the number of load repetitions reached 2 million. At the end of the study, it was reported that recycled fibers in conventional concrete improved fatigue performance with the best performance achieved by a fiber mixture of 2% by weight. On the other hand, the traditional RCC mixture yielded better results than RCC mixtures with fibers under fatigue load values above the 0.7 stress ratio. According to the researchers, this was because the repeated high fatigue loading could lead to better compaction of RCC mixtures and better aggregate interlock, otherwise the addition of fibers could result in pore formation in mixtures and also cause a slight decrease in aggregate interlock. On the other hand, all fiber reinforcement RCC mixtures exhibited better fatigue resistance under low fatigue loading, possibly due to better crack control. In the last part of the study, the design of road pavement with conventional concrete and RCC with recycled fiber was compared with a simple case in which only the fatigue effect was considered. As a result of this comparison, it was stated that the design thickness could decrease by up to 26% with an increase in fatigue performance of RCC. In addition, the researchers stated that, for fatigue-related performance of road pavements, while beam samples were used in the literature, the roads normally behaved as plates. They emphasized that the fatigue performance of the beams actually reflected field conditions at a lower level because the plates would be about 30% stiffer than the beams.

The primary purpose of the study by Modarres & Hosseini, (2014) was to determine the mechanical performance of 12 different RCC mix combinations using normal and reclaimed asphalt pavement aggregate (RAP) with rice husk ash (RHA) ranging from 3% to 5% of cement amount in the RCC. A number of tests were performed to determine the mechanical performance, and a fatigue test was performed. In the study, a three-point bending flexural fatigue test was applied at a frequency of 1.0 Hz. Three fatigue samples were tested for three different stress rates: 0.65, 0.75 and 0.85, and a total of nine beam samples ($5x5x30$ cm^3) were used. However, it should be kept in mind that the number of these samples is quite low for achieving fatigue behavior.

When the S-N equations were examined, it could be seen that the increase of RHA content in the mixtures caused an increase in the slopes of the S-N curves. Similarly, the slopes of the S-N curves for RAP-containing mixtures were also significantly increased compared to those from conventional RCC mixtures. A remarkable aspect of that study was investigation of the relationship between fatigue behavior and the energy absorption capacity of the samples, leading to the following equation relating the S-N slope (SV) to the energy absorption capacity (E_a) of RCC.

$$E_a = -120367 \, SV - 287.6 \qquad R^2 = 0.668 \qquad (2.1)$$

As a result, researchers from that study stated that the fatigue life of RCC mixtures containing RAP materials was lower than conventional RCC mixtures, but RCC mixtures containing 3% RHA and the traditional RCC mixture gave close results.

2.3.5. Literature Review Discussion- Part III

Permanent and progressive damage or instantaneous and brittle fracture can be observed in the internal structures of materials, components, or structures exposed to repeated loads, even if these loads are significantly less than their static strength. This fatigue effect is mostly seen in designs in aircraft, automotive, and manufacturing industries, and it also appears in the design of many bridges, coastal structures, or road pavement related to civil engineering. The literature study of fatigue behavior of metallic materials is quite voluminous because fatigue effects are responsible for many of the failures in mechanical structures. On the other hand, since the fatigue effect is often not addressed in traditional concrete designs, relatively fewer studies on this topic are found in the literature. Another reason for this lack is that determination of the fatigue behavior of the concrete is not as easy as determining static strengths; the process is very complex, time-consuming, and costly.

With respect to the very limited number of fatigue studies related to RCC, it could be seen that the studies were mostly focused on the development of fatigue design models used in road pavement design in the USA. In fact, there are generally two different threads in the guidelines or software tools for RCC pavement design. The first is the

use of traditional concrete S-N fatigue models in fatigue design of RCC pavement, acknowledging that RCC acts much like a conventional concrete pavement. The second is distinguishing RCC from the traditional concrete and determining the fatigue behavior of the RCC. Fatigue behavior studies on RCC have mostly been performed by those with a second opinion aimed at developing new RCC fatigue models that differ from those of conventional concrete, and RCC fatigue studies in the literature generally have supported this second opinion. With respect to the limited number of RCC fatigue behavior found in the literature, the following findings can be summarized.

- It has been reported that RCC exhibited better fatigue performance than conventional concrete, with fatigue strength of the RCC varing between about 55% and 60% of the ultimate static strength.

- In all studies except Tayabji & Okamoto, (1987), RCC fatigue tests were performed on the beam specimens produced in the laboratory, but it was seen that no standard compaction procedure was applied in most of them. However, the ratio of compaction in RCC specimens is known to affect mechanical performance significantly.

- One of the most comprehensive studies on the fatigue behavior of RCC was carried out by Tayabji & Okamoto, (1987). In four different RCC mixtures, river gravel was used with a binder ratio ranging from 170 to 190 kg/m^3. A total of 23 beam samples were cut from RCC pavements compacted by 10-ton vibratory rollers in the field and subjected to fatigue testing after seven months and the S-N curve obtained from the study compared with conventional concrete S-N curves. From this study, researchers stated that RCC and conventional concrete had similar mechanical properties with respect to compressive, flexural strength, and elastic modulus, and RCCs pavement design could be performed similarly to that of traditional concrete.

- RCC beams were subjected to fatigue loads between 50% and 90% of the ultimate static strength and fatigue testing was mostly completed using 2 million load repetitions, at loading frequencies generally selected to lie between 10 and 15 Hz.

CHAPTER 3

EXPERIMENTAL STUDY

In this thesis, the experimental program was conducted in three phases. In the first phase, various laboratory compaction methodologies were applied to different RCC mixtures and relationships between strength, density, and compactability were examined, and a compaction methodology using a double drum vibratory hand roller (DDVHR) was developed for simulating field compaction procedures in the laboratory. In the second phase, the effects of RCC mixture parameters (binder amount, aggregate gradation) on RCC mechanical properties and fracture parameters were observed for different RCC mixtures produced by the DDVHR compaction methodology developed in the previous phase. Finally, in the third phase, for the three RCC mixes of different strength performance obtained in the previous phase, flexural fatigue performance was determined in terms of S-N curves. In this chapter, the materials and experimental methods used in this three-phase study is described.

3.1. Phase I: Effect of Laboratory Compaction Methodologies on the Properties of RCC

Since different compaction methods have been used to produce RCC specimens described in the literature, but there is still no fully efficient method that can be used in laboratories to represent field compaction procedures (Mehta and Monteiro, 2006), the aim of the first phase was to develop an appropriate compaction methodology and ensure an optimization between strength, density and compactability in simulating the RCCs field compaction process under laboratory conditions. For this purpose, RCC mixtures were prepared with different cement dosages, aggregate sizes, and water amounts, the three main factors affecting RCC properties (Table 3.1). A total of twenty RCC mixtures were prepared and compacted by four different laboratory compaction

methods: modified proctor, (ASTM D1557, 2012), vibrating hammer, (ASTM C1435, 2014), vibrating table (ASTM C1176, 2013), and Superpave gyratory compactor, SGC, (ASTM C1800, 2016). 150 mm diameter cylindrical specimens were prepared using these compaction methods for each mixture, and concrete fresh densities, 28-day compressive and splitting tensile strengths, and porosity values were determined from these specimens. A pilot RCC road section was then prepared in the laboratory using DDVHR to represent field compaction conditions for the selected mixtures and values were found for concrete densities, 28-day compressive and splitting tensile strengths, porosity values, and shrinkage.

Table 3.1. *RCC mixtures and compaction methods used in this phase*

| Mix ID | Mixture Proportions | | | Compaction Methods |
| | Cement | Aggregate | Water | |
	Amount (kg/m^3)	D_{max} (mm)	Ratio by weight	
1	200	12		Modified Proctor (ASTM D1557)
2	200	19	%3, %4,	Vibrating Hammer (ASTM C1435)
3	400	12	%5, %6,	Vibrating Table (ASTM C1176)
4	400	19	%7	Superpave Gyratory Compactor (SGC)*

*SGC could not be used in some water ratios.

Material selection and mixture design, compaction methods, test procedures, and the results related to the purpose of the thesis plan are presented below under separate subheadings.

3.1.1. Material Selection and Mixture Design

In all RCC mixtures, CEM I 42.5 R type ordinary portland cement produced in accordance with the TS EN 197-1 and crushed limestone aggregates were used. In the second and third phases of the experimental study, fly ash and silica fume were also used to produce high-performance RCC mixtures. The fly ash obtained from the

Sugözü Thermal Power Plant is designated as Class F according to ASTM C618-19, (2019), and the silica fume was obtained from Antalya Etibank Electrometallurgy Incorporation. Chemical composition of the cementitious materials is given in Table 3.2. The specific gravities of the cement, fly ash, and silica fume used in the study were determined as 3.11, 2.61 and 2.20, respectively, and the Blaine specific surface area of cement and fly ash were determined as 3341 and 2900 cm^2/g, respectively.

Table 3.2. *Chemical composition of cementitious materials used in the study*

Chemical Composition	CEM I 42.5 R Portland Cement	Class F Fly Ash (Sugözü Thermal Power Plant)	Silica Fume (Antalya Etibank Electrometallurgy Inc.)
CaO %	63.7	1.64	0.71
SiO$_2$ %	18.5	56.22	91.00
Al$_2$O$_3$ %	4.6	25.34	0.58
Fe$_2$O$_3$ %	3.1	7.65	0.24
MgO %	1.62	1.80	0.33
SO$_3$ %	3.05	0.32	1.06
K$_2$O %	0.91	1.88	-
Na$_2$O %	0.45	1.13	-
Loss of Ignition %	4.37	2.1	1.84

The physical properties of the aggregates as determined by the related ASTM standards (ASTM C125-19, 2019; ASTM C127-15, 2015; ASTM C128-15, 2015) are presented in Table 3.3.

The aggregate grain size distribution (ASTM C136M-14, 2014; ASTM C33M-18, 2018) for three different aggregate sizes (0-5 mm, 5-12 mm, 12-19 mm) used in the study is given in Figure 3.1.

Table 3.3. *Basic physical properties of fine and coarse aggregates.*

Physical Properties	Fine Aggregate FA (0-5 mm)	Coarse Aggregate CA (5-12 mm)	Coarse Aggregate CA (12-19 mm)
Maximum aggregate size (mm)	5 mm	12 mm	19 mm
Specific gravity (SSD)	2.67	2.69	2.71
Specific gravity (OD)	2.64	2.68	2.70
Bulk density in compacted condition	1791 kg/m^3	1540 kg/m^3	1488 kg/m^3
Bulk density in loose condition	1668 kg/m^3	1466 kg/m^3	1395 kg/m^3
Absorption %	1.24 %	0.29 %	0.18 %
Fineness modulus	3.2	-	-
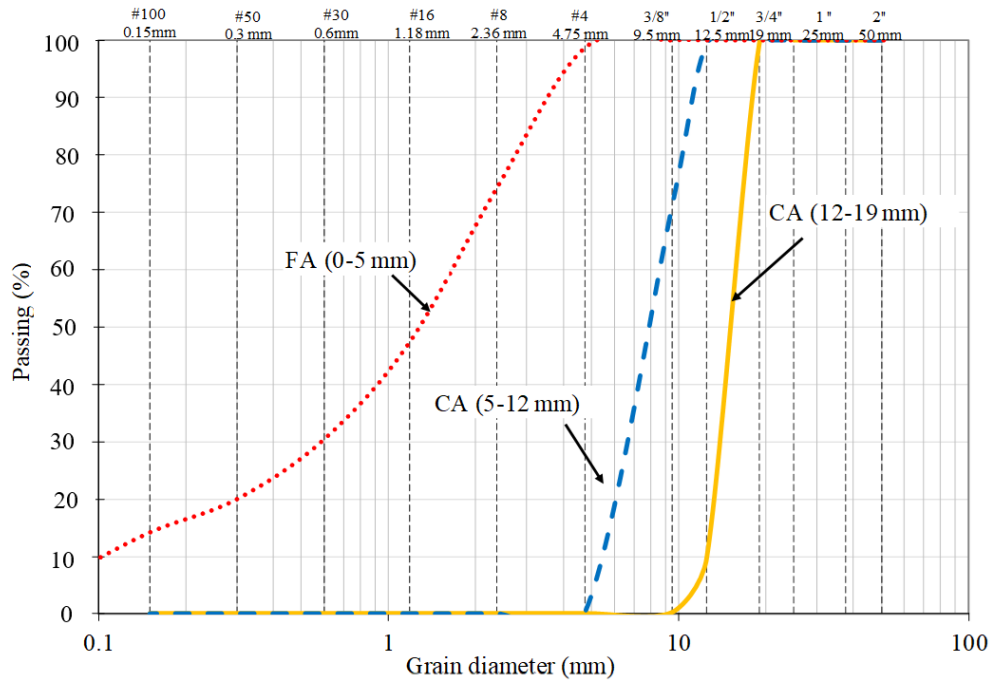
Figure 3.1. Fine and coarse aggregates gradation

The desired gradation of the aggregate combination was determined by considering the recommended RCC gradation band from the American Concrete Pavement Association (ACPA, 2014) and hot mix asphalt (HMA) gradation limits from the

Turkish General Directorate of Highways (GDH) (KGM, 2013) (Table 3.4). The reason for consideration of HMA gradation is that both RCC and HMA pavements use similar compaction methods in the field. For the combined gradation, 0.45 power curves are also provided on the plot. An illustration of the selected combined gradation curves for the maximum aggregate size of 12 mm and the maximum aggregate size of 19 mm is given Figure 3.2. The optimal aggregate combinations were found to be 65% (0-5 mm) - 35% (5-12 mm) - 0% (12-19 mm) for mixes with 12 mm maximum aggregate size, and 50% (0-5 mm) - 40% (5-12 mm) - 10% (12-19 mm) for mixes with 19 mm maximum aggregate size.

Table 3.4. *Lower and upper limits used to determine aggregate grading in RCC mix designs (ACPA, 2014; KGM, 2013)*

Combined Aggregate Gradation Ranges for HMA (KGM, 2013)				
Sieve Size (mm)	Lower Limit (D_{max} 19 mm)	Upper Limit (D_{max} 19 mm)	Lower Limit (D_{max} 12 mm)	Upper Limit (D_{max} 12 mm)
19	100	100	100	100
12.5	88	100	100	100
9.5	72	90	80	100
4.75	45	52	55	72
2	25	35	36	53
0.425	10	20	16	28
0.18	7	14	8	16
0.075	3	8	4	8
Combined Aggregate Gradation Ranges for RCC (ACPA, 2014)				
19	95	100	100	100
12.5	70	95	81	100
9.5	60	85	71	91
4.75	40	60	49	70
2.36	30	50	33	54
1.18	20	40	24	40
0.6	15	30	15	30
0.3	10	25	10	25
0.15	2	16	2	16
0.075	0	8	0	8
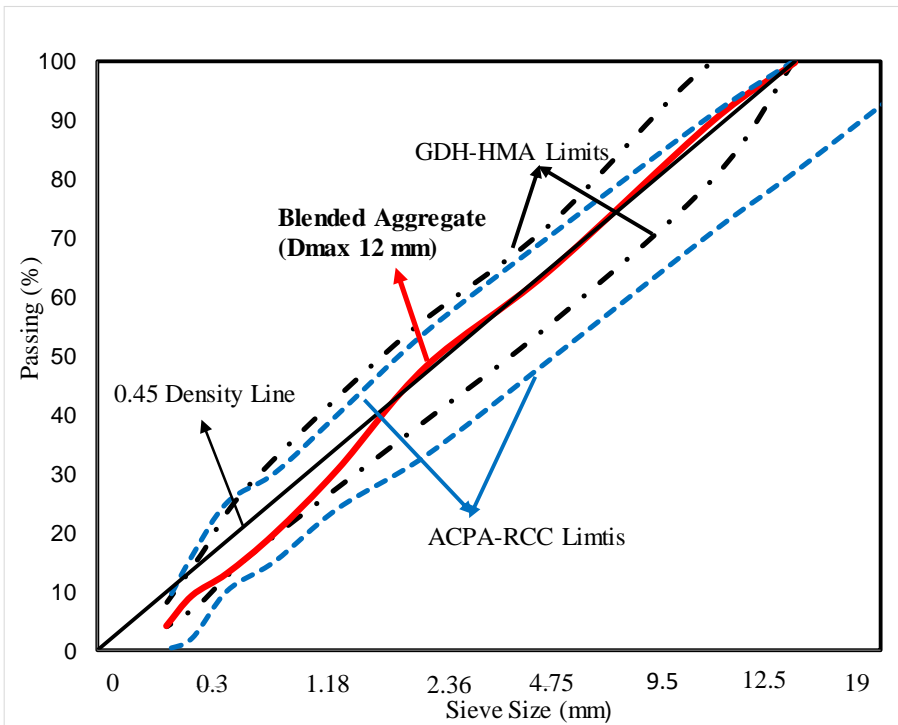
(a)
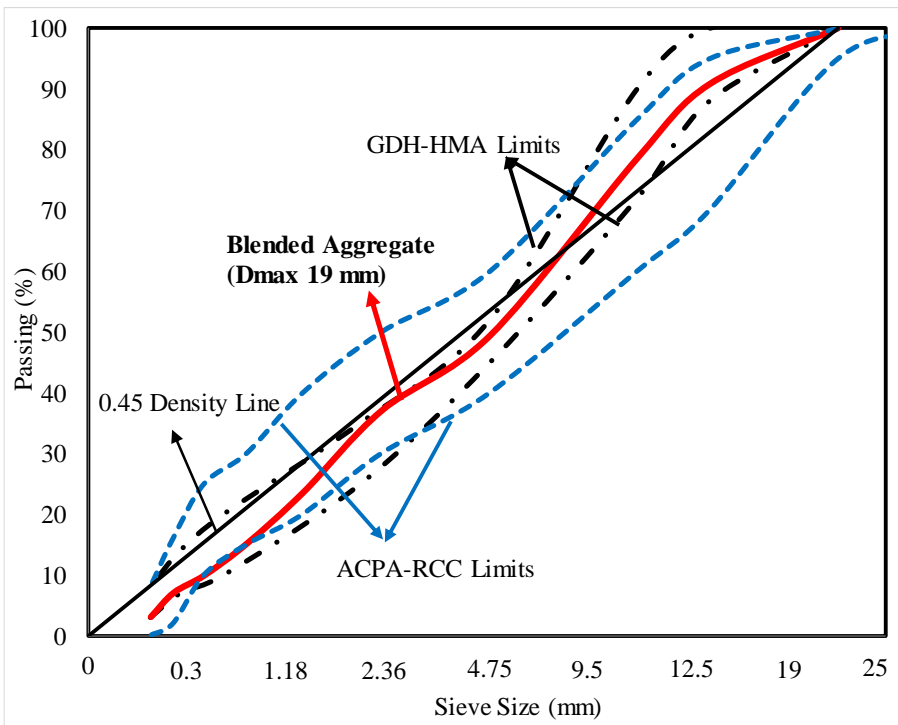
(b)

Figure 3.2. The combined aggregate gradations (a) D_{max} 12 mm (b) D_{max} 19 mm

A total of twenty RCC mixture designs were fabricated using two different aggregate gradations (D_{max} 12 and 19 mm), two different cement dosages (200 and 400 kg/m^3), and five different water ratios; 3-4-5-6-7%. The mixture designs were selected to be consistent with the classical weight/volume calculations of concrete-mixture proportioning described by CP Tech Center RCC guidelines (Harrington et al., 2010) assuming an entrapped air volume of 2%. The proportions for each RCC mixture are given in Table 3.5.

Table 3.5. *RCC mixture proportions for a cubic meter*

No	Mix ID	C (kg)	D_{max} (mm)	W (%)	Water Content (kg)	FA (0-5 mm) (kg)	CA (5-12 mm) (kg)	CA (12-19 mm) (kg)	w/c	C (%)	S/A
1	C200-D12-W3	200	12	3	74	1463	790	-	0.37	8.15	0.65
2	C200-D12-W4	200	12	4	96	1424	770	-	0.48	8.35	0.65
3	C200-D12-W5	200	12	5	117	1388	750	-	0.59	8.55	0.65
4	C200-D12-W6	200	12	6	137	1353	731	-	0.69	8.76	0.65
5	C200-D12-W7	200	12	7	156	1319	713	-	0.78	8.96	0.65
6	C200-D19-W3	200	19	3	74	1125	903	228	0.37	8.98	0.50
7	C200-D19-W4	200	19	4	96	1095	880	222	0.48	9.20	0.50
8	C200-D19-W5	200	19	5	117	1067	857	216	0.59	9.42	0.50
9	C200-D19-W6	200	19	6	137	1040	835	211	0.69	9.64	0.50
10	C200-D19-W7	200	19	7	156	1015	815	206	0.78	9.85	0.50
11	C400-D12-W3	400	12	3	74	1351	730	-	0.19	16.12	0.65
12	C400-D12-W4	400	12	4	97	1312	709	-	0.24	16.52	0.65
13	C400-D12-W5	400	12	5	118	1275	689	-	0.30	16.92	0.65
14	C400-D12-W6	400	12	6	139	1240	670	-	0.35	17.32	0.65
15	C400-D12-W7	400	12	7	158	1206	652	-	0.40	17.71	0.65
16	C400-D19-W3	400	19	3	74	1039	835	211	0.19	17.59	0.50
17	C400-D19-W4	400	19	4	97	1009	810	205	0.24	18.03	0.50
18	C400-D19-W5	400	19	5	118	981	788	199	0.30	18.44	0.50
19	C400-D19-W6	400	19	6	139	953	766	194	0.35	18.88	0.50
20	C400-D19-W7	400	19	7	158	928	745	188	0.40	19.30	0.50

Notes. Mix ID consists of the cement dosage (C), the maximum aggregate size (D_{max}) and the water content percentage (W). FA: fine aggregate, CA: coarse aggregate.

The water ratio, w/c, C and S/A indicated in the table are defined as follows:

water ratio   = Water amount/(binder and aggregates amount),

w/c   = Water amount/binder amount,

C   = Binder amount/(binder and aggregates amount),

S/A   = Fine aggregate amount/total aggregate amount.

As can be seen in Table 3.5, w/c ratios of 200 kg/m^3 binder dosage mixtures varied from 0.37 to 0.78, and w/c ratios of 400 kg/m^3 binder dosage mixtures varied from 0.19 to 0.40. The amount of binding materials ranged from 8.2% to 19.3% by weight.

3.1.2. Test Procedures and Compaction Methods

The gradual RCC casting plan for producing the 20 different RCC mixtures used the five different compaction methods designated in Table 3.1 and, at the same time, to permit the concrete mixer to work more efficiently and distribute the mixture homogeneously. The laboratory-based compaction methods used were: modified proctor (ASTM D1557, 2012), vibrating hammer (ASTM C1435, 2014), vibrating table (ASTM C1176, 2013), and SGC (ASTM C1800, 2016). For each RCC mixture, six cylindrical specimens of ϕ15x30 cm produced by the first three compaction methods were used to determine density, 28-day compressive and splitting tensile strength, and porosity, consistent with ASTM C642, (2013). For the SGC, three cylindrical specimens of diameter 15 cm and height 15 cm were produced; these sizes were subject to equipment height limits. Three different gyration numbers: 50, 60, and 75, were also used in the production of specimens by this method.

The concrete batches were prepared using a tilting drum mixer, having a capacity of 350 dm^3. Since the RCC mixtures required longer mixing times, the following mixing procedure was adopted. Firstly, aggregates and cement were added to the concrete mixer and mixed for 2 minutes. Later, water was added and the concrete was mixed continuously for an additional 5 minutes. For better homogenization of dry RCC

52

mixture, the mixture was poured to the pre-moistened ground and mixed again with the help of a shovel (Figure 3.3).

Figure 3.3. Mixing RCC mixture with rotary drum mixer and shovel on the ground

After preparing each concrete batch, a Vebe test (ASTM C1170, 2014) was performed to determine the RCC mixture consistency. ASTM C1170 describes two different procedures (Procedure A and Procedure B) for RCC consistency testing. Procedure A, with a surcharge mass of 22.7 kg, is recommended for drier, fairly solid RCC, while Procedure B, with a surcharge mass of 12.5 kg, should be applied for RCC with relatively low consistency (normal dry solid consistency). For all mixtures in the experimental study, the Vebe time was determined according to Procedure A, since it stated as the preferred procedure in most studies found in the literature. The Vebe durations were terminated when a mortar ring was sighted around the specimen under a surcharge mass of 22.7 kg on the vibrating table. In some cases, especially the extremely drier mixes, it was hard to observe a complete mortar ring and some necessary repetitions were performed. Also, for mixtures for which the mortar ring could not be fully visible, such as mixtures with a 3% water ratio, the Vebe time was determined by the partial appearance of the mortar ring (Figure 3.4).

Figure 3.4. RCC mixture consistency and applied Vebe test

After determining the Vebe time for the RCC mixtures, cylindrical specimens of 15x30 cm were prepared using the first three laboratory compaction methods specified in Table 3.1. Since there was not yet a standard for the preparation of RCC specimens by the modified proctor compaction method, the ASTM D1557, (2012) standard used for soil compaction was taken as a reference when preparing the RCC specimens. Cylindrical molds were compacted in five layers as for soil samples, the standard rammer was freely dropped 25 times for each layer, and six cylindrical specimens of φ15x30 cm were prepared for each mixture, as shown in Figure 3.5.

Figure 3.5. Compaction of RCC mixtures by modified proctor method (ASTM D1557)

While preparing the RCC specimens using the vibrating hammer (ASTM C1435) method, the mold was filled with four layers, as specified in the standard. The standard specifies that the period of application of the vibrating hammer should be terminated when a mortar ring appears around the specimen or, if such a mortar ring is not observed, should be held for a maximum of 20 seconds. However, when preparing the RCC mixtures in the first stage, especially in mixtures where the mortar ring could not be fully observed, fixed 10, 15, and 20-second reference times were used depending on the water ratio in the mixtures with the vibrating hammer applied within these periods. Six cylindrical specimens of ϕ15x30 cm were prepared for each mixture (Figure 3.6). In the light of experience gained during the first phase, in all mixtures fabricated during the second and third phases of the experimental study, the vibrating hammer was applied for 30 seconds to better compact the specimens.

Figure 3.6. Compaction of RCC mixtures by vibrating hammer method (ASTM C1435).

When preparing the RCC specimens with the vibrating table (ASTM C1176) the third compaction method, molds were compacted with three layers with each layer vibrated under a surcharge load of 9 kg, as specified in the standard. To increase the number

of specimens, an apparatus for holding a second sample was placed the vibrating table and the two samples were simultaneously compacted. In the related standard, as for the vibrating hammer, the vibration time on the vibrating table was limited by observation of a mortar ring around the specimen. Also, as for the vibrating hammer, especially in mixtures for which a mortar ring could not be precisely observed, depending on the water ratio, fixed 10, 15, and 20 second reference times were used and table vibrations applied within these periods. Six cylindrical specimens of ϕ15x30 cm were prepared for each mixture as in the other methods (Figure 3.7).

Figure 3.7. Compaction of RCC mixtures by vibrating table method (ASTM C1176).

In addition to the above-mentioned methods, SGC, commonly used for preparation of more sensitive asphalt concrete samples, was selected as a fourth method. Unlike other compaction methods that use impact compaction, SGC uses both vertical consolidation pressure and a gyratory kneading effort, a combination thought to properly represent field compaction conditions in the laboratory. SGC also offers the significant advantage of achieving desired density and compaction rates with different gyration numbers. As stated in the literature review, a new standard for the preparation of RCC specimens using SGC has been proposed (ASTM WK33682) but has not yet been published. On the other hand, there is a standard test method for determining

RCC specimen density using the gyratory compactor (ASTM C1800). Based on this standard, SGC in the METU Civil Engineering Transportation Laboratory was used to prepare the RCC specimens. The ASTM C1800 standard states that the expected density of RCC mixtures can be reached after 50-60 gyrations. Within the scope of this study, three different gyration numbers, 50-60-75, were selected for examining the effects on RCC physical and mechanical properties of choosing different gyration numbers. For each mixture, three specimens were produced at each gyration number, and a total of 9 specimens were obtained using SGC. As mentioned earlier, for SGC, the target size was $\phi 15 \times 15$cm because height was limited by equipment size (Figure 3.8). However, when mixtures prepared with 6% water ratio were compacted with 75 gyrations, water leakage was seen in the gyratory machine equipment, so, to avoid damage to the equipment, no specimen production was performed in the cases of all mixtures prepared with 7% water ratio at all gyration numbers and of for mixtures with 6% water ratio at 75 gyrations.

Figure 3.8. Compaction of RCC mixtures by SGC method.

When fabricating all RCC specimens in the laboratory, the four compaction methods were performed simultaneously, and time between first preparation of the mixture and

the end of production by all compaction methods did not exceed thirty to forty minutes.

As mentioned earlier, during the first phase of the experimental study, cylindrical specimens of ϕ15x30 cm (length/diameter=2) were produced with the first three compaction methods, with cylindrical specimens of ϕ15x15 cm (length/diameter=1) were obtained using the SGC method. To more accurately compare the results from the two different types of cylindrical specimens, with reference to slenderness ratio of 1 (length/diameter=1), cylindrical ϕ15x15 cm specimens were formed by cutting them from the ϕ15x30 cm specimens obtained using the first three methods. To begin this process, the top 2 cm of the of ϕ15x30 cm cylindrical specimens was cut off to account for the possibility of inadequate compaction. A 15-cm section was then cut and a sulfur head established to obtain 28th day compressive strengths (ASTM C39). The density, percent water absorption, and percent voids in hardened concrete according to ASTM C642 were obtained from the remaining sample by cutting the 2 cm (350 cm^3) minimum volume specified in the specification. The remaining cylindrical part of the 10 cm sample was then used to determine splitting tensile strength (ASTM C496) (Figure 3.9). To compare splitting tensile strength results from the first three methods with SGC results, additional RCC mixtures (4-5-6%) were prepared and splitting tensile strength tests also performed on specimens produced by SGC (50-60-75 gyration numbers). Specimens after cutting are shown in Figure 3.10, and photographs of the related tests are presented in Figure 3.11.

2 cm from the top surface was cut and not used.

Ø15x15 cm compressive strength specimen

Ø15x2 cm (350 cm^3) porosity specimen

Remaining part~Ø10x10 cm splitting tensile strength specimen
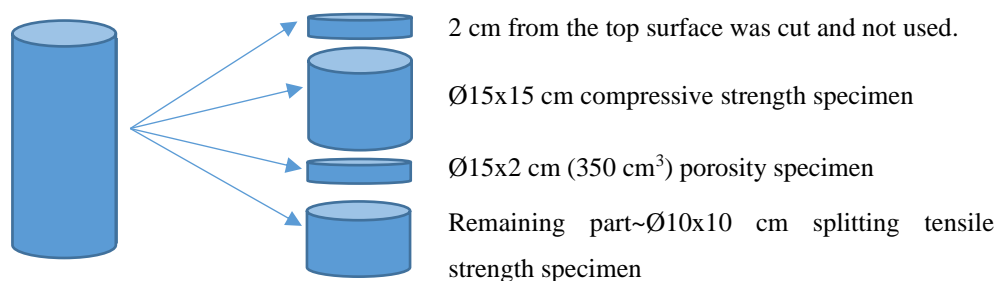
Figure 3.9. Test specimens prepared from Ø15x30 cm cylindrical samples

Figure 3.10. Specimens for 28-day compressive strength (ASTM C29), splitting tensile strength (ASTM C496) and density, water absorption and voids in hardened concrete (ASTM C642)

| (a) | (b) | (c) |
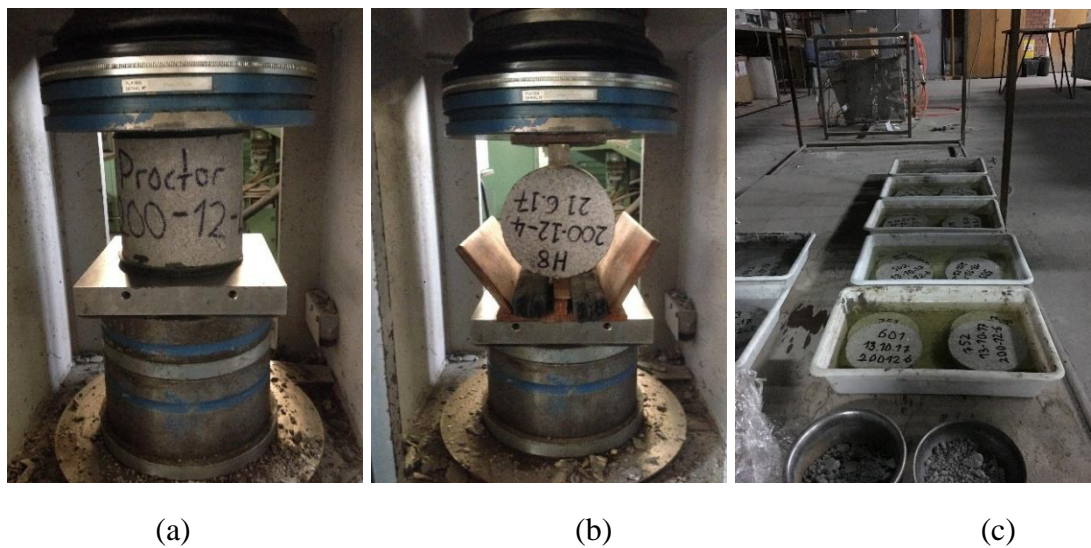
Figure 3.11. Tests on specimens for; (a) 28-day compressive strength (ASTM C29), (b) 28-day splitting tensile strength (ASTM C496), (c) density, water absorption and voids in hardened concrete (ASTM C642)

Prior to compaction of the RCC mixtures using the laboratory DDVHR, the density and strength results obtained from the modified proctor (ASTM D 1557), vibrating hammer (ASTM C1435), vibrating table (ASTM C1176), and SGC method (ASTM C1800), for 20 different RCC mixtures, were examined, and the relationships among water ratio, density ,and compressive strength of 20 different RCC mixtures for these four different compaction methods are shown in Figure 3.12.
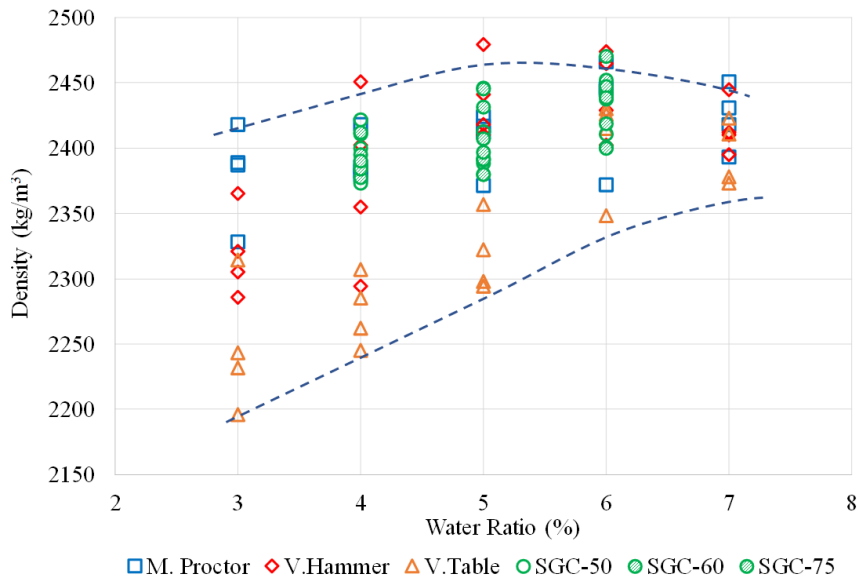
(a)
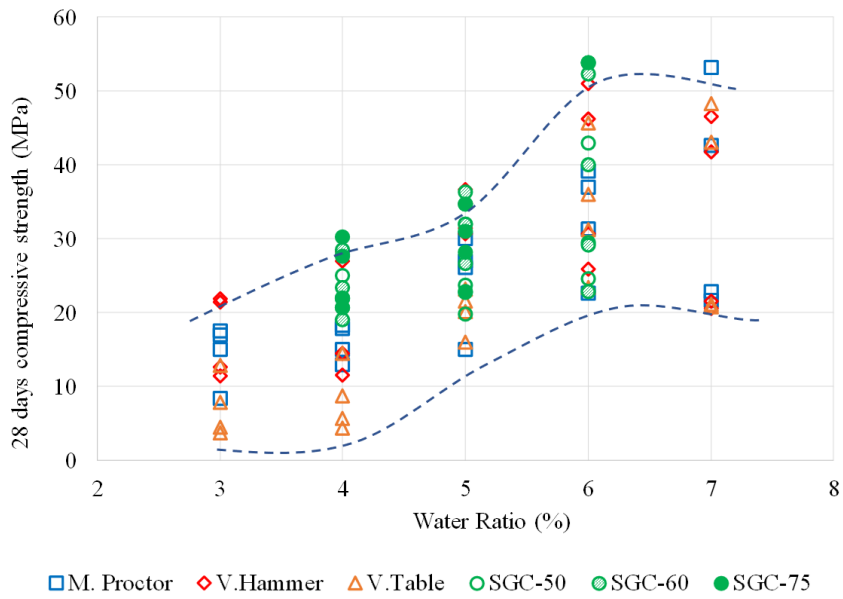
(b)

Figure 3.12. (a) Density- water ratio (b) 28-day compressive strength- water ratio relationships for RCC design mixtures.

Vebe time, reflecting sufficient dry solid consistency required to carry the 10-ton vibratory roller while the RCC is fresh in the field, and water ratio relationships are also displayed in Figure 3.13.
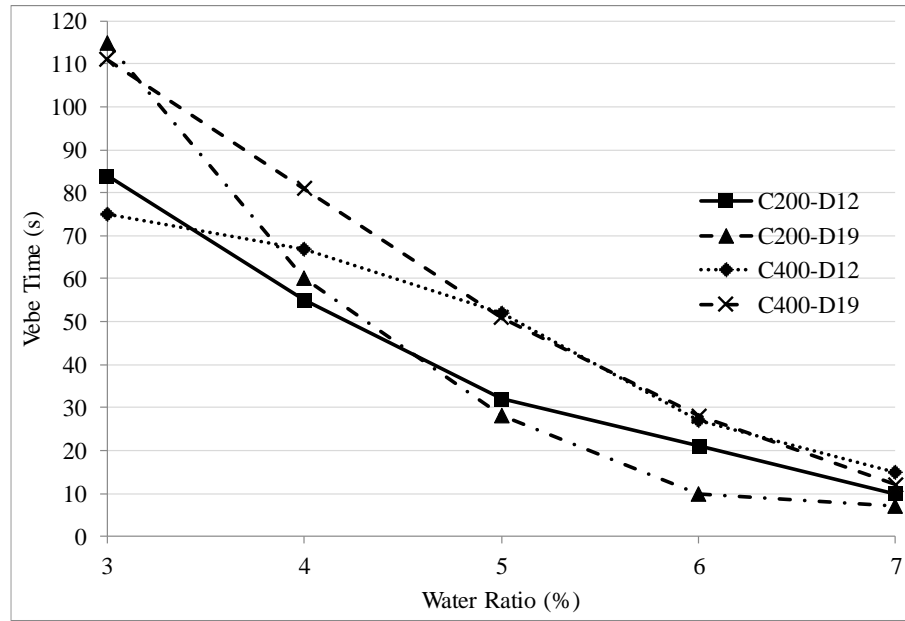
Figure 3.13. Relationship between Vebe time and water ratio for RCC design mixtures

As can be clearly seen in Figure 3.12, when different compaction procedures are used, both RCC density and strength can vary considerably. When the water content in the mixture increases, the difference between the densities obtained from the different compaction procedures decreases (dashed lines in the graph), but this tendency is not repeated for strength. It is also apparent from Figure 3.12 that the highest 28-day compressive strength and density values for all mixtures were generally obtained for water ratios between 5 and 7%. However, as stated in the literature, the consistency Vebe time of the RCC mixtures generally lies in the range 30-40, desirable in terms of field and mechanical performance. In the lab tests, Vebe time decreased to less than 30 seconds for the 6-7% water ratio in all mixtures, as shown in Figure 3.13. In this context, when water ratio, density, compressive strength, and Vebe time (Figure 3.12,

Figure 3.13) are considered together for 20 different RCC mixtures, it is more appropriate to focus only on 5-6% water ratio rather than testing with all water ratios because it is quite difficult and time-consuming to compact all RCC mixtures using a DDVHR under laboratory conditions.

After determination of field-related RCC mixtures to be compacted with a DDVHR, trial batches were prepared to develop the most appropriate compaction methodology. It is know that asphalt pavers are generally used to compact RCC roads, and compaction of a typical asphalt pavement takes place in two stages, as shown in Figure 3.14. During the first stage, a screed connected to the asphalt paver compresses the material through weight and vibration, after which the second compaction stage is carried out using a vibratory roller. To simulate such a two-stage compaction processes used in the field, two-stage compaction was also performed in the laboratory. First, a vibratory plate compactor (VPC) with bottom plate dimensions of 35×45 cm, weight of 100 kg, and vibrating force of 18 kN was used, after which the DDVHR was applied.
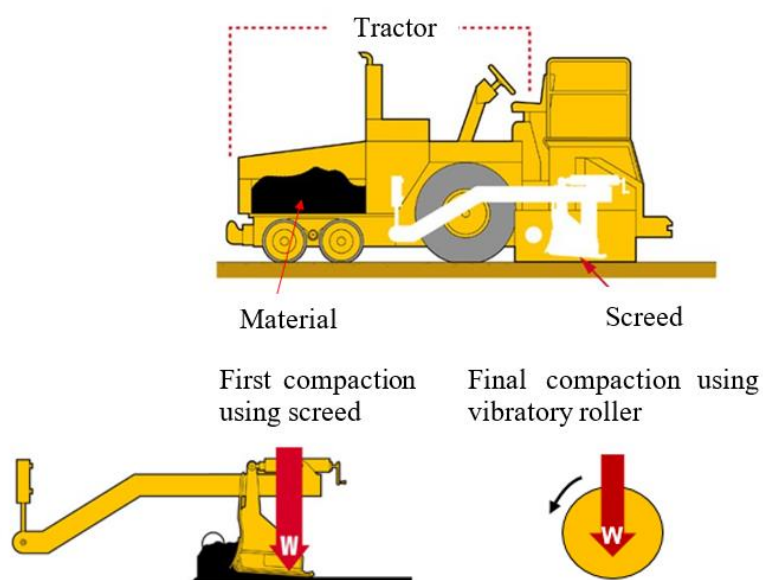
Figure 3.14. Typical compaction process for asphalt paver

The DDVHR used in this study weighed 700 kg and had a capacity of 3900 vibrations per minute provided by two vibrating cylinders, each of 65 cm width and 40 cm diameter. To make more effective use of the DDVHR, the size of the plate mold was chosen as $85{\times}200{\times}15$ cm^3. Cylinder core samples of size $\phi15{\times}15$cm were taken from the plate to determine simulated RCC pavement performance under different tests. In the first phase of the experimental study, since a wooden mold was rapidly destroyed, especially when a concrete cutting saw was used during removal of the beam cores, a second mold made of steel was chosen (Figure 3.15).

Figure 3.15. Wood and steel molds used for DDVHR

Since approximately 650 kg concrete was required for each mix (mold size 85x200x15 cm^3), three-stage casting with water ratios ranging from 5-6% was performed in the concrete mixer to produce RCC with a DDVHR for the four different mixtures. As for the other four laboratory compaction methods, the concrete preparation and mixing procedures were applied, and two Vebe consistency tests performed on each mixture. The Vebe times obtained from this method were within the range of 30 ± 10 sec. The concrete was poured as a single layer on the plate, then a VPC with bottom plate dimensions of $35{\times}45$ cm, weight of 100 kg, and vibrating force of 18 kN was used to apply pre-compaction similar to that provided by a paver prior to application of the vibratory roller under field conditions (Figure 3.16). After pre-compaction with the VPC, DDVHR was introduced. During the first applications, the compaction process

was completed by passing the DDVHR 4 times with vibration followed by 4 times without vibration (Figure 3.17).

Figure 3.16. Vibratory plate compactor (VPC) application representing field paver compaction process prior to DDVHR application for RCC mixtures
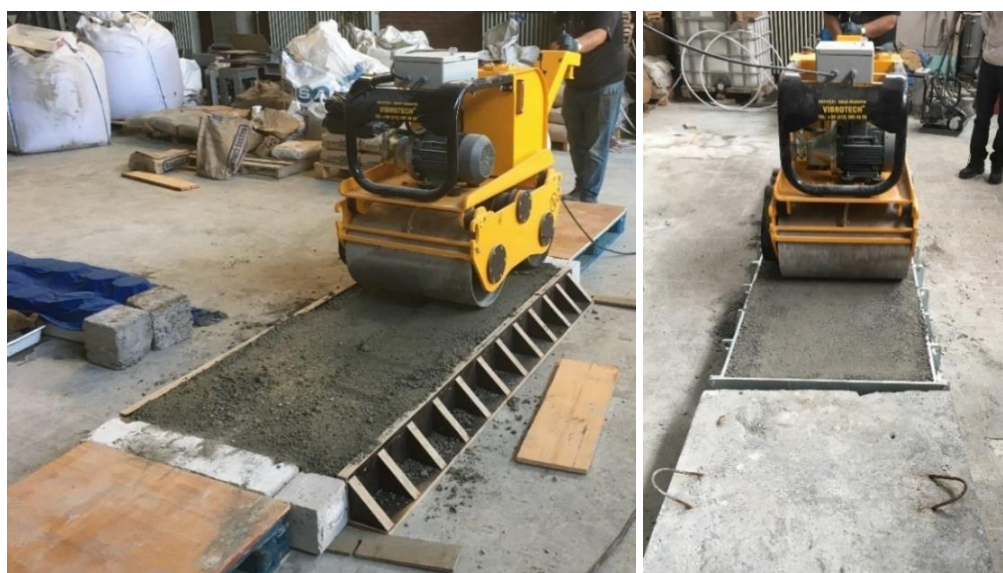
Figure 3.17. Process of preparation of RCC mixtures using vibrating and non-vibrating double drum hand roller

The main problems encountered in this method are due to the fact that the DDVHR is quite heavy (700 kg), can move in only one direction, has no gradual transition at the vibrating-mode level, and is difficult to use at a constant speed, especially in vibrating mode. For these reasons, in some mixtures surface undulation due to changes in the speed level was observed, especially when operating in vibration mode (Figure 3.18).

Figure 3.18. Surface undulations for some RCC mixtures during DDVHR application

To see the shrinkage behavior of RCC mixtures prepared using DDVHR, daily and weekly shrinkage measurements were made by attaching pins at different points on the plates, as shown in Figure 3.19.

After completion of the compaction process, the samples were covered with a damp cloth to cure the mixtures in the molds, and when the 28-day strength had been reached, the beam samples were cut with a concrete-cutting saw and 15 cm cylindrical cores were removed from the plates using a core drilling machine (Figure 3.20). Tests were carried out on core samples to determine compressive strength (ASTM C39), splitting tensile strength (ASTM C496) and density, water absorption, and void ratio (ASTM C642) after 28th days, as in the other four laboratory compaction methods.

Figure 3.19. Shrinkage measurements on RCC road produced in the laboratory

Table 3.6 (a) summarizes the properties of the cylindrical specimens produced during the first phase of the experimental study by four different laboratory compaction methods and prism specimens produced from DDVHR, showing the different RCC mixtures for determined water ratios (4 different RCC mixtures). The tests performed on the specimens are presented in Table 3.6 (b).

The results obtained from the cylindrical specimens and core samples produced during the first phase of the experimental study by four different laboratory compaction methods and DDVHR to represent field conditions in the laboratory are examined in the experimental results section.

(a)

(b)

Figure 3.20. Cutting beam specimens (a) and cylindrical coring specimens of 15 cm (b) from RCC road compacted by DDVHR

Table 3.6. *(a) The total number of specimens prepared for the first phase of experimental study and (b) experimental plan*

(a)

Methods	Shape	Dimensions (cm)	Total number of specimens		
			Number of each sample	Number of mixtures	Total
Modified Proctor (ASTM D1557)	Cylindrical	Ø15x30	6	20	120
Vibrating Hammer (ASTM C1435)	Cylindrical	Ø15x30	6	20	120
Vibrating Table (ASTM C1176)	Cylindrical	Ø15x30	6	20	120
SGC (50-60-75 gyrations)	Cylindrical	Ø15x15	~18	16	240*
DDVHR	Prism	85x200x15	1	4	4

* For some mixtures, specimens with 60 and 75 gyrations could not be produced and were subtracted from the total number.

		Total	604

(b)

Applied Test	Shape	Dimensions (cm)	Number of specimens				
			Tested for each mixture				
			MP (ASTM D1557)	VH (ASTM C1435)	VH (ASTM C1176)	SGC (50-60-75 gyrations)	DDVHR
Compressive strength (ASTM C39)	Cylindrical	ϕ15x15	6	6	6	9	3
Splitting tensile strength (ASTM C496)	Cylindrical	ϕ15x10	6	6	6	9	3
Determination of density, absorption, and voids in hardened concrete (ASTM C642)	Cylindrical	ϕ15x2	3	3	3	9	3

Note: MP, VH, VT, SGC and DDHVR indicate modified proctor, vibrating hammer, Superpave gyratory compactor and double drum vibratory hand roller, respectively.

3.2. Phase II: Mechanical Properties and Fracture Parameters of RCC Mixtures

The second phase of the experimental study examines a total of seven RCC mixtures obtained by adding three new mixtures to the four mixtures determined in the first

phase. The first two added mixtures represented intermediate cement dosage (300 kg/m^3), while the final mixture was selected to achieve high strength and durability. The aim of this phase of the experimental study was to determine compressive and flexural strengths, toughness, and fracture properties of specimens taken from the plate using DDVHR as the compaction procedure representing field conditions.

3.2.1. RCC Mixture Selection

The mixing proportions of the seven different RCC mixtures discussed in the second phase of the experimental study are given in Table 3.7. While the 200 and 400 kg/m^3 cement dosage mixtures of these seven mixtures were determined during the previous phase, in this phase two new mixtures with 300 kg/m^3 cement dosage and maximum aggregate size of 12 and 19 mm were added along with another RCC mixture (shown as B600-D12-W8.5 rather than C400-FA180-SF20-D12) to obtain high strength and durability. To determine the water amount in the new mixtures, since optimum water ratios and Vebe times obtained in previous mixtures that gave the highest strength and density value range were to be considered, water ratios in RCC mixtures with a Vebe time of 30±10 sec were selected to provide the dry solid consistency necessary to carry the vibratory roller in the fresh state, as well as to provide sufficient wetness for homogeneous placement.

Table 3.7. *RCC mixture proportions of the second phase of experimental study for a cubic meter*

No	Mix ID	C	FA	SF	D_{max} (mm)	W (%)	Water	Aggregates			W/C	C (%)	S/A
								0-5 mm	5-12 mm	12-19 mm			
1	C200-D12-W5	200	-	-	12	5.00	117	974	1157	-	0.58	8.58	0.55
2	C200-D19-W5	200	-	-	19	5.00	117	946	866	325	0.58	8.56	0.45
3	C300-D12-W5.5	300	-	-	12	5.50	127	1095	922	-	0.42	12.94	0.55
4	C300-D19-W5.5	300	-	-	19	5.50	128	896	820	308	0.43	12.91	0.45
5	C400-D12-W5.5	400	-	-	12	5.50	128	1048	883	-	0.32	17.16	0.55
6	C400-D19-W5.5	400	-	-	19	5.50	129	857	785	294	0.32	17.12	0.45
7	B600-D12-W8.5	400	180	20	12	8.50	169	863	727	-	0.28	27.39	0.55

Note C: cement, FA: Fly Ash, SF: Silica Fume, W: water ratio, W/C: Water to cementitious ratio, C %: cementitious ratio, S/A: Fine aggregate to total aggregate.

After determination of the RCC mixture designs, ASTM C39, ASTM C78, and JCI-S-001-2003 standards were employed to determine compressive strength, flexural strength and toughness, and fracture energies of RCCs. The RILEM procedure (RILEM TC 89-FMT, 1990) based on non-linear two-parameter fracture model (TPFM) was also used to determine the critical stress intensity factor or fracture toughness (K_{Ic}), critical effective crack length (a_c), modulus of elastic (E_c), critical crack tip opening displacement (CTODc), and initial fracture energy (G_f), all used to determine fracture properties of concrete,.

3.2.2. RCC Specimen Preparation and Test Procedures

To determine the mechanical and fracture properties of the seven different RCC mixtures, DDVHR, first used to represent the field compaction conditions in the previous phase, was also used on the 85x200x15 cm^3 plates during this phase. As in

the previous phase, three-stage castings were performed in the concrete mixer, and since approximately 650 kg of concrete was required for each mix in the production of RCC, with the concrete poured in a single layer. The VPC then used to achieve pre-compaction similar to that provided under field conditions by the paver prior to application of the vibratory roller. Following the pre-compaction provided by the VPC, the application of the DDVHR was initiated. Unlike in the previous phase, a new compaction procedure was developed to prepare the RCC road (plate). The suggested compaction method was sequential, including two passes with a VPC, two passes without vibration by hand roller, two passes from the center of the plate with vibration by the hand roller, two passes from each side of the plate with vibration by the hand roller, and four passes without vibration by the hand roller. This procedure, initially developed for the DDVHR, was used for all mixtures during the second phase of experimental study (Figure 3.21). After concrete casting was completed, the mixtures were cured under a damp cloth cover on the molds, and after one day had passed, the coring process was begun on the plate.

Figure 3.21. Application of VPC and DDVHR for RCC mixtures in the second phase of experimental study

The cutting plan, requiring extraction of core and beam specimens from each mixture's plate, was formed by taking into account the sample numbers and dimensions specified in standards (ASTM C78, JCI-S-001-2003, RILEM TC 89-FMT-1990) for use in determining mechanical and fracture properties of the RCC mixtures (Figure 3.22).

Cylindrical core samples of size Ø 15×15cm were taken from the plates to determine 2, 7, and 28-day compressive strengths (ASTM C39) of the RCC mixtures, with at least four samples taken for each age group.
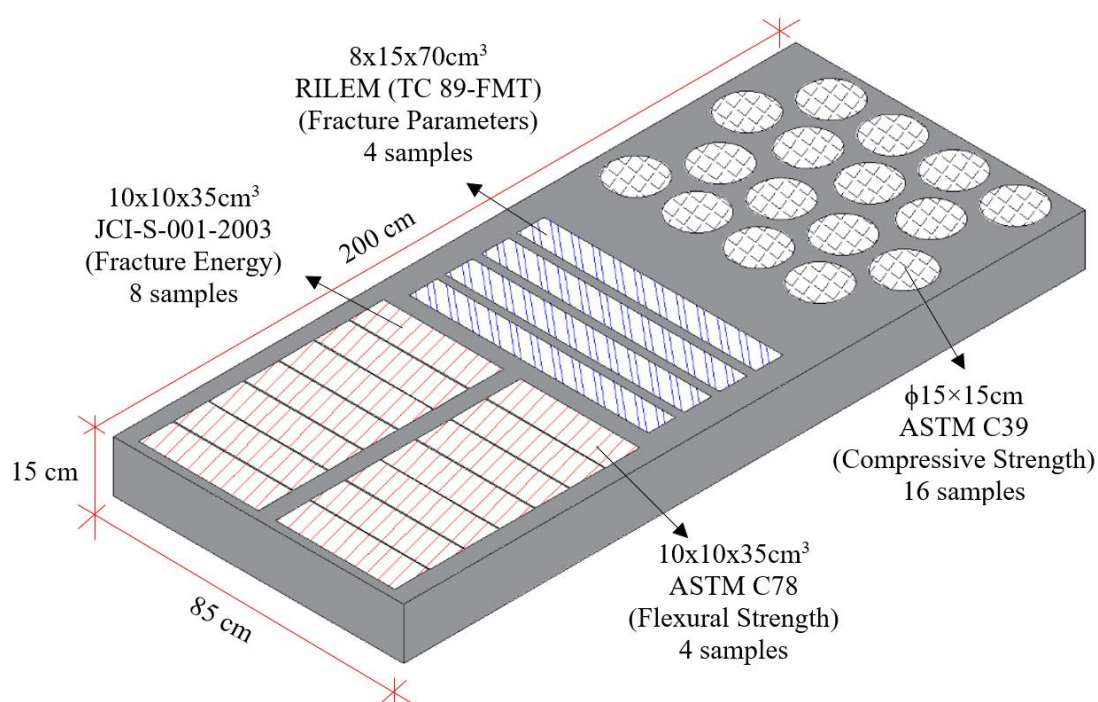
Figure 3.22. Cutting plan of core and beam samples on the plate to determine compressive and flexural strength and fracture parameters of each RCC mixture

A total of four beam specimens of dimensions 10x10x35 cm^3 were cut from the plates for determining 28-day flexural strengths, and the 28-day flexural strength tests were performed according to the ASTM C78 standard, as shown in Figure 3.23.

Eight beam specimens of dimensions 10x10x35 cm^3 were similarly cut from the plates for determining 28 and 90-day fracture energies according to the JCI-S-001-2003 standard, with four samples used for each age group, with specimen sizes and loading apparatus used for the procedure shown in Figure 3.24. In addition, in accordance with JCI-S-001-2003, for each specimen a notch of width 5 mm and depth 3 cm was made under the concrete beams (Figure 3.24).
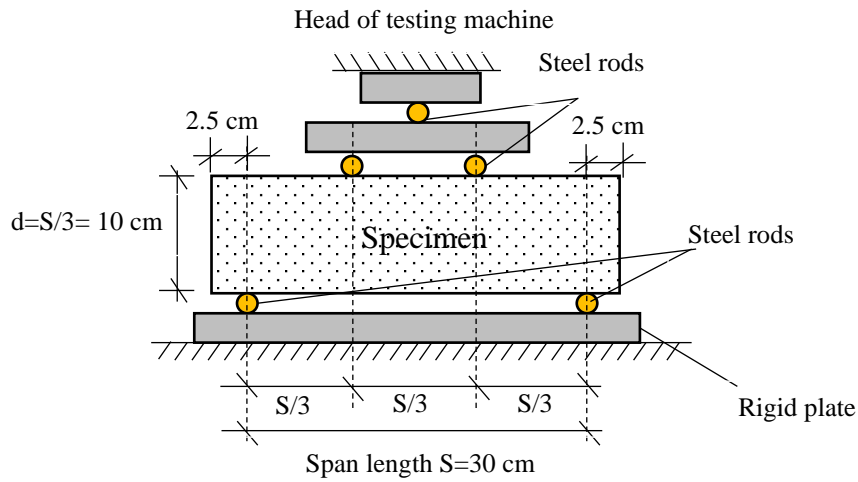
Figure 3.23. Geometry of four-point flexural strength test specimen and the loading configuration (ASTM C78)
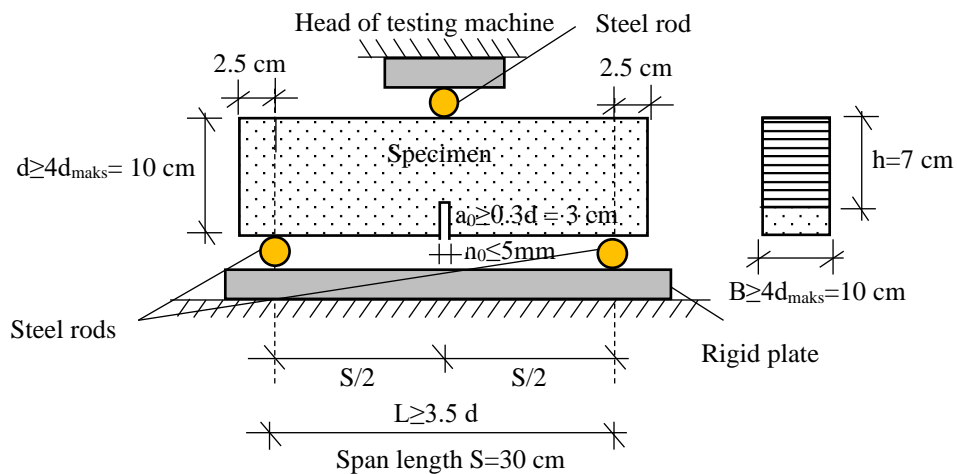
Figure 3.24 Geometry of three-point bending fracture test specimen and loading apparatus (JCI-S-001-2003)

Four beam specimens of dimensions 8x15x70 cm^3 as specified in RILEM (TC 89-FMT,1990) were cut from the plates for to determining 28-day fracture parameters and the three-point bending test was applied on notched beams, shown in

Figure 3.25. As required by the standard, the notch length to beam depth ratio was 1/3 and the notch width did not exceed 5 mm.
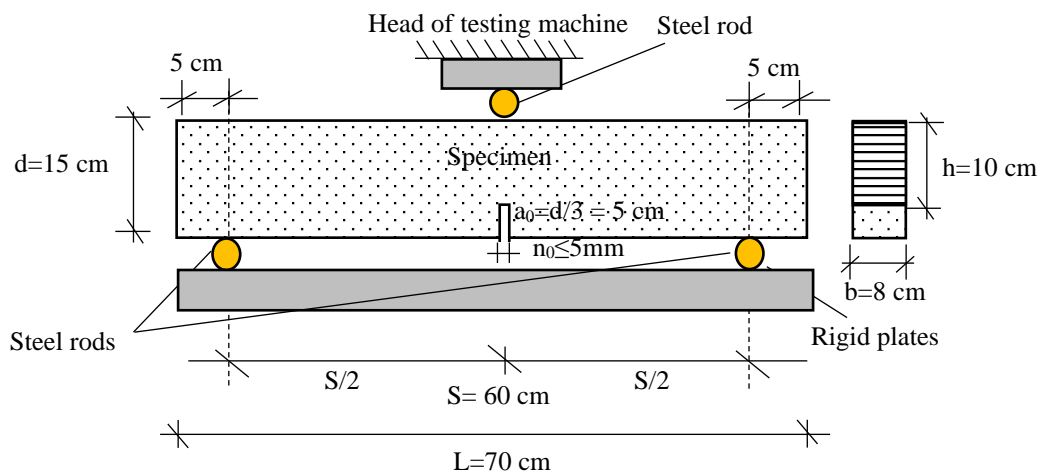
Figure 3.25. *Geometry of three-point bending fracture test specimen and loading apparatus (RILEM TC 89-FMT, 1990)*

To determine 2, 7, and 28-day compressive strengths of the mixtures, at least four samples of Ø15/15 cm were removed with a core-drilling machine for each age group (Figure 3.26).

Figure 3.26 Taking the cores on the RCC plate and reducing the plate sizes with walk-behind concrete saw cutting machine

Beam specimens required to determine flexural strength and fracture properties of mixtures were first extracted from the plates by reducing them to approximate size using a concrete saw, then beam specimens were placed on the specimen-cutting machine to produce more precise dimensions. The notches required by the JCI and RILEM standards were also cut using the specimen-cutting machine Figure 3.27.

(a) (b)

Figure 3.27. Preparation of beam specimens and notching, the example of (a) the cutting of JCI-S-001 beam specimen (b) the notching of the RILEM TC 89-FMT beam specimen

In some cases difficulties were encountered in making cuts on the plate, and irregular samples were cut for RILEM beams since specimen sizes ($8 \times 15 \times 70$ cm^3) were quite large, with non-uniform shaped specimens cut as shown in Figure 3.28, such problems were not encountered in the JCI and ASTM beams.

Figure 3.28. Some RILEM beam samples that could not be adequately obtained due to difficulties encountered during cutting and sample views after the test

Because the preparation of notches of different sizes required for JCI and RILEM beams involves a highly sensitive and challenging process, ±1.5 cm notch-length deviations were observed in some beam specimens.

3.3. Phase III: Fatigue Performance of RCC mixtures

Following the determination of the mechanical and fracture properties of RCCs during the second phase, the final phase of the experimental study was carried out. In this phase, the fatigue performance of three RCC mixers of different strength classes and binder amounts were examined. The relationship between fatigue performance of RCC mixtures and their fracture parameters and mechanical properties were also explored at the end of this phase, with the aim of satisfactorily estimating RCC fatigue behavior using the relatively easier-to-determine fracture parameters rather than costly and time-consuming fatigue testing.

A servo-hydraulic MTS (Landmark 250 kN) load-controlled test machine was used for fatigue tests, and a four-point bending test was performed for flexural fatigue-testing, with the distance between points was chosen as L/3 = 10 cm. Similar to the previous phase, mixtures and specimens were prepared and cured for 28 days, after which flexural strength was determined and maximum loading levels to be used for fatigue tests aimed at being applied for certain ratios of that ultimate static flexural

strength. The loads were separately calculated for the stresses specified by measuring the dimensions of each specimen before the fatigue testing.

3.3.1. RCC Mixture Selection

As mentioned at the beginning of the section, while determining appropriate mixtures for investigating fatigue behavior, different strength classes and binder amounts from RCC mixtures used in the previous phase were taken into account, and three different binder amounts: 200, 400, and 600 kg/m^3 were selected. To eliminate the impact of aggregate size, the maximum aggregate size for the three mixtures was selected as 12 mm, and RCC water ratios were selected to have a Vebe time of 30±10 sec. Table 3.8 displays the mixture designs of RCCs determined for the investigation of RCC fatigue performance.

Table 3.8. *RCC mixture designs to be investigated fatigue performance (kg/m^3)*

| No | Mix ID | C | FA | SF | Water | W/C | D_{max} (mm) | Aggregate | | TAFD |
								0-5 mm	5-12 mm	
1	C200-D12-W5	200	-	-	117	0.58	12	974	1157	2498
2	C400-D12-W5.5	400	-	-	128	0.32	12	1048	883	2510
3	B600-D12-W8.5	400	180	20	169	0.28	12	863	727	2408

Note: C: cement, FA: Fly Ash, SF: Silica Fume, W/C: Water cementitious ratio, TAFD: Theoretical air free density.

3.3.2. RCC Specimen Preparation and Test Procedure

As stated in the literature review part, since fatigue tests can be quite complicated and time-consuming processes compared to quasi-static tests, during the first part of the experimental study four-point flexural fatigue tests were carried out for trial purposes using a Servo-hydraulic MTS (Landmark 250 kN) load-controlled test machine on several mixture specimens. Since a pouring plan is important for application of fatigue

tests on the 28th day of all mixtures, a pouring plan was also prepared during the trial tests by noting how many hours or days the fatigue tests took for each specimen at different stress ratios. In addition, in light of the experiences obtained from the trial tests, some stress-ratio and specimen dimension updates to be applied during fatigue testing were made. It was therefore decided to apply fatigue tests at five different stress ratios (55%, 62.5%, 70%, 77.5% and 85%) reflecting the ratio of maximum fatigue load (S_{max}) to ultimate flexural strength to obtain more realistic fatigue curves of RCC mixtures. It was also thought appropriate at the end of the trial tests to select beam specimen sizes to be used in four-point flexural fatigue tests as $10x15x35$ cm^3. There was, however, no change in the loading rate of 10 Hz (10 cycles per second) used in trial fatigue tests and the minimum load level ($S_{min} = 20\% * MR$) to be applied for all fatigue tests.

To perform fatigue testing for RCC mixtures of three different strength classes, a pouring plan was first established and RCC mixtures were poured according to this schedule. As detailed for the other two phases of the experimental studies, three-stage concrete casting was performed and the mixtures compacted on a $85x200x15$ cm^3 steel plate. The VPC was first used for pre-compaction of the RCC mixtures in the plate, and was followed by compaction with DDVHR to simulate field conditions. While the same procedures used in the second phase were applied in preparation, placing, and compacting of RCC mixtures, unlike in the previous phase, a very thin layer of cement grout was applied to the plate surface to the small size undulations that could result in a negative effect caused by load heads not being balanced. Another separate part of the previous phase was the change in cutting plan resulting from modification of dimensions of beam samples subjected to fatigue tests. The plate cutting plan for the beam specimens used in flexural fatigue and fracture testing is shown in Figure 3.29. A total of 38 beam specimens were obtained from the plate for each RCC mixtures. Four specimens from each mixture were subjected to four-point static flexural tests (ASTM C78) to determine the maximum load for each fatigue stress level. At least four specimens from each mixture were also performed to find fracture

parameters. A total of approximately 90 specimens, about 30 specimens per mixture, was separated to perform four-point flexural fatigue test.
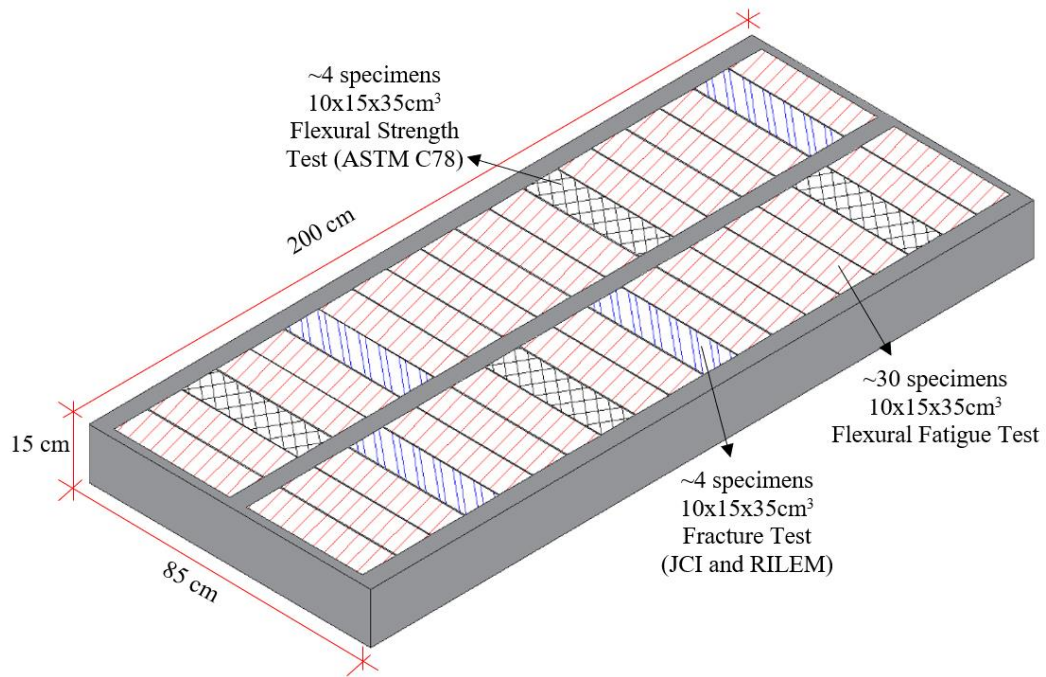
Figure 3.29. The plate cutting plan for the beam specimens used in flexural fatigue and fracture tests (Note: sample locations are not fixed, test samples are selected as mixed)

In the second phase of the experimental studies, specimen sizes specified by standards (JCI-S-001-2003, 2003; RILEM TC 89-FMT, 1990) were used for determining fracture energies and fracture parameters. However, in this phase, $10x15x35 \text{ cm}^3$ beam specimens were used in fatigue tests and fracture parameter tests. The motivation for investigating fracture parameters again can be explained as follows. As mentioned at the beginning of this section, while one objective of this phase was to investigate relationships between the fracture energies and parameters found in the second part and the fatigue behavior obtained in this phase, it is assumed that use of samples from different castings may result in some uncertainty, even though the same mix design and compaction procedures were used. In making comparisons, since it is significant to compare specimen results produced from the same casting, it was also thought

79

desirable to find out fracture parameters and fracture energies on beam specimens extracted from the same plate. The second reason for the repeated testing was to understand differences between fracture results obtained from different specimen sizes and standard sizes, so fatigue beam specimen size was utilized to determine fracture properties of RCC mixtures in this phase.

Figure 3.30 shows photographs of the beam specimens ($10x15x35$ cm^3) cut from the plates on whose surface the very thin cement grout layer was laid fatigue, static bending and fracture tests. The beam specimens cut from the plates were then covered with a damp cloth for curing until the testing days.

Figure 3.30. RCC plate prepared for fatigue test and test specimens of $10x15x35$ cm^{3}cut from plate (C400-D12-W5.5)

To perform the stress/load controlled fatigue tests, ultimate flexural strengths of the RCC mixtures were first obtained in accordance with ASTM C78, after which these flexural strengths were multiplied by the predetermined stress ratios of 55%, 62.5%, 70%, 77.5%, and 85% to determine maximum fatigue stresses that were then

separately converted in to load for each specimen and recorded in the test device. The minimum fatigue load was similarly calculated by converting the load to 20% of the ultimate flexural strength.

Table 3.9 provides 28-day flexural strengths (ASTM C78), the ratios, number of samples tested and maximum and minimum load values from four-point flexural fatigue tests of the RCC mixtures.

Table 3.9. *Load parameters for RCC fatigue tests*

No	Mix ID	28-day Flexural Strength (MPa)	Number of specimens	Stress Ratio (S)	Max. Flexural Load - P_{max} (kN)	Applied Max. Load (%S P_{max}) (kN)	Applied Min. Load (%20 P_{max}) kN)
1	C200-D12-W5	**4.00** [0.68]	3	**0.550**	32.8	18.0	6.5
			4	**0.625**	30.8	19.3	6.2
			5	**0.700**	30.9	21.6	6.2
			6	**0.775**	31.0	24.1	6.2
			6	**0.850**	31.9	27.1	6.4
2	C400-D12-W5.5	**5.06** [8.13]	4	**0.625**	37.5	23.4	6.5
			5	**0.700**	40.1	28.1	8.0
			5	**0.775**	37.4	29.0	7.0
			5	**0.850**	39.2	33.3	7.8
3	B600-D12-W8.5	**5.16** [5.23]	3	**0.550**	37.5	20.6	7.5
			5	**0.625**	36.7	22.9	7.3
			5	**0.700**	38.1	26.7	7.6
			5	**0.775**	36.8	28.5	7.4

Note: The coefficient of variation (%) is given in square brackets.

After determining the loading parameters, four-point flexural fatigue testing was carried out with load control by the servo-hydraulic (MTS Landmark 250 kN) test machine. The cyclic loading rate was applied at a frequency of 10 Hz (10 cycles per second) and fatigue testing continued either until the specimen failed or 2 million load cycles/repetitions had occurred (Figure 3.31). During the tests, the number of cycles/load repetitions to failure (N) was recorded for each specimen. For specimens

reaching 2 million cycles without failing, N was recorded as 2 million. From the literature review, 2 million load repetitions is generally accepted as a sufficient number of cycles for fatigue strength in plain concrete studies (Graeff, et al., 2012; Lee & Barr, 2004; Zhang, Phillips, & Wu, 1996), and since to reach 2 million load repetitions the fatigue load must be applied for approximately 54 hours without intervals, fatigue tests take quite a long time. Because of problems, such as electricity and water interruption, fatigue testing of some samples had to be continued after such interruptions.
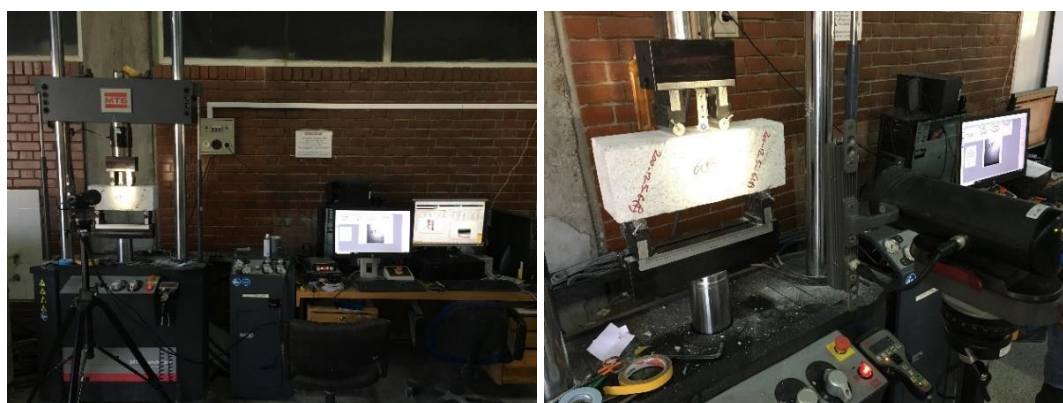
Figure 3.31. Photos from four-point flexural beam fatigue testing (C200-D12-W5).

Figure 3.32 shows load time, displacement time and load-displacement graphs obtained from the fatigue tests for a 70% stress ratio as an example. As the figure shows, an increase in deflection was measured for each specimen while upper and lower load limits are constant, and this deflection is continued until the material cannot bear the specified load due to formation and growth of micro cracks.
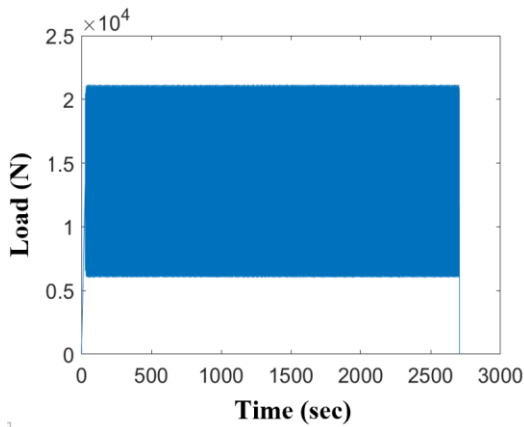
(a) Cycling loading between 0.70*Pmax and
0.2*Pmax (Load-Time
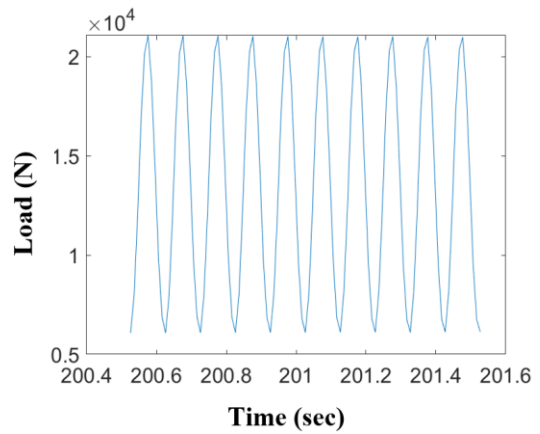
(b) Load - time graph for 1 sec
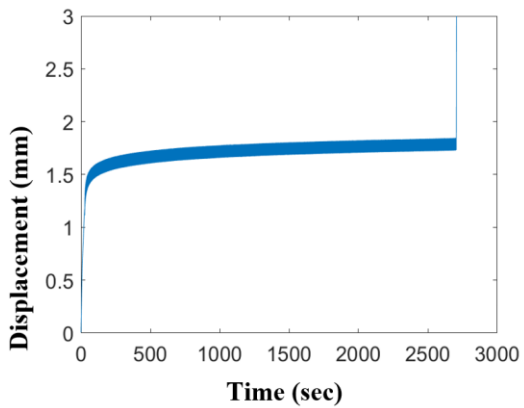
(c) Displacement - time graph
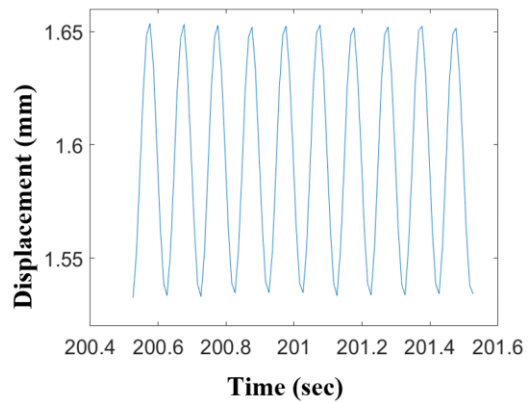
(d) Displacement - time graph for 1 sec
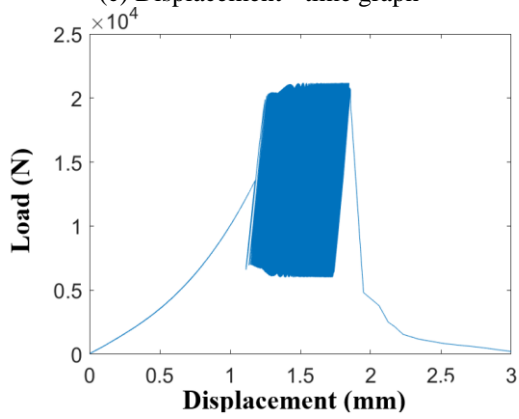
(e) Load – displacement graph
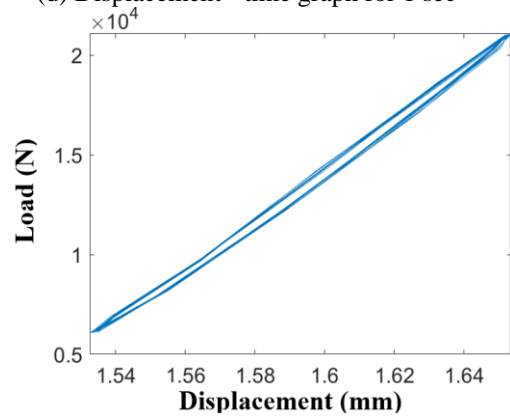
(f) Load – displacement graph for 1 sec

Figure 3.32. Typical results from fatigue test (between 0.70*P_{max} and 0.20*P_{max}) applied on a specimen 10 times per second. (Number of cycles to failure =26776).

CHAPTER 4

EXPERIMENTAL TEST RESULTS AND DISCUSSION

The results of the experimental studies are examined in the three phases explained earlier and evaluations of these results are presented under three separate subtitles of this chapter.

4.1. Phase I Results

As explained in detail Chapter 3.1, specimens were produced for a total of 20 different RCC mixtures by using four different laboratory compaction methods and DDVHR which can simulate field compaction procedures in the laboratory. In this chapter, the results obtained from these specimens are given in tables and the discussions are made with the help of the prepared graphics.

4.1.1. Experimental Results of Different Compaction Methods

The fresh properties, dry and bulk densities, and porosity properties of the RCC mixtures prepared using four different compaction methods are provided in Table 4.1, Table 4.2, and Table 4.3, respectively. In these tables, the mean and the coefficient of variations (CoV %) shown in square brackets were obtained as averages of three specimens.

Table 4.4 and Table 4.5 show the 28-day compressive strengths (ASTM C39) and splitting tensile strengths (ASTM C496) with coefficient of variations (CoV) obtained from the average of six cylindrical specimens (except for the SGC that utilized three specimens) for each mixture. The size of each cylindrical specimen was Ø15x15cm.

Table 4.1. *Fresh properties of RCC mixtures (CoV % in square brackets).*

	RCC mixture design			Mean fresh density (kg/m³)					
No	Mix ID	Vebe Time (sec)	Theo. Air Free Density (kg/m³)	Modified Proctor	Vibrating Hammer	Vibrating Table	SGC-50	SGC-60	SGC-75
1	C200-D12-W3	84	2579	2119 [0.7]	2189 [0.5]	1912 [0.7]	2268 [0.3]	2279 [0.1]	2293 [0.1]
2	C200-D12-W4	55	2541	2160 [0.9]	2306 [1.5]	2006 [3.0]	2322 [0.5]	2330 [0.7]	2338 [0.3]
3	C200-D12-W5	32	2505	2203 [0.9]	2395 [0.5]	2151 [1.1]	2313 [0.8]	2351 [0.3]	2384 [0.1]
4	C200-D12-W6	21	2470	2316 [2.1]	2379 [0.2]	2334 [1.5]	2454 [0.1]	2460 [0.3]	**
5	C200-D12-W7	10	2438	2361 [0.8]	2358 [0.6]	2351 [2.5]	**	**	**
6	C200-D19-W3	115	2583	2151 [0.9]	2180 [2.5]	2006 [1.3]	2218 [1.2]	2243 [0.1]	2241 [0.1]
7	C200-D19-W4	60	2544	2174 [1.2]	2254 [3.3]	2039 [0.9]	2377 [0.1]	2381 [0.5]	2408 [0.4]
8	C200-D19-W5	28	2508	2268 [1.4]	2387 [2.1]	2168 [0.7]	2388 [0.6]	2423 [0.2]	2431 [0.3]
9	C200-D19-W6	10	2473	2396 [0.3]	2397 [2.1]	2360 [0.5]	2478* [0.2]	2493* [0.3]	**
10	C200-D19-W7	7	2441	2385 [0.6]	2386 [2.4]	2365 [0.4]	**	**	**
11	C400-D12-W3	75	2608	2150 [0.6]	2109 [2.6]	1900 [1.0]	2298 [0.2]	2303 [0.1]	2320 [0.4]
12	C400-D12-W4	67	2569	2163 [0.9]	2099 [2.7]	1917 [0.9]	2298 [0.3]	2299 [0.4]	2306 [0.3]
13	C400-D12-W5	52	2534	2238 [0.9]	2268 [1.0]	2170 [3.2]	2353 [0.5]	2353 [0.2]	2365 [0.4]
14	C400-D12-W6	27	2499	2296 [3.5]	2363 [3.4]	2185 [5.4]	2481 [0.5]	2501* [0.4]	**
15	C400-D12-W7	15	2465	2350 [0.8]	2389 [0.9]	2396 [2.3]	**	**	**
16	C400-D19-W3	111	2611	2168 [0.9]	2117 [2.2]	1908 [0.7]	2252 [0.6]	2258 [0.5]	2268 [0.4]
17	C400-D19-W4	81	2573	2184 [0.9]	2134 [2.2]	1927 [1.2]	2260 [0.2]	2270 [0.5]	2291 [0.2]
18	C400-D19-W5	51	2537	2232 [0.9]	2338 [2.3]	2092 [1.3]	2336 [0.3]	2342 [0.6]	2345 [0.5]
19	C400-D19-W6	28	2502	2323 [1.3]	2439 [2.4]	2349 [1.3]	2475 [0.6]	2488 [0.5]	2499 [0.9]
20	C400-D19-W7	12	2468	2379 [0.5]	2423 [2.2]	2382 [0.6]	**	**	**

* data is slightly above the theoretical air free density.
**data could not be obtained due to water seepage in Superpave gyratory machine.

Table 4.2. *28-day dry density and bulk density of RCC mixtures (CoV % in square brackets).*

No	Mix ID	Dry density (kg/m³) (ASTM C642)						Bulk density after immersion and boiling (kg/m³) (ASTM C642)					
		M. Proctor	V. Hammer	V. Table	SGC-50	SGC-60	SGC-75	M. Proctor	V. Hammer	V. Table	SGC-50	SGC-60	SGC-75
1	C200-D12-W3	2141 [1.9]	2145 [5.7]	1972 [5.2]	-	-	-	2328 [1.1]	2305 [6.0]	2196 [4.6]	-	-	-
2	C200-D12-W4	2258 [1.7]	2324 [2.2]	2116 [2.1]	2252 [0.3]	2247 [1.2]	2273 [0.9]	2418 [1.1]	2451 [1.3]	2307 [0.9]	2400 [0.3]	2392 [1.0]	2411 [0.8]
3	C200-D12-W5	2222 [1.2]	2386 [0.4]	2210 [1.9]	2274 [0.8]	2245 [0.6]	2264 [0.6]	2371 [0.7]	2479 [0.2]	2357 [1.1]	2411 [0.5]	2391 [0.4]	2400 [0.3]
4	C200-D12-W6	2356 [0.4]	2365 [0.2]	2327 [0.9]	2274 [0.8]	2335 [0.4]	2337 [1.1]	2466 [0.2]	2474 [0.1]	2426 [0.6]	2395 [0.7]	2446 [0.3]	2447 [0.9]
5	C200-D12-W7	2311 [0.7]	2264 [0.9]	2228 [0.6]	**	**	**	2431 [0.5]	2395 [0.8]	2373 [0.3]	**	**	**
6	C200-D19-W3	2270 [0.9]	2204 [1.8]	2133 [2.2]	-	-	-	2418 [0.6]	2365 [0.8]	2314 [1.5]	-	-	-
7	C200-D19-W4	2243 [1.5]	2279 [0.7]	2092 [1.3]	2295 [0.8]	2279 [0.5]	2287 [0.3]	2386 [1.0]	2402 [0.4]	2262 [0.9]	2421 [0.4]	2411 [0.3]	2412 [0.2]
8	C200-D19-W5	2292 [1.6]	2308 [1.7]	2148 [1.6]	2286 [0.6]	2311 [0.4]	2337 [0.4]	2424 [1.0]	2410 [1.1]	2294 [2.0]	2412 [0.5]	2431 [0.2]	2445 [0.5]
9	C200-D19-W6	2340 [0.9]	2320 [0.6]	2328 [0.6]	2268 [0.6]	2290 [1.0]	2319 [0.6]	2444 [0.7]	2429 [0.5]	2430 [0.2]	2400 [0.5]	2419 [0.7]	2437 [0.4]
10	C200-D19-W7	2296 [0.3]	2277 [0.2]	2290 [0.4]	**	**	**	2418 [0.1]	2410 [0.2]	2411 [0.3]	*	**	**
11	C400-D12-W3	2209 [1.8]	2110 [1.7]	2019 [1.8]	-	-	-	2389 [1.1]	2321 [0.5]	2243 [1.0]	-	-	-
12	C400-D12-W4	2207 [1.2]	2077 [1.3]	1996 [0.9]	2209 [0.5]	2216 [0.5]	2238 [0.5]	2379 [0.8]	2294 [0.9]	2245 [0.4]	2373 [0.3]	2377 [0.4]	2384 [0.3]
13	C400-D12-W5	2292 [2.0]	2325 [2.3]	2150 [1.6]	2244 [0.2]	2235 [1.3]	2272 [0.2]	2412 [1.3]	2418 [2.2]	2322 [1.4]	2388 [0.2]	2380 [0.8]	2407 [0.2]
14	C400-D12-W6	2227 [2.1]	2283 [3.8]	2193 [1.7]	2350 [0.3]	2358 [0.6]	2382 [0.4]	2372 [1.1]	2402 [2.3]	2348 [1.1]	2443 [0.2]	2452 [0.6]	2470 [0.2]
15	C400-D12-W7	2287 [0.4]	2306 [0.2]	2266 [0.4]	**	**	**	2393 [0.2]	2412 [0.2]	2378 [0.3]	*	*	*
16	C400-D19-W3	2222 [1.2]	2068 [0.9]	1988 [1.9]	-	-	-	2387 [0.7]	2286 [0.4]	2232 [0.9]	-	-	-
17	C400-D19-W4	2240 [1.5]	2170 [0.6]	2082 [1.2]	2235 [0.1]	2230 [1.3]	2238 [0.2]	2382 [1.3]	2355 [0.3]	2285 [0.4]	2388 [0.2]	2384 [1.0]	2390 [0.2]
18	C400-D19-W5	2293 [1.0]	2338 [1.8]	2128 [0.5]	2242 [0.6]	2261 [0.4]	2270 [0.3]	2417 [0.6]	2441 [1.1]	2298 [0.2]	2380 [0.6]	2391 [0.2]	2397 [0.1]
19	C400-D19-W6	2350 [1.8]	2376 [0.3]	2312 [1.3]	2336 [0.3]	2333 [0.2]	2336 [0.4]	2446 [1.3]	2465 [0.3]	2415 [1.0]	2440 [0.1]	2438 [0.1]	2438 [0.4]
20	C400-D19-W7	2355 [0.2]	2340 [0.4]	2308 [0.2]	**	**	**	2451 [0.1]	2445 [0.2]	2423 [0.1]	**	**	**

 - Specimens compacted with SGC with 3% water could not be prepared due to unavailability of the equipment at that time.
**data could not be obtained due to water seepage in SGC machine.

Table 4.3. *28-day volume of permeable pore void and water absorption capacity of RCC mixtures (CoV % in square brackets).*

No	Mix ID	Volume of Permeable Pore Voids (%) (ASTM C642)						Water Absorption Capacity (%) (ASTM C642)					
		M. Proctor	V. Hammer	V. Table	SGC-50	SGC-60	SGC-75	M. Proctor	V. Hammer	V. Table	SGC-50	SGC-60	SGC-75
1	C200-D12-W3	18.7 [7.7]	16.0 [11.3]	22.4 [0.8]	-	-	-	8.7 [9.7]	7.4 [7.4]	11.4 [5.9]	-	-	-
2	C200-D12-W4	15.9 [7.8]	12.8 [14.5]	19.1 [11.9]	14.8 [6.7]	14.5 [5.5]	13.8 [2.7]	7.1 [9.6]	5.5 [17]	9.1 [14]	6.6 [6.9]	6.5 [6.2]	6.0 [3.0]
3	C200-D12-W5	14.9 [7.4]	9.3 [3.7]	14.8 [14.3]	13.7 [5.4]	14.6 [4.0]	13.7 [5.8]	6.7 [8.6]	3.9 [4.0]	6.7 [16]	6.0 [6.0]	6.5 [4.5]	6.0 [6.3]
4	C200-D12-W6	10.9 [5.5]	10.8 [1.9]	10.5 [6.3]	12.1 [2.8]	11.2 [4.8]	11.1 [5.3]	4.6 [6.0]	4.6 [2.0]	4.7 [7.2]	5.3 [3.4]	4.8 [5.1]	4.7 [6.3]
5	C200-D12-W7	12.0 [4.4]	13.1 [2.4]	14.4 [4.1]	**	**	**	5.2 [5.1]	5.8 [3.3]	6.5 [4.7]	**	**	**
6	C200-D19-W3	14.8 [3.3]	16.2 [12.5]	18.2 [7.6]	-	-	-	6.5 [4.1]	7.4 [14]	8.5 [9.9]	-	-	-
7	C200-D19-W4	14.3 [5.4]	12.2 [6.0]	17.0 [4.0]	12.7 [7.6]	13.3 [6.1]	12.5 [6.0]	6.4 [7.9]	5.4 [6.7]	8.1 [5.2]	5.5 [8.3]	5.8 [6.5]	5.5 [6.3]
8	C200-D19-W5	13.2 [8.5]	10.1 [15.0]	14.6 [10.9]	12.6 [3.0]	12.1 [5.1]	10.8 [2.6]	5.8 [9.9]	4.4 [17]	6.8 [10]	5.5 [3.6]	5.2 [5.4]	4.6 [2.2]
9	C200-D19-W6	10.4 [3.6]	10.8 [3.7]	10.2 [9.0]	13.2 [2.1]	12.9 [4.6]	11.9 [4.5]	4.4 [4.6]	4.7 [4.1]	4.4 [9.6]	5.8 [2.6]	5.6 [5.6]	5.1 [5.1]
10	C200-D19-W7	12.2 [4.0]	13.2 [2.7]	12.1 [1.9]	**	**	**	5.3 [4.3]	5.8 [2.9]	5.3 [2.2]	**	**	**
11	C400-D12-W3	17.9 [8.0]	21.1 [11.0]	25.8 [1.5]	-	-	-	8.1 [9.8]	10.0 [13]	12.9 [1.8]	-	-	-
12	C400-D12-W4	17.2 [5.0]	21.7 [4.2]	24.9 [3.7]	16.4 [6.4]	16.2 [1.7]	14.6 [3.3]	7.8 [6.1]	10.4 [5.3]	12.5 [4.6]	7.4 [6.8]	7.3 [2.1]	6.5 [3.8]
13	C400-D12-W5	12.0 [14]	9.3 [11.4]	17.2 [5.6]	14.4 [3.2]	14.5 [8.0]	13.5 [1.4]	5.2 [16]	4.0 [12]	8.0 [6.4]	6.4 [3.2]	6.5 [9.4]	6.0 [1.5]
14	C400-D12-W6	14.4 [6.2]	10.4 [0.5]	16.2 [9.4]	9.3 [3.5]	9.4 [0.8]	8.8 [5.5]	6.5 [16]	4.3 [3.8]	7.0 [9.4]	4.0 [3.8]	4.0 [0.2]	3.7 [5.8]
15	C400-D12-W7	10.6 [3.6]	10.6 [0.8]	11.3 [2.5]	**	**	**	4.7 [3.9]	4.6 [1.0]	5.0 [2.7]	**	**	**
16	C400-D19-W3	16.5 [6.8]	21.8 [5.1]	24.5 [6.6]	-	-	-	7.4 [7.8]	10.5 [6.0]	12.3 [8.5]	-	-	-
17	C400-D19-W4	14.2 [5.4]	18.4 [3.7]	20.4 [7.8]	15.3 [3.2]	15.4 [2.3]	15.2 [2.0]	6.4 [6.1]	8.5 [4.3]	9.8 [9.0]	6.9 [3.3]	6.9 [3.6]	6.8 [2.1]
18	C400-D19-W5	12.4 [7.0]	9.3 [3.9]	17.0 [7.6]	13.8 [0.3]	13.1 [6.0]	12.6 [4.8]	5.4 [8.0]	4.4 [19.7]	8.0 [8.0]	6.1 [0.8]	5.8 [6.5]	5.6 [5.1]
19	C400-D19-W6	9.6 [9.7]	8.9 [1.6]	10.3 [6.1]	10.5 [4.1]	10.5 [1.9]	10.2 [3.9]	4.1 [12]	3.7 [1.3]	4.5 [7.4]	4.5 [4.4]	4.5 [2.1]	4.4 [4.0]
20	C400-D19-W7	9.5 [0.9]	10.5 [3.8]	11.5 [3.7]	**	**	**	4.1 [1.0]	4.5 [4.2]	5.0 [3.9]	**	**	**

 - Specimens compacted with SGC with 3% water could not be prepared due to unavailability of the equipment at that time.

**data could not be obtained due to water seepage in SGC machine.

Table 4.4. *28-day compressive strength of RCC mixtures (CoV % in square brackets).*

No	Mix ID	M. Proctor (MPa)	V. Hammer (MPa)	V. Table (MPa)	SGC-50 (MPa)	SGC-60 (MPa)	SGC-75 (MPa)
1	C200-D12-W3	8.4 [7.4]	21.4 [5.9]	7.8 [7.9]	14.4 [35.0]	14.4 [6.3]	21.1 [9.7]
2	C200-D12-W4	13.0 [4.6]	27.0 [14.2]	8.7 [10.6]	21.9 [2.6]	23.4 [5.0]	27.6 [5.3]
3	C200-D12-W5	15.0 [9.9]	31.4 [4.6]	16.0 [7.8]	20.0 [0.8]	22.7 [0.2]	22.9 [9.2]
4	C200-D12-W6	22.6 [9.4]	25.9 [6.8]	23.4 [14.4]	24.6 [2.8]	22.8 [5.9]	**
5	C200-D12-W7	21.6 [5.0]	20.6 [3.4]	20.8 [4.8]	**	**	**
6	C200-D19-W3	15.1 [24.6]	23.0 [7.5]	12.9 [13.4]	13.3 [8.5]	14.5 [8.6]	12.9 [12.5]
7	C200-D19-W4	18.3 [6.7]	28.2 [5.4]	14.5 [7.1]	27.8 [5.0]	28.5 [4.2]	30.2 [6.6]
8	C200-D19-W5	27.0 [5.3]	34.8 [8.3]	20.2 [4.5]	25.0 [7.2]	26.6 [2.2]	28.1 [1.7]
9	C200-D19-W6	31.3 [3.4]	30.7 [3.4]	31.2 [4.9]	29.4 [0.8]	29.2 [2.2]	**
10	C200-D19-W7	22.8 [4.6]	21.6 [2.1]	21.1 [2.4]	**	**	**
11	C400-D12-W3	17.5 [7.8]	12.7 [14.1]	4.5 [12.4]	23.0 [4.0]	23.9 [2.9]	23.9 [1.3]
12	C400-D12-W4	15.0 [8.9]	11.6 [9.4]	4.4 [10.8]	25.3 [10.4]	22.5 [5.4]	22.3 [1.3]
13	C400-D12-W5	26.9 [7.3]	32.0 [12.7]	23.2 [10.8]	31.9 [9.6]	32.4 [0.6]	31.4 [12.4]
14	C400-D12-W6	37.0 [7.3]	51.0 [8.7]	36.0 [2.5]	42.7 [3.5]	40.4 [5.0]	**
15	C400-D12-W7	53.2 [4.5]	46.6 [7.1]	48.2 [6.9]	**	**	**
16	C400-D19-W3	16.9 [5.8]	11.4 [8.3]	3.7 [5.8]	19.0 [0.3]	20.6 [7.4]	20.0 [4.3]
17	C400-D19-W4	17.8 [3.9]	14.4 [8.4]	5.7 [13.6]	20.7 [7.0]	19.1 [4.3]	20.7 [4.6]
18	C400-D19-W5	30.0 [13.2]	36.6 [9.9]	21.5 [8.4]	34.7 [8.2]	36.3 [0.3]	34.7 [5.3]
19	C400-D19-W6	38.0 [8.2]	46.3 [7.7]	45.7 [7.4]	53.8 [4.1]	52.3 [3.9]	53.8 [1.0]
20	C400-D19-W7	45.0 [9.6]	41.7 [3.6]	43.1 [6.0]	**	**	**

**data could not be obtained due to water seepage in SGC machine.

Table 4.5. *28-day splitting tensile strength of RCC mixtures (CoV % in square brackets).*

No	Mix ID	M. Proctor (MPa)	V. Hammer (MPa)	V. Table (MPa)	SGC-50 (MPa)	SGC-60 (MPa)	SGC-75 (MPa)
1	C200-D12-W3	1.2 [8.3]	2.7 [6.8]	0.7 [13.6]	-	-	-
2	C200-D12-W4	1.8 [10.0]	3.4 [9.6]	1.2 [11.3]	2.4 [9.4]	2.2 [6.0]	2.4 [5.5]
3	C200-D12-W5	1.7 [5.2]	3.9 [7.1]	2.3 [9.5]	2.4 [14.4]	2.2 [4.3]	2.7 [5.7]
4	C200-D12-W6	3.2 [11.2]	3.5 [6.7]	2.7 [11.4]	2.7 [10.7]	3.0 [13.2]	3.0 [13.7]
5	C200-D12-W7	3.2 [6.5]	3.0 [11.6]	2.8 [6.4]	**	**	**
6	C200-D19-W3	1.7 [8.2]	2.2 [10.2]	1.5 [10.5]	-	-	-
7	C200-D19-W4	2.0 [5.6]	2.5 [9.3]	2.0 [12.0]	2.3 [14.1]	2.3 [8.7]	2.5 [6.9]
8	C200-D19-W5	2.9 [8.6]	3.5 [5.6]	2.7 [8.6]	2.5 [11.0]	2.4 [4.1]	3.0 [10.0]
9	C200-D19-W6	3.8 [12.2]	3.1 [11.8]	2.7 [9.9]	2.7 [3.4]	2.3 [2.0]	2.9 [9.4]
10	C200-D19-W7	2.7 [10.4]	2.6 [11.0]	2.4 [7.1]	**	**	**
11	C400-D12-W3	2.1 [5.4]	1.2 [8.8]	0.4 [11.8]	-	-	-
12	C400-D12-W4	1.6 [12.1]	1.1 [10.8]	0.4 [8.2]	2.6 [5.5]	2.6 [3.2]	2.7 [12.6]
13	C400-D12-W5	3.1 [7.9]	3.7 [7.7]	2.5 [18.8]	3.2 [3.2]	3.5 [3.9]	3.9 [7.7]
14	C400-D12-W6	3.5 [9.4]	4.7 [10.2]	3.7 [16.3]	4.9 [8.6]	5.2 [10.5]	5.7 [9.4]
15	C400-D12-W7	4.7 [12.0]	3.8 [9.1]	3.9 [8.1]	**	**	**
16	C400-D19-W3	1.6 [11.8]	0.9 [9.4]	0.3 [4.6]	-	-	-
17	C400-D19-W4	1.7 [6.8]	1.4 [8.8]	0.6 [8.4]	1.8 [12.5]	2.1 [4.6]	2.0 [12.4]
18	C400-D19-W5	2.6 [11.6]	3.9 [9.1]	2.1 [11.6]	2.1 [9.5]	2.7 [1.6]	2.5 [7.2]
19	C400-D19-W6	3.5 [9.9]	4.4 [7.1]	3.9 [4.7]	4.4 [10.8]	4.0 [5.8]	3.8 [3.0]
20	C400-D19-W7	4.3 [11.7]	4.3 [11.5]	4.0 [17.5]	**	**	**

- Specimens for splitting tensile strength compacted with SGC with 3% water could not be prepared due to unavailability of the equipment at that time.

** data could not be obtained due to water seepage in SGC machine.
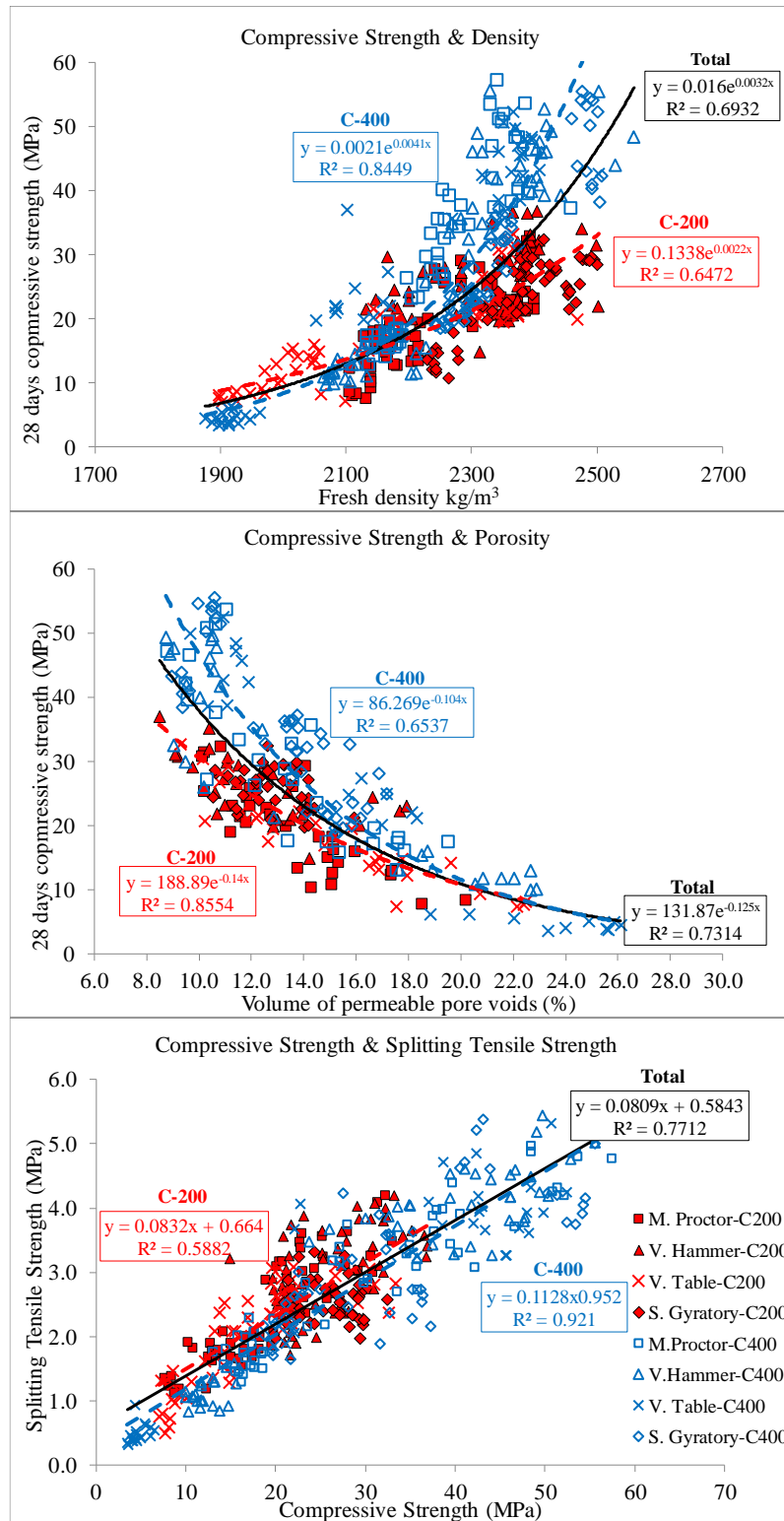
Figure 4.1. Relationship between 28-day compressive strength and density, porosity, 28-day splitting tensile strength (red 200 kg/m³ - blue 400 kg/m³)

91

Density, porosity, and 28-day splitting tensile strength values with respect to the 28-day compressive strengths for all specimens are plotted in Figure 4.1. These relationships were derived for separate 200 and 400 kg/m^3 dosage mixtures as well for a combined dosage. A linear relationship ($R^2 = 77\%$) between compressive strength and splitting tensile strength of mixtures was found, and exponential growth between compressive strength and density of the RCC mixtures was observed, while an increase in permeable pore voids exhibited an exponential decay with respect to compressive strength.

4.1.1.1. Effects of Mix Parameters on Physical and Mechanical Performance of RRC Mixtures

The effect of the cement dosage (200 and 400 kg/m^3) and aggregate size (D_{max}-12 and 19 mm) on strength was examined for all RCC mixtures, and, as expected, there was an increase in strength with enhanced cement dosage independent of compaction methods. Figure 4.2 show that while D_{max}-19 mm mixtures exhibited higher compressive strength at low cement dosage (200 kg/m^3) than the D_{max} -12 mm mixtures, it was not possible to make such a generalization for high cement dosage mixtures (400 kg/m^3).
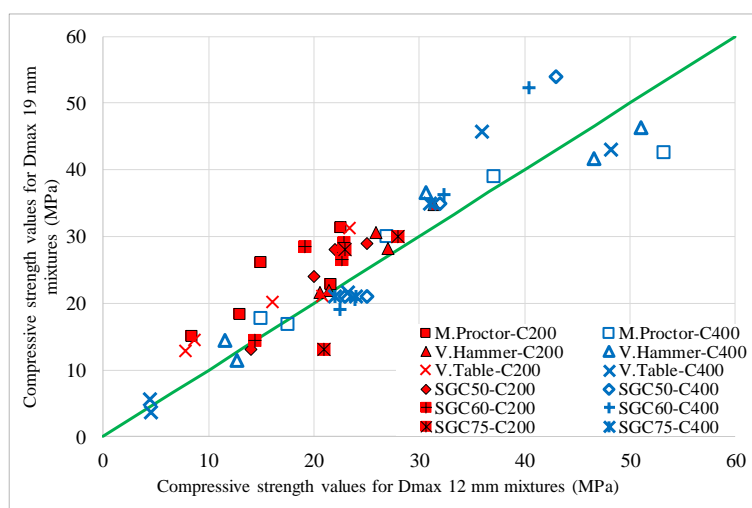
Figure 4.2. A comparison between the compressive test results based on the maximum aggregate sizes for the same RCC mixtures (red 200 kg/m^3 - blue 400 kg/m^3)

Figure 4.3 shows the density-water amount and compressive strength-water amount relationships when the first three compaction methods: modified proctor, vibrating hammer, and vibrating table, were compared.

(a)

(b)
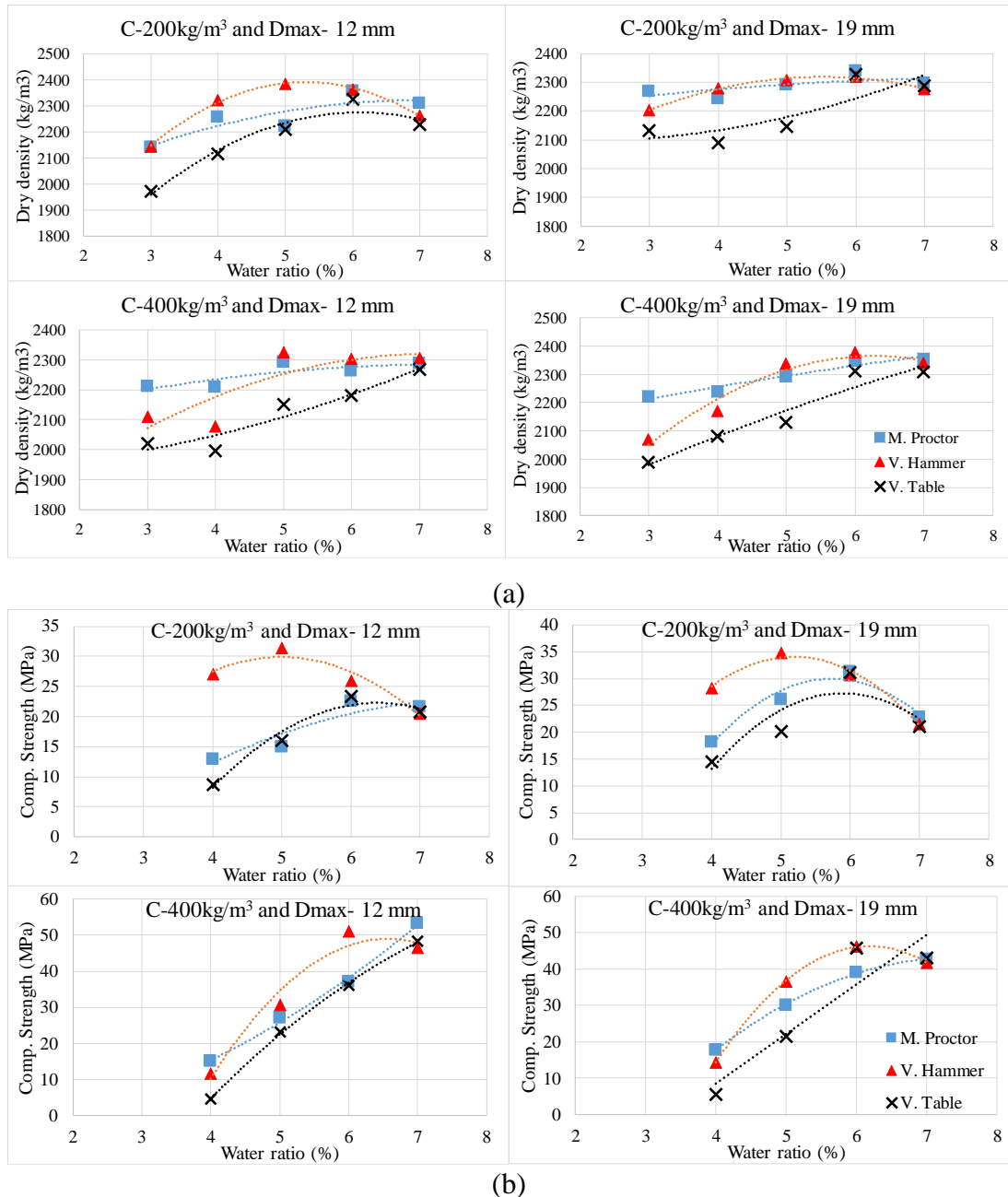
Figure 4.3. a) Density-water ratio and b) compressive strength-water ratio relationship obtained by the production of RCC mixtures by modified proctor, vibrating hammer and vibrating table

Figure 4.3(b) show that the relationship between compressive strength and water amount was generally obtained as a parabolic curve for mixtures with lower cement dosage (200 kg/m^3). Such mixtures show actual soil behavior, and their approximate 5% water content results in maximum compressive strength. However, higher cement dosage mixtures (400 kg/m^3) act as conventional concrete, so for the water content values considered in this study, any increase in water content value results in an increase in compressive strength, so such a clear parabolic curve cannot be drawn. The reason for this behavior lies in the well-known explanation by Abrams, (1918) depicted in Figure 4.4. As the W/C ratio increases, the compressive strength reduction can be represented by a power curve, but this is true only for a fully or well-compacted concrete mixture, and as the W/C diminishes, the specimen compaction will become harder, leading to reduced strength. RCC mixtures fall into the region where increasing the water amount along with adequate compaction will lead to an increase in the compressive strength. For the water amounts used in this study, an increase in water amount for low-cementitious mixtures resulted in a moisture level optimum for achieving the highest compressive strength, although the optimum water amount varies with compaction methods.
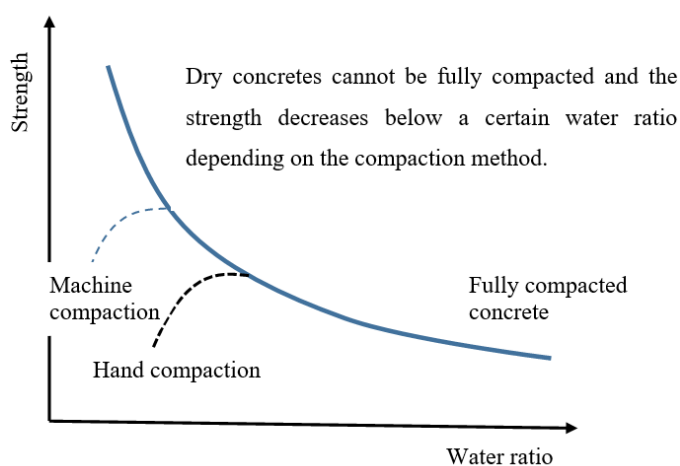
Figure 4.4. Relationship between compressive strength, water ratio and compaction method (Abrams, 1918)

To provide better understanding, the compressive strength of RCC mixtures with respect to water amount for the different compaction methods is also presented in Figure 4.5. As seen in these graphs, for all compaction methods, as the water amount is increased the low-cementitious mixtures represented in red follow a parabolic trend, while the high-cementitious mixtures represented in blue follow a linear trend.
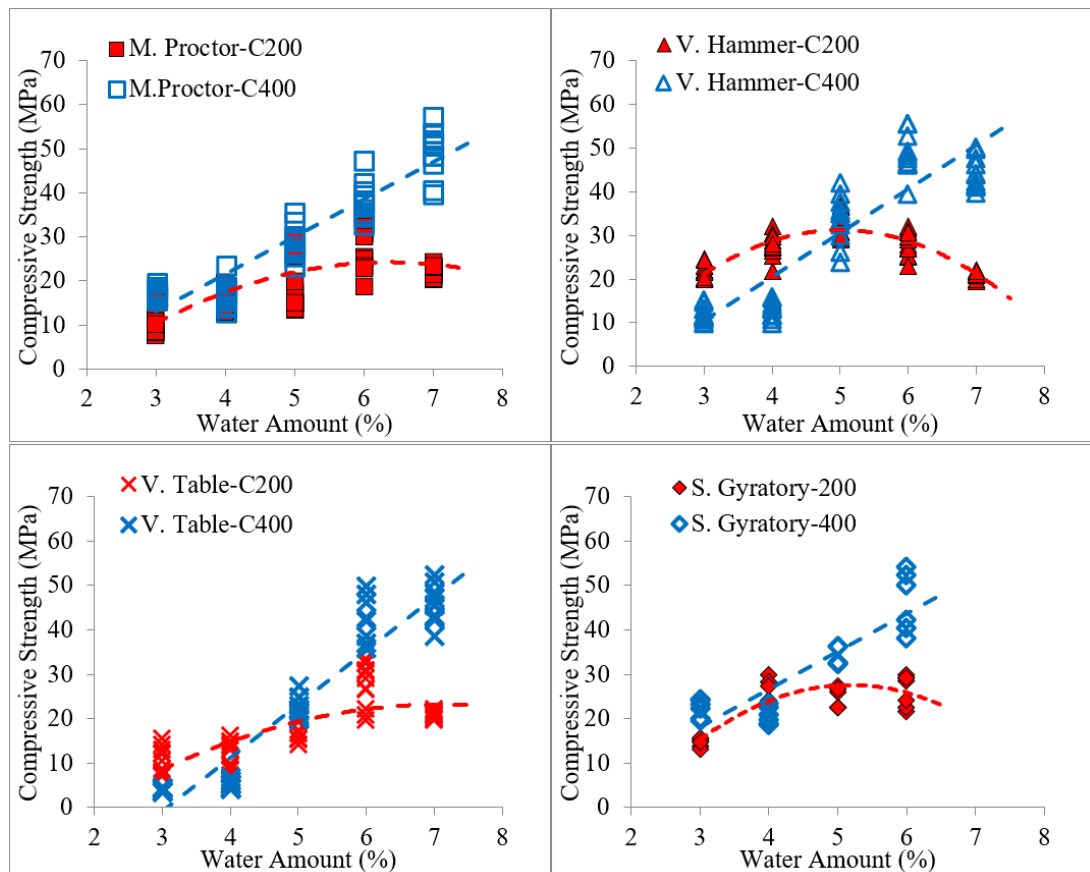
Figure 4.5. Relationship between water amount and compressive strength at 28 days for each compaction method

The results for SGC, another method within the scope of this study, were examined and the effects of gyration numbers on the strength and density of RCC samples were explored. In Figure 4.6, since it can be observed that gyration numbers have no significant effect on strengths and densities of RCC specimens, it can be said that

gyration levels in the range of 50 to 60 gyrations should be selected in order to simulate the actual field conditions in the laboratory.

In Figure 4.7, the compressive and splitting tensile strengths of RCC mixtures compacted at targeted 60 gyrations, specified in the ASTM C1800 standard as recommended gyration numbers for RCC mixtures, are separately compared to those compacted at 50 and 75 gyrations. It can be observed that compressive and splitting tensile strengths of the RCC mixtures were virtually independent of the compaction effort.

When the effect of water amount on RCC compressive strengths and densities for SGC is investigated, while a significant relationship cannot be found for low cement dosage (200 kg/m^3), for high cement dosage (400 kg/m^3) a linear relationship can be observed between water amount and compressive strength, along with a parabolic relationship between water amount and density (Figure 4.8 and Figure 4.9).
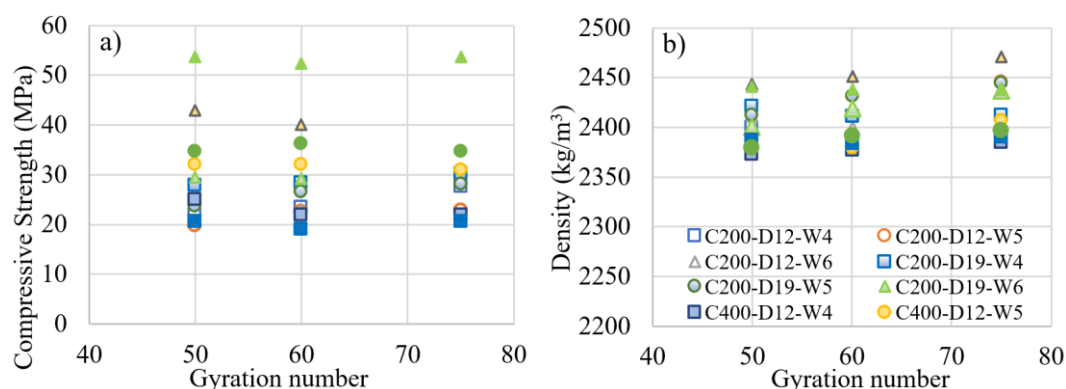
Figure 4.6. Effect of the gyration numbers on RCC mixture design a) 28-day compressive strength (ASTM C39) b) density (ASTM C642)
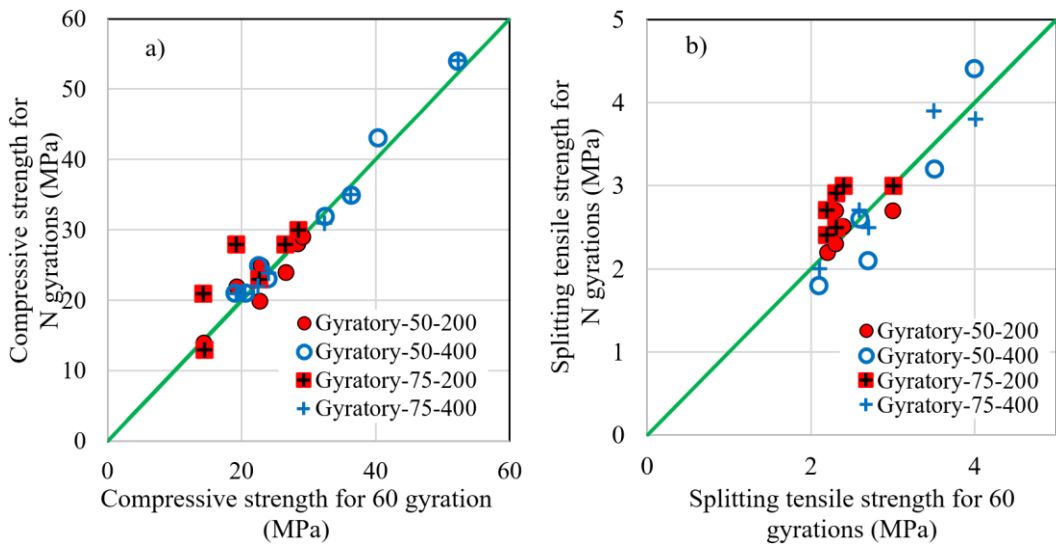
Figure 4.7. a) Compressive strength comparison with respect to gyration numbers, b) Splitting tensile strength comparison with respect to gyration numbers (red 200 kg/m^3 - blue 400 kg/m^3)
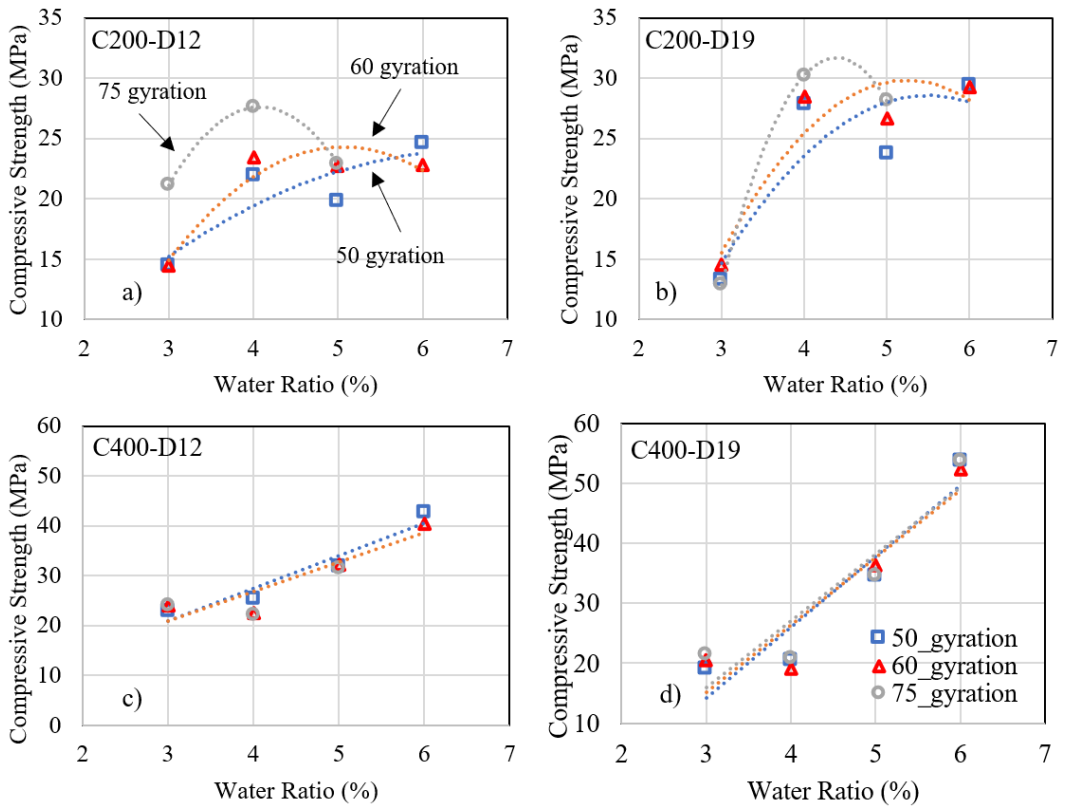
Figure 4.8. Relations between compressive strength and water ratio for SGC method a) C200-D12, b) C200-D19, c) C400-D12, d) C400-D19

It is noteworthy that similar cases have been seen in the literature related to RCC mixtures prepared by SGCs. Those researchers also observed a rising trend between water amount and density rather than the expected parabolic behavior, and noted that water leakage occurred from the equipment above a certain water amount (Amer, et al., 2003, 2004; S. Williams, 2013). Similarly, in this study water leakage occurred at 75 gyrations for mixtures with a 6% water ratio, while water leakage occurred at all gyrations in mixtures with a 7% water ratio during preparation of the SGC samples, so for the SGC method a 5-6% water ratio is determined as the range that can be used in these mixtures without resulting water leakage.
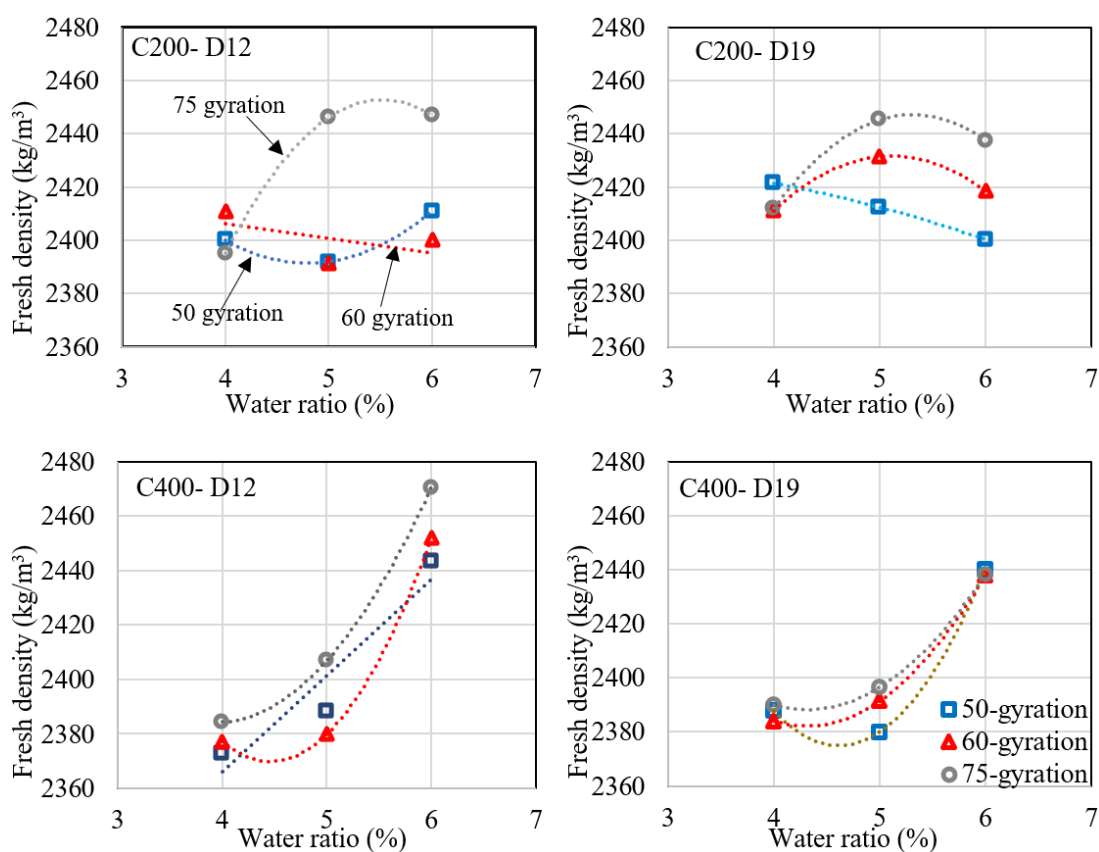
Figure 4.9. Relations between density and water ratio for SGC method a) C200-D12, b) C200-D19, c) C400-D12, d) C400-D19

Compressive strengths obtained from the first four compaction methods were compared for low and high cement mixtures with reference to the vibrating hammer. As can be seen in Figure 4.10, use of the vibrating hammer results in the highest strength for low cement-dosage mixtures, while it gives lower strength than the modified proctor and the SGC for high cement-dosage mixtures, especially at low water ratios (3-4%). Conversely, when the SGC is taken as a reference, it can be seen that higher strength is obtained than for the other three methods for higher cement dosage mixtures (Figure 4.11).
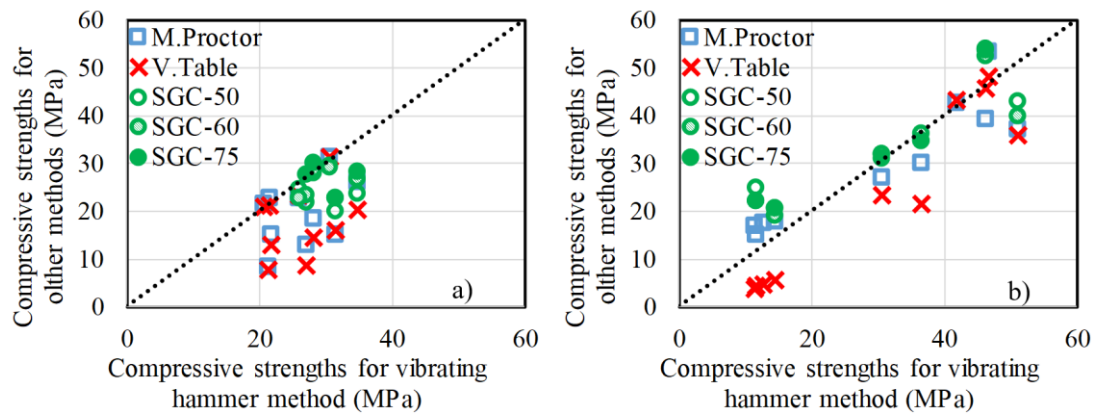
Figure 4.10. Comparison of compressive strengths obtained from the first four compaction methods w.r.t vibrating hammer a) 200 kg/m^3 cement dosage b) 400 kg/m^3 cement dosage

The relationship between concrete consistency (Vebe time) and compressive strength was examined for the first four compaction methods, and the relationships between Vebe consistency time and the compressive strength of all mixtures are also presented in Figure 4.12. From this figure it can be seen that the most appropriate water amounts in the specified Vebe range are approximately 6% for high-dosage mixtures and approximately 5% for low-dosage mixtures. Moreover, the relationship between Vebe time and compressive strength is best described as linear (R^2=0.70) for high cement dosage RCC mixtures, while no relationship (R^2=0.12) was found for low cement dosage RCC mixtures.

99
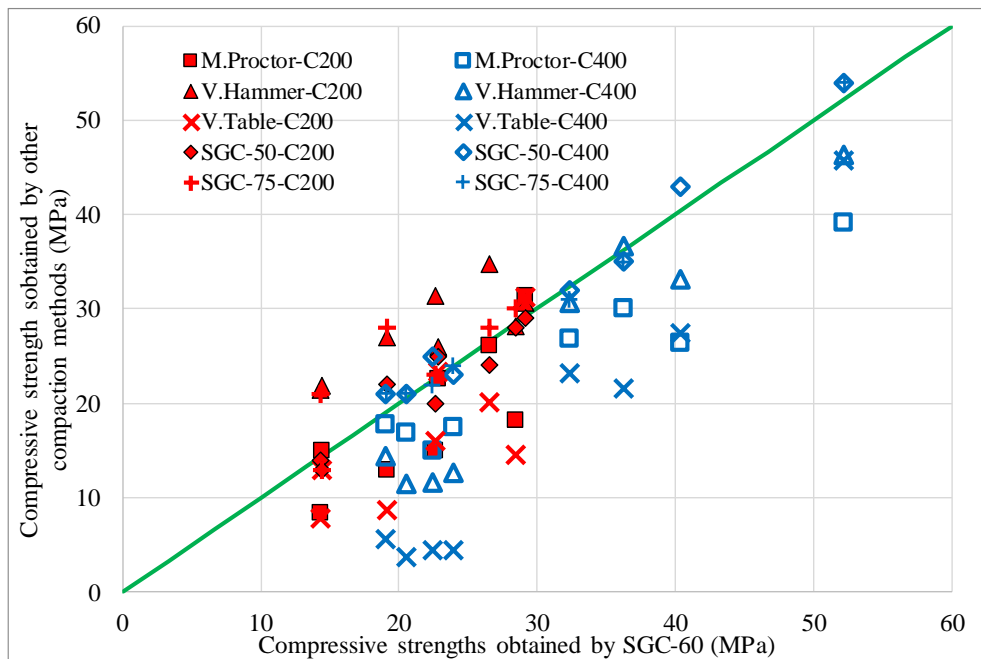
Figure 4.11. Comparison of compressive strengths obtained from the first four compaction methods with reference to SGC (60 gyrations) (red 200 kg/m^3 - blue 400 kg/m^3)
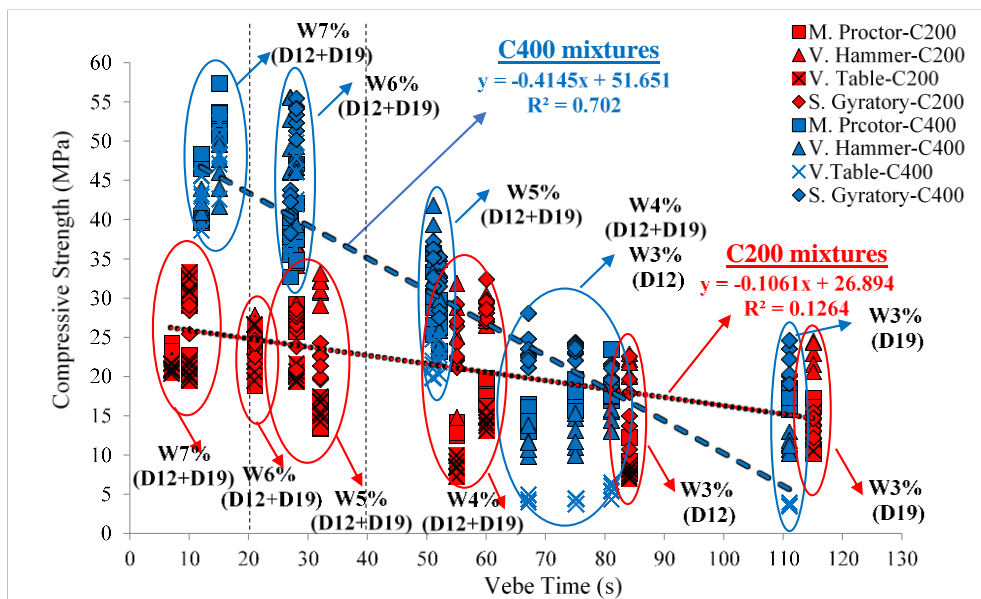
Figure 4.12. The relations between the compressive strength and Vebe time of all RCC mixtures. (red 200 kg/m^3 - blue 400 kg/m^3)

4.1.1.2. Effect of Compaction Ratio on Physical and Mechanical Performance of RRC Mixtures

While the compaction ratio for RCC specimens was calculated based on the maximum theoretical fresh density of concrete (air free) in this study, it is known that the compaction ratio for soil applications is calculated based on dry density. This ratio is used to compare the physical and mechanical properties of the RCC samples produced by different laboratory compaction methods. Eq. (4.1) was used to calculate the compaction ratio of the RCC specimens.

$$\text{Compaction ratio } (\%) = \frac{\text{Fresh Density}}{\text{Theoretical Air Free Density}} \qquad (4.1)$$

The compressive strengths corresponding to compaction ratio of RCC mixtures are shown in Figure 4.13, showing that, for low cement dosage mixtures, compaction ratios of least 96% can be achieved with compressive strengths of 20 MPa, higher for all compaction methods, while for high cement dosage mixtures, compaction ratio of at least 96% yields a strength of 40 MPa or higher.
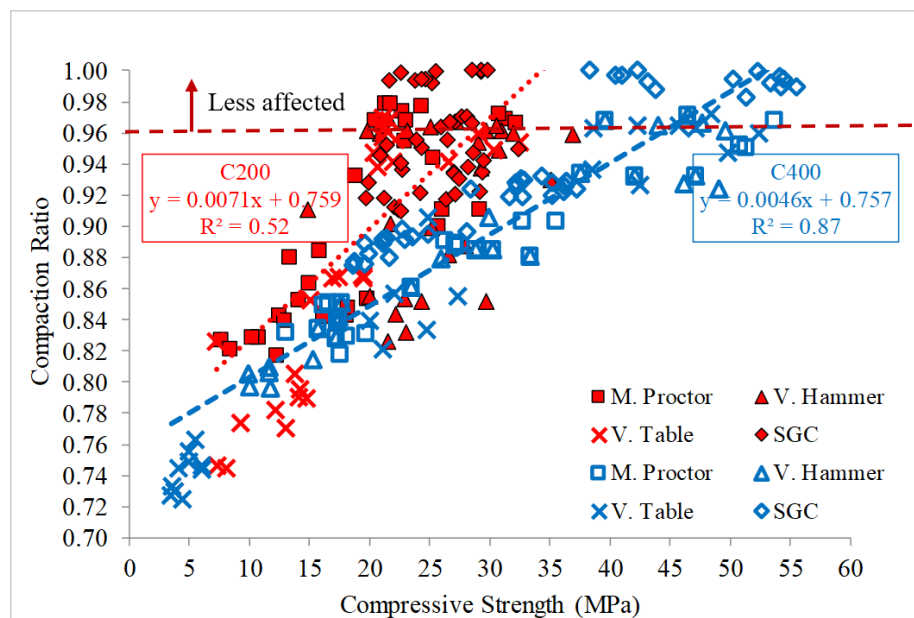
Figure 4.13. Relationship between compressive strength and compaction ratio for RCC mixtures (red 200 kg/m^3 - blue 400 kg/m^3)

As it can be seen in Figure 4.14, the compaction ratio is affected by not only compaction methods but also mixture parameters such as binder dosage and water amount. For all mixes and all compaction procedures, as the amount of water in the mixture increases the compaction ratio approaches 1.0, i.e., the fresh wet density of the sample approaches the theoretical air-free density.

a) C200-D12   b) C200-D19

c) C400-D12   d) C400-D19
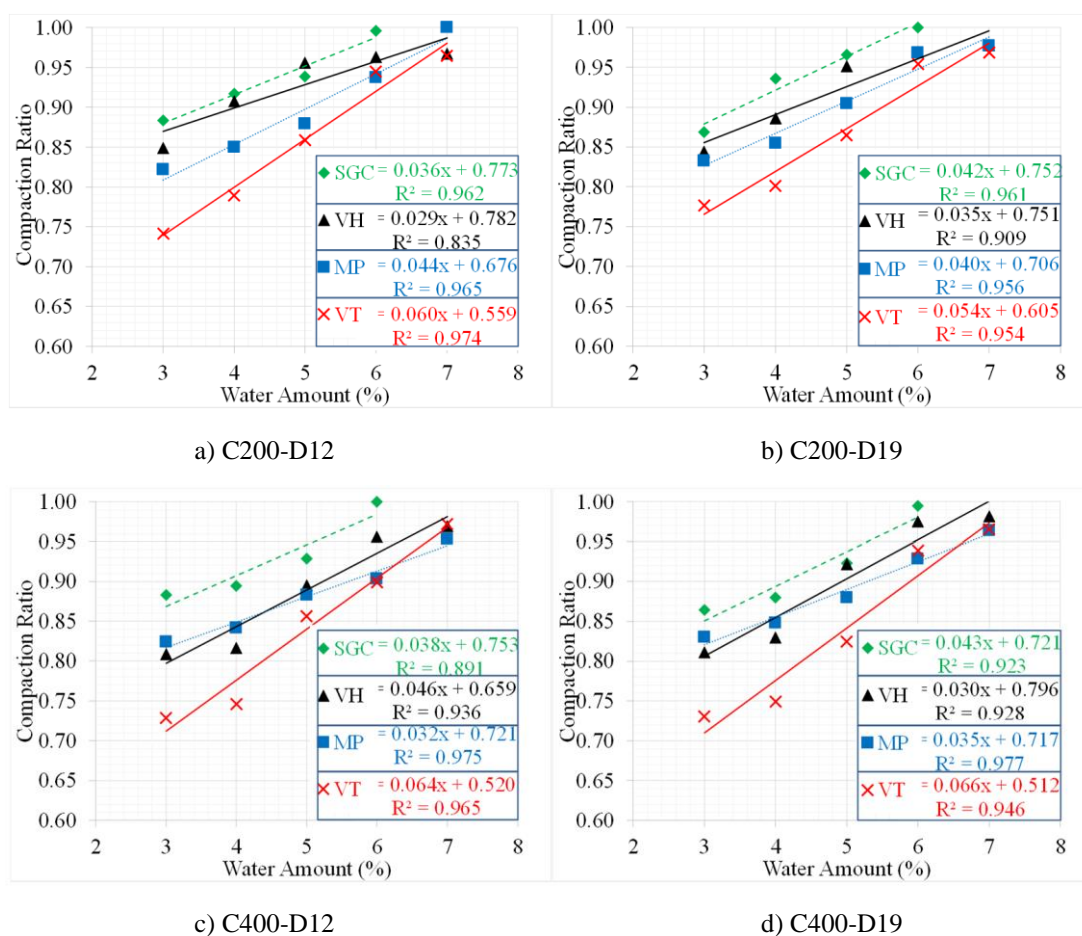
Figure 4.14. Effect of RCC mix parameters on the compaction ratio (VH, MP and VT are abbreviations of vibrating hammer, modified proctor and vibrating table, respectively).

For all mixtures, use of the vibrating table resulted in the least compaction, and SGC resulted in the highest amount of compaction, as can be seen from the red and green regression lines separated from the others. With respect to low cement dosage

mixtures (C200-12 and C200-19), use of the vibrating hammer resulted in a higher degree of compaction than the modified proctor, although the difference was only marginally significant for the high cement dosage mixtures (C400-12 and C400-19). On the other hand, no significant trend was observed with respect to aggregate size, and this is also evident from the regression line parameters provided on the graphs.

The relationship between Vebe consistency time and the compaction ratio is given in Figure 4.15, and the relationship can be seen to take on a logarithmic form for all compaction methods (R^2=0.71-0.93). As the figure shows, when the effects of a change in the compaction method for both low and high cement content RCC mixtures are examined, a considerable change in compaction ratio especially at high Vebe times can be observed, while for Vebe times below 15 seconds the compaction ratio values for the different methods are close to one another. The highest compaction ratio for the same Vebe durations for almost all RCC mixtures was obtained from SGC, vibrating hammer, modified proctor and vibrating table, respectively.
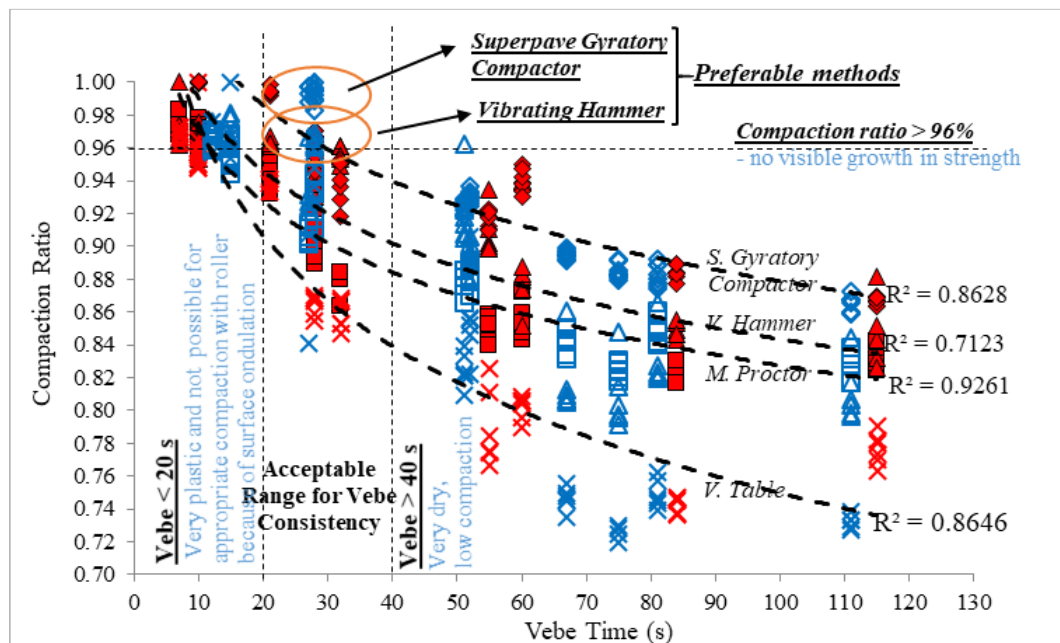
Figure 4.15. Vebe time and compaction ratio relationship (red 200 kg/m^3 - blue 400 kg/m^3).

In this study, when considering strength, density, compaction ratio, and applicability (in the field) of the RCC mixtures, it was found that the ideal water amounts were approximately 6% for high-dosage mixtures and approximately 5% for low-dosage mixtures.

4.1.1.3. Comparison of Laboratory Compaction Methods with DDVHR Practices on RCC Pavement

At the end of this phase, the results obtained from the first four laboratory compaction methods were compared with the core results produced by the DDVHR that simulated field compaction in the laboratory for selected RCC mixtures. The results obtained from the core specimens taken from the plate compacted by a DDVHR are given in Table 4.6. These preliminary results showed that DDVHR compaction methodology can be applied successfully under laboratory conditions with vebe time of about 30 sec. The results of 28-day compressive strength, density, and compaction ratio tests for all the compaction methods were compared with the DDVHR results, as shown in Figure 4.16. The figure shows that the closest results for the DDVHR with respect to 28-day compressive strength, density, and compaction ratio values were obtained for the SGC and vibrating hammer methods.

Table 4.6. *Results of double drum vibratory hand roller (DDVHR) for specified water amounts*

No	Mix ID	Vebe time (s)	Theoretical air free density (kg/m^3)	Fresh Density (kg/m^3)	Dry density (kg/m^3)	Compaction ratio	28-day compr. Strength (MPa)	Cov %	28-day splitting tensile strength (MPa)	Permeable pore voids %
1	C200-D12-W5	45	2505	2370	2266	95%	25	3	1.6	10.4
2	C200-D19-W5	35	2508	2399	2293	96%	30	7	3.3	10.6
3	C400-D12-W5	57	2534	2384	2280	94%	42	1	2.1	10.4
4	C400-D19-W6	23	2502	2400	2302	96%	44	2	3.5	9.8
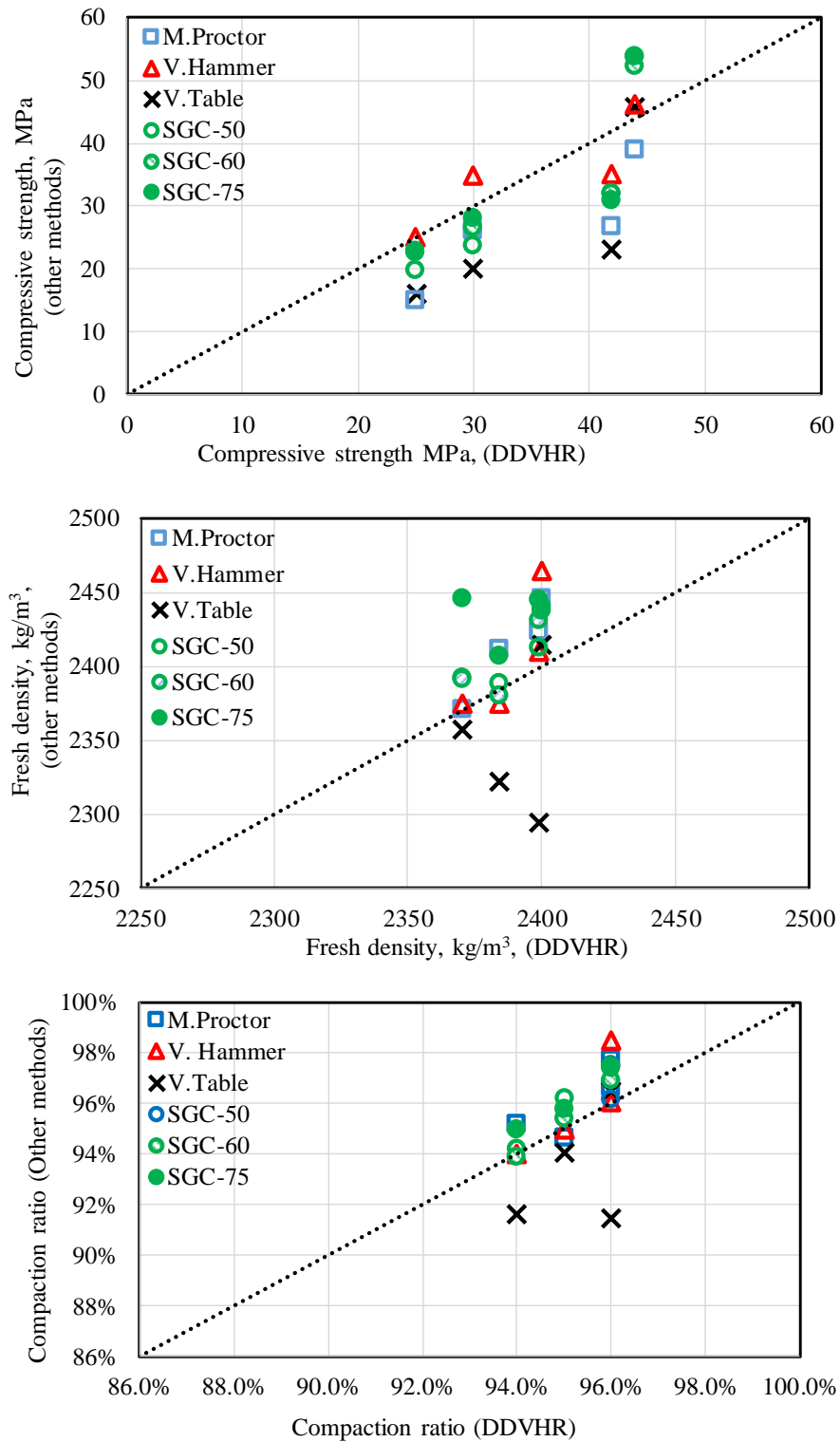
Figure 4.16. Comparison of the results obtained from the DDVHR with the other four laboratory compaction methods a) 28-day compressive strength b) density c) compaction ratio

Figure 4.17 also shows long term-shrinkage results for these RCC specimens, revealing that shrinkage values in 200 kg/m^3 cement dosage specimens were quite low compared to those in 400 kg/m^3 cement dosage mixtures. All shrinkage values were also very low (< 350 µstrain) compared to those of conventional concrete (typically around 600-800 µstrain).
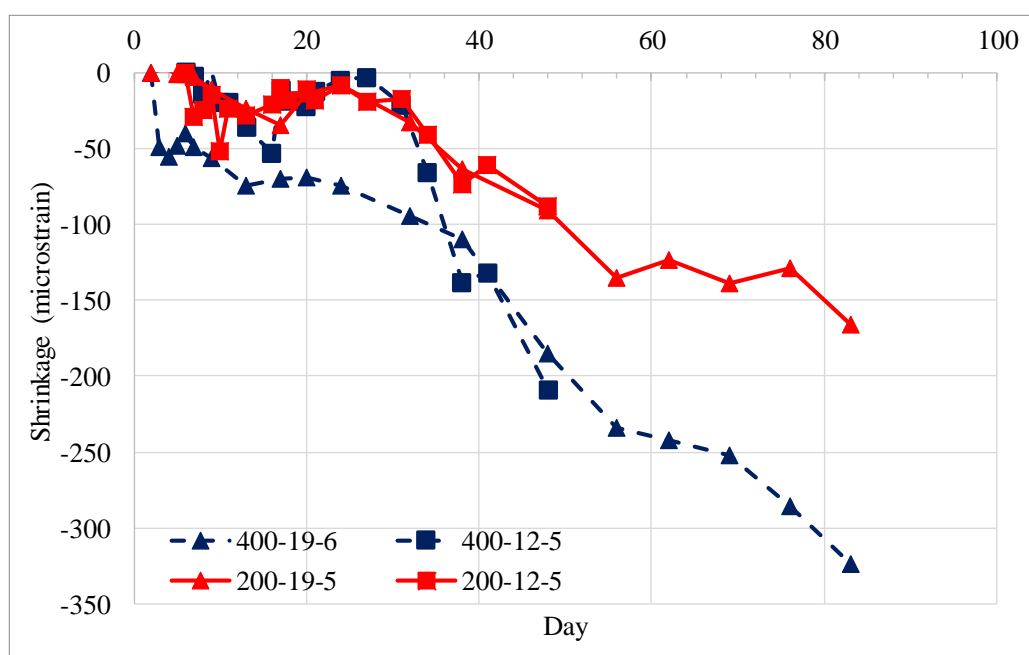
Figure 4.17. The shrinkage results obtained from RCC specimens.

4.1.2. Discussion

In the first phase of the experimental study, a total of 600 cylindrical specimens (15x30 cm^2 and 15x15 cm^2) were produced by four different laboratory compaction methods (modified proctor (ASTM D1557), vibrating hammer (ASTM C1435), vibrating table (ASTM C1176), SGC (ASTM C1800)) and four plate specimens (15x85x200 cm^3) were produced by DDVHR. Vebe consistency test (ASTM C1170), 28-day compressive (ASTM C39) and splitting tensile strength (ASTM C496) and density

106

tests, and water absorption and permeable pore void tests (ASTM C642) were performed on those specimens, leading to the following conclusions:

- Laboratory compaction techniques have a profound effect on the physical and mechanical properties of RCC mixtures. For all mixtures, the vibrating table caused least compaction, while SGC resulted in highest compaction.

- Compaction ratio, which is one of the most important parameters defining RCC properties, is highly affected by not only compaction methods but also mixture parameters such as binder amount and water content.

- The use of a higher cement dosage (400 kg/m^3) both increased density and enhanced compressive strength. In terms of compressive strength, maximum aggregate size has a considerable effect on mixtures with a cement content of 200 kg/m^3, with the 28-day compressive strength values increasing with the use of larger aggregate size. However, this was not true for the higher cement content for which about half of the test results reflected decrease in strength with the larger aggregate. In addition, when the 28-day compressive strength and splitting tensile strength obtained from all RCC specimens were correlated, there was a linear relationship between them.

- For the first three laboratory compaction methods (Modified Proctor, Vibratory Hammer, Vibrating Table), the ideal water ratio for RCC mixture designs was found to be in the range of 5-6%, while the expected ideal parabolic relations between water ratio and density or compressive strength in soils has not been observed in produced RCC mixtures except for when the vibrating hammer method was used. Also, when these three methods are compared, it was found that vibrating hammer use generally led to higher strengths than other methods.

- For RCC specimens prepared by the SGC method, RCC mixtures of 7% water ratio could not be prepared because of water leakage in the SGC equipment. The relationship between water amount and compressive strength for SGC was

also examined, and especially for high cement dosage, a linear increase in compressive strength with water ratio was observed. Similar water leakage and behavior in SGC have also been reported in the literature (Amer et al., 2003, 2004; S. Williams, 2013). The optimum water content for SGC method was determined around 6% in this study, where the ideal water amount was taken to be highest for which no water leakage was experienced by the researchers.

- When the effects of gyration levels for SGC method on compressive strength, density, and water ratio of RCC samples were investigated, it was found that changes in the number of gyrations did not lead to a significant change for 50, 60, and 75 gyrations.

- While the effect of the compaction ratio on the compressive strength of high cement content mixtures is quite clear, it is not very noticeable for mixtures with low cement content. However, for all the mixtures, after a compaction ratio of 96%, this effect becomes even smaller.

- The relationship between compaction method and compaction ratio is significantly affected by Vebe time. For low Vebe times, the compaction ratios for all the methods applied were close to one another, but the differences increase with an increase in Vebe time.

- DDVHR compaction methodology, which can simulate the field compaction procedures, can be applied to produce RCC plates successfully under laboratory conditions with vebe time of about 30 sec.

- The results for cylindrical specimens produced by four laboratory compaction methods and the results for core samples extracted from plates produced by DDVHR for the determined RCC mixtures were compared in terms of compressive strength, density, and compaction ratios, and it was observed that the closest results to the DDVHR were obtained by the SGC and the vibrating hammer methods.

In view of the findings from the first phase of the experimental study, it was clear that it would be more appropriate to design water ratios of RCC mixtures in the range of 5-6% and Vebe times in the range of 30±10 sec for the second phase of the experimental study.

4.2. Phase II Results

In the second phase of the experimental study, in which the mixture design, compaction methodology and testing procedures are explained in detail Chapter 3.2, the compressive and flexural strengths and fracture properties of seven different RCC mixtures are examined. All RCC mixtures were prepared by DDVHR on the plates to simulate the field compaction conditions and core samples were taken from the plates for determination of compressive strengths (ASTM C39) for 2, 7 and 28 days. Four-point flexural strength test (ASTM C78) was carried out on beam specimens cut from the plates to determine the flexural strength of the RCC mixtures for 28 days. Two different test procedures, JCI-S-001-2003, (2003), RILEM TC 89-FMT, (1990), were applied to determine the fracture properties of RCC mixtures. The results of the tests applied to the RCC mixtures in order to determine the fracture parameters and mechanical properties are given in the following section.

4.2.1. Experimental Results

4.2.1.1. Compressive and Flexural Strengths

The theoretical air free density, average Vebe (consistency) time, compaction ratios and compressive strengths after 2,7 and 28 days for seven different RCC mixtures are presented in Table 4.7. The compaction ratio was calculated by dividing the densities of the cores by the theoretical air free density, as explained in Phase I of this study, although in Phase I, fresh densities of samples compacted in cylindrical molds were used to calculate the compaction ratio, while in this phase the average densities obtained from the hardened specimens were used because of inability to measure it from the plate in fresh state. The compressive strength values given in the table show the average value for each age group of at least four Ø15 /15 cm core samples taken

from the plate. In addition, for comparison, three Ø15/30 cm cylindrical molds for each mixture were prepared using the vibrating hammer (ASTM C1435), and the 28-day compressive strength results are also given in Table 4.7. While the water ratios of the RCC mixtures were determined with reference to Vebe times of about 30 seconds, for 300 kg/m^3 and 600 kg/m^3 binder dosage mixtures, it was realized that the consistency was slightly higher expected, so the Vebe times decreased to approximately 20 seconds, as shown in Table 4.7. It is believed that this might have been caused by the fine aggregate containing a little more moisture during mixture preparation. High mixture consistency resulted in undulations in some parts of the RCC surface during compaction of 300 kg /m^3 binder dosage mixtures with DDVHR. On the other hand, as expected, RCC mixtures began behaving as normal concrete with an increase in consistency and more compaction was observed.

Table 4.7. *Average Vebe time, compaction ratio (CR) and compressive strength at 2,7 and 28 days for RCC mixtures.*

Physical properties of RCC mixtures					2, 7 and 28 days compressive strength of RCC mixtures				
					DDVHR			V. Hammer	
No	Mix ID	TAFD	Vebe time (sec)	CR (%)	2 days (MPa)	7 days (MPa)	28 days (MPa)	CR (%)	28 days (MPa)
1	C200-D12-W5	2498	32	95.1	16.6 [4.7]	22.6 [5.8]	26.9 [4.9]	98.8	36.0 [4.4]
2	C200-D19-W5	2504	32	97.0	18.9 [4.6]	23.8 [4.3]	29.0 [9.3]	99.5	37.4 [3.8]
3	C300-D12-W5.5	2495	22	98.6	22.0 [9.4]	30.2 [9.8]	**40.6** [6.6]	98.9	**46.7** [10.6]
4	C300-D19 W5.5	2501	20	97.8	23.0 [4.6]	29.0 [8.6]	**43.3** [7.1]	98.4	**47.9** [11.0]
5	C400-D12 W5.5	2510	35	95.3	26.3 [6.1]	29.5 [9.9]	39.2 [3.9]	98.0	56.8 [9.3]
6	C400-D19 W5.5	2515	32	94.6	26.9 [2.6]	30.4 [6.5]	31.3 [4.3]	98.9	50.2 [9.9]
7	B600-D12 W8.5	2408	21	99.0	31.0 [4.4]	36.8 [7.6]	**48.0** [3.7]	98.1	**45.5** [9.1]

Note: Values in boldface indicate statistical similarity between vibrating hand roller and vibrating hammer for 28-day compressive strength.

Figure 4.18 shows the observed increase in compressive strength as the binder dosage and specimen age. However, the maximum aggregate size used in the mixtures was found to be less effective with respect to compressive strength (Figure 4.18), while the 28-day compressive strengths obtained by DDVHR, representing the field, were lower than the compressive strengths of samples obtained with a vibrating hammer, representing laboratory compaction conditions. Considering all the mixtures, the average compressive strength of DDVHR was 25% lower than when using the vibrating hammer, not only for the last mixture expected to yield high strength and durability, with both compaction procedures yielding statistically-similar results. While these results were significant in terms of the extent to which the compaction process can affect the compressive strength of RCC mixtures, a t-test with 95% confidence revealed that 28-day compressive strength pairs of DDVHR cores and laboratory vibrating-hammer specimens (for RCC mixtures with an approximate 20-second Vebe consistency time) produced the same results statistically, and this might have caused the convergence of compaction ratios with increasing consistency. As expected, with an increase in consistency, RCC began to exhibit conventional concrete behavior and yielded higher compaction ratios.

As it can be seen in Figure 4.18, 300 kg/m^3 binder dosage mixtures exhibited higher 28-day compressive strengths than 400 kg/m^3 binder dosage mixtures due to the previously-mentioned Vebe times and higher compaction ratios. That is, the increase in the consistency of the mixture resulted in a higher compaction ratio, leading to an increase in compressive strength. On the other hand, some problems with surface roughness and undulations were encountered during compaction of higher consistency mixtures with the DDVHR. In other words, even though increasing the consistency of RCC mixtures leads to higher compaction ratios of compressive strength values, it can cause RCC insufficiency in carrying the weight of the vibratory roller in fresh states, possibly resulting in surface problems during field application. It is therefore vital to take into consideration the Vebe consistency time of the RCC laboratory studies to obtain results consistent with field conditions.
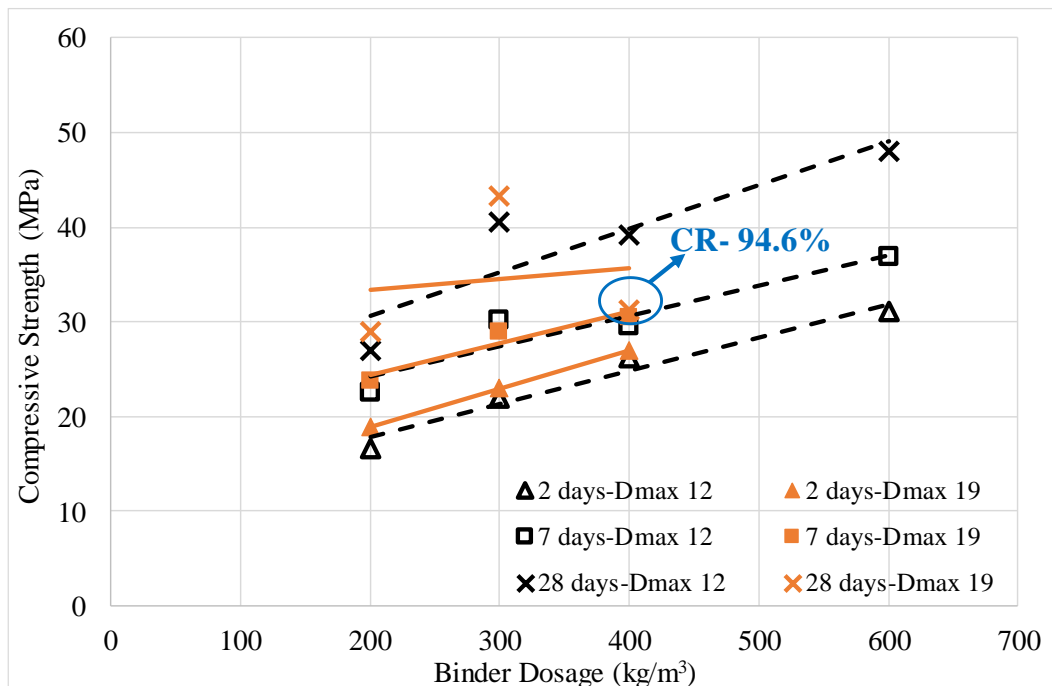
Figure 4.18. Relationship between cement dosage and compressive strength of 2, 7 and 28 days for DDVHR.

It was also observed that RCC mixtures reached about 65% of their nominal strengths after 2 days, making them sufficiently strong for carrying light traffic even at the lowest cement dosage (> 15 MPa) (Harrington, et al., 2010). The mixtures also reached about 80% of their nominal strength after 7 days, (Figure 4.19), one of the essential factors that can separate RCC from traditional concrete in pavement application.

Four-point bending tests (ASTM C78) were performed on four beam specimens of geometry $10\times10\times35$ cm^3 cut from the plates for determination of flexural strengths after 28 days (Figure 4.20), with a servo-hydraulic MTS (Landmark 250 kN) displacement-controlled test machine used for the flexural test. The rate of displacement was 0.5 mm/min for the flexural test. The results of flexural strength of average four beams for RCC mixtures are given in Table 4.8.
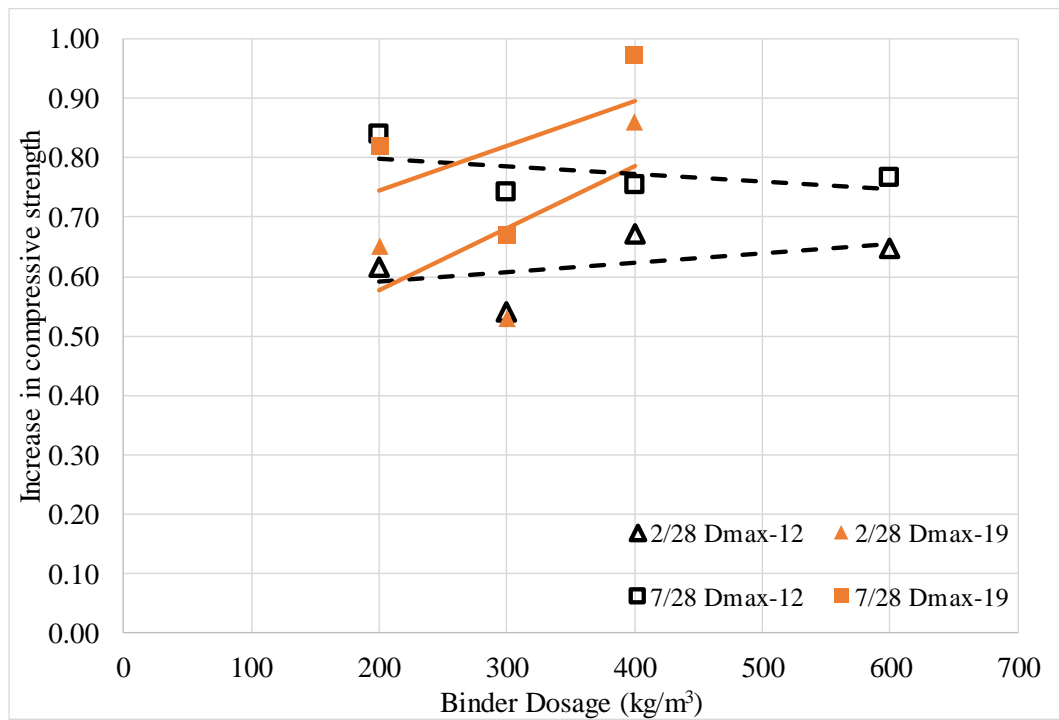
Figure 4.19. Relationship between cementitious dosage and compressive strength development with respect to concrete age for DDVHR.

Figure 4.20. Determination of flexural strength of RCC mixtures according to ASTM C78.

113

Table 4.8. *Average 28-day flexural strength values and coefficient of variations of RCC mixtures*

No	Mix ID	Maximum Load* (P)	Span Length (L)	Beam width* (b)	Beam depth* (d)	Modulus of Rupture MR	
						Mean	CoV
		N	mm	mm	mm	MPa	%
1	C200-D12-W5	11676	300	95.0	93.5	**4.22**	7.5
2	C200-D19-W5	12813	300	92.6	102.2	**4.19**	13.3
3	C300-D12-W5.5	15423	300	101.5	102.9	**4.33**	10.7
4	C300-D19-W5.5	15018	300	100.5	101.4	**4.35**	4.9
5	C400-D12-W5.5	16168	300	101.6	101.4	**4.64**	9.0
6	C400-D19-W5.5	14577	300	102.2	105.6	**3.84**	5.0
7	B600-D12-W8.5	18615	300	95.7	101.0	**5.65**	4.4

*It was measured separately for each specimen and the average value is given in the table.

As it can be seen in Table 4.8 and Figure 4.21, there was no clear relationship between flexural strengths of the RCC mixtures and binder dosage and the maximum aggregate size. Because the C400-D19 mixture with the lowest degree of compaction (94.6%) (Table 4.7), showed the lowest performance with flexural strength. It is seen that compaction ratios of RCC specimens also affected flexural strength results as in the compressive strength results. At this point, it should be noted that the beams were subjected to two cutting operations; they were first removed from the plate, after which the specimen height was reduced to 10 cm. As expected, the highest flexural strength was obtained from the blended mixture (B600-D12) that, was planned to have high strength and durability.
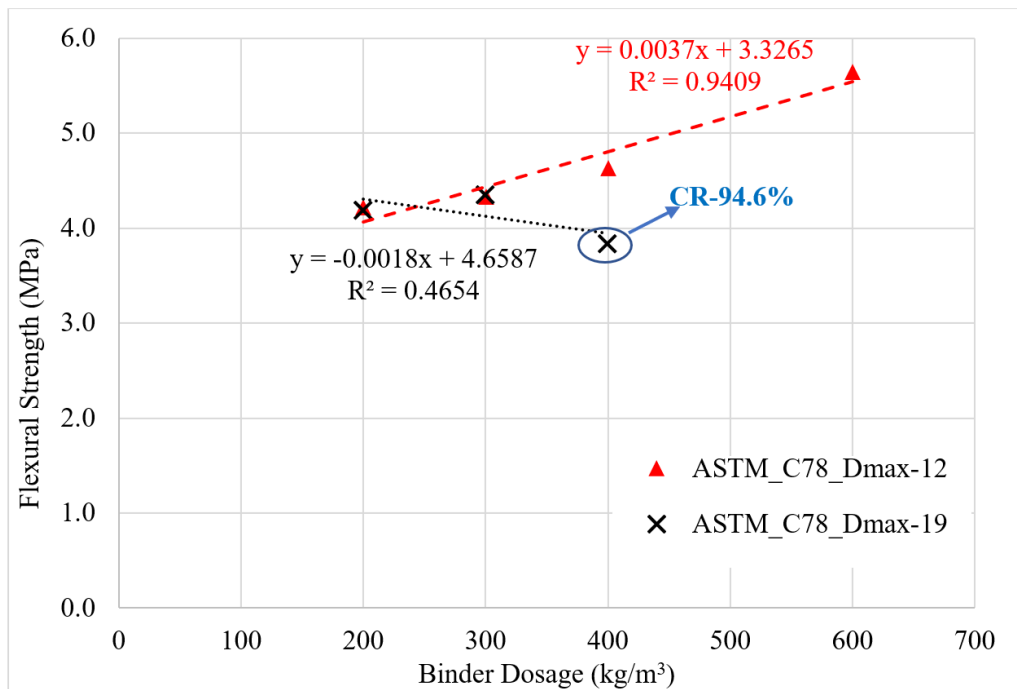
Figure 4.21. Relationship between binder dosage and flexural strength.

4.2.1.2. Fracture Parameters - RILEM Procedure

The RILEM (TC 89-FMT 1990) procedures based on nonlinear TPFM (Jenq and Shah 1985), described in detail in the previous section, were applied on beam specimens with the dimensions specified in

Figure 3.25. Three-point bending tests were conducted at a constant crack mouth opening displacement (CMOD) rate using a closed-loop servohydraulic universal testing machine, the MTS Landmark, with a capacity of 250 kN, as shown in Figure 4.22. The loading rate was set at 0.02 mm/min.

The testing guidelines require that after the beam reaches its ultimate strength and the load begins to decrease, the specimen should be unloaded at 95% of peak load. When the applied load comes down to zero, the reloading process is applied, and this

procedure continues until the specimen fails. Each beam was subjected to one such cycle of loading-unloading, as shown in Figure 4.23.

Figure 4.22. Three-point bending fracture test (RILEM TC 89-FMT 1990) on notched RCC specimen.
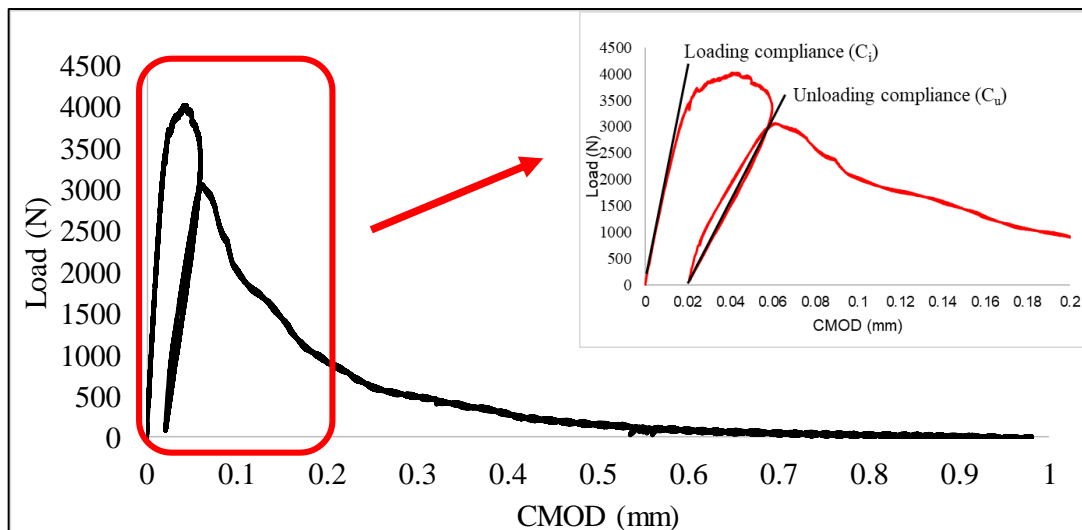
Figure 4.23. Loading and unloading compliances (C_i and C_u) from Load-CMOD curve (C400-D19-W5.5).

As part of the TPFM (Jenq & Shah, 1985), the loading and unloading CMOD compliance values (C_i and C_u) were calculated to determine the fracture parameters as the inverses of the slopes of the loading and unloading curves, respectively.

For those calculations, Young Modulus (E) was first calculated to determine the value of the effective crack length (a_c) from Eq. (4.2).

$$E = \frac{6Sa_0V_1(\alpha_0)}{C_id^2b}$$

$$V_1(\alpha_0) = 0.76 - 2.28\,\alpha_0 + 3.87\,\alpha_0{}^2 - 2.04\,\,\alpha_0{}^3 + \frac{0.66}{(1-\alpha_0)^2}$$

$$\alpha_0 = (a_0/d)$$

(4.2)

where S=span length, a_0=initial notch depth, d= depth, b= width, C_i= initial loading compliance value, $V_1(\alpha_0)$=geometric factor for the beam specimen, and α_0=initial notch depth ratio,1/3.

The critical effective crack length, a_c, can be then calculated from Eq. (4.3).

$$a_c = \frac{EC_ud^2b}{6SV_1(\alpha_c)}$$

$$V_1(\alpha_c) = 0.76 - 2.28\,\alpha_c + 3.87\,\alpha_c{}^2 - 2.04\,\alpha_c{}^3 + \frac{0.66}{(1-\alpha_c)^2}$$

$$\alpha_c = (a_c/d)$$

(4.3)

where a_c= critical effective crack length, and C_u= unloading compliance value.

After the critical effective crack length, a_c, has been determined, the critical stress intensity factor or fracture toughness, $K_{Ic}{}^s$, can be calculated using Eq. (4.4).

$$K_{Ic}{}^s = 3(P_{max} + 0.5\,W_0S/L)\frac{S\sqrt{\pi a_c}F(\alpha_c)}{2d^2b}$$

$$F(\alpha_c) = \frac{1.99 - \alpha_c\,(1-\alpha_c)(2.15 - 3.93\,\alpha_c + 2.7\,\alpha_c{}^2)}{\sqrt{\pi}(1 + 2\,\alpha_c)(1-\alpha_c)^{3/2}}$$

(4.4)

where P_{max} = the measured maximum load, W_0=self-weight of the beam.

Finally, the critical crack tip opening displacement can be calculated using Eq. (4.5).

$$CTODc = \frac{6P_{max}Sa_cV_1\ (\propto_c)}{Ed^2b}\sqrt{[(1-\beta)^2 + (1.081 - 1.149 \propto_c)(\beta - \beta^2)]}$$

$$\beta = (a_c/a_0)$$

(4.5)

The initial fracture energy (or energy release rate), G_f, can also be determined based on the values of K^s_{IC} and modulus of elasticity, E, for plane stress, using Eq. (4.6).

$$G_f = \frac{(K^s_{IC})^2}{E}$$

(4.6)

In this study, K^s_{Ic} which indicates that the critical stress intensity factor or fracture toughness is obtained from TPFM was expressed with the typical K_{Ic} abbreviation.

Figure 4.24 shows the load-CMOD graphs required for determination of fracture parameters according to the RILEM TC 89 FMT procedure for seven different RCC mixtures.
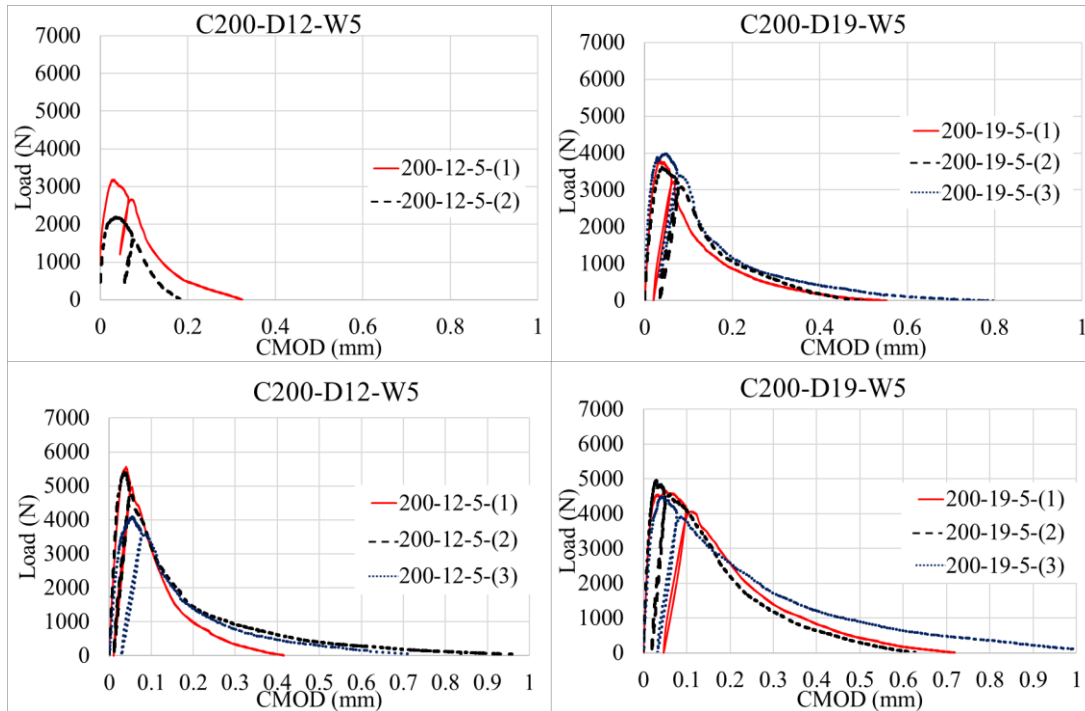
(a) 200 kg/m³ binder dosage RCC mixture (tests were repeated with new mixture due to damage of the sample before the test)
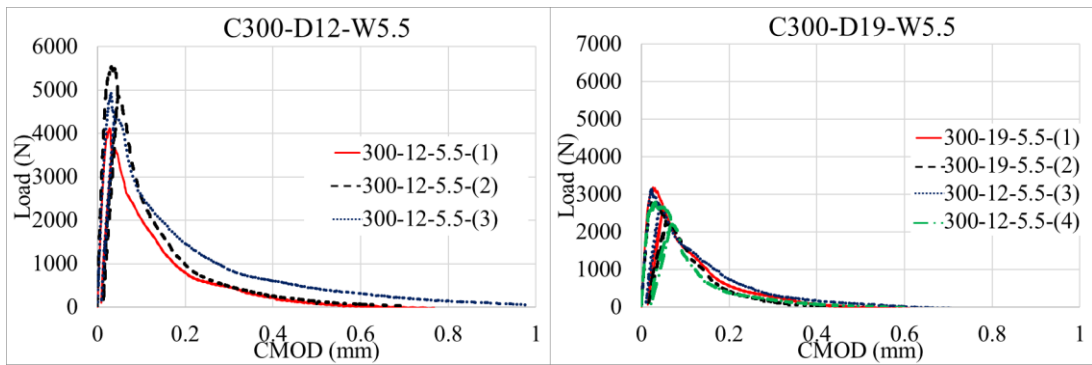
(b) 300 kg/m³ binder dosage RCC mixture
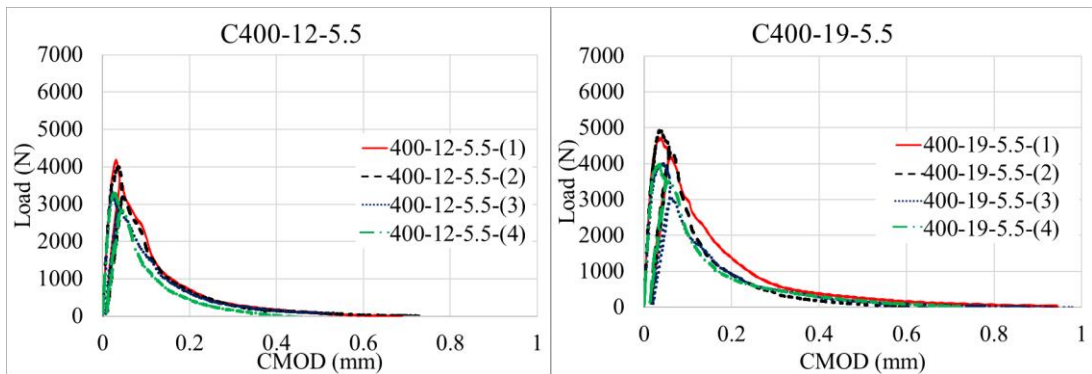
(c) 400 kg/m³ binder dosage RCC mixture
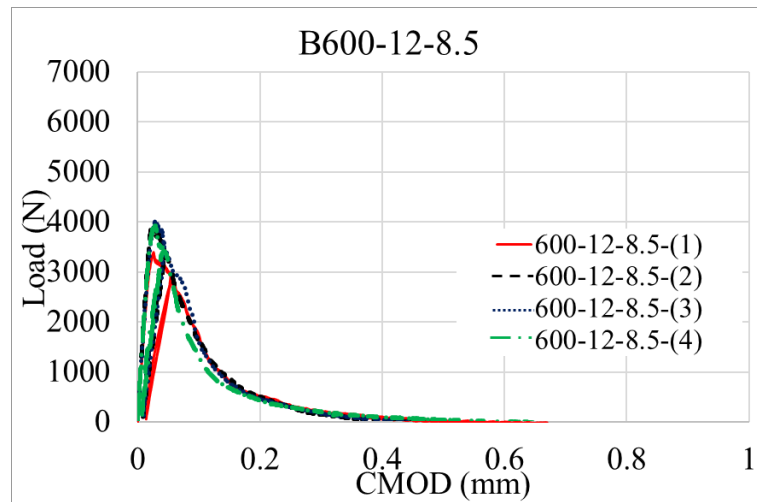
(d) 600 kg/m³ binder dosage RCC mixture

Figure 4.24. The load-CMOD graphs obtained by RILEM TC 89 FMT procedure for seven different RCC mixtures.

For each RCC mixture, required for the RILEM fracture equations (Eq. 4.2-6) , the average specimen geometry values and input parameters such as maximum load (P_{max}), and loading and unloading compliances (C_i and C_u) are presented in Table 4.9(a).

 The average fracture parameters -the modulus of elasticity (E), the critical effective crack length (a_c), the critical stress intensity factor (K_{Ic}), the critical crack-tip opening displacement ($CTOD_c$), and the energy release rate/initial fracture energy (G_f) obtained from RILEM fracture equations (Eq. 4.2-6) for each RCC mixture are shown in Table 4.9(b). As can be seen in that table, the coefficient of variations values is generally lower than values obtained from fracture tests found in the literature for conventional concrete, where it is recommended to set the coefficient of variation limit to 20% for K_{Ic} and 40% for $CTOD_c$ (Shi et al., 2018).

TPFM contains two valid fracture parameters for cementitious materials, the critical stress intensity factor (K_{Ic}) and the critical crack-tip opening displacement ($CTOD_c$), and the other parameters, maximum load (P_{max}), modulus of elasticity (E), and critical effective crack length (a_c), can be derived to find these two parameters. The relationships between these parameters and the RCC mixture properties represented by the aggregate size and the binder content are shown in Figure 4.25.

The first remarkable result is that the critical stress intensity factor or fracture toughness (K_{Ic}) of mixtures, which is a measure of the resistance to crack propagation in materials, were found higher than 1.0 MPa.m$^{1/2}$ even in the lowest dosage mixture which is the typical value of conventional concrete pavements. In addition, the highest K_{Ic} was obtained from C300-D19 mixture. However, this result may be related to size effect since the average specimen's width and depth of this mixture were smaller than other mixtures as shown in Table 4.9(a).

It was also observed that K_{Ic} enhanced with the increase of binder dosage in RCC mixtures as shown Figure 4.25(c). Similarly, with the increase of the maximum aggregate size, the growth in stress intensity factor was detected in all RCC mixtures,

and this amount of growth varied between 11% and 15% depending on the binder content. The results also showed that the critical stress at which a crack occurs was higher in D_{max} 19 mm than D_{max} 12 mm.

Table 4.9. *Fracture test results of RCC mixtures according to the RILEM TC 89-FMT (1990) procedure*

(a) Average of the measured geometric data for each specimen.

No		1	2	3	4	5	6	7
Mix ID		C200 - D12- W5**	C200 - D19- W5**	C300 - D12- W5.5	C300 - D19- W5.5	C400 - D12- W5.5	C400 - D19- W5.5	B600 - D12- W8.5
Beam weight* W_0	kg	27.3	24.1	21.8	16.2	18.5	19.7	17.9
Beam length* L	mm	676	648	733	669	663	660	645
Span length* S	mm	600	600	600	600	600	600	600
Beam width* b	mm	122.3	106.0	81.2	75.0	81.0	81.9	83.2
Beam depth* d	mm	150.1	151.1	144.1	132.5	143.9	150.1	144.9
Notch depth* a_0	mm	52.00	45.00	37.65	41.60	44.98	43.94	49.31
Initial compliance* C_i	-	4.91E-06	3.69E-06	3.74E-06	5.44E-06	5.08E-06	4.33E-06	5.34E-06
Unloading compliance* C_u	-	9.87E-06	1.09E-05	6.94E-06	1.51E-05	1.02E-05	1.05E-05	1.16E-05
Max. crack mouth opening displacement* CMODc	mm	0.71	0.78	0.81	0.66	0.67	0.83	0.65
Max. load* P_{max}	kN	4.72 [19.1]	4.73 [4.3]	4.88 [14.8]	3.13 [11.0]	4.08 [10.9]	4.52 [9.5]	3.98 [11.0]
Theoretical flexural strength* σ_{tfs}	MPa	3.84 [3.7]	3.61 [4.3]	4.78 [2.4]	4.55 [3.4]	4.32 [9.8]	4.44 [14.2]	4.62 [3.7]

* It was measured separately for each beam sample and the average value is given in the table.
** Tests were repeated with new mixture due to damage of sample before the test.

No	Mix ID	Modulus of Elasticity E (GPa)	Critical Effective Crack Length α_c (mm)	Critical Stress Intensity Factor K^s_{IC} (N/m$^{3/2}$)	Critical Crack Tip Opening Displacement CTOD$_c$ (mm)	Energy Release Rate/Initial Fracture Energy G_f (N/m)
1	C200-D12-W5*	27.36 [6.3]	71.26 [12.2]	1.07 [2.5]	0.0139 [1.3]	41.76 [1.3]
2	C200-D19-W5*	32.05 [10.9]	74.90 [7.7]	1.23 [9.9]	0.0153 [22.5]	48.43 [28.6]
3	C300-D12-W5.5	35.39 [2.6]	54.47 [9.92]	1.26 [8.6]	0.0127 [19.0]	45.03 [20.2]
4	C300-D19-W5.5	38.25 [6.0]	66.23 [7.8]	1.42 [10.3]	0.0136 [17.8]	53.04 [25.2]
5	C400-D12-W5.5	33.71 [3.8]	65.16 [4.8]	1.19 [11.0]	0.0128 [9.0]	44.91 [17.2]
6	C400-D19-W5.5	34.62 [13.3]	69.05 [3.8]	1.37 [11.2]	0.0156 [5.2]	54.52 [12.9]
7	B600-D12-W8.5	37.61 [4.9]	70.73 [4.1]	1.32 [4.7]	0.0127 [8.5]	46.64 [9.5]

*The results obtained from the new mixtures.

The second fracture parameter calculated by TPFM is CTOD$_c$; it provides an idea of the fracture behavior and the crack in the material. It was observed that an increase in the size of aggregates led to an increase in CTOD$_c$ as in K_{Ic} results. The increase in fracture parameters values associated with an increase in the size of aggregates can be explained by the bridge effect in concrete (B. Wang, Zhang, Dai, & Xu, 2011; Zhou, Barr, & Lydon, 1995). Unlike K_{Ic}, while CTOD$_c$ exhibited a downward trend with an increase in binder dosage, no clear behavior was observed for the maximum aggregate size of 19 mm, while the effect of the compaction ratio on fracture parameters was significant as it was for strength behavior. The fracture parameters exhibited trends different from the overall trend in 300 and 400 binder-dosage mixtures, the second highest (98.6%) and the lowest (94.6%) compaction ratio, respectively.

(a) Modulus of elasticity   (b) Critical effective crack length

(c) Critical stress intensity factor   (d) Critical crack tip opening displacement

(e) Initial fracture energy
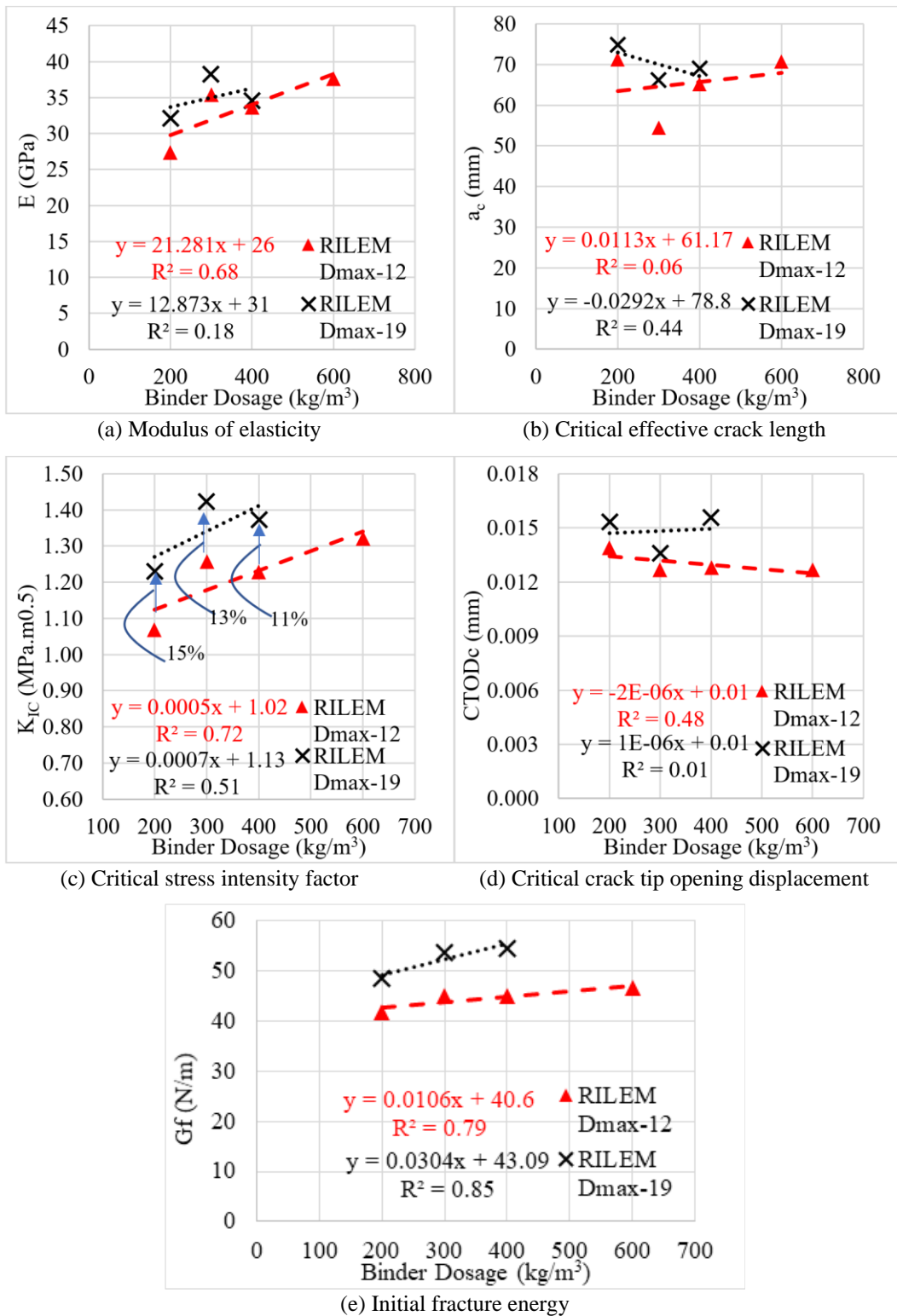
Figure 4.25. Relationship between fracture parameters obtained by RILEM procedure and binder dosage.

Relationships between fracture parameters and strengths are shown in Figure 4.26. The relationship between all fracture parameters and strengths was found to exhibit a linear relationship for small maximum aggregate size RCC mixtures, while it was not valid for mixtures with a maximum aggregate size of 19 mm. K_{Ic} increased linearly with an increase in compressive strength for all RCC mixtures, and the crack resistance for the maximum aggregate size of 19 mm RCC mixtures was higher than that for 12 mm at the same compressive strength, and these results are consistent with the literature for conventional and high strength concrete (Jenq & Shah, 1985; Sarker, Haque, & Ramgolam, 2013; B. Wang et al., 2011; Zhou et al., 1995). Simply put, when cracks propagate, they require higher energy to go around or through larger aggregate. Unlike the K_{Ic}, $CTOD_c$ that tended to decrease with an increase in compressive strength except for one mixture (C400-D19), (Figure 4.26 (b)). As expected, the specimens exhibited more brittle behavior through an increase in compressive strength from a reduction of the water-binder ratio in the mixtures. At this point, $CTOD_c$ might also be reduced by increasing the brittleness of RCC mixtures, although it can be seen that there is no agreement in published studies about the effect of the compressive strength on $CTOD_c$ for normal concrete. Some studies, for example, state that the effect of compressive strength on $CTOD_c$ is negligible (Lin, Jin, & Li, 2004; Wang, et al., 2011), while another study asserted that $CTOD_c$ decreases with an increase in compressive strength when the aggregate size remains constant (Zhao & Xu, 2001).
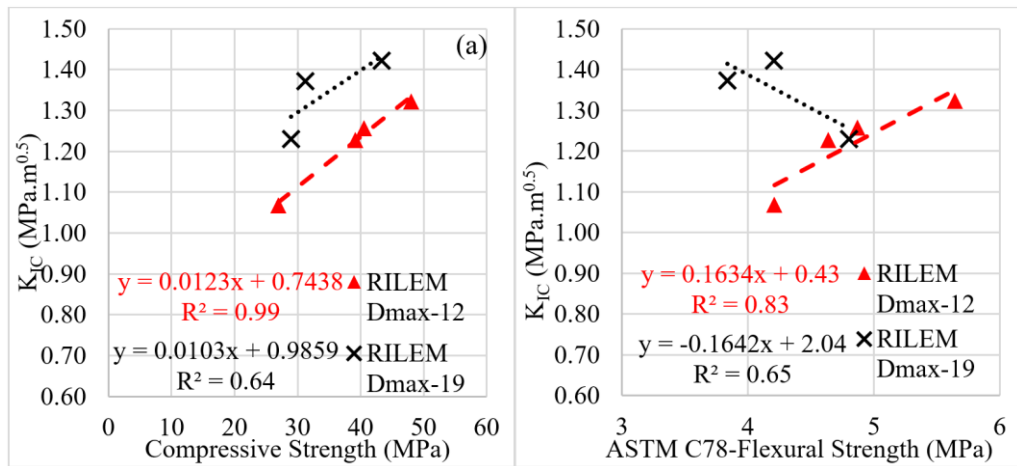
(a) Critical stress intensity factor/fracture toughness (K_{Ic})
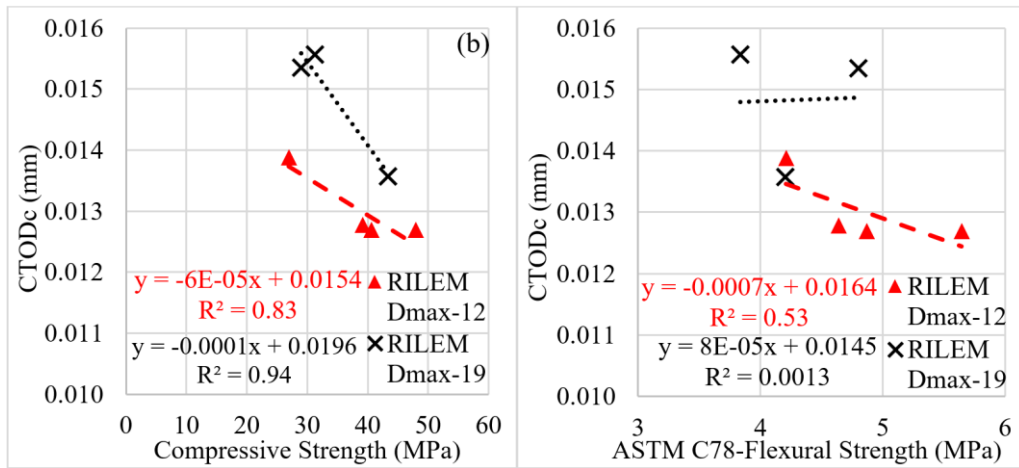
(b) Critical crack tip opening displacement ($CTOD_c$)
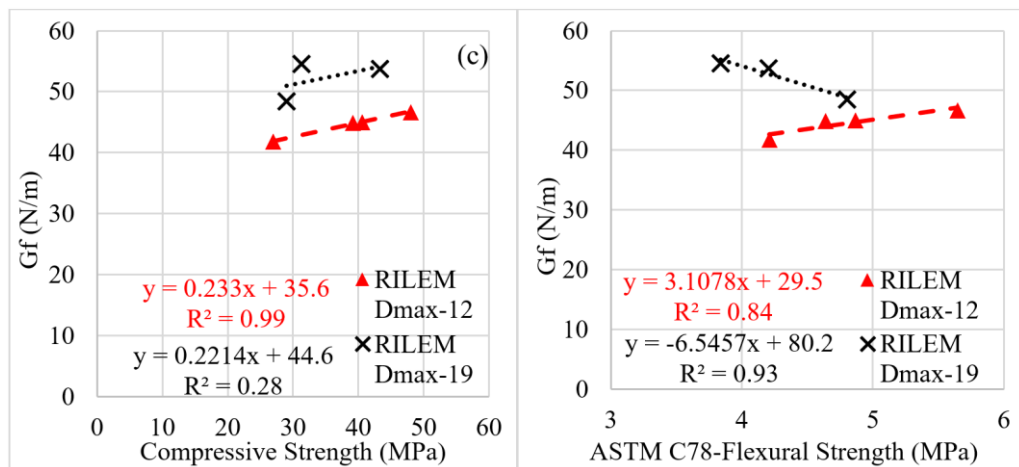
(c) Initial fracture energy (G_f)

Figure 4.26. Relationship between strengths and fracture parameters, (a) critical stress intensity factor, (b) critical crack tip opening displacement, (c) initial fracture energy

It can also be said that RCC mixtures exhibited more pronounced fracture properties with respect to critical stress intensity factor compared to results in the literature related to conventional concrete pavement mixtures (LaHucik, et al., 2017;LaHucik & Roesler, 2017; Roesler, Paulino, Gaedicke, Bordelon, & Park, 2007).

Typical fractured surfaces of specimens from each mixture at the end of the fracture test (RILEM procedure) are shown Figure 4.27, where it can be seen that the cracks follow the aggregate perimeters of and fracture occurs throughout the cement matrix, especially in mixtures of 200 and 300 kg/m^3 binder dosage with maximum aggregate size of 19 mm. It can also be observed that some aggregates are broken in the 400 and 600 kg/m^3 dosage mixtures. In particular, the fracture surfaces of mixtures with a maximum aggregate size of 12 mm are smoother than those with a maximum aggregate size of 19 mm, indicating that some cracks follow a shorter path before specimen failure, i.e., mixtures with maximum aggregate size of 12 mm may require less fracture energy than mixtures with 19 mm aggregate size.
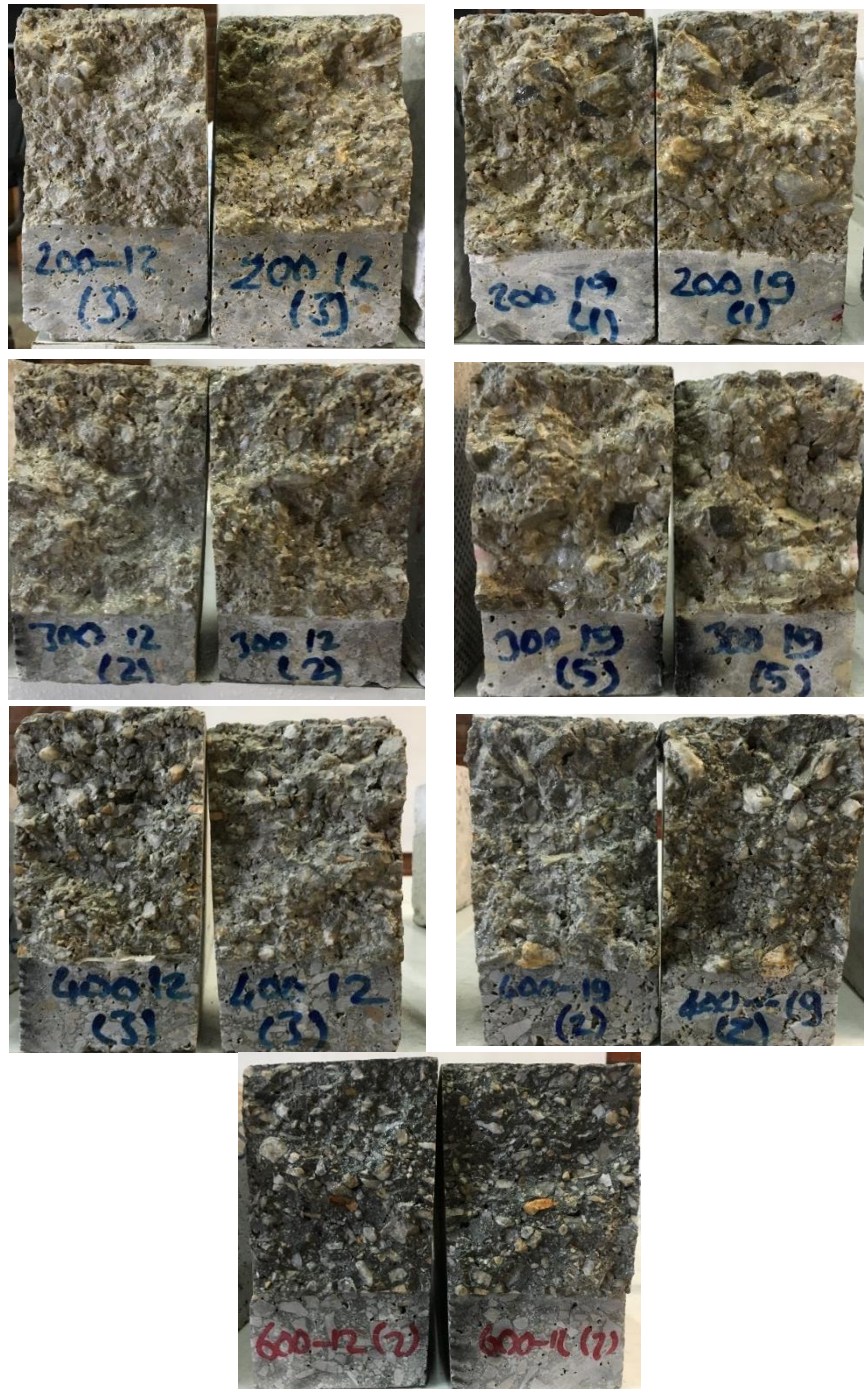
Figure 4.27. Typical fractured surfaces of specimens from each RCC mixture at the end of the RILEM test procedure

4.2.1.3. Total Fracture Energy - JCI Procedure

In the method developed by the Japanese Concrete Institute (JCI-S-001 2003), load-CMOD curves of notched beams under three-point bending test were used to determine toughness and total fracture energy of RCC specimens. As described in detail in the previous chapter, the specimen sizes and loading setup for the procedure are shown in Figure 3.24. 28 and 90 day fracture-energy tests were performed for the first three mixtures, while testing of the last four mixtures was delayed due to a problem with the cutting machine. For the first three mixtures, since no significant difference was observed in the fracture energy results for the two ages, the average of eight specimens (40±10 days) was evaluated for each mixture, mainly because of the small difference in ultimate strength development between those two ages.

With respect to the RILEM test, a three-point bending test was conducted at a CMOD rate using the servohydraulic universal testing machine (MTS Landmark 250 kN) (Figure 4.28), with a 0.05 mm/min loading rate. The measurement of load and CMOD was performed from the beginning of testing until the specimen completely ruptured.

Figure 4.28. *Determination of fracture energy of RCC mixtures by three-point bending test applied on notched beam according to JCI-S-001-2003 standard*

Load-CMOD curves for seven different RCC mixtures are shown in Figure 4.29 and Figure 4.30. Since the testing was performed by controlling the CMOD at a slow loading rate, the specimens had not been completely ruptured at the end of the fracture test because the load amount required to continue the test was nearly zero. When the cracks had reached a certain size, the specimen remained stable and its dead weight was almost enough to increase the value of the CMOD, i.e., the load-CMOD graph exhibited significant differences from the specimens in the tail section, as shown in Figure 4.29. In this study, complete failure in this test was defined to be when the load had diminished to 1% of the ultimate load.

At the end of the tests, the following equations were utilized to calculate fracture energy (G_F) consistent with the related standard.

$$G_F = \frac{0.75 \times W_0 + W_1}{A_{lig}}$$
$$W_1 = 0.75 \times \left(\frac{S}{L} m_1\right) \times g \times CMOD_c \qquad (4.7)$$

where G_F= Total fracture energy (N/m), W_0= area below load-CMOD curve up to the rupture of the specimen (N.mm), m_1=specimen weight (kg), S= span length (mm), L= total length of specimen (mm), g= gravitational acceleration (9.807 m/s^2), $CMOD_c$= crack-mouth opening displacement at the time of rupture (mm), and A_{lig}= area of broken ligament (mm^2).

The fracture energy of RCC mixtures was calculated from the above equations, and Table 4.10 shows the average of measured geometric data, including average toughness (W_0) and fracture energies (G_F) values for RCC mixtures. As it can be seen in Table 4.10 and Figure 4.31, all RCC mixtures (except for C300-D12) exhibited similar fracture energies (G_F). It should be kept in mind that C300-D12 and C400-D19 mixtures, the second most (98.6%) and at least (94.6%) compacted respectively, affected all the investigated relationships. In addition, this unexpected rising in fracture energy may be also related to size effect as in K_{Ic} results since this mixture has lowest effective depth among the other mixtures. Contrary to expectations, neither

increases in binder dosage or maximum aggregate size led to a significant change in the fracture energy, and the seventh mixture developed for obtaining a high strength RCC appeared to exhibit the lowest fracture energy. Increasing the brittleness of the material is thought to decrease both the toughness and the fracture energy.

Figure 4.32 shows typical fractured surfaces of specimens obtained for each mixture at the end of the experimental tests.

Table 4.10. *Fracture energy (G_F) test results according to the JCI-S-001-2003 procedure.*

No		1	2	3	4	5	6	7
Mix ID		C200 -D12- W5	C200 -D19- W5	C300 -D12- W5.5	C300 -D19- W5.5	C400 -D12- W5.5	C400 -D19- W5.5	B600 -D12- W8.5
Average of measured geometric data								
Sample weight* (m_1)	kg	8.5	9.9	8.8	8.6	8.3	8.4	8.8
Sample length* (L)	mm	351	345	351	344	351	351	350
Span length* (S)	mm	300	300	300	300	300	300	300
Sample width* (b)	mm	101.1	91.4	101.0	95.9	99.6	100.2	103.9
Sample depth* (d)	mm	102.2	100.9	102.7	105.1	99.6	103.7	103.6
Notch depth* (a_0)	mm	30.1	29.7	34.6	31.6	28.2	31.1	26.7
Effective depth* (h=d-a0)	mm	72.1	71.2	68.1	73.6	71.3	72.6	76.8
Crack mouth opening displacement* (CMODc)	mm	0.88	0.69	0.81	0.79	0.78	0.94	0.75
Average of fracture energy test results								
Max. Load* (P_{max})	kN	**4.7** [11.5]	**5.6** [16.5]	**5.3** [21.0]	**4.7** [12.5]	**5.4** [18.3]	**4.3** [10.8]	**8.6** [9.5]
Theoretical Flexural Strength* (σ_{tfs})	MPa	**3.97** [6.8]	**4.70** [9.3]	**5.11** [9.8]	**4.07** [10.4]	**4.75** [13.4]	**3.80** [9.1]	**6.29** [2.7]
Toughness* (**W_0**)	N.mm	**649** [25.2]	**674** [27.7]	**783** [26.8]	**669** [22.1]	**639** [16.0]	**628** [17.2]	**593** [20.5]
Fracture Energy * (**G_F**)	N/m	**72.3** [22.7]	**72.4** [18.7]	**92.0** [20.1]	**77.0** [17.7]	**73.2** [13.0]	**72.1** [15.1]	**63.8** [10.7]

* It was measured separately for each beam sample and the average value is given in the table.
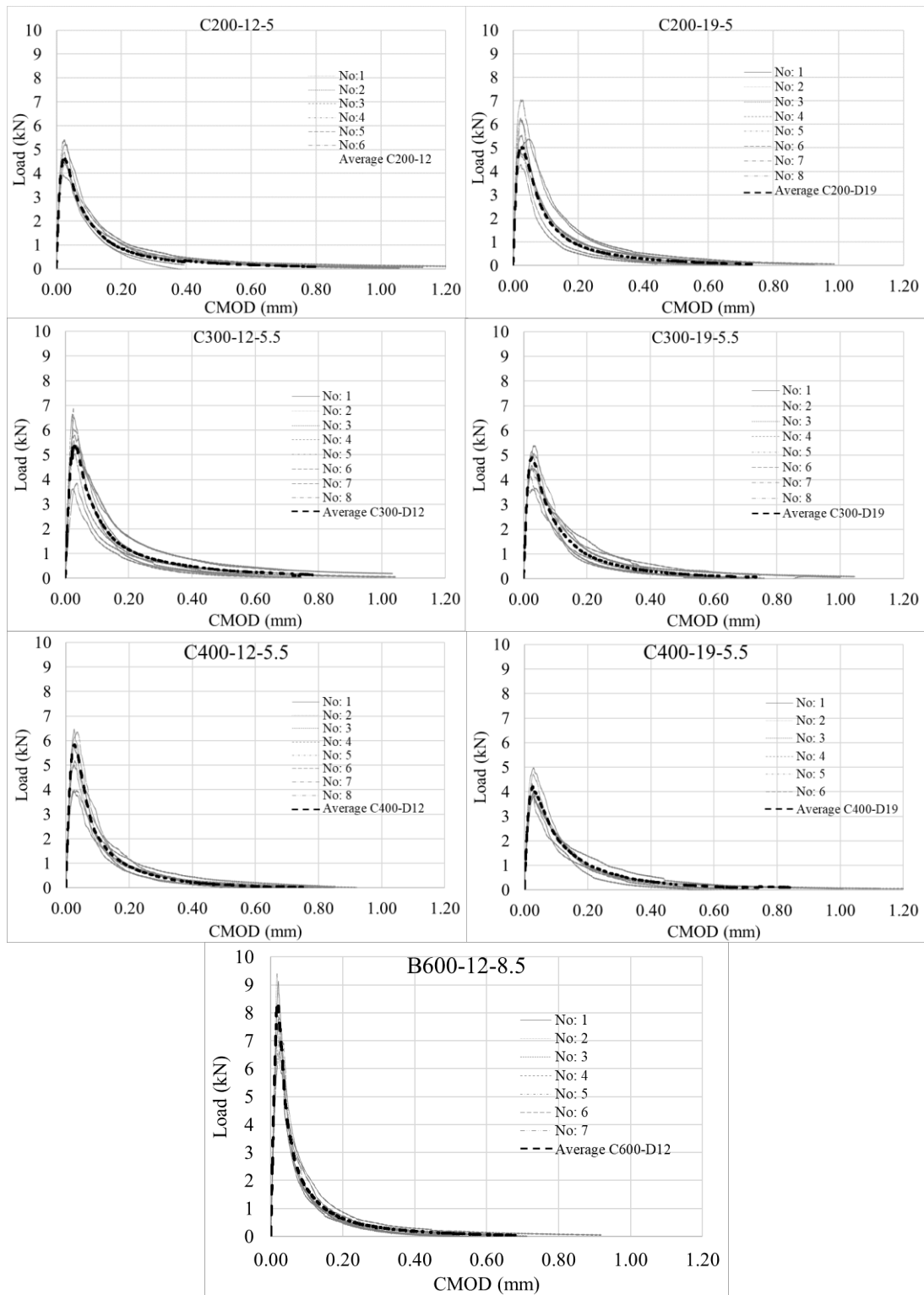
Figure 4.29. Load-CMOD curves for each RCC mixtures obtained by JCI procedure.
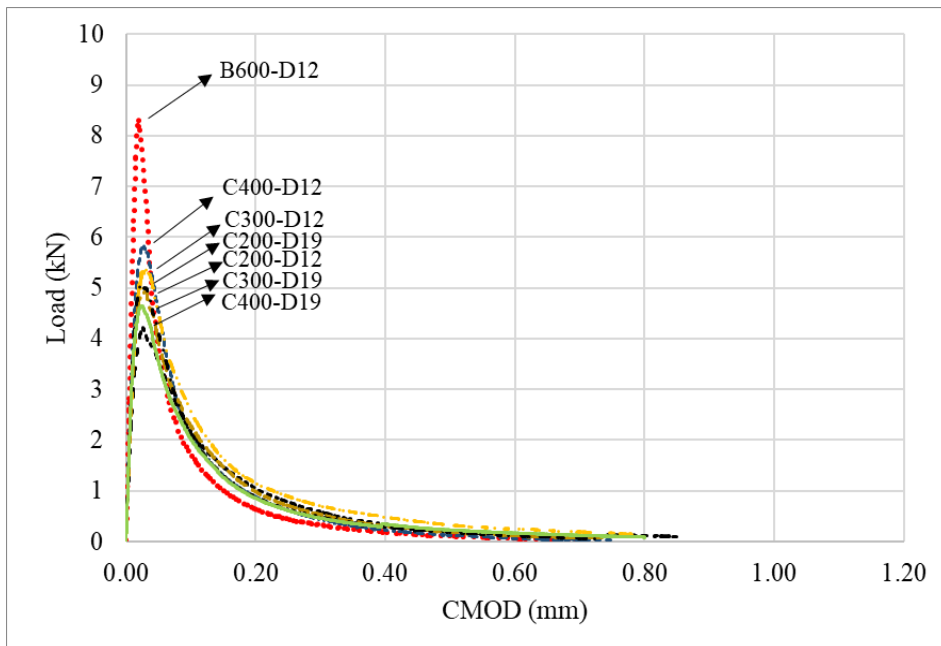
Figure 4.30. Average Load-CMOD curves for RCC mixtures.
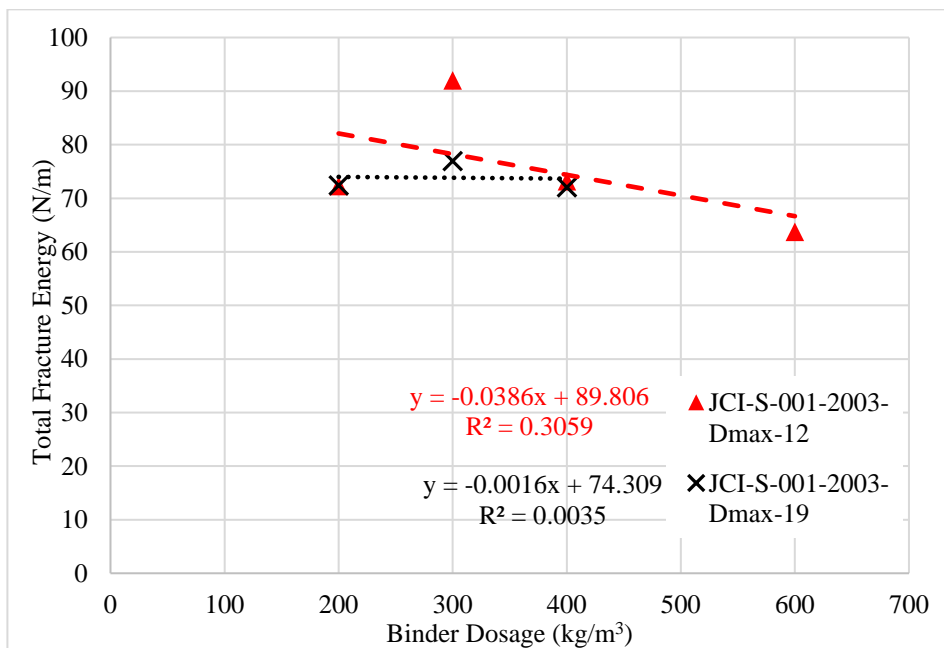
Figure 4.31. Relationship between total fracture energy (JCI-S-001-2003) and binder dosage.

132
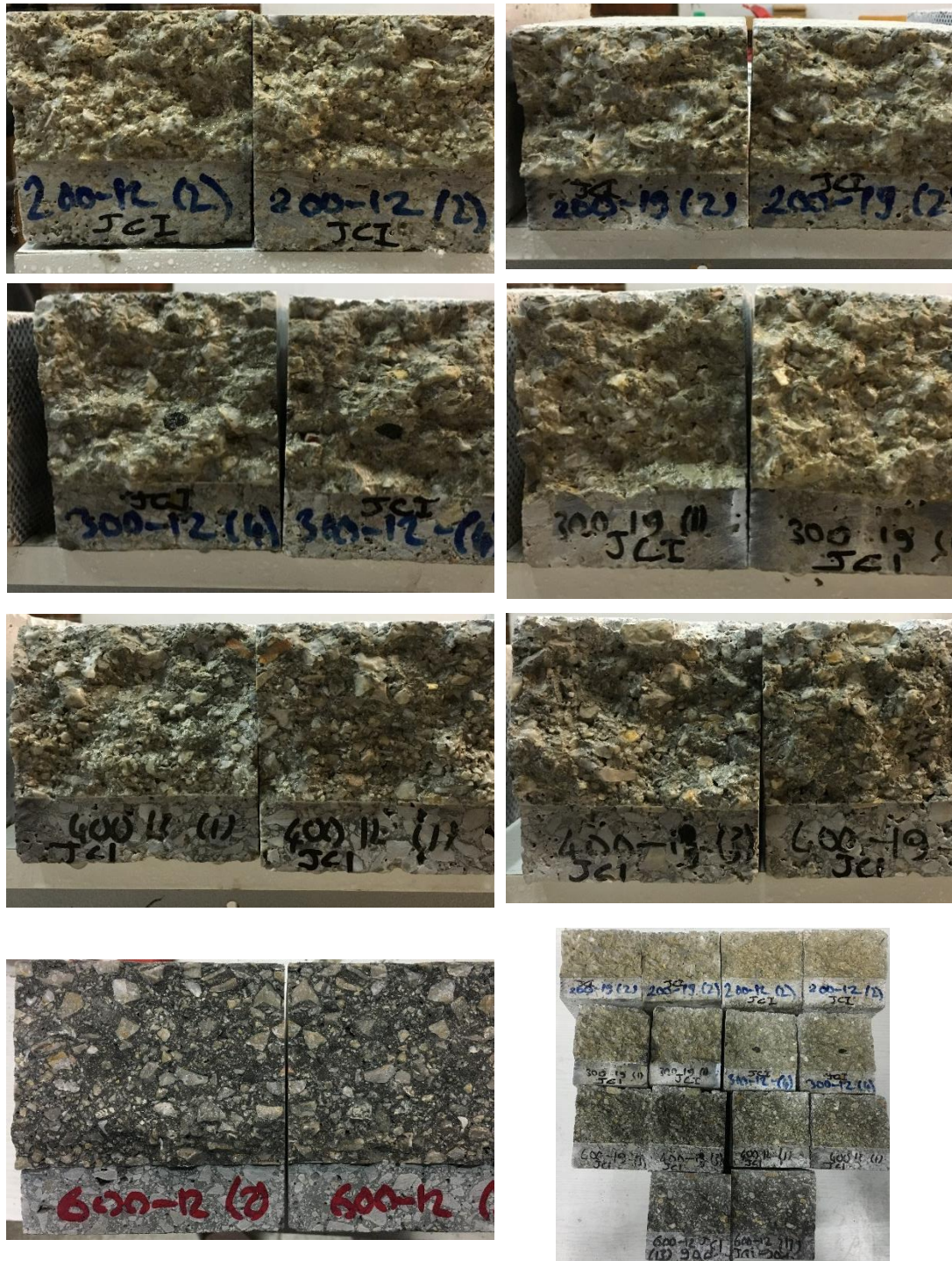
Figure 4.32. Typical fractured surface of the samples at the end of the JCI test procedure.

4.2.1.4. Characteristic Length

One of the most frequently-used parameters in the fracture mechanics concept is the characteristic length (l_{ch}), developed by Hillerborg, et al., (1976) as an inverse measure of material brittleness. Characteristic length (l_{ch}) is a material property defined in Eq. (4.8), as a function of total fracture energy (G_F), tensile strength (f_t) and elastic modulus (E_c).

$$l_{ch} = \frac{E_c G_F}{(f_t)^2} \tag{4.8}$$

This parameter can be useful in structural design since it controls strength, fracture mode and crack growth (Akkaya, et al., 2003). While is value will usually vary between 100-200 mm for mortar and 200-500 mm for concrete, it can be lower or higher than these values (Hillerborg, 1985). The variation in characteristic length with respect to the binder dosage and maximum aggregate size is given obtained for each RCC mixture in Figure 4.33, where it can be seen to show a decreasing tendency with increasing binding amount, i.e., the specimens exhibited more brittle behavior with such an increase. While this linear tendency was clearly seen for mixtures with a maximum aggregate size of 12 mm, mixtures with a maximum aggregate size of 19 mm showed a downward trend while not representing linear behavior. The figure shows that the seventh mixture with a binding amount of 600 kg/m^3 had the lowest characteristic length, so this mixture would be expected to exhibit the highest brittle behavior among the examined mixtures.

The change in characteristic length with respect to compressive and flexural strengths and the RILEM fracture parameters are illustrated in Figure 4.34.
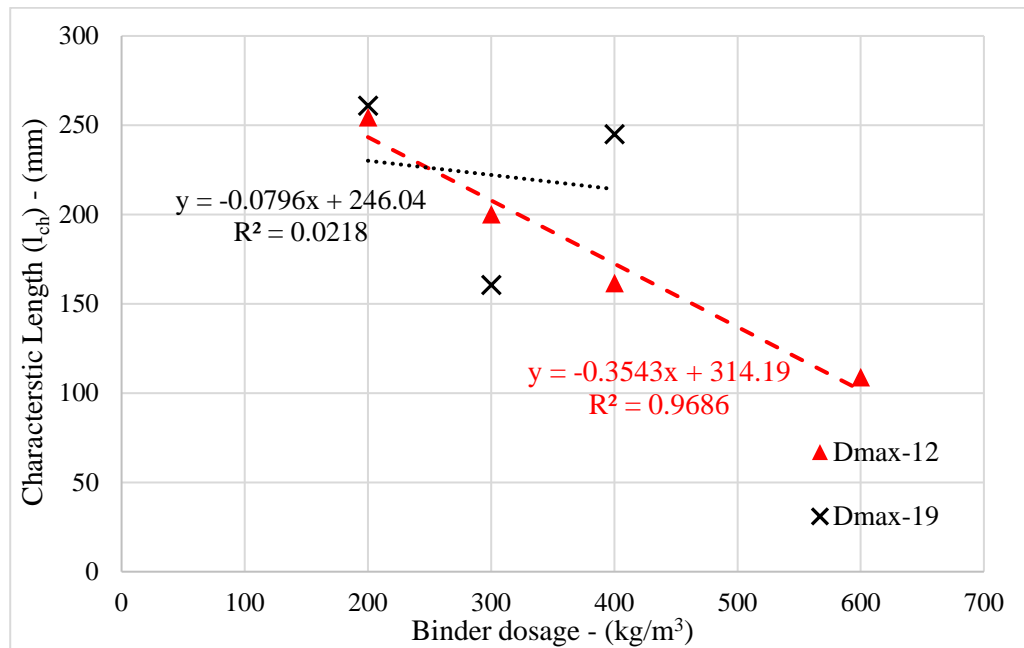
Figure 4.33. Variation of the characteristic length with regards to the binding amount and maximum aggregate size.

Figure 4.34 (a) shows that there is a clear decreasing trend of the characteristic length with an increase of in either compressive or flexural strengths, mixtures exhibited more brittle fracture with an increase in compressive strength. The comparison between the RILEM fracture parameters and the characteristic length in Figure 4.34(b) reveals that l_{ch} is inversely proportional to the critical stress intensity factor (K_{Ic}) but directly proportional to the crack tip mouth opening displacement ($CTOD_c$). In other words, the mixture with larger K_{Ic} exhibited more brittle behavior, while the one with a larger $CTOD_c$ would be expected to exhibit less brittle behavior. One of the most striking results to emerge from the figures is that an increase in maximum aggregate size in RCC mixtures resulted in a growth in the characteristic length, i.e., the mixtures with smaller maximum aggregate size became less brittle. These results are consistent with other studies which have shown that characteristic length is increased when either compressive strength decreases or maximum aggregate size increases in concrete mixtures (Akcay, et al., 2012; Akkaya, et al., 2003; Kornbak & Karihaloo, 1996; M. A. Tasdemir & Karihaloo, 2001).
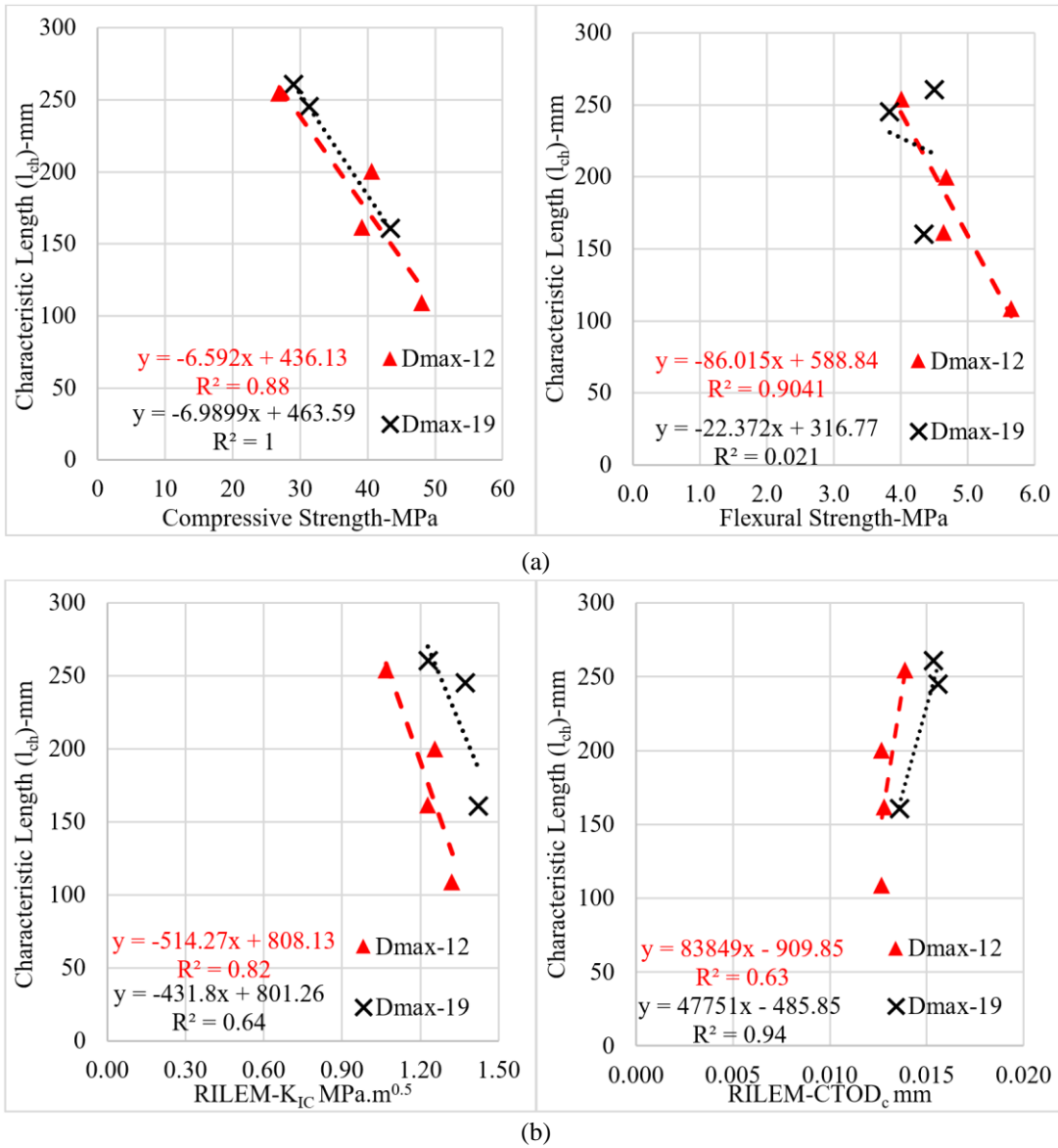
Figure 4.34. The relationship between characteristic length and (a) strengths, (b) RILEM fracture parameters in RCC mixtures.

4.2.2. Discussion

In the previous phase of the experimental study, twenty different RCC mixtures comprised of two different cement dosages (200 and 400 kg/m^3), two different maximum aggregate sizes (12-19 mm) and five different water ratios (3,4,5,6,7%) were prepared using different compaction methodologies, and their physical and

mechanical performances were investigated. Four RCC mixtures were then selected from these twenty different mixtures by considering compressive and tensile strengths, compaction ratios, and ideal Vebe consistency times for field applications. In this phase, three new RCC mixtures were added to the four different RCC mixtures discussed in the first phase. Two were formed as mixtures of 12 mm and 19 mm maximum aggregate sizes with a cement amount of 300 kg/m^3 to provide a clearer understanding of the effect of binder dosage, while the third was formed as a mixture with 12 mm maximum aggregate size and 600 kg/m^3 binder dosage, with cement weight of 45% fly ash and 5% silica fume, to represent behavior of high-performance RCC. To simulate field consistency conditions, the water ratio of the mixtures was chosen based on Vebe times of 30 ± 10 seconds. All RCC mixtures were compacted in a plate with dimensions of 15x85x200 cm^3 by applying a VPC and a DDVHR to simulate compaction under actual field conditions.

The compressive strengths at 2, 7 and 28 days of cores taken from the plates and at 28 days of cylindrical samples produced by vibrating hammer were determined. Third-point bending test was performed on beam specimens that were cut out of the plate to determine the 28-day flexural strengths. Three-point bending test was also applied to notched beams at constant CMOD rates specified in standards to determine the fracture parameters of seven different RCC mixtures by using two different procedures, RILEM TC 89-FMT, (1990) and JCI-S-001-2003, (2003). The calculated fracture parameters were E_c, K_{Ic}, $CTOD_c$, a_c, G_f, G_F and l_{ch}.

Conclusions from the strength and fracture tests, relationships among them, and effects of the mixture designs on the results are as follows:

- The highest compaction ratio was obtained for 300 kg/m^3 98.6-97.8% binding mixtures (ignoring the blended mixture), while the lowest compaction was obtained from 400 kg/m^3 95.3-94.6%. binding mixtures. This clearly and significantly affected all the test results obtained from these mixtures. Vebe times are thought to be effective at these compaction ratios. For the 300 kg/m^3

and 400 kg/m^3 binder mixtures, respective Vebe times in the range of 22-20 sec and 35-32 sec were obtained. Even though increasing the consistency of RCC mixtures leads to higher compaction ratios, it makes the RCC insufficiently capable of carrying the weight of the vibratory roller at fresh state, creating surface problems during field application, so it is vital to consider the Vebe consistency time of the RCC laboratory studies to obtain results consistent with field conditions.

- When compressive strengths after 2, 7, and 28 days of (Ø15x15cm) cores taken from the plates compacted with DDVHR were examined, an increase in the compressive strength with increased binder dosage and specimen age was observed, although the maximum aggregate size used in mixtures has been found have less influence on compressive strength. On the other hand, for 300 kg/m^3 binder dosage mixtures, because of the effect of high compaction ratio the compressive strength at 28 days was approximately 41 MPa and it reached same compressive strength as the 600 kg/m^3 binding mixture. It also exhibited higher compressive strength than 400 kg/m^3 binding mixtures that have the lowest degree of compaction.

- The RCC mixtures reached about 65% of their 28 day-compressive strength after 2 days, sufficient to carry light traffic even at the lowest cement dosage (> 15 MPa) (Harrington, et al., 2010), and about 80% after 7 days. This is a critical point that can RCC apart from traditional concrete in pavement applications.

- The 28 day-compressive strengths of RCC samples produced by DDVHR that represented field conditions were lower (about 25% less) than for samples produced with the vibrating hammer that represented laboratory conditions. This is related to the lower compaction ratio, except for the blended mixture (B600-12) that exhibited higher compaction ratio and compressive strength in the DDVHR specimens. The compressive strength results obtained by both

138

methods were statistically similar to one another for low Vebe times (approximately 20 s) when the compaction ratios were close to one another.

- When the 28-day flexural strengths (ASTM C78) of RCC mixtures were examined, it was seen that the highest flexural strength was obtained from the blended mixture (B600-D12), which was planned to have high strength and durability. The C400-D19 mixture, which has the lowest degree of compaction (%94.6), presented the lowest performance in flexural strength.

- K_{Ic}, which is a measure of the resistance to crack propagation in materials, was found higher than 1.0 MPa.m$^{1/2}$ even in the lowest dosage mixture which is the typical value of conventional concrete pavements. It was also observed that K_{Ic} enhanced with an increase in binder dosage in RCC mixtures. Similarly, as maximum aggregate size increased, increases varying between 11% and 15% depending on the binding contents were detected in all RCC mixtures. Moreover, an increase the aggregate size led to an increase in CTOD$_c$.

- K_{Ic} increased linearly with increase in compressive strength for all RCC mixtures, while the CTOD$_c$ conversely tended to decrease with increasing compressive strength except for one mixture, C400-D19.

- Increases in binder dosage or maximum aggregate size did not produce significant changes in the fracture energy, and fracture energies of all RCC mixtures except for C300-D12 were close. However, since the fracture energy test was performed by controlling the CMOD with applying a slow displacement rate, the specimens had not completely ruptured at the end of the fracture test when the applied load had diminished to a value near to zero, even though, this had no notable effect on the fracture parameters because since the test only lasted until the load had gone down to 1% of the ultimate force.

- The characteristic length tends to decrease with an increase in either compressive or flexural strength, and the mixtures exhibited more brittle

fracture when the compressive strength increased. A comparison between the RILEM fracture parameters and the characteristic length revealed that the latter is inversely proportional to K_{Ic} but directly proportional to $CTOD_c$, i.e., the mixture with a larger K_{Ic} exhibits more brittle behavior, and the one with a smaller $CTOD_c$ would similarly be expected to exhibit more brittle behavior.

- An increase in maximum aggregate size in RCC mixtures resulted in a characteristic length growth, i.e., mixtures with smaller maximum aggregate size became more brittle.

Last but not least, fracture parameters of RCC mixtures are affected by compaction ratio and size effect such as notch depth, notch width, specimen height and width.

4.3. Phase III Results

In the previous phase, mechanical and fracture properties of seven different RCC mixtures were examined. In this last phase of the experimental study, for three RCC mixes of different binder amount, the flexural fatigue performance was determined in terms of S-N curves and the relationship between its fracture parameters are investigated. In addition, the effect of mixture design on the RCC fatigue behavior is explored. The mixture design, compaction methodology and fatigue testing procedures for RCC mixtures are explained in Chapter 3.3.

Flexural fatigue test results and S-N curves of RCC mixtures, comparison with S-N curves of conventional concrete in literature, their relationship with its fracture parameters and effects of mixture design on its fatigue behavior is discussed in detail in the following section.

4.3.1. Flexural Fatigue Test Results of RCC mixtures

Fatigue testing of concrete mixtures is typically performed on specimens in load/stress control to develop Stress-Life (S-N) curves that indicate the number of load cycles/repetitions to failure (N) corresponding to the stress/load ratio (S).

In this study, the S-N approach used in all conventional concrete studies described in the literature was utilized to analyze fatigue behavior of RCC mixtures. Fatigue loads calculated for each stress ratio, shown in Table 4.11, were applied to specimens at a loading frequency of 10 Hz (10 cycles per 1 second) and fatigue tests were continued either until the specimen failed or 2 million number of load cycles/repetitions had occurred. During the tests, the number of load cycles/repetitions to failure was recorded for each specimen, and for specimens reaching 2 million cycles without failing, the number of load cycles/repetitions (N) was recorded +2 million. To evaluate how far specimens might last after 2 million load cycles, testing was continued for some specimens until 4 million cycles had occurred.

Table 4.11. *Load parameters for fatigue test.*

No	Mix ID	28-day Flexural Strength (MPa)	Number of specimens	Stress Ratio (S)	Max. Flexural Load - P_{max} (kN)	Applied Max. Load (%S P_{max}) (kN)	Applied Min. Load (%20 P_{max}) kN
1	C200-D12-W5	4.00 [0.68]	3	0.550	32.8	18.0	6.5
			4	0.625	30.8	19.3	6.2
			5	0.700	30.9	21.6	6.2
			6	0.775	31.0	24.1	6.2
			6	0.850	31.9	27.1	6.4
2	C400-D12-W5.5	5.06 [8.13]	4	0.625	37.5	23.4	6.5
			5	0.700	40.1	28.1	8.0
			5	0.775	37.4	29.0	7.0
			5	0.850	39.2	33.3	7.8
3	B600-D12-W8.5	5.16 [5.23]	3	0.550	37.5	20.6	7.5
			5	0.625	36.7	22.9	7.3
			5	0.700	38.1	26.7	7.6
			5	0.775	36.8	28.5	7.4

At the end of fatigue testing, the number of load cycles/repetitions (N) corresponding to the stress ratio (S) was plotted in semi-logarithmic form, and the slope obtained for the equation was recorded as the fatigue slope. Table 4.12 shows the number of load cycles/repetitions (N) corresponding to the stress ratio (S) and the number of samples tested for each stress ratio.

Fatigue testing for each mixture was continued for approximately 1-1.5 months. The longest fatigue tests were observed at the lowest stress ratio of 55%, and the 2 million cycles were continued non-stop for 54 hours, so it was thought that there was no more need for further tests when the number of cycles exceeded 2 million for the first three test samples tested at low-stress ratios, e.g., a 55% stress ratio. The remaining samples were either used for other stress ratios in which the variation was higher or used to determine fracture parameters. Outliner test results were ignored. Figure 4.35 shows S-N diagrams plotted in semi-logarithmic form by carrying out a linear regression on each RCC mixtures.

Table 4.12. *Results of 28-day flexural fatigue test for RCC mixtures*

Mix ID	Stress Ratio (S)	Number of samples	Number of load cycles/repetitions to failure (N) Results of each sample	Average	S-N equations
C200-12-5	0.550	3	3 x 2000001+	+2 million	
	0.625	4	4 x 2000001+	+2 million	
	0.700	5	4571; 21090; 26776; 55343; 897986;	201153	$S=0.9291-0.0503\log(N)$ $R^2=0.813$
	0.775	6	73; 100; 385; 1407; 5083; 9878	2821	
	0.850	6	5; 78; 81; 136; 528; 2992	637	
C400-12-5.5	0.625	4	4 x 2000001+	+2 million	
	0.700	5	34784; 102829; 121785; 123837; 199230	116493	$S=0.9188-0.0431\log(N)$ $R^2=0.889$
	0.775	5	340; 1995; 3663; 50750; 116052	34560	
	0.850	5	12; 24; 32; 70; 121	52	
B600-12-8.5	0.550	3	3 x 2000001+	+2 million	
	0.625	5	146233; 293777; 554264; 1140130; 1333509	693583	$S=0.8644-0.0436\log(N)$ $R^2=0.879$
	0.700	5	1132; 9564; 20837; 53397; 53860	27758	
	0.775	5	15; 106; 119; 125; 435	160	
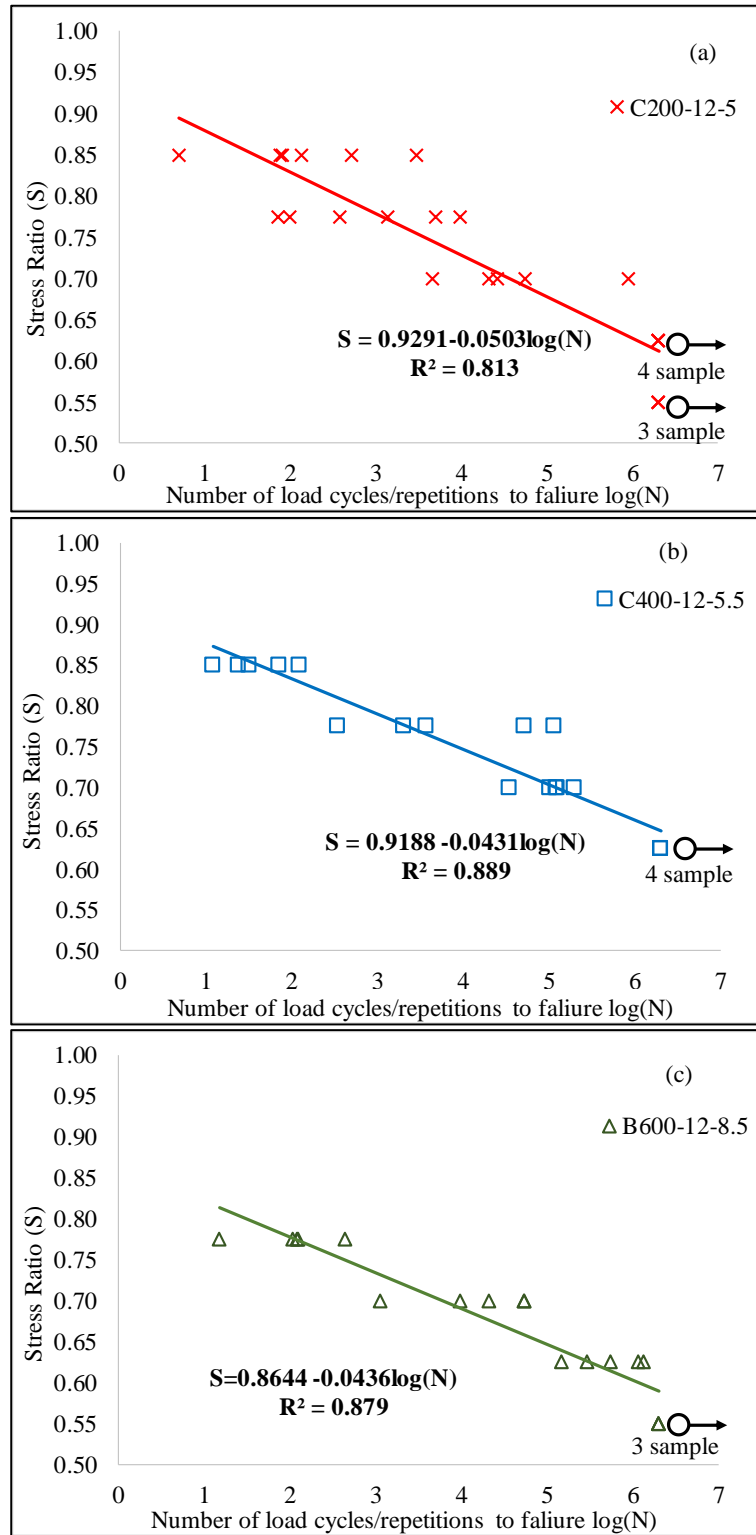
Figure 4.35. S-N curve for each RCC mixture under flexural fatigue loading (a) 200 kg/m³ binder dosage (b) 400 kg/m³ binder dosage (c) 600 kg/m³ binder dosage

As can be seen in Figure 4.35, samples that did not fail after 2 million load cycles are shown with arrows and the sample numbers tested are also indicated in the figures. The stress ratio, corresponding to 2 million load cycles/repetitions in the S-N curve, which is generally accepted as the sufficient number of cycles for fatigue strength in plain concrete, was determined as the average fatigue strength of RCC mixtures. From Figure 4.35, the average fatigue strength of blended mixture was found as about 58% of its ultimate static strength, while 200 and 400 kg/m^3 binder dosage mixtures were found as about 62% and 65% of its ultimate static strength, respectively. Figure 4.36 shows S-N fatigue curve and equations obtained by combining three different RCC mixtures from 61 beam specimens (10x15x35 cm^3). When fatigue data of all RCC mixtures are evaluated together, the average fatigue strength corresponding to 2 million load cycles was approximately 62.5% of the ultimate static strength.
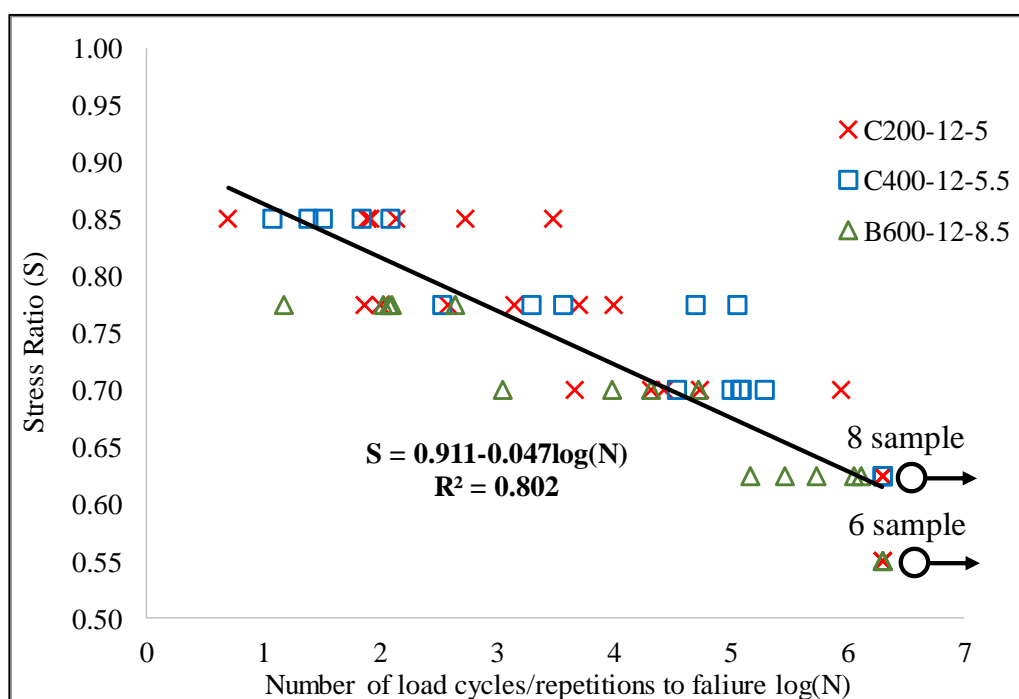
Figure 4.36. S-N fatigue curve and equation for all RCC mixtures (total of 61 samples)

4.3.2. Comparison with Fatigue Curves in Literature

While it would be useful to compare fatigue curves of this study with those found in the literature for conventional concrete and RCC but, as previously mentioned, fatigue tests are quite time-consuming, complex, and expensive, so few fatigue curves on RCC can be found in the literature. The first comparison is with the S-N curve obtained by CTL (Tayabji & Okamoto, 1987), one of the most comprehensive studies on this subject whose test procedure details are given in the literature review. The most interesting aspect of that study is that four different RCC mixtures were subjected to fatigue tests on beam samples taken from the field after being compacted with a 10-ton vibratory roller in the field. S-N fatigue curves were obtained from fatigue tests performed on 23 beam samples (15x15x75 cm^3) over approximately seven months. Comparisons with the fatigue curves developed in this study (61 beam samples) and CTL (Tayabji & Okamoto, 1987) and ACPA (Roden, 2013) are given in Figure 4.37. As discussed in the literature review, it should be noted that the fatigue curve presented by ACPA (Roden, 2013) used fatigue data obtained by Tayabji & Okamoto, (1987). It can be seen in this figure that the fatigue slope obtained from this study is significantly lower than the fatigue slope obtained by Tayabji & Okamoto, (1987). If two fatigue models for a road pavement design are compared, the developed fatigue model would be more conservative (safer) at loads higher than 68% of the ultimate strength, the intersection point of the two fatigue models, while for stress ratios below this value (greater number of loading cycles), the fatigue model developed by Tayabji & Okamoto, (1987) is more conservative.

When the fatigue strength of RCC mixtures obtained from both fatigue curves are examined, for 2 million load cycles the fatigue strengths are approximately 50% and 62% of the ultimate static strengths found by the Tayabji & Okamoto, (1987) fatigue model and the developed fatigue model, respectively. However, since the study done by Tayabji & Okamoto, (1987) was performed about 30 years ago, improvements in both design techniques and test procedures are to have been expected. The extent to which such improvements changes might affect fatigue behavior could be another

subject of research. As indicated in literature review, it is known that when fatigue performance of plain concrete samples produced in the laboratory is compared with that in the field, superior performance is generally obtained under laboratory conditions. Most importantly, the study done by Tayabji & Okamoto, (1987) used four different RCC mixes with binder amounts ranging from 170 to 190 kg/m^3, while in this study binder amounts varied from 200 to 600 kg/m^3. Also, bank run gravel was used in that study while crushed limestone aggregate was used in this study, a difference that might possibly affect fatigue behavior significantly.
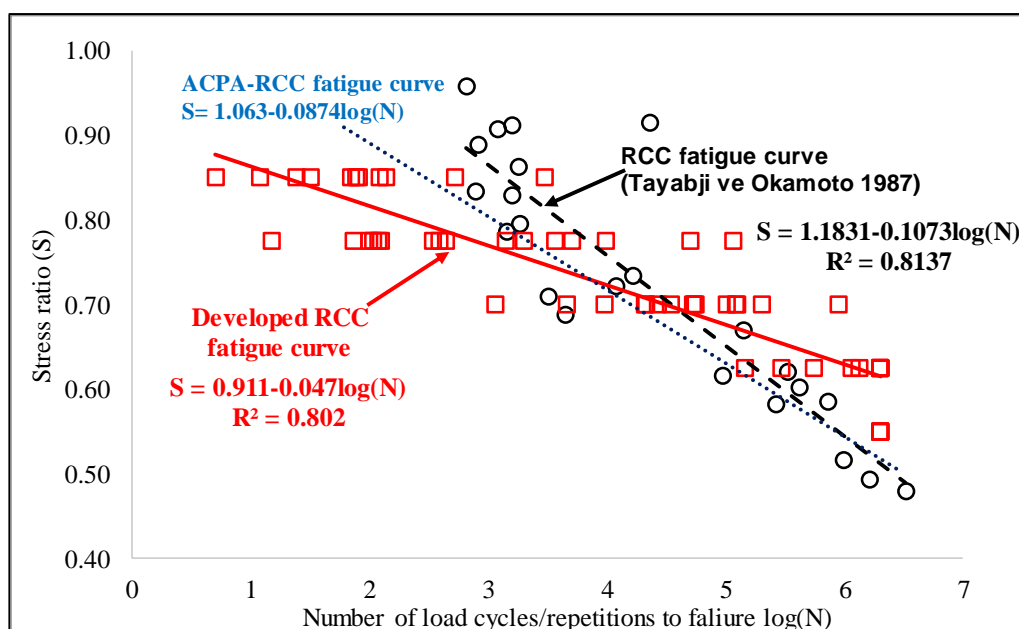
Figure 4.37. A comparison between the fatigue curve developed in this study and the fatigue curve obtained by Tayabji & Okamoto, (1987) and ACPA (Roden, 2013)

Figure 4.38 is a comparison of fatigue curves obtained from this study from RCC fatigue studies with earlier-developed RCC fatigue curves. The slope of this study's RCC fatigue curve is seen to lie between the slopes of RCC fatigue curves developed by Modarres & Hosseini, (2014) and by Sun et al., (1998). While the slope of RCC fatigue curves developed by Graeff, et al., (2012) is quite high and close to the slope of fatigue curve obtained by Tayabji & Okamoto, (1987), it should be noted that in

146

the current RCC fatigue studies, only a limited number of samples were subjected to fatigue tests (commonly three samples for each stress ratio except for the Sun, et al., (1998) study). Because there is as yet no standard procedure for compaction of beams in the laboratory and different laboratory compaction methodologies were utilized to compact beam samples, these effects may also affect the fatigue behavior of RCC mixtures.
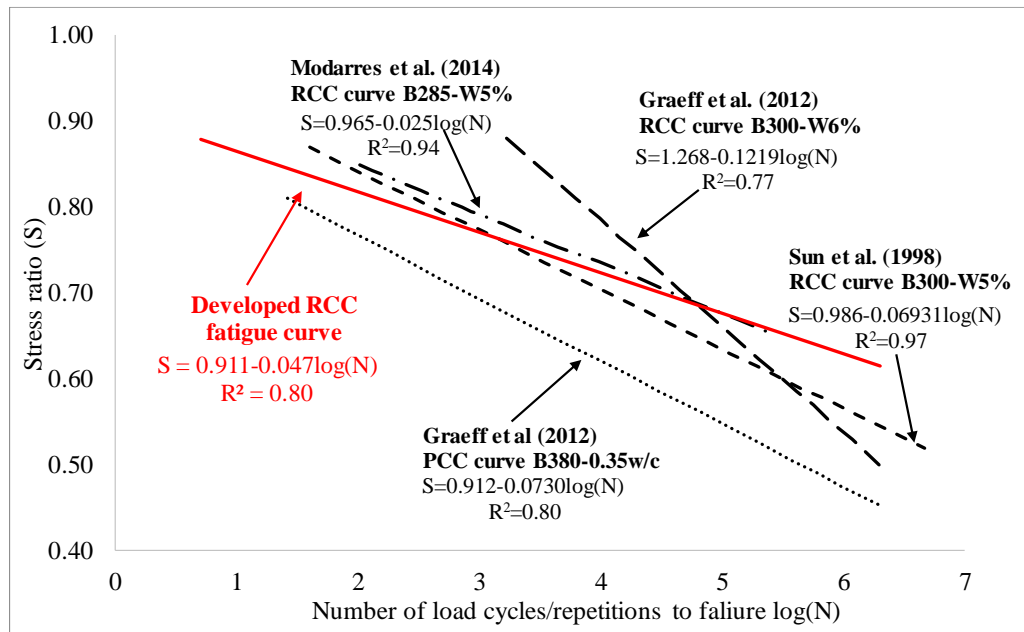
Figure 4.38. Comparison of developed RCC fatigue curve with current RCC fatigue curves in the literature (B: binder content (kg/m^3; W: water ratio by weight, w/c: water to cement ratio)

When fatigue strengths obtained from current RCC fatigue curves for 2 million load cycles are compared , the fatigue strength is about 62% of the ultimate static strength for the fatigue model developed by Sun, et al., (1998), while fatigue strength is about 50% of the ultimate static strength for the fatigue model developed by Graeff, et al., (2012). However, no results were obtained from an RCC fatigue curve developed by Modarres & Hosseini, (2014) because a total of 9 beams were tested and the samples failed after only about 200,000 load cycles. In that study conducted by Graeff, et al., (2012), as explained in detail in the literature, the fatigue behavior of RCC mixtures

was determined by using a special fatigue test setup in which three beams were placed atop one another and loads were transferred to the combination, so fatigue tests were applied on three samples simultaneously.

Since the fatigue curve used by PCA, (1984) in the design of concrete pavements is also employed in some RCC pavement design guides or software, it is also important to compare the developed RCC fatigue curves with those obtained for conventional concrete (PCC). For this purpose, in Figure 4.39 compares conventional concrete fatigue curves in literature and fatigue curves used in concrete pavement design by PCA with the RCC fatigue curve from this study.

In particular, the fatigue curve for PCC obtained by Murdock & Kesler, (1958) is quite similar to the fatigue curve obtained for RCC mixtures in this study, with both curves yielding the same fatigue strength of 62% for 2 million load cycles. However, when the PCA, (1984) fatigue curve is examined, it can be seen that it gives more conservative results for RCC pavement designs. In other words, if a RCC pavement thickness design decision made according to the PCA fatigue curve, the pavement thickness will result in thicker pavement thickness than one according to the RCC fatigue design obtained from this study. However, it should be noted that a probability of failure parameter is not considered in the RCC curve, and taking into account some probability of failure, e.g., 95% reliability, this curve will be slightly lower. It can also be seen that the fatigue strength of the PCA, (1984) curve corresponds to about 50% of its ultimate static strength for 2 million load cycles.
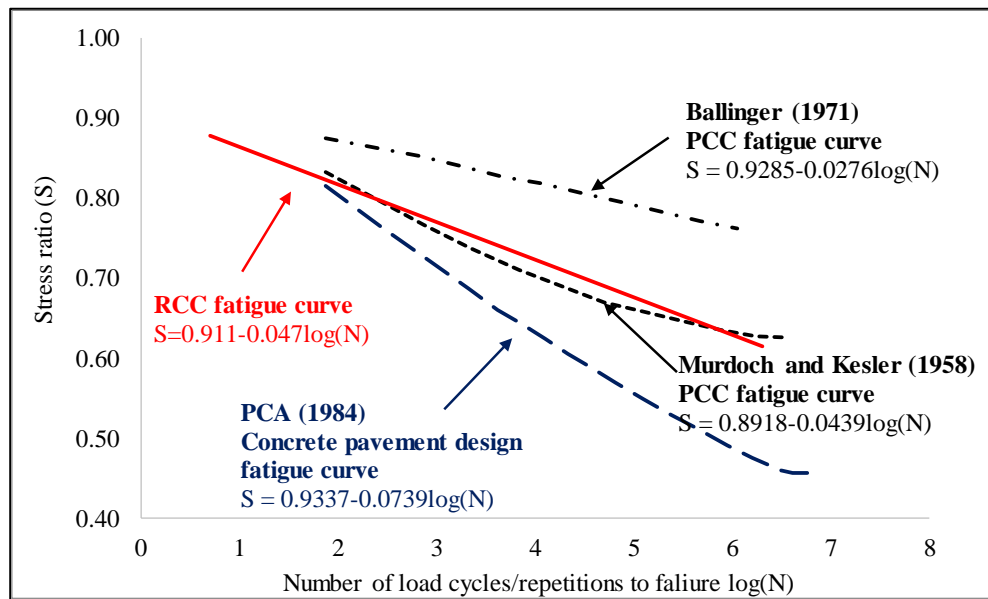
Figure 4.39. Comparison of RCC fatigue curve with conventional concrete fatigue curves

4.3.3. The Relationship between Fracture Parameters and Fatigue Behavior of RCC mixtures

Although the fracture parameters of the RCC mixtures were determined during the second phase of the experimental study, to achieve more accurate correlation with fatigue test results, it was decided to determine fracture parameters and total fracture energies for beam samples obtained from the plate prepared for fatigue samples. RILEM TC 89-FMT (1990) and JCI-S-001-2003 (2003) procedures, described in detail in the second phase of the experimental study, were utilized to find the fracture parameters and total fracture energies, but when the specimen sizes in the relevant standards were taken into account in determining fracture parameters and total fracture energies in the previous phase, in this phase the fracture tests were carried out on beam specimens of $10 \times 15 \times 35$ cm^3, the same size as the fatigue beam specimens. Moreover, according to the two-parameter fracture model (TPFM), a nonlinear fracture mechanics approach, it is claimed that fracture parameters are independent of the sample sizes. In this study, to what extent fracture parameters are affected by the size effect will also be found.

149

As can be seen in Figure 4.40, CMOD-controlled fracture tests on 10x15x35 cm^3 notched beam samples were performed in accordance with relevant procedures. The notches on beams were cut to 5 cm for the RILEM test and to 3 cm for the JCI test, again in accordance with relevant procedures.

Figure 4.40. Determination of fracture parameters in the third phase of the experimental study

Figure 4.41 shows the load-CMOD relationships for three-point bending notched beams obtained for each mixture according to the JCI procedure. To determine total fracture energy, the first three samples from each mixture were tested using JCI procedure, but no additional samples were tested because of the low standard deviation. The load-CMOD relation of three-point bending notched beams obtained for each RCC mixture according to the RILEM procedure is also shown in Figure 4.42.

Table 4.12 gives average values of fracture parameters (RILEM) and total fracture energy (JCI) obtained by at least three beam specimens of dimensions 10x15x35 cm^3 along with coefficients of variation (CoV) for each mixture. In addition, the average results obtained from the beam samples of the standard dimensions specified in the relevant procedures (RILEM and JCI) in the previous phase are given in the same table. Figure 4.43 compares the fracture parameters of the same mixtures for these two sample sizes. As can be seen from these graphs, while the change in specimen size

partially affected the fracture parameters, total fracture energies were very close to one another. The fact that the two sizes (10x10x35 cm^3 and 10x15x35 cm^3) were close to one another is thought to affect these results. On the other hand, different specimen sizes resulted in some serious changes within the fracture parameters, especially in K_{Ic}, and larger K_{Ic} was obtained by decreasing the sample size. CTOD$_c$ in contrast increased with increasing sample size. It should be noted, however, that these fracture properties were obtained from mixtures poured at different times, and although mixtures were prepared and compacted with the same procedure, there are inevitable differences between concrete mixtures poured at different times.

Table 4.13. *Comparison of fracture parameters obtained with fatigue sample sizes (10x15x35 cm^3) in this phase and standard sizes (RILEM 8x15x70 cm^3; JCI 10x10x35 cm^3) in the previous phase*

Mix ID	Age at test (day)	RILEM TC 89-FMT-1990						JCI-S-001-2003			
		Max. Load (P_{max})	Elastic Modulus (E)	Critical crack length (a_c)	Critical stress intensity factor (K^s_{Ic})	Critical crack tip opening displacement (CTOD$_c$)	Initial fracture energy (G_f)	Max. Load (P_{max})	Max. crack mouth opening displacement (CMODc)	Toughness (W_0)	Total fracture energy (G_F)
		kN	GPa	mm	MPam$^{1/2}$	mm	N/m	kN	mm	Nmm	N/m
C200-D12	90[*]	11.9	36.7 [9.5]	65.17 [14.0]	1.32 [14.3]	0.0125 [17.6]	47.6 [23.6]	6.5	0.79	768	84.2 [5.5]
	40[§]	4.72	27.4 [6.3]	71.26 [12.2]	1.07 [2.5]	0.0139 [1.3]	41.76 [1.3]	5.0	0.72	534	72.3 [22.7]
C400-D12	56[*]	13.5	42.5 [9.9]	61.43 [7.7]	1.44 [10.6]	0.0117 [13.6]	49.1 [14.8]	6.4	0.75	704	78.8 [1.7]
	40[§]	3.73	33.7 [3.8]	65.16 [4.8]	1.23 [9.9]	0.0128 [9.0]	44.91 [17.2]	5.4	0.78	639	73.2 [13.0]
B600-D12	45[*]	14.8	35.8 [6.8]	52.27 [5.2]	1.40 [4.9]	0.0111 [13.9]	53.3 [12.6]	7.5	0.62	625	62.8 [0.7]
	40[§]	3.98	37.6 [4.9]	70.73 [4.1]	1.32 [4.7]	0.0127 [8.5]	46.64 [9.5]	8.6	0.75	593	63.8 [10.7]

[*] *These tests were carried out on beam samples of the dimensions (RILEM-JCI 10x15x35cm^3) specified in the third phase of the thesis study.*

[§] *These tests were carried out on beam samples of the dimensions specified (RILEM 8x15x70 cm^3; JCI 10x10x35 cm^3)in the relevant standard in the second phase of the thesis study.*
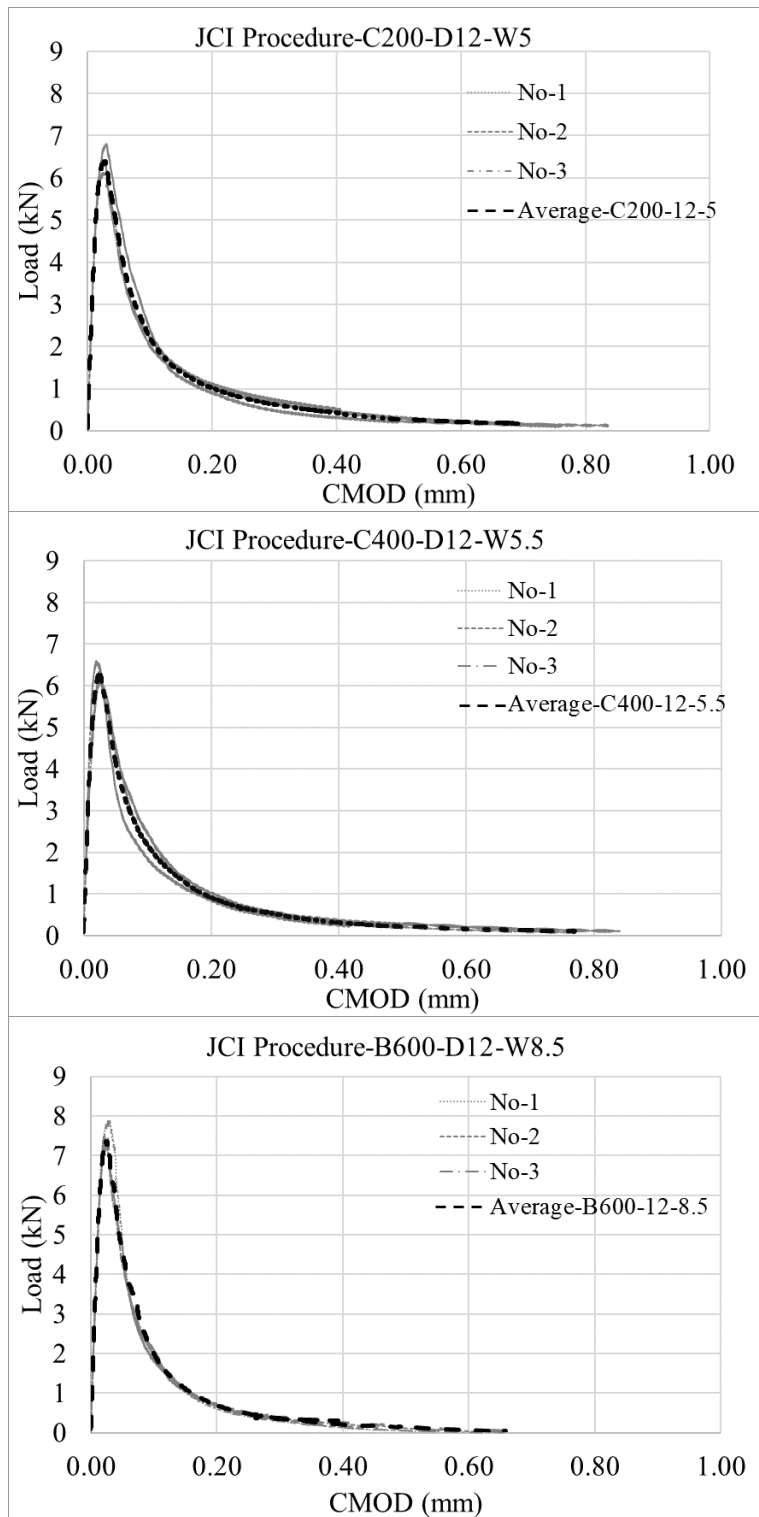
Figure 4.41. Load-CMOD graphs obtained by three-point bending beam specimens with the dimension of 10x15x35 cm^3 for each mixture according to the JCI procedure (JCI-S-001 2003).

152
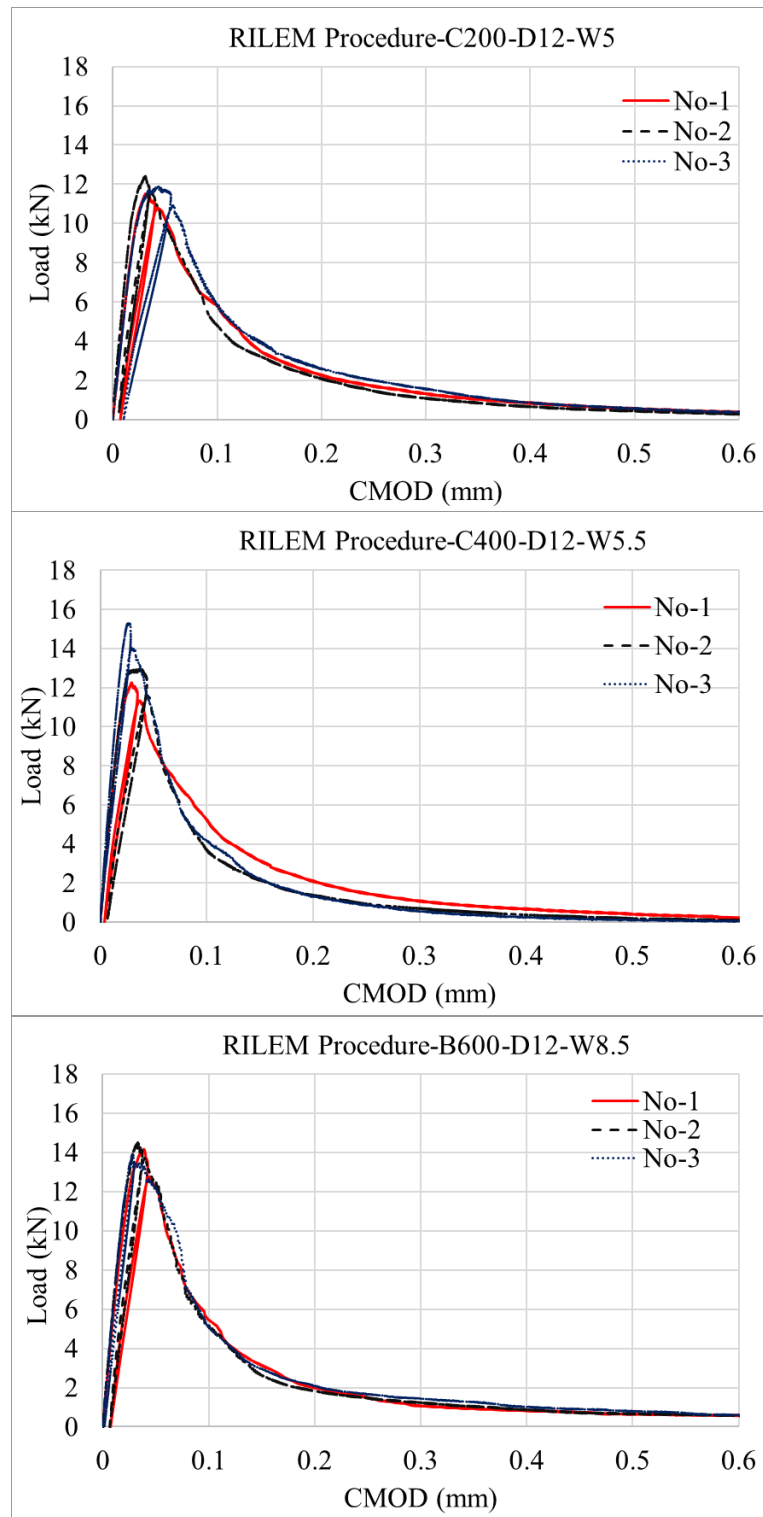
Figure 4.42. Load-CMOD graphs obtained by three-point bending beam specimens with dimension of 10x15x35 cm^3 for each mixture according to the RILEM procedure (RILEM TC-89 FMT 1990)

153
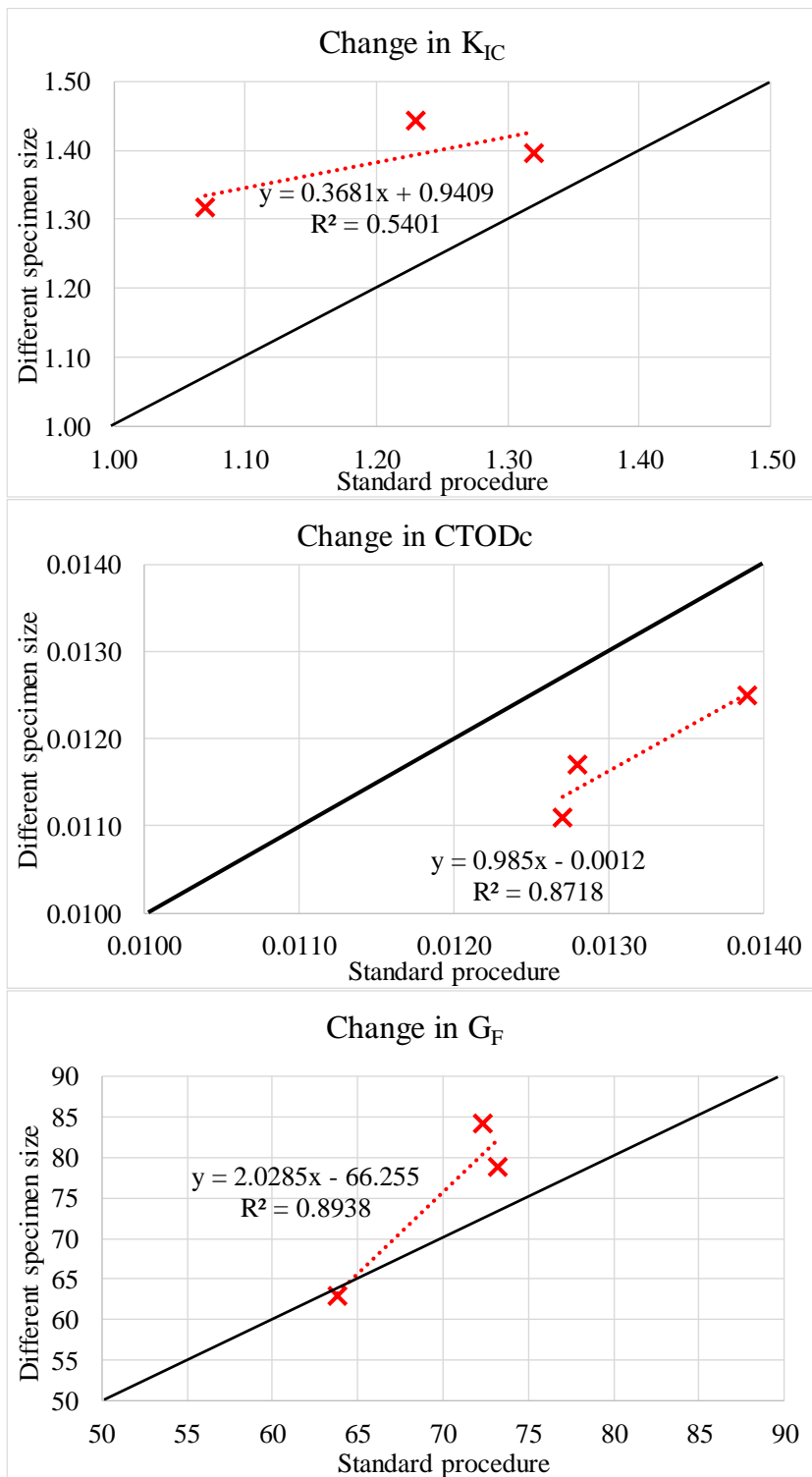
Figure 4.43. Comparison of fracture parameters obtained by standard specimen sizes and fatigue specimen sizes for the same mixtures

Relationships between the fracture parameters and the slopes of the fatigue curves of the mixtures were investigated to permit easier estimation of RCCs fatigue strength. As can be seen in Table 4.12, slopes of slopes of S-N curves for each 200, 400, and 600 kg/m^3 binder dosage RCC mixture were found to be 0.0503, 0.0431, and 0.0436, respectively.

For each mixture, the relationships between fracture parameters (K_{Ic} and $CTOD_c$) and the slopes of fatigue curves are given in Figure 4.44. As can be seen from the graphs, there is a relationship between nonlinear two parameter fracture model (TPFM) parameters: critical stress intensity factor (K_{Ic}) and critical crack tip opening displacement ($CTOD_c$) and slopes of RCC fatigue curves. However, the linear relationship between the slope of fatigue curves and other fracture parameters, the initial critical crack length (a_c) and total refractive energies, (G_f and G_F) is at low.

The following equations are proposed for predicting the slopes of S-N fatigue curves (S_F) from the critical stress intensity factor (K_{Ic}) and the critical crack-tip opening displacement ($CTOD_c$), but while further studies are needed for them to be verified, it should be noted that it takes at least two to three months for a concrete mixture to achieve a dependable fatigue curve slope.

$$S_F = -0.0602\ K_{Ic} + 0.129 \qquad R^2 = 0.90$$
$$S_F = -6.439\ CTOD_c - 0.0439 \qquad R^2 = 0.73$$

(4.9)
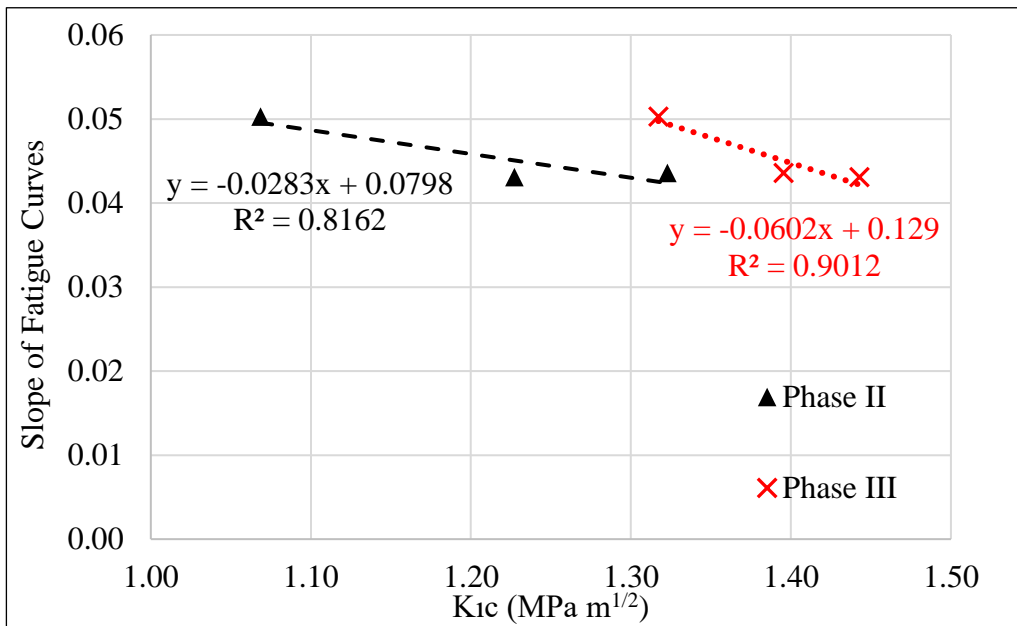
(a)
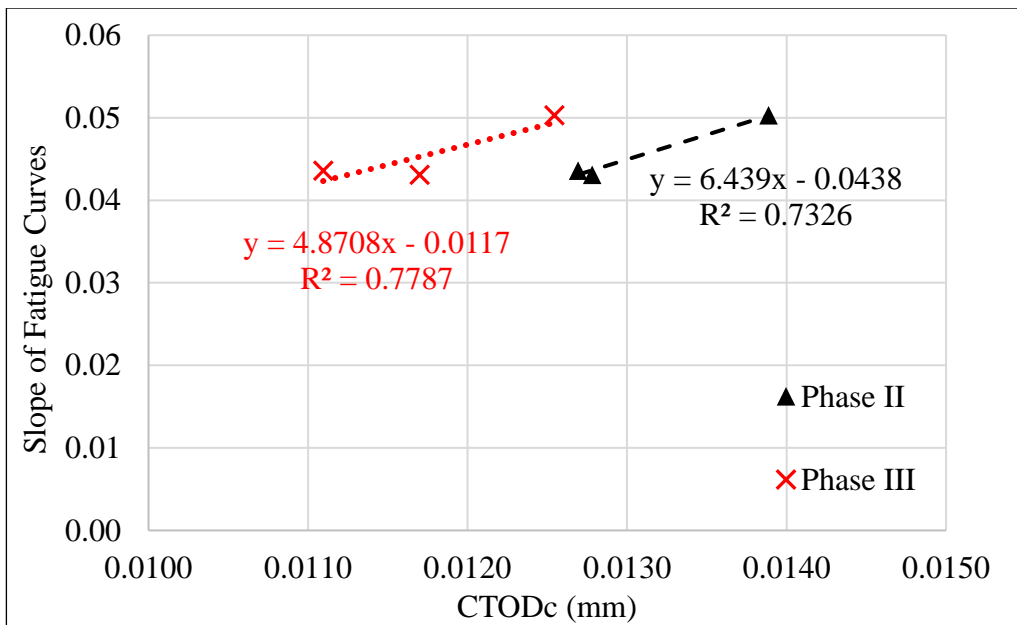
(b)

Figure 4.44. The relations between slopes of fatigue curves and fracture parameters (a) K_{IC} (b) $CTOD_c$ obtained from Phase II and Phase III

156

4.3.4. The Effects of Binder Content on RCC Fatigue Behavior

As found in phase I of this study, since the compaction ratio is a unique property for RCC mixtures, its effect on fatigue behavior is much sought for. For further analysis, the densities of beam specimens subjected to fatigue test were measured using width, length, depth and weight data before testing, and the compaction ratio of each specimen was calculated by dividing the hardened densities to the maximum theoretical air-free density of each corresponding mixture. Bivariate correlations (Pearson's correlation coefficient), Regression Analysis, and ANOVA (Analysis of variance) tests were performed using IBM SPSS 22.0 (IBM Corp, 2013) software to investigate the relationship between the number of load cycles to failure (N) and stress ratios (S) and mixture design parameters such as compaction ratios (CR), binder amount (B) and water-to-binder ratio (W/B) for each RCC specimen data. Results of Pearson's correlation coefficients for each RCC mixture are presented in Table 4.14.

Table 4.14. *Results of Pearson's correlation coefficient for RCC mixture.*

	N	S	CR	B	W/B
Pearson Correlation	1	-0.896[**]	0.475[**]	0.067	-0.048
Sig. (2-tailed)		0.000	0.000	0.610	0.716
n	61	61	61	61	61

** Correlation is significant at the 0.01 level (2-tailed).

As can be seen in Table 4.14, the number of load cycles to failure (N) (up to 2 million cycles) yielded the maximum linear correlation with the stress ratios (S). As expected, this is a negative relationship, and increasing the number of fatigue stresses/loads reduces the number of load cycles/repetitions before failure. In Table 4.14, the second statistically-significant correlation (sig<0.001) is seen as a positive relationship between the number of load cycles to failure and the compaction ratios of the beam specimens. In other words, a high compaction ratio suggests that the RCC specimen

can withstand more load cycles under the same stress/load. On the other hand, no correlation is seen between the binder amount and the water/binder ratio for the number of load cycles.

After the correlation procedure to study the strength of relationships between the variables before fitting a model was completed, linear regression analysis was used to model the value of a dependent scale variable (number of load cycles to failure-N) based on its linear relationship to predictors (stress ratio-S; compaction ratio-CR; binder ratio-B; water to binder ratio-W/B). ANOVA analysis was also performed to check regression model fit, and the results of the linear regression analysis and an ANOVA table for the model are summarized in Table 4.15. As seen in the model summary, Adj. $R^2 = 85\%$ represents the predictive power of the model. The regression model is statistically significant since the significance level (p value) is less than 0.05 in the ANOVA table. In other words, this ANOVA table indicates that using the model is better than guessing the mean. Statistically significant contribution to the model came from the stress ratio (sig. <0.001) followed by binder amount (sig. <0.01), compaction ratio (sig. <0.01) and water-to-binder ratio (sig. <0.05).

As a result of the regression analysis, the fatigue life equation for estimating the number of load cycles/repetitions to failure (N) for RCC mixtures can be obtained as follows.

$$\text{Log(N)} = 4.826\text{-}17.136 \ (S)+15.597 \ (CR)\text{-}10.828 \ (B)\ \text{-}3.908 \ (W/B)$$
$$\text{Adj. } R^2=0.85$$

(4.10)

The fatigue life model developed by considering binder dosage, compaction ratio and water/binder ratio, critical parameters for RCC mixtures, is more realistic and novel than other RCC fatigue life estimation models found in the literature that contain only stress ratios.

Table 4.15. *Results of the linear regression analysis and ANOVA table*

Model Summary

Model	R	R Square	Adjusted R Square	Std. Error of the Estimate
1	.928[*]	.862	**.850**	.71056

ANOVA[*]

Model	Sum of Squares	df	Mean Square	F	Sig.
1 Regression	154.195	4	38.549	76.350	**.000**[**]
Residual	24.740	56	.505		
Total	178.934	60			

Coefficients[a]

Model		Unstandardized Coefficients B	Std. Error	Standardized Coefficients Beta	t	Sig.
1	(Constant)	**4.826**	6.253		0.772	**.444**
	S	**-17.136**	1.194	-.872	14.356	**.000**
	CR	**15.597**	5.746	.187	2.714	**.009**
	B	**-10.828**	3.157	-.449	-3.430	**.001**
	W/B	**-3.908**	1.763	-.295	-2.217	**.031**

*Dependent Variable: N (logarithmic scale)
**Predictors: (Constant), B, W/B, S, CR

4.3.5. Discussion

In the second phase of the experimental study, mechanical performance and fracture properties of seven different RCC mixtures produced with DDVHR, that can simulate field compaction conditions in the laboratory, were investigated. In this phase, the last part of the experimental study, three mixtures of different strength levels were selected from seven RCC mixtures whose mechanical performance and fracture properties were determined, and their 28-day fatigue performances were examined. The relationship between fatigue behavior of RCC mixtures and its fracture parameters as well as its mixture design were explored with the goal of improving accuracy in estimating fatigue strength of the RCC mixtures with fracture parameters derived from relatively easier and shorter processes rather than costly and lengthy processes

involved in fatigue tests. In the preparation, placing, and compacting of the selected RCC mixtures (C200-12, C400-D12, B600-D12), previously-determined procedures were followed and each mixture laid on a steel plate of 85x200x15 cm^3 was first pre-compacted using a VPC, after which a DDVHR was used for full-size compaction to simulate field compaction conditions in the laboratory. However, unlike in the previous phase, a very thin cement grout layer was applied to the plate surface to prevent small-sized undulations that could result in a negative effect caused by load heads not being balanced. Beam specimen sizes of 10x15x35 cm^3 were cut and removed from the plates of each RCC mixture to be used in fatigue tests. Four specimens from each mixture were subjected to four-point static flexural tests (ASTM C78) to determine maximum and minimum fatigue loads for each stress level. A four-point flexural fatigue test was carried out with load control provided by a servo-hydraulic (MTS Landmark 250 kN) test machine. Fatigue loads calculated for each stress ratio (55%, 62.5%, 70%, 77.5%, and 85%) were applied to the specimens at a loading frequency of 10 Hz (10 cycles per 1 second) and this test continued until either the specimen failed or reached 2 million load cycles/repetitions. Similarly, the minimum fatigue load was calculated by converting the load to 20% of the ultimate flexural strength. The S-N approach used in all conventional concrete studies in the literature was also used to analyze fatigue behavior of RCC mixtures. S-N fatigue curves for each mixture were obtained by fatigue tests performed on a total of 61 RCC beam specimens.

Although the fracture parameters of the RCC mixtures were determined during the second phase of the experimental study, to make more accurate correlations with the fatigue test results, fracture parameters and total fracture energies on the beam specimens obtained from the plate prepared for fatigue specimens were determined once again, and at least three specimens from each mixture were used to find fracture parameters in accordance with the new specimen size (10x15x35 cm^3).

For the three different RCC mixtures, the results from the 28-day four-point flexural fatigue tests, JCI, and RILEM fracture tests performed during this phase, and the

relationships between fatigue behavior and its fracture parameters as well mixture design are summarized below.

- The ultimate static flexural strengths (MR) of 200, 400 and 600 kg/m³ binder dosage RCC mixtures were obtained as averages of 4.00 MPa, 5.06 MPa and 5.16 MPa, respectively.

- Since 2 million load cycles/repetitions is reported in the literature as a sufficient number of cycles for determination of fatigue strength in studies investigating fatigue behavior on concrete, it follows that fatigue strength for RCC mixtures with binder dosages of 200 kg/m³ and 400 kg/m³ correspond to about 62 and 65% of their ultimate static flexural strengths. In the last RCC mixture that had a binder dosage of 600 kg/m³, fatigue strength was found as 58% of the ultimate static flexural strength. The average fatigue strength of RCC mixtures was about 62.5% of the ultimate static strength.

- Since studies in the literature indicate that fatigue strength for conventional concrete generally corresponds to 50-55% of ultimate static flexural strengths, it can be stated that RCC mixtures have better fatigue strength than that of conventional concrete.

- The S-N fatigue curve for a single RCC mixture was obtained by considering fatigue data from a total of 61 beams of all RCC mixtures taken together. When the result is compared to other RRC fatigue curves reported in the literature, it can be seen hat the slope of fatigue curves obtained from this study is generally lower than that slope of fatigue curves obtained from other studies.

- Especially in comparison with the fatigue curve obtained by Tayabji & Okamoto, (1987), one of the most comprehensive studies on RCC fatigue found behavior in the literature, the fatigue model developed in this study is more conservative (safer) at loads higher than 68% of the ultimate strength, the intersection point of the two fatigue models, while the fatigue model

developed by Tayabji & Okamoto, (1987) is more conservative below this value (or higher cycle loading). When fatigue strengths corresponding to 2 million load cycles for both fatigue models are compared, Tayabji & Okamoto, (1987) describe fatigue strength of RCC as about 50% of the ultimate static strength, while fatigue strength of RCC in this model is about 62% of the ultimate static flexural strength. In other words, the RCCs obtained from this study reflected better fatigue performance than the RCCs conducted by Tayabji & Okamoto, (1987). However, since the study done by Tayabji and Okamoto (1987) was used lower binder amounts and different aggregate gradations with river gravels, it is to be expected that different behaviors.

- When fatigue curves obtained from current RCC fatigue studies are compared with RCC fatigue curves from this study, the slope of developed RCC fatigue curve lies between the slope of RCC fatigue curves developed by Modarres & Hosseini, (2014) and that of the Sun et al., (1998) study. However, it should be noted that in the current RCC fatigue studies, a limited number of samples were subjected to fatigue tests (commonly three samples for each stress ratio except for Sun et al., (1988)) and different compaction methodologies were used to produce beam samples in laboratory because of lack of a standard procedure for compaction of beams in the laboratory, so differences in fatigue behavior would be expected. When the fatigue strengths obtained from current RCC fatigue curves for 2 million load cycles are compared, the fatigue strength is about 62% of the ultimate static strength for the fatigue model developed by Sun et al., (1988), while fatigue strength is about 50% of the ultimate static strength for the fatigue model developed by Graeff, et al., (2012).

- Fatigue curves obtained from conventional concrete both in in the literature and those used in concrete pavement design by PCA were also compared with the RCC fatigue curve obtained from this study. In particular, the fatigue curve for PCC obtained by Murdock & Kesler, (1958) is quite similar to the fatigue curve obtained for RCC mixtures in this study. While both curves yielded the

same fatigue strength of 62% for 2 million load cycles, when the PCA, (1984) fatigue curve is examined, it can be seen that it produces more conservative results for RCC pavement designs. In other words, if the RCC pavement thickness is chosen according to the PCA fatigue curve, the pavement thickness will be thicker than that corresponding to the RCC fatigue design obtained from this study. It should not be forgotten, however, that the probability of failure parameter was not considered in the RCC curve, and taking into account the probability of failure, e.g., for 95% reliability, this curve will be slightly lower. Furthermore, it can be seen that the fatigue strength corresponding to the PCA, (1984) curve is about 50% of its ultimate static strength for 2 million load cycles.

- When the results from fracture tests performed on beam specimens obtained from the mixtures in this phase in accordance with JCI-S-001-2003 (2003) and RILEM TC 89-FMT (1990) procedures were examined, it could be observed that the results differed from the values obtained for the same mixtures in the previous phase. This occurred because the specimen sizes related to JCI-S-001-2003 (2003) and RILEM TC 89-FMT (1990) procedures in the previous phase were $10x10x35$ cm^3 and $8x15x70$ cm^3, respectively, while in this phase, beam specimens for fatigue testing of size $10x15x35$ cm^3 were used in both JCI and RILEM procedures, and this change in specimen size partially affected the fracture parameters, although total fracture energies were very close to one another. While the fact that the two dimensions ($10x10x35$ cm^3 and $10x15x35$ cm^3) are in pretty close agreement is thought to affect these results, different specimen sizes resulted in some serious changes, especially in the K_{Ic} within the fracture parameters, with a larger K_{Ic} obtained by decreasing the sample size. By contrast, $CTOD_c$ increased with increasing sample size.

- The fatigue curve slope for each RCC mixture was compared with fracture parameters obtained both in this phase and the previous phase to facilitate the fatigue-strength estimation process. After the correlation, it was realized that

there is a strong relationship between two TPFM parameters: critical stress intensity factor (K_{Ic}) and critical crack tip opening displacement ($CTOD_c$), and the slope of the RCC fatigue curves. Even though the coefficient of determination in the regression seems high, further studies are needed to verify this result.

- Pearson's correlation coefficient was utilized to statistically analyze bivariate linear correlations between number of load cycles to failure (N) and stress ratio (S) as well as mixture design parameters such as compaction ratio (CR), binder amount (B), and water-to-binder ratio (W/B) for each RCC specimen data. As expected, the number of load cycles to failure achieved the maximum linear correlation with the stress ratios, a negative relationship, and increasing the number of fatigue stresses/loads reduces the number of load cycles/repetitions to failure. A second significant correlation was found in the positive relationship between the number of load cycles to failure and the compaction ratio of the beam specimens. A linear regression model was also developed using RCC specimen data to predict the number of load cycles to failure based on stress ratio, compaction ratio, binder amount, and water-to-binder ratio, and it was proven to be significant by the ANOVA analysis (p<0.001).

- Therefore, developed fatigue life model by considering the binder amount, compaction ratio and water/binder ratio, which is critical parameters for RCC mixtures, it has been more realistic and novel than the other RCC fatigue life estimation models in the literature which contains only stress ratios.

In conclusion, it is thought that this new RCC fatigue model, by exhibiting similar behavior with respect to fatigue curve slope of conventional concrete to RCC fatigue models in the literature, but much higher fatigue strength than traditional concrete, could with further development be used as a more innovative model in road pavement designs. Remarkable evidence was also found that predicting fatigue performances of RCC mixtures, a time-consuming and complicated process, can be accomplished in

164

relatively shorter time and more easily than with fracture parameters. It was also realized that compaction ratio, one of the critical parameters for RCC mixtures, had a significant effect on fatigue behavior of RCC mixtures and it is included in the regression models for RCC fatigue behavior developed in this study. It would be useful to verify all these suggestions by through future.

CHAPTER 5

SUMMARY, CONCLUSIONS AND RECOMMENDATIONS

RCC technology offers great advantages, especially in road applications, in providing rapid and economic solutions. The main advantage of RCC is its capacity for being compacted using the same equipment used for traditional flexible asphalt pavement. Because of its advantages, its use on pavements have been accelerated in the 21th century not only in Turkey, but also in USA and elsewhere in the world. However, a fully efficient laboratory compaction methodologies that can simulate actual field compaction procedures has not been developed. In addition, the key parameter for a successful RCC pavement application is the choice of correct thickness, which largely depends on mechanical, fracture and fatigue properties of RCC mixtures. However, there is inadequate number of related data since it is not easy to determine these properties under laboratory conditions. This comprehensive three-phase experimental study attempts to address the lack of information found on the subject in academic literature and guide contractors using RCC pavement applications in Turkey.

This thesis describes the preparation of RCC mixtures of different strength classes using compaction methodology that can simulate field compaction conditions in the laboratory, and determine mechanical performance, fracture properties and fatigue behavior of the designed RCC mixtures. In addition, effects of mixture design parameters on these properties of RCC and the relationships between fatigue performance of RCC mixtures and their fracture parameters were also investigated. The first phase of this comprehensive experimental program addressed the process of determination of optimum RCC mix design considering density, strength, and workability (compactability) parameters, as well as development of a proposed DDVHR compaction methodology for simulating field compaction conditions based on these parameters. Since different mixture designs and compaction methods applied

during the preparation of RCC specimens can be found in the literature studies, it is highly significant to determine appropriate mixture design parameters and laboratory compaction methodology for the preparation of RCC specimens, and no fully efficient laboratory method has been found to represent the compaction procedures applied in the field. To this end, RCC mixtures were prepared with different cement dosages, aggregate sizes, and water ratios, which are the three main factors affecting the concrete matrix. A total of twenty RCC mixtures were compacted by four different laboratory compaction methods: modified proctor, vibrating hammer, vibrating table, and SGC, followed by producing 150 mm diameter cylindrical specimens by applying these compaction methods to each mixture. Following the tests carried out on the RCC specimens, optimum RCC mixture-design parameters based on density, strength, and compactability were identified for use in the subsequent phases of the study. A compaction methodology using a DDVHR was also implemented to represent field compaction procedures in the laboratory. During the second phase of the experimental study, taking the optimum RCC mixture-design parameters as a reference, RCC roads (plates) of different strength classes were poured and compacted using DDVHR compaction methodology, after which cylindrical cores and beam specimens were taken from the plates and mechanical and fracture-related properties (RILEM and JCI procedures) of the mixtures were determined. During the final phase of the study, flexural fatigue performance for three RCC mixtures of different strength classes was determined and expressed as S-N curves, and relationships between its fracture parameters and its mixture design parameters were examined.

Based on the experimental results, the following conclusions can be drawn:

- Laboratory compaction methods have a profound effect on the physical and mechanical properties of RCC mixtures. In addition, compaction ratio, which is one of the most important parameters defining RCC properties, is highly affected by not only compaction methods but also mixture parameters such as binder amount and water content.

168

- Ideal RCCs can be achieved from mixtures with water amounts of 5-6% and the compaction ratios higher than 96% and can be produced using DDVHR compaction methodology under laboratory conditions with vebe time of about 30 sec.

- The RCC mixtures reached about 65% of their 28 day-compressive strength after 2 days and about 80% after 7 days, and these levels would be sufficient to carry light traffic even with at lowest cement dosage (> 15 MPa) (Harrington et al. 2010). This is an essential point differentiating RCC from traditional concrete in pavement application.

- K_{Ic}, which is a measure of the resistance to crack propagation in materials, was found higher than 1.0 MPa.m$^{1/2}$ even in the lowest dosage mixture which is the typical value of conventional concrete pavements and enhanced with increasing in binder dosage. Similarly, an increase in maximum aggregate size led to an increase in K_{Ic} in all RCC mixtures, with the amount of growth varying between 11% and 15% depending on the binding content. Furthermore, the K_{Ic} increased linearly with increase in compressive strength for all RCC mixtures.

- An increase in the maximum aggregate size led to increase in $CTOD_c$ and the $CTOD_c$ tended to decrease with an increase in compressive strength. Contrary to expectations, neither an increase in binder dosage nor maximum aggregate size led to a significant change in fracture energy and toughness. The 600 kg/m^3 binding mixture specially developed for obtaining a high strength RCC appeared to have the lowest fracture energy. A comparison between the RILEM fracture parameters and the characteristic length revealed that the latter is inversely proportional to K_{Ic} but directly proportional to $CTOD_c$, i.e., the mixture with a larger K_{Ic} exhibits more brittle behavior, and the one with a smaller $CTOD_c$ would similarly be expected to exhibit more brittle behavior.

- The effect of the compaction ratio on fracture parameters was quite significant as in the compressive and flexural strengths, but fracture properties were highly affected by size effect such as notch depth, notch width or specimens height and width.

- The four-point flexural fatigue tests were performed for three RCC mixtures of different strength classes on a total of 61 beam specimens with dimensions 10x15x35 cm^3 cut from the RCC roads (plates) produced by DDVHR, and the average fatigue strength of the RCC mixtures, corresponding to 2 million load cycles, was found to be about 62.5% of the ultimate static strength.

- The fatigue curve slope for each RCC mixture was compared with fracture parameters obtained both in this phase and the previous phase to facilitate the fatigue-strength estimation process. After the correlation, it was realized that there is a strong relationship between two TPFM parameters: K_{Ic} and $CTOD_c$, and the slope of the RCC fatigue curves. Even though the coefficient of determination in the regression seems high, further studies are needed to verify this result.

- According to the Pearson's correlation coefficient analysis performed on a total of 61 beam specimens, a statistically significant (sig<0.001) positive correlation between the number of load cycles to failure and the compaction ratios of the beam specimens was observed. In other words, since a high compaction ratio suggests that an RCC specimen can withstand more load cycles under the same stress/load,

- The developed fatigue life model, by considering the binder amount, compaction ratio, water to binding ratio, which are the one of the most critical parameters for RCC mixtures, provides a more realistic and novel solution than other RCC fatigue life estimation models found in the literature that consider only stress ratios.

170

In particular, its determination of the number of load cycles corresponding to a stress ratio (S-N fatigue curve) over a total of 61 beam specimens obtained by cutting from the RCC roads (plates) produced by DDVHR to simulate field compaction conditions is a valuable contribution to the literature based on the known fact that S-N fatigue curve studies required for RCC pavement design have been extremely limited because fatigue tests represent highly complex, costly, and time-consuming processes. In practice, the S-N curves obtained about thirty years ago or produced for conventional concrete roads are still utilized both in guidelines and RCC pavement design software, and the use of relatively few specimens in producing those fatigue curves because of cost and time penalties further highlights the potential impact of this study on the academic literature.

However, to integrate the fatigue data obtained from this study into RCC pavement design software in the USA and/or to create RCC pavement design guides or software for use in Turkey requires further and more advanced development of this study's methodology. The scope and other constrains to this study prevented entering into full RCC pavement design, but future studies could significantly advance the study's S-N curve approach by formulating a RCC pavement design fatigue curve and making improvements with respect to design parameters such as reliability and failure probability. The allowable pavement stress consistent with ultimate static strength of material could be related to the number of wheel load applications over a selected design period, using a S-N design fatigue curve through which a design thickness for RCC pavement could be calculated with respect to allowable pavement stress, taking into account both subgrade/subbase strength and environmental factors. This could make possible development of a special RCC pavement design guide with related software for our country.

Finally, as compaction ratio was determined to be the most influential parameter on the compressive and flexural strength, fracture and fatigue properties of RCC, effect of aggregate gradation on the compaction properties as well as fracture parameters can be investigated.

REFERENCES

Abrams, D. A. (1918). Design of concrete mixtures. *Bulletin*, *1*, 1–22.

ACI (American Concrete Institute). (1992). *Considerations for Design of Concrete Structures Subjected to Fatigue Loading* (ACI 215R-92). Farmington Hills, MI: American Concrete Institute.

ACI (American Concrete Institute). (2015). *Guide to roller-compacted concrete pavements (*ACI 327R-14). Farmington Hills, MI: American Concrete Institute.

ACI (American Concrete Institute). (1995). *Report on roller-compacted mass* concrete (ACI 207.5R-99). Farmington Hills, MI: American Concrete Institute.

ACPA (American Concrete Pavement Association). (2014). *Roller-Compacted Concrete Guide Specificaiton*. Retrieved from http://www.acpa.org/wp-content/uploads/2014/11/ACPA-Roller-Compacted-Concrete-Guide-Specification-Version-1.2.pdf

Ağar, E., & Taşdemir, Y. (2007). Silindirle Sıkıştırılabilen Beton Yollar. *Türkiye Hazır Beton Birliği*. Retrieved from http://www. thbb. org/article. aspx.

Aghaeipour, A., & Madhkhan, M. (2017). Effect of ground granulated blast furnace slag (GGBFS) on RCCP durability. *Construction and Building Materials*, *141*, 533–541.

Akcay, B., Agar-Ozbek, A. S., Bayramov, F., Atahan, H. N., Sengul, C., & Tasdemir, M. A. (2012). Interpretation of aggregate volume fraction effects on fracture behavior of concrete. *Construction and Building Materials*, *28*(1), 437–443.

Akkaya, Y., Bayramov, F., & Taşdemir, M. A. (2003). Betonun Kırılma Mekaniği Tasarımda Kullanılan Mekanik Özelikler İle Kırılma Parametreleri Arasındaki Bağıntılar, Türkiye Mühendislik Haberleri. *Türkiye Mühendislik Haberleri*, *426*(4), 70–75.

Amer, N., Delatte, N., & Storey, C. (2003). Using gyratory compaction to investigate density and mechanical properties of roller-compacted concrete. *Transportation Research Record: Journal of the Transportation Research Board*, (1834), 77–84.

Amer, N., Storey, C., & Delatte, N. (2004). Roller-compacted concrete mix design procedure with gyratory compactor. *Transportation Research Record: Journal of the Transportation Research Board*, (1893), 46–52.

Anderson, T. L. (2017). *Fracture mechanics: fundamentals and applications*. CRC press.

Antrim, J. D. (1967). The mechanism of fatigue in cement paste and plain concrete. *Highway Research Record*, (210), 95-107.

ASTM C1170. (2014). *Standard Test Method for Determining Consistency and Density of Roller-Compacted Concrete Using a Vibrating Table*. West Conshohocken, PA.

ASTM C1176. (2013). *Standard Practice for Making Roller-Compacted Concrete in Cylinder Molds Using a Vibrating Table*. West Conshohocken.

ASTM C125-19. (2019). *Standard Terminology Relating to Concrete and Concrete Aggregates*. West Conshohocken, PA.

ASTM C127-15. (2015). *Standard Test Method for Relative Density (Specific Gravity) and Absorption of Coarse Aggregate*. West Conshohocken, PA.

ASTM C128-15. (2015). *Standard Test Method for Relative Density (Specific Gravity) and Absorption of Fine Aggregate*. West Conshohocken, PA.

ASTM C1352M-15. (2015). *Standard Test Method for Flexural Modulus of Elasticity of Dimension Stone*. West Conshohocken, PA.

ASTM C136M-14. (2014). *Standard Test Method for Sieve Analysis of Fine and*

Coarse Aggregates. West Conshohocken, PA.

ASTM C1435. (2014). *Standard Practice for Molding Roller-Compacted Concrete in Cylinder Molds Using a Vibrating Hammer*. West Conshohocken. P.A.

ASTM C1800. (2016). *Standard Test Method for Determining Density of Roller-Compacted Concrete Specimens Using the Gyratory Compactor*. West Conshohocken, PA.

ASTM C33M-18. (2018). *Standard Specification for Concrete Aggregates*. West Conshohocken, PA.

ASTM C39 / C39M-18. (2018). *Standard Test Method for Compressive Strength of Cylindrical Concrete Specimens*. West Conshohocken, PA.

ASTM C496 / C496M-17. (2017). *Standard Test Method for Splitting Tensile Strength of Cylindrical Concrete Specimens*. West Conshohocken, PA.

ASTM C618-19. (2019). *Standard Specification for Coal Fly Ash and Raw or Calcined Natural Pozzolan for Use in Concrete*. West Conshohocken.

ASTM C642-13. (2013). *Standard Test Method for Density, Absorption, and Voids in Hardened Concrete*. West Conshohocken, PA.

ASTM C78 /C78M-18. (2018). *Standard Test Method for Flexural Strength of Concrete (Using Simple Beam with Third-Point Loading)*. West Conshohocken.

ASTM D1557-12e1. (2012). *Standard Test Methods for Laboratory Compaction Characteristics of Soil Using Modified Effort (56,000 ft-lbf/ft3 (2,700 kN-m/m3))*. West Conshohocken, PA.

ASTM D7313-13. (2013). *Standard Test Method for Determining Fracture Energy of Asphalt-Aggregate Mixtures Using the Disk-Shaped Compact Tension*

Geometry. West Conshohocken, PA.

ASTM WK33682. (n.d.). *Testing of Roller-Compacted Concrete Specimens to Be Covered in Proposed New ASTM Standard* | www.astm.org. Retrieved May 25, 2018, from https://www.astm.org/newsroom/testing-roller-compacted-concrete-specimens-be-covered-proposed-new-astm-standard

ASTM WK59339. (2017). *New Test Method for Laboratory Compaction Characteristics of Roller-Compacted Concrete Using Modified Effort (56,000 ft-lbf/ft3 (2,700 kN-m/m3))*. West Conshohocken, PA.

Ballinger, C. A. (1971). Cumulative fatigue damage characteristics of plain concrete. *Highway Research Record*, (370), 48–60.

Barenblatt, G. I. (1962). The mathematical theory of equilibrium cracks in brittle fracture. *Advances in applied mechanics*, *7*, 55–129.

Basquin, O. H. (1910). The exponential law of endurance tests. In *Proc Am Soc Test Mater*, *10*, 625–630.

Bauschinger, J. (1886). On the change of the elastic limit and the strength of iron and steel, by drawing out, by heating and cooling, and by repetition of loading (summary). *Minutes of Proceedings of the Institution of Civil Engineers with Other Selected and Abstracted Papers*, *87*, 463.

Bazant, Z. P. (2014). *Fracture Mechanics of Concrete Structures: Proceedings of the First International Conference on Fracture Mechanics of Concrete Structures (FraMCoS1), held at Beaver Run Resort, Breckenridge, Colorado, USA, 1-5 June 1992*. CRC Press.

Bažant, Z. P. (1984). Size effect in blunt fracture: concrete, rock, metal. *Journal of Engineering Mechanics*, *110*(4), 518–535.

Bažant, Z. P., & Oh, B. H. (1983). Crack band theory for fracture of concrete.

Matériaux et Construction, *16*(3), 155–177.

Bazant, Z. P., & Sun, H.-H. (1987). Size effect in diagonal shear failure: influence of aggregate size and stirrups. *ACI Materials Journal*, *84*(4), 259–272.

Bordelon, A., Roesler, J., & Hiller, J. (2009). *Mechanistic-Empirical Design Concepts for Jointed Plain Concrete Pavements in Illinois*. Illinois, USA.

Browne, M. J. (2006). *Feasability of using a gyratory compactor to determine compaction characteristics of soil.* Montana State University-Bozeman, College of Engineering.

Carpinteri, A. (1982). Application of fracture mechanics to concrete structures. *Journal of the Structural Division*, *108*(4), 833–848.

CEB Bultenin No.189. (1988). *Fatigue of Concrete Structures - State of the Art Report*. Belgium.

Cerni, G., & Camilli, S. (2011). Comparative analysis of gyratory and Proctor compaction processes of unbound granular materials. *Road Materials and Pavement Design*, *12*(2), 397–421.

Chhorn, C., Hong, S. J., & Lee, S.-W. (2017). A study on performance of roller-compacted concrete for pavement. *Construction and Building Materials*, *153*, 535–543.

Chhorn, C., & Lee, S. W. (2016a). Consistency control of roller-compacted concrete for pavement. *KSCE Journal of Civil Engineering*, *21*(5), 1757–1763.

Chhorn, C., & Lee, S. W. (2016b). Influencing compressive strength of roller-compacted concrete. *Proceedings of the Institution of Civil Engineers-Construction Materials*, *171*(1), 3-10.

Choi, Y.-K., & Groom, J. L. (2001). RCC Mix Design-Soils Approach. *Journal of Materials in Civil Engineering*, *13*(1), 71–76.

Clemmer, H. F. (1922). Fatigue of concrete. *Proc. Amer. Soc. Test. Mater, 22,* 402–419.

Coffin Jr, L. F. (1954). A study of the effects of cyclic thermal stresses on a ductile metal. *Transactions of the American Society of Mechanical Engineers, New York*, *76*, 931–950.

Collins, R., Watson, D., Johnson, A., & Wu, Y. (1997). Effect of aggregate degradation on specimens compacted by superpave gyratory compactor. *Transportation Research Record: Journal of the Transportation Research Board*, (1590), 1–9.

Cook, D. J., & Crookham, G. D. (1978). Fracture toughness measurements of polymer concretes. *Magazine of Concrete Research*, *30*(105), 205–214.

Crepps, R. B. (1923). Fatigue of mortar. *Proc. Amer. Soc. Test. Mater, 23,* 329–340.

Dugdale, D. S. (1960). Yielding of steel sheets containing slits. *Journal of the Mechanics and Physics of Solids*, *8*(2), 100–104.

Ferrebee, E., Brand, A., Kachwalla, A., Roesler, J., Gancarz, D., & Pforr, J. (2014). Fracture properties of roller-compacted concrete with virgin and recycled aggregates. *Transportation Research Record: Journal of the Transportation Research Board*, (2441), 128–134.

Filho, J. M., Paulon, V. A., Monteiro, P. J. ., Andrade, P. de, & Dal Molin, D. (2008). Development of Laboratory Device to Simulate Roller-Compacted Concrete Placement. *ACI Materials Journal*, *105*(2), 125–130.

Glucklich, J. (1963). Fracture of plain concrete. *Journal of the Engineering Mechanics Division*, *89*(6), 127–138.

Glucklich, J. (1965). Static and fatigue fractures of portland cement mortar in flexure. *Transportation Research Board, 90*(2), 1343-1382.

Graeff, A. G., Pilakoutas, K., Neocleous, K., & Peres, M. V. N. N. (2012). Fatigue resistance and cracking mechanism of concrete pavements reinforced with recycled steel fibres recovered from post-consumer tyres. *Engineering Structures*, *45*, 385–395.

Griffith, A. A., & Eng, M. (1921). VI. The phenomena of rupture and flow in solids. *Phil. Trans. R. Soc. Lond. A*, *221*(582–593), 163–198.

Guo, L.-P., Carpinteri, A., Spagnoli, A., & Sun, W. (2010). Experimental and numerical investigations on fatigue damage propagation and life prediction of high-performance concrete containing reactive mineral admixtures. *International Journal of Fatigue*, *32*(2), 227–237.

Harrington, D., Abdo, F., Adaska, W., Hazaree, C. V, Ceylan, H., & Bektas, F. (2010). *Guide for roller-compacted concrete pavements*. Concrete Pavement Technology Center, Iowa, USA.

Hatt, W. K. (1925). Fatigue of concrete. *Highway Research Board Proceedings*, 4, 47-60.

Hazaree, C., Ceylan, H., & Wang, K. (2011). Influences of mixture composition on properties and freeze–thaw resistance of RCC. *Construction and Building Materials*, *25*(1), 313–319.

Hillerborg, A. (1985). The theoretical basis of a method to determine the fracture energyG F of concrete. *Materials and Structures*, *18*(4), 291–296.

Hillerborg, Arne, Modéer, M., & Petersson, P.-E. (1976). Analysis of crack formation and crack growth in concrete by means of fracture mechanics and finite elements. *Cement and Concrete Research*, *6*(6), 773–781.

IBM Corp, N. (2013). IBM SPSS statistics for windows. *Version 22.0.*

Inglis, C. E. (1913). Stresses in a plate due to the presence of cracks and sharp corners. *Transactions of the Institute of Naval Architects*, *55*(219–241), 193–198.

Irwin, G. R. (1957). Analysis of stresses and strains near the end of a crack traversing a plate. *J. Appl. Mech. Transactions of the ASME, 24,* 351-369.

Japan Concrete Institute Standard (JCI-S-001-2003). (2003). *Method of test for fracture energy of concrete by use of notched beam.* Retrieved Sep 27, 2019, from http://www.jci-net.or.jp/j/jci/study/jci_standard/JCI-S-001-2003-e.pdf

Jenq, Y., & Shah, S. P. (1985). Two parameter fracture model for concrete. *Journal of Engineering Mechanics*, *111*(10), 1227–1241.

Jimenez Pique, E. R. A. (2002). *Fracture process zone of quasi-brittle materials : a model material approach.* (PhD Thesis). Technische Universiteit Eindhoven.

Kaplan, M. F. (1961). Crack propagation and the fracture of concrete. *Journal Proceedings*, *58*(11), 591–610.

Kesler, Clyde E. (1953). Effect of speed of testing on flexural fatigue strength of plain concrete. In *Highway Research Board Proceedings*, *32*, 251-258.

Kesler, C. E., Naus, D. J., & Lott, J. L. (1972). Fracture mechanics-its applicability to concrete. *Proceedings of the Society of Materials Science Conference on the Mechanical Behavior of Materials.* 113-124.

Kesler, C. E. (1970). *Fatigue and fracture of concrete*, Stanton Walker Lecture Series of the Materials Sciences,National Sand and Gravel Association and National Ready Mixed Concrete, Association. University of Maryland, College Park.

KGM. (2013). *Karayolu Teknik Şartnamesi (Yol Üstyapısı, Sanat Yapıları, Köprü ve*

Tüneller, Üstyapı ve Çeşitli İşler). Retrieved September 20, 2019, from https://www.tamyol.com.tr/UserFiles/Content/KGM_Teknik_Sartnamesi_2013.pdf.

Khalilpour, S., BaniAsad, E., & Dehestani, M. (2019). A review on concrete fracture energy and effective parameters. *Cement and Concrete Research*, *120*, 294–321.

Kim, H., & Buttlar, W. G. (2009). Discrete fracture modeling of asphalt concrete. *International Journal of Solids and Structures*, *46*(13), 2593-2604.

Kim, J.-K., & Kim, Y.-Y. (1996). Experimental study of the fatigue behavior of high strength concrete. *Cement and Concrete Research*, *26*(10), 1513–1523.

Kumar, S., & Barai, S. V. (2011). *Concrete fracture models and applications*. Springer Science & Business Media.

LaHucik, Jeff, Dahal, S., Roesler, J., & Amirkhanian, A. N. (2017). Mechanical properties of roller-compacted concrete with macro-fibers. *Construction and Building Materials*, *135*, 440–446.

LaHucik, Jeffrey, & Roesler, J. (2017). Field and Laboratory Properties of Roller-Compacted Concrete Pavements. *Transportation Research Record: Journal of the Transportation Research Board*, (2630), 33–40.

Lange-Kornbak, D., & Karihaloo, B. L. (1996). Design of concrete mixes for minimum brittleness. *Advanced Cement Based Materials*, *3*(3–4), 124–132.

Lee, M. K., & Barr, B. I. G. (2004). An overview of the fatigue behaviour of plain and fibre reinforced concrete. *Cement and Concrete Composites*, *26*(4), 299–305.

Lee, S. W., Cho, Y.-H., & Park, C. (2014). Mechanical performance and field application of low cement based concrete under compaction energy. *KSCE Journal of Civil Engineering*, *18*(4), 1053–1062.

Lin, C., Jin, X., & Li, Z. (2004). Experimental study on some factors affecting fracture property of concrete [J]. *China Concrete and Cement Products*, *5*, 7–9.

Masad, E., Muhunthan, B., Shashidhar, N., & Harman, T. (1999). Quantifying laboratory compaction effects on the internal structure of asphalt concrete. *Transportation Research Record: Journal of the Transportation Research Board*, (1681), 179–185.

McCall, J. T. (1958). Probability of fatigue failure of plain concrete. *Journal Proceedings*, *55,* 233–244.

Mindess, S., & Nadeau, J. S. (1976). Effect of notch width on KIc for mortar and concrete. *Cement and Concrete Research*, *6*(4), 529–534.

Modarres, A., & Hosseini, Z. (2014). Mechanical properties of roller compacted concrete containing rice husk ash with original and recycled asphalt pavement material. *Materials & Design*, *64*, 227–236.

Mokwa, R., Cuelho, E., & Browne, M. (2008). Laboratory Testing of Soil Using Superpave Gyratory Compactor. *Transportation Research Board*, *1*(1), 14-17.

Murdock, J. W., & Kesler, C. E. (1958). Effect of range of stress on fatigue strength of plain concrete beams. In *Journal of the American Concrete Institue Proceedings*, *55,* 221–231.

Nallathambi, P., & Karihaloo, B. L. (1986). Determination of specimen-size independent fracture toughness of plain concrete. *Magazine of Concrete Research*, *38*(135), 67–76.

Neal, J. A., & Kesler, C. E. (1964). *Fifth Progress Report Mechanism of Fatigue Failure in Concrete*. Department of Theoretical and Applied Mechanics, University of Illinois.

Neocleous, K., Angelakopoulos, H., Pilakoutas, K., & Guadagnini, M. (2011). Fibre-

reinforced roller-compacted concrete transport pavements. *Proceedings of the ICE-Transport*, *164*(TR2), 97–109.

Neocleous, K., Pilakoutas, K., & Guadagni, M. (2009). EcoLanes: Paving the Future for Environmentally-Friendly and Economical Concrete Roads. *Intersections, 6*(2), 59-74.

Okamoto, P. A. (2008). *Roller Compacted Concrete Pavement Properties* (RCA R&D Serial No. SN2996). Portland Cement Association, Skokie, IL.

Özcan, S. (2008). *Bonding Efficiency Of Roller Compacted Concrete With Different Bedding Mixes*. Middle East Technical University. Retrieved from http://etd.lib.metu.edu.tr/upload/12610189/index.pdf

Öztürk, H. I., Tan, B. E., Şengün, E**,** Yaman, İ. Ö. (2019), "Comparison of Jointed Plain Concrete Pavement Systems Designed by Mechanistic-Empirical (M-E) Method for Different Traffic, Subgrade, Material and Climatic Conditions", *Journal of the Faculty of Engineering and Architecture of Gazi University,* 34(2), 771-783.

Packard, R. G. (1984). *Thickness design for concrete highway and street pavements,* Portland Cement Association (PCA).Skokie, III.

Paris, P. C., Gomez, M. P., & Anderson, W. E. (1961). A Rational Analytical Theory of Fatigue, *The Trend in Engineering, 13*(1), 9-14.

Pasetto, M., & Baldo, N. (2014). Comparative analysis of compaction procedures of unbound traditional and non-conventional materials. In *Pavements Unbound: Proceedings of the 6th International Symposium on Pavements Unbound (UNBAR 6), 6-8 July 2004,* Nottingham, England.

Peterson, R., Mahboub, K., Anderson, R., Masad, E., & Tashman, L. (2003). Superpave® laboratory compaction versus field compaction. *Transportation Research Record: Journal of the Transportation Research Board*, (1832), 201–208.

Pittman, D. (2012). "U.S. Army Corps of Engineers Experience with Roller Compacted Concrete Pavements." *Symposium on Integrated Cement Based Pavement Soluations, Part 2: Roller Compacted Concrete Pavements*. American Concrete Institute.

Planas, J., & Elices, M. (1989). Size effect in concrete structures: Mathematical approximations and experimental validation. *Cracking and Damage', Edited by J. Mazars and ZP Bažant (Elsevier, London, 1989)*, 462–476.

RILEM, (1990). 89-FMT Committee Fracture Mechanics of Concrete,Determination of fracture parameters of plain concrete using three-point bend tests. *Materials and Structures*, *23*(6), 457–460.

Roden, R. (2013). *RCC Fatigue Model Development by the American Concrete Pavement Association (ACPA) – Interim Report*. American Concrete Pavement Association (ACPA).

Roesler, J., Paulino, G., Gaedicke, C., Bordelon, A., & Park, K. (2007). Fracture behavior of functionally graded concrete materials for rigid pavements. *Transportation Research Record: Journal of the Transportation Research Board*, (2037), 40–49.

Sarker, P. K., Haque, R., & Ramgolam, K. V. (2013). Fracture behaviour of heat cured fly ash based geopolymer concrete. *Materials & Design*, *44*, 580–586.

Schrader, E. (1992). Roller-Compacted Concrete for Dams – State of the Art. In *International Conference on Advances in Concrete Technology*. Athens, Greece.

Schrader, E. (2003). Appropriate laboratory compaction methods for different types of Roller Compacted Concrete (RCC). In *Proceeding of the 4th International symposium on RCC Dams, Madrid, España*.

Sengun, E., Aykutlu, M. A., & Yaman, O. (2017). Silindirle Sıkıştırılmış Beton Yollar Üzerine Güncel Bir Tarama-Bölüm 1: Özellikleri ve Karışım Tasarımı. *Cement and Concrete World*, *22*(130), 93–114.

Service d'Expertise en Matériaux, S. (2003). *Rapport de l'étude des caractéristiques du béton compacté au rouleau routier*. Montréal, Québec, Canada.

Shah, S. P., & McGarry, F. J. (1971). Griffith fracture criterion and concrete. *Journal of the Engineering Mechanics Division*, *97*(6), 1663–1676.

Shi, X., Mirsayar, M., Mukhopadhyay, A., & Zollinger, D. (2019). Characterization of two-parameter fracture properties of portland cement concrete containing reclaimed asphalt pavement aggregates by semicircular bending specimens. *Cement and Concrete Composites*, *95,* 56-69.

Stephens, R. I., Fatemi, A., Stephens, R. R., & Fuchs, H. O. (2000). *Metal fatigue in engineering*. John Wiley & Sons.

Strange, P. C., & Bryant, A. H. (1979). Experimental tests on concrete fracture. *Journal of the Engineering Mechanics Division*, *105*(2), 337–342.

Sun, W., Liu, J., Qin, H., Zhang, Y., Jin, Z., & Qian, M. (1998). Fatigue Performance and Equations of Roller Compacted Concrete with Fly Ash. *Cement and Concrete Research*, *28*(2), 309–315.

Tasdemir, C., Tasdemir, M. A., Grimm, R., & König, G. (1995). Microstructural effects on the brittleness of high strength concrete. *Fracture Mechanics of Concrete Structures*, 125–134.

Tasdemir, M. A., & Karihaloo, B. L. (2001). Effect of aggregate volume fraction on the fracture parameters of concrete: a meso-mechanical approach. *Magazine of Concrete Research*, *53*(6), 405–415.

Tayabji, S. D., & Okamoto, P. A. (1987). Engineering properties of roller-compacted concrete. *Transportation Research Record*, (1136).

TS EN. (2002). 197-1. Cement–Part 1: compositions and conformity criteria for common cements. *Turkish Standard Institution*.

Van Ornum, J. L. (1903). The fatigue of cement products. *Transactions of the American Society of Civil Engineers*, *51*(2), 443–445.

Wang, B., Zhang, X., Dai, J., & Xu, S. (2011). Critical crack tip opening displacement of different strength concrete. *Journal of Central South University of Technology*, *18*(5), 1693.

Wang, C., Chen, W., Hao, H., Zhang, S., Song, R., & Wang, X. (2018). Experimental investigations of dynamic compressive properties of roller compacted concrete (RCC). *Construction and Building Materials*, *168*, 671–682.

Westergaard, H. M. (1939). Bearing pressures and cracks. *Journal of Applied Mechanics*, *6*(2), A49–A53.

Williams, H. A. (1943). Fatigue Tests of Lightweight Aggregate Concrete Beams. In *Journal Proceedings*, 39, 441–448.

Williams, S. (2013). Comparison of the Superpave Gyratory and Proctor Compaction Methods for the Design of Roller-Compacted Concrete Pavements. *Transportation Research Record: Journal of the Transportation Research Board*, (2342), 106–112.

Wöhler, A. (1860). Versuche zur Ermittlung der auf die Eisenbahnwagenachsen einwirkenden Krafte und die Widerstandsfaihigkeit der Wagen-Achsen. *Zeitschrift Fur Bauwesen*, *X*, 583–616.

Xu, S., & Reinhardt, H. W. (1999). Determination of double-K criterion for crack propagation in quasi-brittle fracture, Part II: Analytical evaluating and practical measuring methods for three-point bending notched beams. *International Journal of Fracture*, *98*(2), 151–177.

Xu, S., & Zhang, X. (2008). Determination of fracture parameters for crack propagation in concrete using an energy approach. *Engineering Fracture Mechanics*, *75*(15), 4292–4308.

Yaman, İ. Ö., & Ceylan, H. (2013). Silindirle sıkıştırılmış beton yollar. *T.H.B.B Hazır Beton Dergisi*, 69–82.

Yan, A., Wu, K.-R., Zhang, D., & Yao, W. (2001). Effect of fracture path on the fracture energy of high-strength concrete. *Cement and Concrete Research*, *31*(11), 1601–1606.

Yimprasert, P., & McCullough, B. F. (1973). *Fatigue and stress analysis concepts for modifying the rigid pavement design system.* Texas Transportation Institute. Arlington, TX United States.

Zhang, B., Phillips, D. V, & Wu, K. (1996). Effects of loading frequency and stress reversal on fatigue life of plain concrete. *Magazine of Concrete Research*, *48*(177), 361–375.

Zhao, Z., & Xu, S. (2001). Influence of compressive strength of concrete upon new K_R-curve based on the cohesive force. *Journal of Hydroelectric Engineering*, *74*, 11–21.

Zhou, F. P., Barr, B. I. G., & Lydon, F. D. (1995). Fracture properties of high strength concrete with varying silica fume content and aggregates. *Cement and Concrete Research*, *25*(3), 543–552.

CURRICULUM VITAE

PERSONAL INFORMATION

Surname, Name	: Şengün, Emin
Nationality	: Turkish (TC)
Date and Place of Birth	: 1 January 1989, Tokat
Phone	: +90 312 210 22 92
E-mail	: esengun@ybu.edu.tr

EDUCATION

Degree	Institution	Year of Graduation
MS	ITU Civil Engineering	2013
BS	YTU Civil Engineering	2010
High School	Tokat Anadolu High School, Tokat	2006

WORK EXPERIENCE

Year	Place	Enrollment
2013-Present	AYBU Civil Engineering	Research Assistant
2010-2013	YTU Civil Engineering	Research Assistant

FOREIGN LANGUAGES

Advanced English,

PUBLICATIONS

Journals

1. Şengün, E., Alam, B., Shabani, R., Yaman, İ. Ö., "The Effects of Compaction Methods and Mix Parameters on the Properties of Roller Compacted Concrete Mixtures", Construction and Building Materials, Vol: 228, pp: 116807, 2019.

2. Öztürk, H. I., Tan, B. E., Şengün, E., Yaman, İ. Ö., "Comparison of Jointed Plain Concrete Pavement Systems Designed by Mechanistic-Empirical (M-E) Method for Different Traffic, Subgrade, Material and Climatic Conditions", Journal of the Faculty of Engineering and Architecture of Gazi University, 34:2, 771-783, 2019.

3. Şengün, E., Aykutlu, M. A., Yaman, İ. Ö., "State of Art Review of Roller Compacted Concrete Pavements – Part II: Compaction Methodology and Field Applications", Cement and Concrete World, Vol:23, No:134, ISSN 1301-0859, 2018, pp. 60-78.

4. Şengün, E., Aykutlu, M. A., Yaman, İ. Ö., "State of Art Review of Roller Compacted Concrete Pavements – Part I: Properties and Mixture Design", Cement and Concrete World, Vol:22, No:130, ISSN 1301-0859, 2017, pp. 93-114.

5. Şengün, E., Yaman, İ. Ö., Ceylan H.,"An Overview on Rigid Pavement Specifications in Developed Countries ", Cement and Concrete World, Vol:21, No:123, ISSN 1301-0859, 2016, pp. 77-86.

6. Şengün, E., Kıran, E., Yaman, İ. Ö., "Opportunities for Concrete Pavements and Concrete Safety Barriers in Turkey", Cement and Concrete World, Vol:22, No:126, ISSN 1301-0859, 2017, pp. 72-82.

International Conferences

1. Şengün, E., Shabani, R., Alam, B., Yaman, İ. Ö., "The Effect of Set Retarding and Plasticizer Admixtures on the Fresh and Hardened Properties of Roller Compacted Concrete", 10. International Concrete Congress-Recent Advances in Concrete Technology, Cilt:1, Sayfa: 288-296, BAOB Campus, Bursa, Turkey, 2-4 May 2019.

2. Şengün, E., Yaman, İ. Ö., "Concrete Road… Why not?", 10. International Concrete Congress-Recent Advances in Concrete Technology, Cilt:1, Sayfa: 288-296, BAOB Campus, Bursa, Turkey, 2-4 May 2019.

3. Shabani, R., Şengün, E., Öztürk, H. I., Alam, B., Yaman, İ. Ö., "Evaluation of Superpave Gyratory Compaction Method (SGC) for Roller Compacted Concrete (RCC) Mixture Design", Transportation Record Board (TRB) 98th Annual Meeting, Poster Presentation, Washington DC, US, January 2019.

4. Şengün, E., Shabani, R., Alam, B., Yaman, İ. Ö., "Comparison of Several Laboratory Compaction Practices Applied on Roller Compacted Concrete Pavements" 12th International Congress on Civil Engineering (ACE 2018), presented, Ege University, İzmir, Turkey, 12-14 September 2018.

5. Şengün, E., Aykutlu, M. A., Shabani, R., Alam, B., Yaman, İ. Ö., "Comparison of Laboratory Practices for Roller Compacted Concrete Pavements", 13th International Symposium of Concrete Roads (13th ISCR-2018), presented, Berlin, Germany, 19-22 June 2018.

6. Ardoğa, M. K., Şengün,E., Alam B., Yaman, İ. Ö., "Determination of the Tensile Strength of Different Fiber Reinforced Concrete Mixtures",12 th International Congress on Civil Engineering (ACE 2016), presented, Boğaziçi University, Istanbul, Turkey, 21-23 September 2016.

7. Şengün,E., Alam B., Yaman, İ. Ö., "High Performance Fiber Reinforced Concrete for Pavements",12th International Congress on Civil Engineering (ACE 2016), presented, Boğaziçi University, Istanbul, Turkey, 21-23 September 2016.

8. Şengün,E., Alam B., Yaman, İ. Ö., "Effect of Synthetic Fibers on Energy Absorption Capacity of Normal and High Performance Concrete ", 2st International Scientific Conference: Civil Engineering- Present Problems, Innovative Solutions (CEPPIS 2016) , presented, UTP University of Science and Technology, Bydgoszcz, Poland, 8 June 2016.

9. Şengün,E., Alam B., Yaman, İ. Ö., "Effect of synthetic fibers on flexural performance of normal and high performance concrete,9 th RILEM International Symposium on Fiber Reinforced Concrete (BEFIB 2016),Vancouver, Canada, pp. 925-934,19-21 September 2016.

10. Şengün, E., Berilgen, M., Incecik, M., "Effects of Using Different Constitutive Soil Models for The Cavity Expansion Problem", 8th European Conference on numerical Methods in Geotechnical Engineering, vol.1, pp. 205-208, Delft, The Netherlands, 18-20 June 2014.